CRITICAL SAMPLE SIZE AND SATELLITE IMAGE SELECTION FOR THE RECOGNITION OF POPPY AND PYRETHRUM CROPS IN NORTH WEST TASMANIA

UNIVERSITY OF TASMANIA

Rachel Michelle Barrett

B.Sc.Agr (Hons)

School of Agricultural Science
University of Tasmania
PO Box 447, Burnie
Tasmania, Australia, 7320

A thesis submitted in fulfillment of the requirements for the degree of
Masters in Agricultural Science
University of Tasmania
October 2002

DECLARATION OF ORIGINALITY

I, Rachel Michelle Barrett, do hereby declare that this submission is my own work and that, to the best of my knowledge and belief, it contains no material previously published or written by another person, nor material, which to a substantial extent, has been accepted for the award of any other degree or diploma of the University or any other institute of higher learning, except where due acknowledgement is made in the text.

Rachel Michelle Barrett

October 2002

STATEMENT OF AUTHORITY OF ACCESS

This thesis may be made available for loan and limited copying in accordance with the Copyright Act 1968.

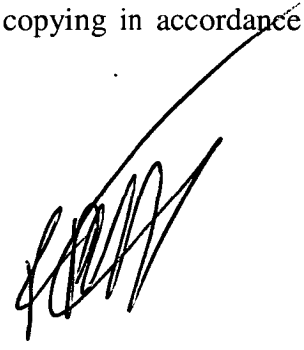

Rachel Michelle Barrett

October 2002

PREVIOUS PUBLICATIONS

Parts of the material presented in this thesis were published as:

Barrett, R.M., Crowther, P., Laurence, R.C.N. and Lincolne, R. (2000). Agricultural Crop Identification Using SPOT and LANDSAT Images in Tasmania. *International Archives of Photogrammetry and Remote Sensing. Volume XXXIII Part B7/1 Commission VII.* pp. 133-139.

Laurence, R.C.N., Barrett, R.M., Crowther, P., and Lincolne, R. (2001). *Remote Sensing as an Aid to Horticultural Crop Recording and Husbandry.* Final Report to Horticulture Australia Ltd. HRDC Project No. VG97011.

Barrett, R.M., Crowther, P; Laurence, R.C.N. and Lincolne, R. (2001). Remote Sensing as an Aid to Tasmanian Horticultural Crop Recording and Husbandry. *Proceedings of IEEE 2001 International Geoscience and Remote Sensing Symposium.* 09 – 13 July, 2001. Sydney.

ABSTRACT

Determination of the critical level of training data, and investigation of targeting the time of image acquisition to specific crop growth cycles, will increase the efficiency of remote sensing data analysis, for recognition of poppies and pyrethrum. The objective of this project, was to determine whether the amount of training data (critical sample size) contributed significantly to classification, using three methods of analysis of two season's data for, poppy and pyrethrum crops, on the North West Coast of Tasmania and to investigate the timing of image acquisition. Distinction between class types was not an objective of the study.

Eight Landsat 5 TM, two SPOT XS and three SPOT XI images were acquired between 02 July 1997 and 28 March 1999.

Observations of the spectral response of poppies showed that, Landsat TM bands one, two, three and five in November and January, provided significantly different, peak pixel values for the poppy crop. SPOT XS band two in February also provided peak pixel values for poppies. The spectral response of pyrethrum indicated that an increase in pixel value for the January Landsat TM data in bands five and seven was distinct, as was the peak in SPOT XI band three during December.

A principal component analysis, (PCA) was carried out separately on each image. For all Landsat TM imagery, over 98.482% of variance was contained within the first three principal components. Similarly, for all SPOT XI data, over 99.189% of variance was contained within the first three principal components. When SPOT XS data was analysed, the first and second components accounted for over 98.909% data variance.

The merged spectral response patterns generated from the automatic internal average relative reflectance (AIARR), normalised difference vegetation index (NDVI) and PCA images by an unsupervised, iterative self-organising data analysis technique (ISODATA) for the poppy and pyrethrum AOIs, provided the input for a supervised classification. As the AIARR, NDVI and PCA data were normally distributed, and the spectral response patterns were parametric, a maximum likelihood parametric decision rule was selected.

The amount of training data had a significant effect on the contribution to classification for the three analysis methods, over two season's data for each of the crop types.

To achieve a classification accuracy of 90% for poppies, the acquisition of Landsat data in either November or January, required a PCA with 80% of the total poppy area used as training (calibration) data. To achieve a classification accuracy of 96% for poppies, the acquisition of SPOT XI data in either October or December, required a NDVI analysis with 50% of the total poppy area used as training (calibration) data.

For pyrethrum, a classification accuracy of 80% was achieved by acquiring imagery in the post harvest and dormancy stage (late February to October), using a PCA method and 90% of the total amount of data available for training. When imagery was acquired in late December or early January, using 40% of the total amount of pyrethrum data for training contributed, on average, to the classification of 87% of the crop, when analysed using the NDVI method.

The findings of this research showed that the choice of the training set (quality and quantity) had an influence on the success of a classification approach as well as the choice of image analysis technique. Timely acquisition of imagery was shown to be required to achieve a satisfactory level of contribution to classification from training data of poppies and pyrethrum.

ACKNOWLEDGEMENTS

The work in this thesis has been supported by the University of Tasmania's School of Agricultural Science and Faculty of Science and Engineering through the funding of a Scholarship and the Tasmanian Institute of Agricultural Research funded my participation at ISPRS 2000 and IGARS 2001 conferences.

Many thanks are due to my supervisors, Dr. Rowland Laurence (Tasmanian Institute of Agricultural Research, Burnie) and Dr. Paul Crowther (Sheffield Hallam University, United Kingdom) for their guidance, assistance, influence and constructive criticism.

I thank Mr Ross Lincolne (Central Science Laboratory, Hobart) for his tutoring in the use of ERDAS Imagine (Version 8.4)® and introduction to the world of remote sensing.

I would also like to thank my colleagues, particularly the Research Higher Degree candidates, Dr Danny Donaghy and Dr Ali Salardini at the Tasmanian Institute of Agricultural Research, Burnie, for their valuable advice and support in the preparation of papers and this thesis.

Finally, a most sincere thanks to my parents who, whilst not having an intrinsic knowledge of my research, provided moral support and the educational opportunities to enable the achievement of my goals.

TABLE OF CONTENTS

LIST OF FIGURES

2. A LITERATURE REVIEW OF REMOTE SENSING AND METHODS OF DATA ANALYSIS

4. A REVIEW OF THE AGRONOMY AND PHYSIOLOGY OF POPPY (*PAPAVER SOMNIFERUM*) AND PYRETHRUM (*TANACETUM CINERARIIFOLIUM*)

5. REGIONAL SETTINGS

6. MATERIALS AND METHOD

7. RESULTS AND DISCUSSION

APPENDIX A:

APPENDIX F:

APPENDIX G:

LIST OF TABLES

APPENDIX A:

APPENDIX C:

CHAPTER 1

INTRODUCTION

"Great spirits have always found violent opposition from mediocrities. The latter cannot understand it when a man does not thoughtlessly submit to hereditary prejudices but honestly and courageously uses his intelligence."

Albert Einstein

In this chapter the background research undertaken by Laurence *et al.* (2001), which lead to the instigation of this project is briefly presented. The aims of the research and a chapter plan are also presented.

1.1 Historical Background to Thesis

In October 1997, an investigation commenced into the ability of current technology to identify and differentiate between the many horticultural crops grown in Tasmania using commercially available multi-spectral satellite images (HRDC Project VG97011, Laurence *et al.* 2001). The overall objective of individual crop recognition in this project was, to initiate a database of crop location and characteristics, which would support farm/crop management software and whole of industry performance records.

While the main focus of this project was the recognition of multiple crop types, industry showed significant interest in the specific recognition of individual crops (poppies and pyrethrum) and the possibility of using the technology to assist with yield forecasting and crop area measurement.

This previous work by Laurence *et al.* (2001), showed encouragingly that several crops were recognised simultaneously from the two years' data acquired, some individual crops with about 90 - 95 % accuracy.

Those crops, which are of major importance to the Tasmanian industry, were generally among those best identified. The onion crop stood out as being easily recognised in many situations, with peas, potatoes, poppies and pyrethrum also returning good accuracy in the analyses, particularly in the second year. These crops were also those, which comprised the major part of the data set, as they were most common in the production systems within the study areas. As a result, this allowed for the use of larger numbers of "training" paddocks in the automated methodology in comparison with situations with some less-frequently occurring crops, where the number of "training" paddocks was very probably inadequate. The investigation of the number of data sets, which were required as training data, was not undertaken in project VG97011 but is examined in this thesis. The proportions of data sets used as training data vary with crop type, location, and the effectiveness of imagery acquisition. The extent to which the training data subset can be minimised over seasons and locations will affect costs of analysis.

The approach taken by this previous work in attempting to identify many crop types simultaneously did, however, involve compromise in setting the parameters in the automated procedure and errors of commission tended to be larger than would be the case had one or a few crops been the target of recognition.

The analyses in project VG97011, using segregation of images into early-season (21 July 1998 – 29 January 1999 imagery) and later-season (27 September 1998 – 29 March 1999 imagery) information were found to result only in minor general improvement to classification. Different segregation options were not studied, but these analyses indicated that the investigation of other combinations of image timing might enhance recognition. For example, peas were recognised poorly in the late image selection (coinciding with pod maturation and harvest) indicating that early imagery, coinciding with rapid vegetative growth and flowering, would

give best recognition. Results with identification of potato crops were converse to those with peas, suggesting that late imagery (coinciding with rapid vegetative growth and flowering) was very selective for potato crops.

1.2 Aim of Research

The aim of this thesis is to investigate utilising the technology developed in Project VG97011 in a commercial environment, by tailoring the methodology for two major and commercially significant horticultural crops individually, poppies and pyrethrum. Tasmania supplies about half of the world's production of morphine concentrated poppy straw (CPS) from about ten per cent of the area grown worldwide (Anon 2000; Fist 2001). The Tasmanian pyrethrum industry is a major supplier and multi-million dollar exporter of natural pyrethrum products to the world market. The predictive accuracy in relation to identification for these particular crops was also among the most favourable of the 22 different crops investigated in Project VG97011.

Crops differ not only in their growth cycle, but also in morphology, physiology and agronomy. These differences relating to the plant (leaf area index, canopy architecture, leaf surface characteristics, plant water nutrient status and disease) and soil (colour, moisture status, percentage of the surface discernable beneath the canopy) play a significant role in the measurement of the reflectance of electromagnetic waves from a particular plant. Therefore, the current study will an investigate targeting the time of image acquisition to specific crop growth cycles.

Given the high costs associated with collecting training data, determination of the critical level of training data will enable the use of remote sensing data for crop recognition to become more cost effective. As stated by Cruz-Castillo *et al.* (1994), the combination of too many variables and few observations (i.e. sample sizes) usually causes unreliable estimates. Therefore, if increases in accuracy of prediction are to be achieved, it is imperative that sufficient training data (ground truthing) are obtained. There is, however, a critical level, where any increases in

quantity of training data will no longer result in significant increases in accuracy. The choice of a good training set can also have significant influence on the success of a classification approach (Shine and Wakefield 1999).

1.3 Chapter Plan

The second chapter "A Literature Review of Remote Sensing and Methods of Data Analysis" provides a technical foundation for the reader to the work discussed in this thesis and includes reference to relevant literature. It contains information explaining the concept and definition of remote sensing, and the principals underlying satellite imagery. Widespread image preparation and image interpretation methods are discussed, in addition to a discussion in relation to the classification of imagery data and the methods of determining the accuracy of classification.

Chapter three "A Brief Historical Review of Remote Sensing in Australian Agriculture" reviews and discusses the development and use of remote sensing in Australian grassland and broadacre agriculture. This chapter also demonstrates the practical application of the concepts and the principles underlying satellite imagery discussed in chapter two.

The fourth chapter provides a technical foundation for the reader to the work discussed in this thesis and includes reference to relevant literature. Chapter four provides a brief historical background to the development of the poppy (*Papaver somniferum*) and pyrethrum (*Tanacetum cinerariifolium)* industries in Tasmania, a description of the poppy and pyrethrum plants and the agronomy, physiology and utilisation of the crops.

Chapter five "Regional Settings," provides the reader with background information regarding the geographical location, climatic and soil environment of the study area.

Chapter six "Materials and Method" describes the selection of trial areas, image acquisition, ground-truthing and the distribution of the areas of interest (AOI) for the 1997/98 and 1998/99 poppy and pyrethrum growing seasons in this research. The chapter also describes the image preprocessing techniques used and the preparation of data for classification using the automatic internal average relative reflectance (AIARR), normalised difference vegetation index (NDVI) and principal component analysis (PCA).

Spectral response patterns were obtained for each AOI associated with poppies and pyrethrum in each of the individual images, to determine whether pyrethrum and poppy crops exhibited spectrally distinct patterns using AIARR. The outcome of the AIARR calculation on the data was a relative reflectance value for each pixel, for each layer per image. The result of the AIARR calculation on the data was a set of relative reflectance values per pixel, per crop type, per layer, which were then used in classification, with a decision rule, to assign the pixels to a class.

The NDVI was calculated on the Landsat 5 TM imagery and SPOT imagery. The outcome of the NDVI calculation on the data was a value for each pixel, for each layer per image (one layer in the case of NDVI). The result of the NDVI calculation on the data was a set of vegetation indices per pixel, per crop type per layer to be used in classification, with a decision rule, to assign the pixels to a class.

A PCA was carried out separately on each image in an approach similar to Turner and Congalton (1998). Components were calculated for six layers in the Landsat TM imagery, three layers in the SPOT XS imagery and four layers in the SPOT XI imagery. From the PCA images, new images were created with the desired number of layers based on the examination of the Eigenvalues and Eigenvectors. The result of the PCA calculation on the data was a set of data values per pixel, per crop type per layer to be used in classification, with a decision rule, to assign the pixels to a class.

The classification procedure and the subsequent assessment of classification are also described in Chapter six.

Presentation of the results from the AIARR, NDVI and PCA calculations and their discussion is provided in Chapter seven. The chapter also reports on the classification method where the output from the iterative self organising data analysis ISODATA signature files for each proportion of training data, for all layers per image (three or more for the AIARR, one for the NDVI, and two or three for the PCA) per crop type, is presented and discussed. The assessment of the contribution of the amount of training data to classification is reported and discussed.

Chapter eight draws conclusions in relation to the objective of this project, which was not to distinguish class types but rather to determine whether the amount of training data had a significant effect on the contribution to classification, using three methods, over two season's data for each of the crop types. Determining the critical level of training data, the most appropriate technique for analysis of remote sensing data, in relation to crop type, phenology, physiology, agronomy and time of image acquisition will enable the use of remote sensing data for crop recognition to become more cost effective, given the high costs associated with collecting training data.

CHAPTER 2

A LITERATURE REVIEW OF REMOTE SENSING AND METHODS OF DATA ANALYSIS

Remote sensing has many formal definitions. Campbell (1996) defined remote sensing as: *"...the practice of deriving information about the earth's land and water surfaces using images acquired from an overhead perspective, using electromagnetic radiation in one or more regions, reflected or emitted from the surface of the earth...."* Earlier, (Jupp. *et al.* 1985) defined remote sensing as: *"...the action of observing a target, such as the earth, using physical instruments such as multi-spectral sensors, radar and cameras which are remote from the target..."* Elaborating further *"....most remotely sensed data are measurements of reflected and emitted electromagnetic radiation (light, heat and radio waves) making up an image of the target which is then processed and interpreted in various ways..."* Colwell (1983) and Mather (1991) defined remote sensing as the acquisition of information or data, about an object or scene, without direct contact. It is usually associated with the acquisition of information about the Earths' surface by electronic and/or optical instruments from satellites, airborne platforms or ground observation.

2.1 Electromagnetic Radiation Spectra

Every surface on the Earth reflects the suns electromagnetic radiation and/or is itself a source of electromagnetic radiation (EMR) and thence exhibits a unique spectral response pattern. Star and Estes (1990) described EMR as energy transmitted through space in the form of electric and magnetic waves.

EMR ranges in frequency from radio waves, microwaves, infrared waves, visible light, ultraviolet waves, x-rays, through to gamma rays (Jensen 1996). The series

of electromagnetic waves depicted in Figure 2.1, arranged in order of their frequency, is called the electromagnetic spectrum.

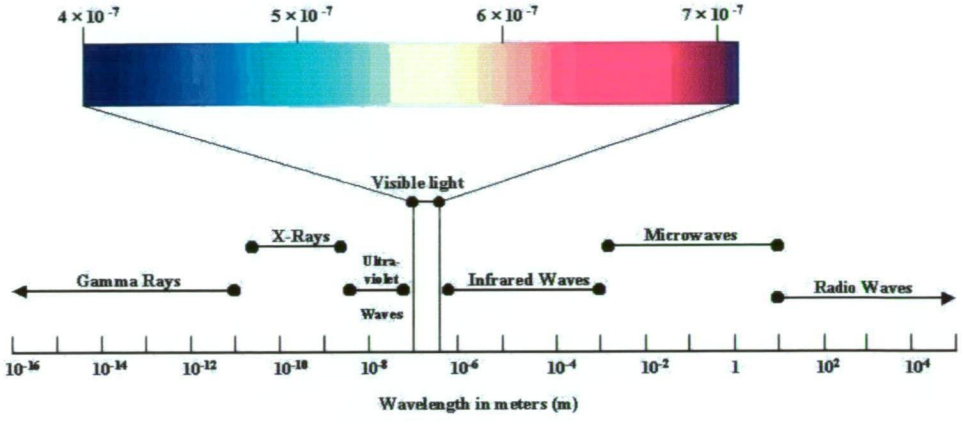

Figure 2.1: The electromagnetic spectrum

There are two ways in which remote sensing can be performed: actively and passively (Richards 1993). Commercial remote sensing satellites carry either active or passive sensor systems, or both types. A passive system consists of an array of small detectors, which record (as digital numbers), the amount of electromagnetic radiation reflected and/or emitted from the Earths' surface. However, there are several photographic devices still in operation and not all sensors are scanning systems (i.e. systems not using an array of small detectors).

Multispectral scanners (such as SPOT and Landsat) are examples of passive systems. An active system propagates its own electromagnetic radiation and measures (as digital numbers) the intensity of the return signal. Synthetic aperture radar (SAR) is an example of an active system.

2.2 Absorption Spectra

In remote sensing, the sun is the radiation source for passive sensors (Richards, 1993). Elachi (1987) stated that, as solar radiation travels through the Earths' atmosphere, it is affected by four phenomena: absorbtion, scattering, scattering source and emission source. These are described below.

2.2.1 Absorption

Absorption is the amount of radiation absorbed by the atmosphere. It is not linear but logarithmic with concentration (Flaschka, 1969). The concentration of atmospheric gasses, particularly water vapour, is variable. Other gases of significance to absorption are carbon dioxide (CO_2) and ozone (O_3). Figure 2.2 diagrammatically represents the effect of absorption on solar radiation.

2.2.2 Scattering

Scattering is the amount of radiation scattered away from the field of view by the atmosphere. Rayleigh scattering is modelled with a commonly used algorithm, which accounts for the scattering of short wavelength energy, by the gas molecules in the atmosphere (Pratt 1991). Figure 2.2 diagrammatically represents the effect of scattering on solar radiation.

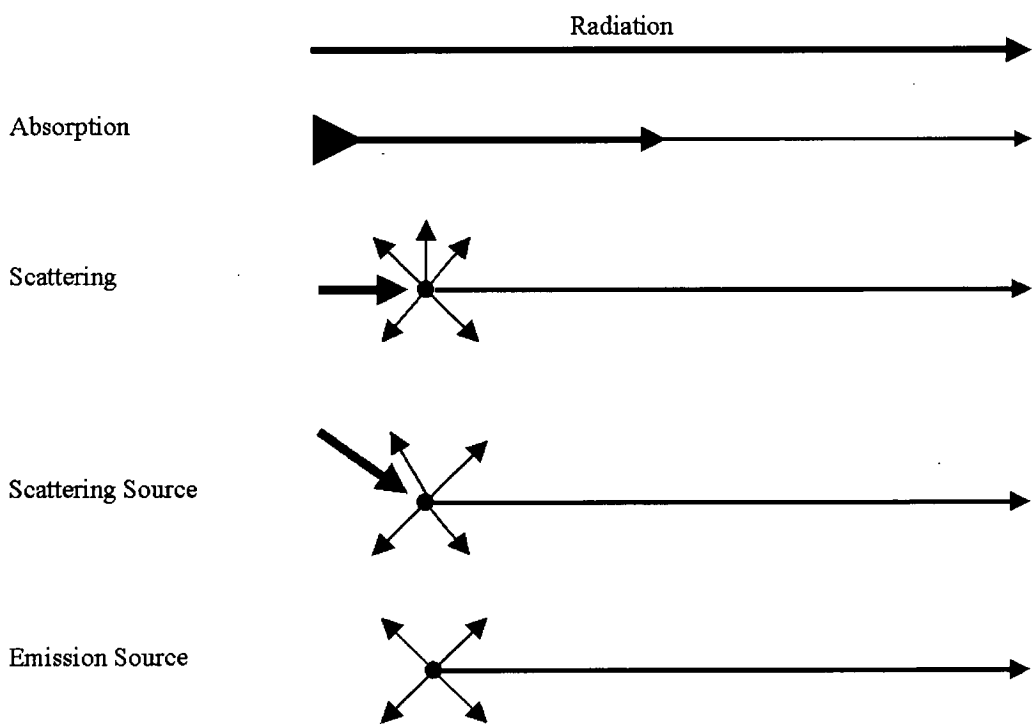

Figure 2.2: Diagrammatic representation of absorption, scattering, scattering source and emission source (after Elachi 1987)

2.2.3 Scattering Source and Emission Source

Scattering source is divergent solar radiation scattered into the field of view, whereas, emission source is radiation re-emitted after absorption. After interaction

with the target material, the reflected radiation travels back through the atmosphere and is subjected to absorption and scattering a second time, before arriving at the remote-sensing platform. Figure 2.2 diagrammatically represents the effect of scattering source and emission source on solar radiation.

2.3 Reflectance Spectra

Elachi (1987) stated that when an electromagnetic wave (solar illumination in the case of passive remote sensing) strikes a surface, three interactions are possible. These are reflection, transmission and scattering. It is the reflected radiation, generally modelled as bi-directional reflectance (Clarke and Roush, 1984), which is measured by the satellite platform. The wavelengths, which are not returned to the sensor, provide information about the imaged area (Pouncey *et al.*1999).

Different remote sensing instruments record different parts (bandwidths) of the spectrum of electromagnetic energy (Figure 2.3) and the portions or bands, which can be recorded by an instrument, are known as that instruments' spectral resolution.

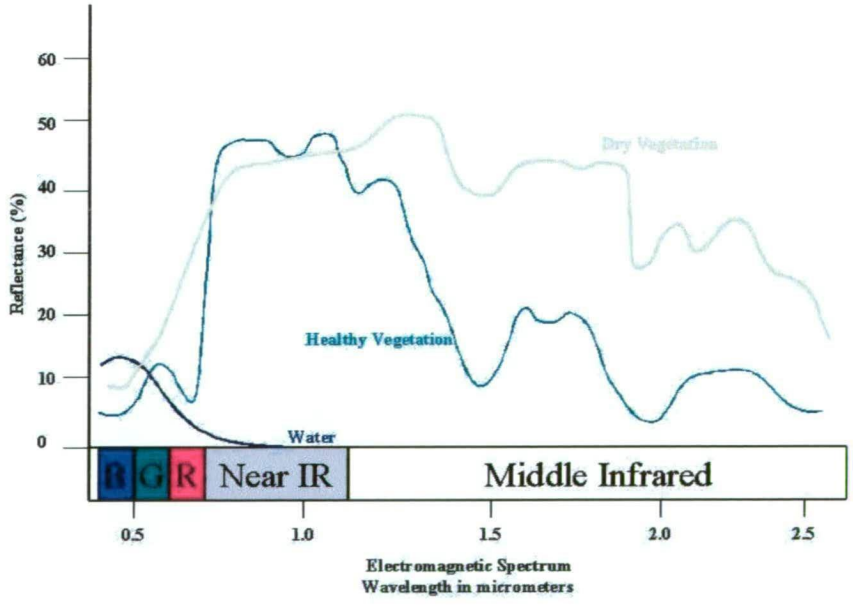

Figure 2.3: Spectral response curves of various surfaces compared to the bandwidths of satellite sensors

The two satellite platforms used in this project (Landsat and SPOT) detect reflected electromagnetic radiation in the visible and infrared region of the spectrum, with the exception of the Landsat thermal band (band 6), which measures emitted radiation. Appendix A provides detailed technical information for the Landsat TM and SPOT sensors.

Every material (rocks, soils, vegetation, cultural features etc) absorbs a portion of the electromagnetic spectrum, and has characteristic spectral response patterns based on the chemical composition of the material Remotely sensed data are made up of reflectance values, translated to discrete digital numbers (or values) recorded by the sensing device.

The optical reflectance of a crop is determined by the unique interaction of solar radiation with a specific crop canopy (Nieuwenhuis 1996). The integration of the interaction between morphology, physiology and agronomy over the life of the crop, soil characteristics and prevailing atmospheric conditions, produces a characteristic spectral response pattern, which can be used for crop recognition.

2.4 Selection of Analysis Software

ERDAS Imagine (Version 8.4)® was selected as the analysis system as it incorporated functions of both image processing and geographic information systems (GIS). These functions included importing, viewing, altering and analysing raster data sets.

ERDAS Imagine (Version 8.4)® provided a map-based graphical tool for viewing, managing and archiving the image data as well as the ability to quickly and accurately register imagery to a specific reference. Sensor modelling techniques gave the ability to orthorectify SPOT and Landsat with ease. Functions for spatial and spectral enhancement were included, enabling extraction of the required information from the imagery. Supervised and unsupervised land cover

classification techniques were also included as well as advanced tools for evaluating the quality and input training data and the resulting thematic maps.

The above mentioned features were required for the analysis of data in this project. Hence, ERDAS Imagine (Version 8.4)® was selected as it provided a single analysis software package, which would meet all the user demands.

2.5 Image Preprocessing

Several types of errors and/or distortions are manifested in remotely sensed data and had to be corrected, to prepare the imagery for analysis.

Rawly gathered, remotely sensed image data represent the surface of the earth, and are distorted by both the curvature of the earth, and the sensor being used. Rectification is the process of projecting the data onto a plane and making it conform to a map projection system.

Image-to-image registration enabled comparison of separate images from differing sources to be compared pixel by pixel and essentially made an image conform to another (Pouncey *et al.* 1999). Image-to-image registration involved georefrencing only. Where both Landsat 5 TM and SPOT images were used to create datasets, their accurate conformation was necessary to prevent the small misalignments between images, causing errors around the edge of the paddocks, where areas from adjacent paddocks could accidentally be included. This enabled comparison between separate images pixel by pixel.

2.5.1 Ground Control Points

Accurate ground control points (GCPs) are necessary for rectification, as the rectified coordinates for all other points in the image are extrapolated from the GCPs. The more evenly dispersed the GCPs are, the more reliable the rectification. Ground control points are specific pixels in an image for which the

output map coordinates (or other coordinates) are known (i.e. identifiable features located on the earths' surface which have known ground coordinates). Ground control points consist of two *x,y* pairs of coordinates. The source coordinates are data file coordinates in the image to be rectified and the reference coordinates are the coordinates of the map or reference image to which the source image is being registered. Once located, GCPs are used to compute and test a transformation matrix.

2.5.2 Transformation Matrix - First-Order Linear Transformation

The transformation matrix consists of coefficients, which are used, in polynomial equations to convert the coordinates (Pouncey *et al.* 1999). The aim of calculating the coefficients of the transformation matrix, is to derive polynomial equations for which there is the least error when they are used to transform the reference coordinates of the GCPs, into the source coordinates. The size of the matrix (minimum number of GCPs) is dependent upon the order of the transformation. Pouncey *et al* (1999) showed that the minimum number of points required, when performing a transformation of order *t* equals:

$$\frac{((t+1)(t+2))}{2}$$

First-order transformations can be used to project raw imagery to a planar map projection, convert a planar map projection to another planar map projection (e.g. SPOT and Landsat Level 1B data), and when rectifying relatively small areas. A first-order transformation is a linear transformation, which can change location in *x* and/or *y*, scale in *x* and/or *y*, skew in *x* and/or *y* and rotation.

The transformation matrix for a first-order transformation consists of six coefficients (three for each coordinate (*x* and *y*)).

$$\begin{matrix} a_0 & a_1 & a_2 \\ b_0 & b_1 & b_2 \end{matrix}$$

The coefficients are used in the first order polynomial as follows:

$$x_0 = a_0 + a_1 x + a_2 y$$
$$y_0 = b_0 + b_1 x + b_2 y$$

where:

x and y are source coordinates (input)
x_0 and y_0 are rectified coordinates (output)

In the case of a first order image rectification, the variables in the polynomial (x and y) are the source coordinates of a GCP. The coefficients are computed from the GCPs and stored as a transformation matrix. The quality of the transformation is represented using a root mean square (RMS) error (Pouncey *et al.* 1999).

2.5.3 Residual and Root Mean Square Error

RMS error is the distance between the input (source) location of a GCP and the retransformed location for the same GCP, (i.e. the difference between the desired output coordinate for a GCP and the actual output coordinate for the same point). RMS error is calculated with a standard statistical distance equation:

$$RMS \quad error = \sqrt{(x_r - x_i)^2 + (y_r - y_i)^2}$$

where:

x_i and y_i are the input source coordinates
x_r and y_r are the retransformed coordinates

RMS error is expressed as a distance in the source coordinate system. The RMS error is a distance in pixel widths. For example, a RMS error of two means that the reference pixel is two pixels away from the retransformed GCP. A large RMS error indicates poor correspondence.

Residuals are the distances between the source and retransformed coordinates in one direction and are given for each GCP. The x residual is the distance between the source x and the retransformed x coordinate. The y residual is the distance

between the source y and the retransformed y coordinate. The RMS error per GCP is reported in ERDAS Imagine (Version 8.4)® to assist in the evaluation of the GCPs and is calculated with the distance formula:

$$R_i = \sqrt{XR_i^2 + YR_i^2}$$

where:

R_i = the RMS error for GCP i
XR_i = the X residual for GCP i
YR_i = the Y residual for GCP i

The spatial relationship between the residuals and the RMS error per point is illustrated in Figure 2.4:

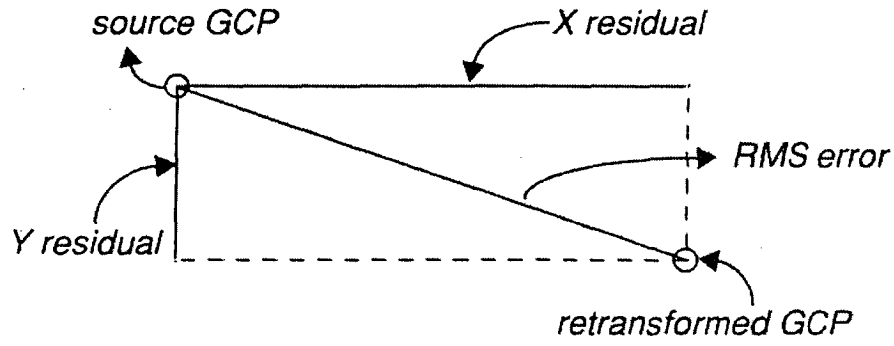

Figure 2.4: Relationship between residuals and RMS error per GCP (after Pouncey *et al.* 1999)

From the residuals, the total RMS error, the x RMS error and the y RMS error are determined:

$$R_x = \sqrt{\frac{1}{n}\sum_{i=1}^{n} XR_i^2}$$

$$R_y = \sqrt{\frac{1}{n}\sum_{i=1}^{n} YR_i^2}$$

$$T = \sqrt{R_x^2 + R_y^2} \qquad \text{or} \qquad T = \sqrt{\frac{1}{n}\sum_{i=1}^{n} XR_i^2 + YR_i^2}$$

where:

R_x = X RMS error
R_y = Y RMS error
T = total RMS error
n = number of GCPs
i = GCP number
XR_i = the X residual for GCP i
YR_i = the Y residual for GCP i

Acceptable RMS error is determined by the end use of the data, the type of data being used, the accuracy of GCPs and ancillary data being used. Therefore, when rectifying SPOT data to an accuracy of within 20 metres, the RMS error should not exceed 1.00 (i.e. retransformed coordinates to be considered "correct" must be within a 1 pixel or 20m radius).

RMS error can be reduced by several approaches. The order of the polynomial may be increased, but use of high order polynomials (greater than first or second order) is not recommended as it can result in less regular and predictable results based on the complex nature of the equation for the transformation (Pouncey *et al.* 1999). Secondly, the GCPs with the highest RMS error can be removed and further transformation calculated from the remaining GCPs. This second approach works on the principle that the highest RMS errors are attributed to inaccurate GCPs. A third and less desirable option is the tolerance of a higher amount of RMS error. A final option of selecting a point, for which the user has the most confidence, is not appropriate as it often results in a decrease in the dispersal of GCPs and thence, inaccuracy of the transformation.

2.5.4 Resampling

As the grid of pixels in a source image rarely matches the grid for a reference image, resampling is required so that the new data file values for the output file can be calculated. The input image with source GCPs and the output grid with reference GCPs must be compared (Figure 2.5).

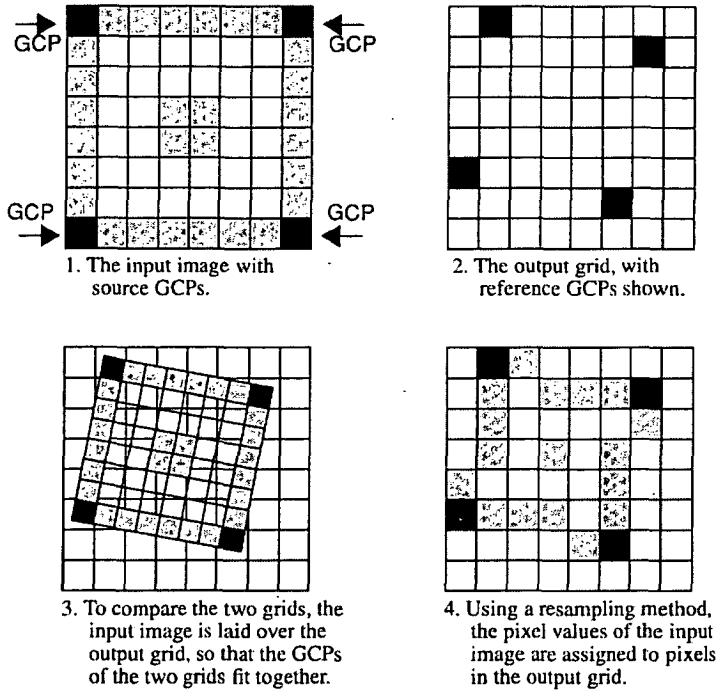

Figure 2.5: Diagrammatic representation of resampling (after Pouncey *et al.* 1999)

To enable comparison of the input image and output grid, the input image is laid over the output grid so that the GCPs of the two grids are aligned. The assignment of the pixel values of the input image to the pixels in the output grid are achieved by the use of a resampling technique such as nearest neighbour, bilinear interpolation or cubic convolution.

2.5.4.1 Nearest Neighbour Technique

A nearest neighbour resampling technique is used to assign the value of the closest pixel to the output value. The rectified coordinates (x_o,y_o, Figure 2.6) are retransformed to the source coordinate system using the inverse of the transformation, to determine an output pixels nearest neighbour. The pixel which is closest to the retransformed coordinates (x_r,y_r) is the nearest neighbour and the data file value for that pixel becomes the data file value of the pixel in the output image (Pouncey *et al.* 1999).

Nearest neighbour resampling transfers original data values without averaging them and therefore the extremes and subtleties of the data values are maintained.

Modification of radiometric values is also avoided (Turner and Congalton 1998). This is an important consideration when discriminating between vegetation types (Jensen 1996).

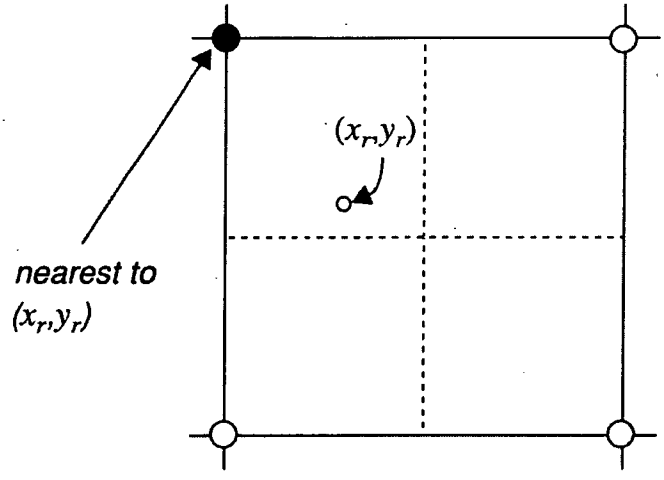

Figure 2.6: Graphical representation of nearest neighbour resampling technique (after Pouncey *et al.* 1999)

Nearest neighbour resampling was considered appropriate by Pouncey *et al.* (1999) for thematic files, which can have data files based on a qualitative (nominal or ordinal) system and a quantitative (interval or ratio system). Nominal data are file values in a raster layer that are simply categorized and named. The actual value used for each category has no inherent meaning, it is simply a class value. An example of a nominal raster layer would be a map showing tree species. Ordinal data are similar to nominal data, except that the file values put the classes in a rank or order. For example, a layer with classes numbered and named "1 = Good," "2 = Moderate," "3 = Poor" is an ordinal system. Interval data file values have an order, but the intervals between the values are also meaningful. Interval data measure some characteristic, such as elevation or degrees centigrade, which does not necessarily have an absolute zero. (The difference between two layers of interval data is meaningful.) Ratio data measure a condition that has a natural zero, such as electromagnetic radiation (as in most remotely sensed data), rainfall, or slope. Ratio data are always positive.

Nominal and ordinal data lend themselves to applications in which categories, or themes, are used. Therefore, these variables are termed categorical or thematic. Interval and ratio data are more likely to measure a condition, causing the file values to represent continuous gradations across the layer. Such layers are sometimes termed continuous.

Nearest neighbour resampling is also a suitable method to use prior to classification and is the easiest of the three methods (nearest neighbour, bilinear interpolation and cubic convolution) to compute and the fastest to use in ERDAS Imagine (Version 8.4)®.

2.5.4.2 Bilinear Interpolation Technique

Bilinear interpolation uses the retransformed coordinates (x_r,y_r), which are obtained from the rectified coordinates (x_o,y_o), as in the nearest neighbour resampling technique. The data file value of the rectified pixel is based, however, on the distances between the retransformed coordinate location (x_r,y_r) and the four closest pixels in the input (source) image (Figure 2.7). In other words, bilinear interpolation uses the data file values of four pixels in a 2 × 2 window to calculate an output value with a bilinear function.

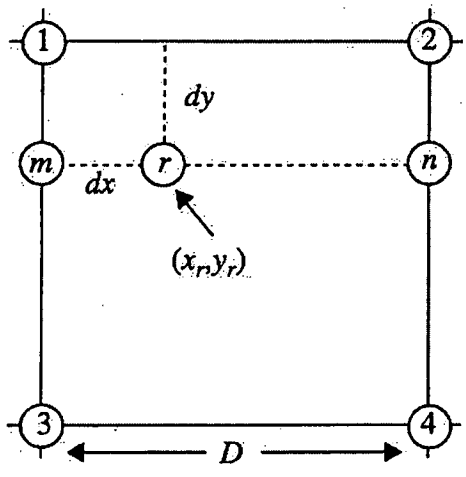

Figure 2.7: Bilinear interpolation where *r* is the location of the retransformed coordinate (after Pouncey *et al.* 1999)

In figure 2.7, the neighbouring pixels are numbered one, two, three and four. Given the data file values on a grid, the data file value for r (V_r) must be calculated. To calculate V_r a linear interpolation is performed, by interpolating V_m and V_n (Figure 2.8).

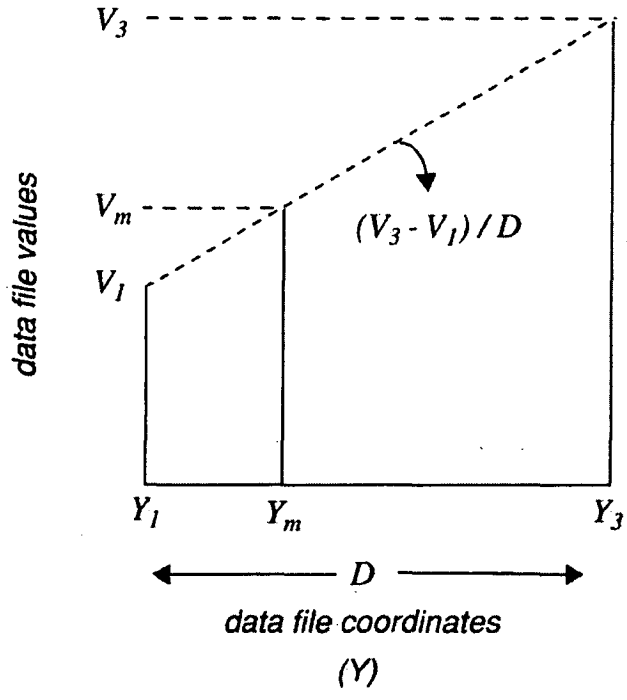

Figure 2.8: Linear Interpolations. Calculating a data file value as a function of spatial distance between two pixels (after Pouncey *et al.* 1999)

Where the data files are plotted in a graph relative to the distance from each other, it can be seen that the data file value of (V_m) is a function of the change in the data between the data file values of pixels three and one. This can be expressed in the following mathematical format:

$$V_r = \sum_{i=1}^{4} \frac{(D - \Delta x_i)(D - \Delta y_i)}{D^2} \times V_i$$

where:

Δx_i = the change in the x direction between (x_r, y_r) and the data file coordinate of pixel i
Δ_{yi} = the change in the y direction between (x_r, y_r) and the data file coordinate of pixel i
V_i = the data file value for pixel i
D = the distance between pixels (in x or y) in the source coordinate system

For each of the four pixels, the closer the pixel to (x_r,y_r), the greater the data file value weighting.

Bilinear interpolation has two advantages over the nearest neighbour resampling technique. Output images are smoother without the "stair-stepped" effect that is possible with nearest neighbour and are more spatially accurate. This method is often used when changing the cell size of the data, such as the merge of SPOT/Landsat TM imagery. Bilinear interpolation does result however, in some extremes of the data file value being lost, as some pixels are averaged and the edges are smoothed.

2.5.4.3 Cubic Convolution

Cubic convolution is similar to bilinear interpolation except a set of 16 pixels in a 4 × 4 array is averaged to determine the output data file value and an approximation of a cubic function rather than a linear function is applied to the 16 input values. To identify the 16 pixels in relation to the retransformed coordinate (x_r,y_r), the pixel (i,j) is used such that:

$$i = \text{int}\ (x_r)$$
$$j = \text{int}\ (y_r)$$

This assumes that (x_r,y_r) is expressed in data file coordinates (pixels). The pixels around (i,j) make up a 4×4 grid of input cells as shown in Figure 2.9.

As a cubic rather than a linear function is used to weight the 16 input pixels, the pixels further from (x_r,y_r) have exponentially less weight than those closer to (x_r,y_r).

Pouncey *et al.* (1999) reports that the cubic convolution used in ERDAS Imagine (Version 8.4)® is a compromise between low frequency and high frequency, and the general effect of the cubic convolution depends upon the data.

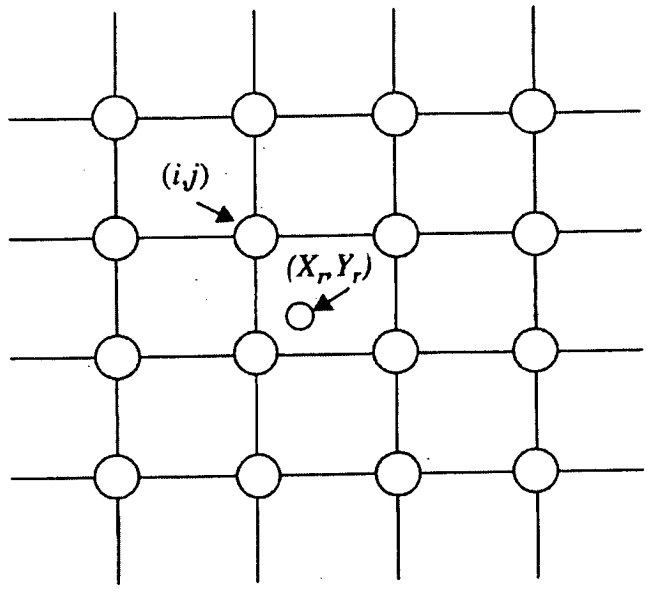

Figure 2.9: Diagrammatic representation of cubic convolution (after Pouncey *et al.* 1999)

The formula used in ERDAS Imagine (Version 8.4)® is:

$$V_r = \sum_{i=1}^{4} V(i-1, j+n-2) \times f(d(i-1, j+n-2)+1)$$
$$+V(i, j+n-2) \times f(d(i, j+n-2))$$
$$+V(i+1, j+n-2) \times f(d(i+1, j+n-2)-1)$$
$$+V(i+2, j+n-2) \times f(d(i+2, j+n-2)-2)$$

where:

i = int (x_r)
j = int (y_r)
d(i,j) = the distance between a pixel with coordinates (i,j) *and* (x_r,y_r)
V(i,j) = the data file value of pixel (i,j)
Vr = the output data file value
a = -0.5 (a constant which differs in other applications of cubic convolution)
$f(x)$ = the following function:

$$f(x) = \begin{cases} (a+2)|x|^3 - (a+3)|x|^2 + 1 & \text{if } |x| < 1 \\ a|x|^3 - 5a|x|^2 + 8a|x| - 4a & \text{if } 1 < |x| < 2 \\ 0 & \text{otherwise} \end{cases}$$

Cubic convolution uses 4 × 4 resampling, and in most cases a value of –0.5 tends to produce layers with a mean and standard deviation matching the mean and

standard deviation of the input pixels more closely than any other resampling method (Atkinson 1985). However, data values may be altered. Atkinson (1985) reports the effects of the cubic curve weighting can both sharpen the image and smooth out noise. The cubic convolution method is most suited when the cell size is being dramatically changed (Landsat TM/aerial photo merges). Fassnacht *et al.* (1997) noted that data resampled using the cubic convolution technique decreased the effectiveness of atmospheric corrections.

2.6 Normalised Difference Vegetation Index (NDVI)

When monitoring vegetation development and crop growth, it is common to use "vegetation indices" (Davenport and Nicholson 1993; Marchetti and Ricotta 1994; Marchetti, *et al.* 1995; Murthy, *et al.* 1996). Indices are related to the contrasting reflectance of the green biomass in the visible and near-infrared parts of the spectrum.

Due to the presence of chlorophyll in the leaves of plants, visible light is absorbed. The leaf structure of plants causes much of the light in the near-infrared part of the spectrum to be reflected, and therefore green vegetation generally has a high reflectance in this wavelength range, compared with wet bare soils.

The most common vegetation index used for the estimation of biomass by crop-specific empirical relationships, is the normalised difference vegetation index (NDVI). Birth and McVey (1968) developed the near infrared to red reflectance ratio as an index of green vegetation:

$$\frac{NearIR}{red} \approx \frac{TMBand\,4}{TMBand\,3}$$

Rouse *et al.* (1974) further developed this relationship into the now generally accepted NDVI, defined as:

$$NDVI = \frac{r_{nir} - r_{vis}}{r_{nir} + r_{vis}} \approx \frac{TMBand4 - TMBand3}{TMBand4 + TMBand3}$$

where r is the measured reflectance and the suffixes *nir* and *vis* indicate the near-infrared band and the visible band respectively. Values for NDVI range between -1 (high biomass) and +1 (bare soil). This index responds to changes in amount of green biomass (Deering *et al.* 1975; Tucker 1979), chlorophyll content, and leaf water stress (Tucker *et al.* 1980; Ajai 1983).

Blasco *et al.* (1986) determined that a normalised difference vegetation index could be calculated from the red and infrared SPOT XS bands two and three:

$$NDVI = \frac{r_{nir} - r_{vis}}{r_{nir} + r_{vis}} \approx \frac{SPOTBand3 - SPOTBand2}{SPOTBand3 + SPOTBand2}$$

2.7 Principal Components Analysis

Orlóci (1966) first described principal components analysis (PCA). PCA aims to find fewer than the original number of variables to explain the total variation in the data (i.e. reduce dimensionality), (Chavez and Kwarteng 1989; Cruz-Castillo *et al.* 1994). PCA is based on the Karhunen-Loeve (K-L) expansion (Kittler and Young 1973) and, according to Byun *et al* (1997), is a well known statistical method for data projection and widely used in pattern recognition and data analysis.

Lillesand and Kiefer (1994) stated that PCA rearranges the variance of all bands in an image to produce a new set of uncorrelated components, in which the information content is unevenly distributed (Faust 1989; Jensen 1996). The uncorrelated components are calculated by linear combinations of the original variables, termed "principal components." The principal components are orthogonal (non-correlated) to each other, which maximises variation among the original variables (Cruz-Castillo *et al.* 1994). Using analysis of Euclidean distance (to calculate the distance between two points in multi-dimensional spectral space) and PCA, successional trends can be displayed and provide the best insight into vegetation patterns (Mazzoleni *et al.* 1991).

Euclidean spectral distance is distance between n dimensional spectral space. It allows two measured vectors to be compared for similarity. The spectral distance between two pixels is calculated as follows:

$$D = \sqrt{\sum_{i=1}^{n} (d_i - e_i)^2}$$

where:

D = spectral distance
n = number of bands (dimensions)
i = a particular band
d_i = the data file value of pixel d in band i
e_i = the data file value of pixel e in band i

This equation, after Swain and Davis (1978), is in two dimensions (when $n = 2$) and it can be simplified to the Pythagorean Theorem ($c^2 = a^2 + b^2 + c^2$):

$$D^2 = (d_i - e_i)^2 + (d_j - e_j)^2$$

The PCA technique has been shown to highlight low variance dimensions in multi-spectral space in an image, such as fallow blocks, in the latter principal components of the transformation (Ceballos and Bottino 1997). Chavez and Kwarteng (1989), confirmed that the largest amount of the total variance was mapped to the first component, with decreasing variance going to each of the following components. This can be seen quite clearly in a graphical representation (Figure 2.10) by visually interpreting the PCA layers of the 10 January 1998 Landsat 5 TM image in this research. Green *et al.* (1998) reported similar findings, in which 95% of the variability of the data was accounted for in the first and second principal components. The sum of the variance in all components is equal to the total variance in the original input imagery. PCA is a powerful tool in change detection (Dwivedi 1996). Findings by Green *et al* (1998) confirmed Mather's (1987) conclusion that the most accurate classification of Landsat TM necessitated the calculation of principal components and band ratios.

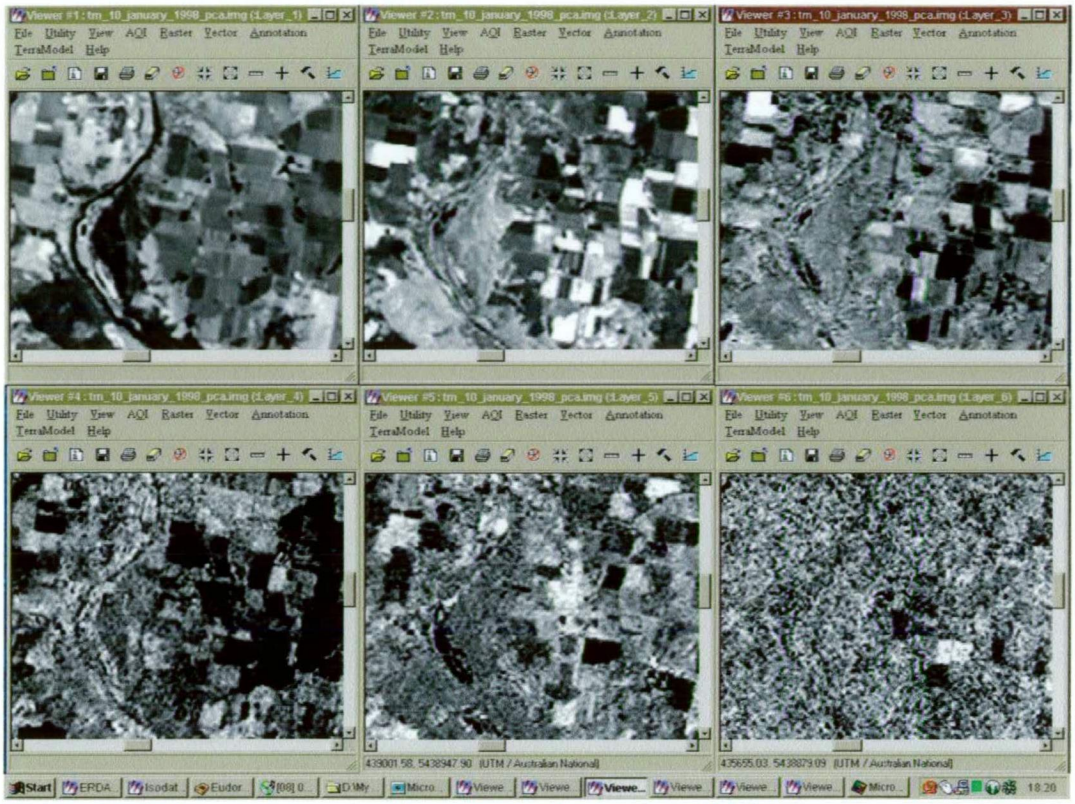

Figure 2.10: PCA layers of 10 January 1998 Landsat TM image

Crist and Cicone (1984a, 1984b) analysed the fundamental spectral dimensionality of six reflective bands in agricultural areas of the United States and suggested, that it essentially occupied three dimensions (Eigenvectors). Torigoe *et al* (1992) summarised the Eigenvectors as follows: *The first feature, "brightness," is the weighted sum of all the bands and defined in the direction of principal variation in soil reflectance. The second feature "greenness," is a contrast between the near infrared bands and the visible bands. Greenness responds to the combination of high absorption in the visible bands and high reflectance in the near infrared that is characteristic of green vegetation. The third feature, which contrasts the sum of the visible and near infrared bands, has been tentatively named "wetness."*

To perform a PCA, the axes of the spectral space are rotated, changing the coordinates of each pixel in spectral space, as well as the data file values. In ERDAS Imagine (Version 8.4)®, a linear transformation is performed on the data. The result of the transformation is that the axes in *n* dimensional spectral space are shifted and rotated. To perform the linear transformation, the Eigenvectors and

Eigenvalues of the n principal components must be mathematically derived from the covariance matrix, as show in the following equation after Faust (1989):

$$V = \begin{bmatrix} v_1 & 0 & 0 & .... & 0 \\ 0 & v_2 & 0 & .... & 0 \\ & & .... & & \\ 0 & 0 & 0 & .... & v_n \end{bmatrix}$$

$$ECov\ E^T = V$$

where:

Cov = the covariance matrix
E = the matrix of eigenvectors
^{T} = the transposition function
V = a diagonal matrix of eigenvalues, in which all nondiagonal elements are zeros

V is computed so that its nonzero elements are ordered from greatest to least so that:

$$V_1 > V_2 > V_3 ..... V_n$$

The matrix V is the covariance matrix of the output principal component file. The zeros represent the covariance between bands (i.e. there is none), and the eigenvalues are the variance values for each band. As the Eigenvalues are ordered from V_1 to V_n, the first Eigenvalue is the largest and represents the most variance in the data.

Each column of the resulting Eigenvector matrix, E, describes a unit-length vector in spectral space, which shows the direction of the principal components. The column of the resulting Eigenvector matrix, E, are used as coefficients in the following equation (modified by Pouncey *et al.* (1999) from Gonzalez and Wintz (1977), to transform the original data file values into the principal component values:

$$P_e = \sum_{k=1}^{n} d_k E_{ke}$$

where:

e = the number of the principal components (first, second)
P_e = the output principal component value for principal component band e
k = a particular input band
n = the total number of bands
d_k = an input data file value in band k
E = the eigenvector matrix, such that E_{ke} = the element of the matrix at row k, column e.

Williams (1983) and Chavez *et al.* (1984) reported that information not mapped to the first three components of the six Landsat TM bands can be of significant interest, depending on the degree of correlation and spectral contrast that exist (e.g. fallow blocks). Williams (1983) also stated, that a colour composite made from three of the six components can be difficult to visually interpret. Abdel-Razik *et al.* (1984) reiterated that use of the PCA worked well with some vegetation data but not with others. Principal components analysis can also show distortion problems (Mazzoleni *et al.* 1991) such as the "arch effect" (when an arch is formed as displacement occurs along an axis which is of little concern so long as the trend displayed can be interpreted in a biologically sensible manner). The "arch effect" is attributed to the large number of zeros in the data matrix (Swan 1970).

Bryun *et al.* (1997) reported some disadvantages of PCA. These included problems of interpreting the meanings of the axes used for plotting the dimensionally reduced data and problems with singular matrices when highly correlated data were introduced.

2.8 Classification

Classification is the process of sorting pixels into a finite number of individual classes. A data class (or spectral class) is a set of pixels, which is statistically similar. Image classification schemes are applied to satellite images to identify the

spectral response pattern of features such as crop types (Lark 1995; Campbell 1996). For each pixel in an image, the spectral brightness values are recorded for the spectral bands. Each pixel may therefore, have a spectral response pattern consisting of many reflectance values from the bands. In a multi-spectral classification scheme the information is extracted and a spectral class is assigned to each pixel based upon similar spectral response pattern in the image (Gong *et al.* 1992).

There are two major approaches to multi-spectral classification, supervised and unsupervised. The basic steps for both supervised and unsupervised classifiaction are similar (Figure 2.11) and the choice of method by the user is largely dependent on the dataset to be analysed.

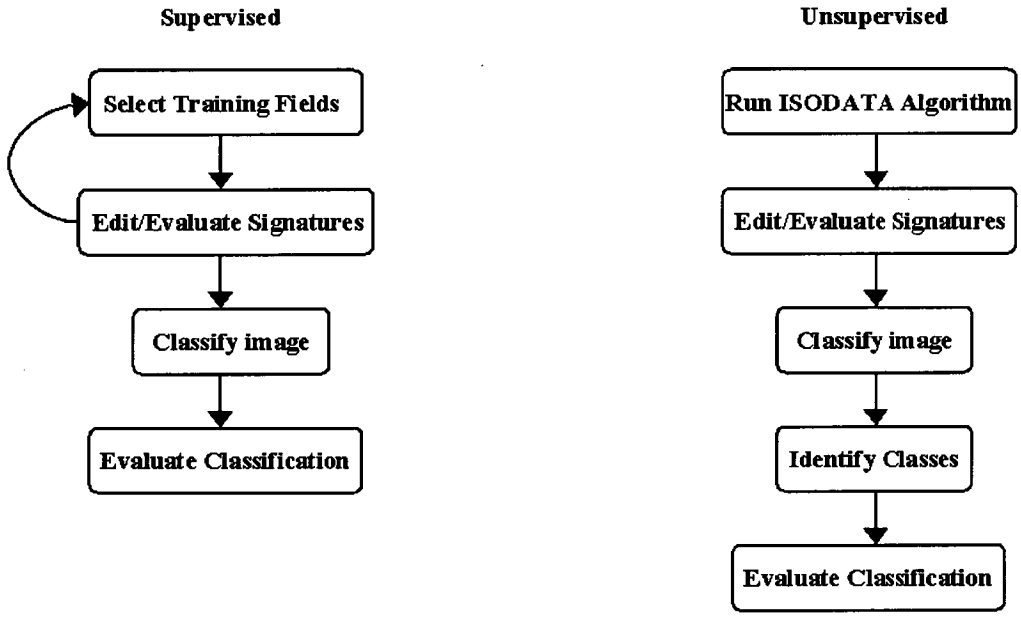

Figure 2.11: Diagrammatic representation of supervised and unsupervised classification methods

The user closely controls a supervised classification, and hence, knowledge of the data, desired classes and the algorithm to be used is required before the training (or calibration) samples are selected. By the identification of patterns in the imagery, the user trains the computer system to identify pixels with similar

characteristics. By setting priorities to these classes, the classification of pixels is supervised as they are assigned to a class value.

Supervised classification is appropriate when relatively few classes are required to be identified, when selected training sites can be verified with ground truth data or when distinct, homogenous regions that represent each class are present in the data.

Unsupervised classification is more automated and allows the user to specify parameters as guidelines for the computer system to determine statistical patterns in the data.

Unsupervised classification is more suited to the determination of classes by spectral distinctions that are inherent in the data, allowing these classes to be defined by the user (Jensen 1996). The unsupervised method of classification enables the user to define many classes easily and to identify classes that are not in contiguous, easily recognised regions.

As with any computerised data analysis method, the quality and suitability of the input data determine the success or failure of a method. Hence, the failure or lack of significant improvement in the results of a classification method, can be attributed to site specific factors, such as, fire (Fiorella and Ripple 1993), flood (Noonan 1999), optimum time of image acquisition for target vegetation (Peştemalci *et al.* 1995), or forest attributes (Skidmore 1989). The apparent failure or lack of significant improvement in the results of a classification method can also be attributed to analysis factors, such as the inclusion or exclusion of relative sun incidence (Fiorella and Ripple 1993), elevation and slope (Franklin 1994), choice of image processing method prior to classification (Green *et al.* 1998), adequacy of training data (Jupp and Mayo 1982; Shine and Wakefield 1999), and spatial or spectral resolution of the sensor (Vickery 1983).

2.8.1 Classification Training

Prior to classification commencing, the computer system must be trained to recognise patterns within the data. Hord (1982) defined training as the process of defining the criteria by which the patterns are recognised. Training can be performed with either a supervised or unsupervised method.

Supervised training requires the selection of pixels that represent the required land cover, by using other sources such as ground truth data. Once patterns have been identified, the computer can be instructed to identify pixels with similar characteristics. Accuracy of the classification at this point depends largely on the data originally identified (Pouncey *et al.* 1999).

Unsupervised training is reliant on the computer system uncovering statistical patterns inherent within the data, based on user defined parameters. The subsequent statistical patterns are at this point not meaningful, but rather clusters of pixels with similar spectral characteristics. The user must then assign meaning to the resulting classes (Jensen 1996).

5.8.2 Classification Signatures

The result of training data is a set of signatures, which define the training sample or cluster. Each signature corresponds to a class and is used with a decision rule to assign the pixels in an image file to a class. ERDAS Imagine (Version 8.4)® enables signatures to be parametric or non-parametric.

2.8.2.1 Parametric Signature

A parametric signature is based on the mean and covariance matrix statistical parameters of the pixels, which are in the training sample or cluster. Both supervised and unsupervised training can generate parametric signatures. A set of parametric signatures can be used to train a statistically based classifier (i.e. maximum-likelihood) to define the classes. It is important to note that a parametric signature requires normal distribution of the data (Kloer 1994).

2.8.2.2 Non-parametric Signature

Feature space, defined by Pouncey *et al.* (1999) is an abstract space, which is defined by spectral units, such as an amount of EMR. A non-parametric signature is based on discrete objects (polygons) in a feature space image. The feature space objects are used to define the boundaries for the class. Supervised training only, is used to generate non-parametric signatures.

2.8.3 Iterative Self Organising Data Analysis Technique

The iterative self-organising data analysis (ISODATA) clustering algorithm was first reported by Tou and Gonzalez (1974). ISODATA is iterative, in that it repeatedly performs an entire classification and recalculates the statistics. Self-organising refers to the way in which it locates clusters, with minimum user input.

The ISODATA method uses minimum spectral distance to assign a cluster for each pixel. The process begins with a specified number of cluster means and then iterative processing of the image data, assigns each of the pixels to one of the class means. After each iteration, the initial cluster means shift to represent the new statistical means of the clusters in the data.

2.8.4 Classification Decision Rule

Subsequent to the signatures being defined, the image pixels must be sorted into classes based on the signatures. This is achieved by using a classification decision rule. This is a mathematical algorithm that sorts the pixels into distinct class values using the data contained within the signatures.

2.8.4.1 Parametric Decision Rule

The parametric signatures train a parametric decision rule. These signatures are defined by the mean vector and covariance matrix for the data file values of the pixels in the signatures. When a parametric decision rule is used, every pixel is assigned to a class since the parametric decision space (the abstract space which is defined by spectral units) continuous (Kloer 1994).

2.8.4.2 Non-parametric Decision Rule

A non-parametric decision rule is not based on statistics and hence is independent of the properties of the data. A non-parametric decision rule determines whether or not the pixel is located inside a non-parametric boundary.

2.8.4.3 Maximum-Likelihood Classifier

The foundation of the maximum likelihood classifier (decision rule) is the Bayes' Theorem, which expresses the relationship of evidence, *a priori* knowledge and the likelihood that a specific hypothesis is true (Eastman, 1993). The maximum likelihood decision rule is based on the probability that a pixel belongs to a particular class. The basic equation assumes that these probabilities are equal for all classes, and that the input bands have normal distributions. Should the user have *a priori* knowledge that the probabilities are not equal for all classes, weight factors can be specified. This variation of the maximum likelihood is the Bayesian decision rule (Hord 1982).

The maximum likelihood decision rule is the most accurate of the classifiers in the in ERDAS Imagine (Version 8.4)® (Pouncey *et al* 1999) as it takes the variability of classes into account by using the covariance matrix. The equation for the maximum likelihood/Bayesian classifier in ERDAS Imagine (Version 8.4)® is as follows:

$$D = \ln(a_c) - [0.5\ln(|Cov_c|)] - [0.5(X - M_c)T(Cov_c - 1)(X - M_c)]$$

where:

D = weighted distance (likelihood)
c = a particular class
X = the measurement vector of the candidate pixel
M_c = the mean vector of the sample class c
a_c = percent probability that any candidate pixel is a member of class c (defaults to 1.0, or is entered from *a priori* knowledge)
Cov_c -= the covariance matrix of the pixels in the sample of class c
$|Cov_c|$ = determinant of Cov_c (matrix algebra)
$Cov_c - 1$ = inverse of Cov_c (matrix algebra)
ln = natural logarithmic function
T = transposition function (matrix algebra)

The pixel is assigned to the class c, for which D is the lowest.

There are also some disadvantages. Maximum likelihood is parametric and, hence, relies on a normal distribution of the data in each input band. Another disadvantage is that it tends to over-classify signatures with relatively large values in the covariance matrix (Pouncey *et al* 1999).

2.9 Methods of Determining Accuracy of Classification Methods

Three methods commonly used in remote sensing to determine accuracy of classification methods are one-way analyses of variance (Koppi *et al.* 1994), correlation matrices (Story and Congalton 1986) and the KHAT (estimation of KAPPA) statistic (Congalton 1991).

2.9.1 One-way Analysis of Variance

A simple method to determine the accuracy of a classification method, is to consider how well the class predicts a nominated crop type, which depends upon how well the classification partitions the variance within and between classes. A highly accurate classification would have little within class variation and consequently all variation would be between classes. This class variation can be measured by the one-way analysis of variance (Koppi *et al.* 1994).

Two measures, which are useful in the interpretation of the results of the one-way analysis of variance, are the percentage variance and probability of the F-distribution. The smaller the values the higher the accuracy of classification.

Many variables and few observations usually cause unreliable estimates (Cruz-Castillo *et al.,* 1994; Laurence 2001). As the percentage variance is dependent on sample size, and the probability of the F-distribution takes into account the sample size, the probability of the F-distribution is frequently the reporting value.

2.9.2 Correlation Matrix

Perhaps the most common method of accuracy of classification determination is the correlation matrix described by (Story and Congalton 1986).

The matrix is an array of numbers set out in rows and columns to express the number of areas of interest assigned to a particular class, relative to the actual class, as identified on the ground via ground-truthing.

The simplest statistic is the overall accuracy, which is calculated by dividing the total of correct areas of interest (the sum of the major diagonal), by the total number of areas of interest.

The "producer's accuracy" (error of exclusion or omission) indicates the probability of an area of interest being correctly classified. This accuracy is calculated by dividing the total number of correct areas of interest in a class by the total number of areas of interest of that class derived from the reference data (column total). This calculation informs the producer of the classification method as to how well, a certain area of interest has been classified.

The "user's accuracy" (error of inclusion or commission) indicates the probability that an area of interest classified on the image actually represents that class on the ground. This accuracy is calculated by dividing the total number of correct AOIs in a class by the total number of AOIs, which were classified in that class.

While both the "user" and "producer" accuracy measures are important, in measuring success of analyses, the ultimate aim of a selected methodology is for the user's accuracy for a singular class and, indeed, all classes to be as close to 100% as possible.

2.9.3 KHAT Statistic (Estimation of KAPPA)

Congalton *et al.* (1983) proposed the use in remote sensing accuracy assessment of a discrete multivariate technique known as the KAPPA analysis, which produces a KHAT statistic (Cohen 1960).

The KHAT statistic expresses the proportional reduction in error, generated by a classification process compared with the error of a completely random classification. For example, a value of 0.82 implies that the classification process is avoiding 82 percent of the error that a completely random classification generates (Congalton 1991). Another way to express this, is that KAPPA, is highest in the classes that can be considered the most homogeneous (Perakis *et al.* 1998). Congalton (1991) redefined the KHAT equation as:

$$\hat{K} = \frac{N \sum_{i=1}^{r} x_{ij} - \sum_{i-1}^{r} (x_{i+} * x_{+j})}{N^2 - \sum_{i=1}^{r} (x_{i+} * x_{+j})}$$

where:

r = number of rows in matrix
x_{ij} = number of observations in row i and column j
x_{i+} and x_{+j} = marginal totals of row i and column j
N = total number of observations

The redefinition was required to clear up confusion caused by a typographical error in Congalton *et al.* (1983).

Shine and Wakefield (1999) summarised the definition of the KAPPA coefficient as a measure of association between two categorical variables. In other words it is used to measure the agreement between the classification approach and the actual result. A value of zero indicates no agreement between the classification approach and the actual result, except that, expected by chance. A value of one indicates perfect agreement with all the values falling on the diagonals (Agresti 1990).

CHAPTER 3

A BRIEF HISTORICAL REVIEW OF REMOTE SENSING IN AUSTRALIAN AGRICULTURE

Most remote sensing in Australian Agriculture has been carried out with the Landsat TM and SPOT sensors. The value of Landsat TM and SPOT data in relation to agricultural applications lies in the spatial resolution at which it is acquired (30m pixels for Landsat and 20m pixels for SPOT). This resolution is useful for detecting spatial variation in crop spectral response patterns within paddock and farm scales, which are common in Australian agriculture (Button 2001).

3.1 Grassland Agriculture

Vickery *et al.* (1980) identified that the use of remote sensing (in particular Landsat imagery), could discriminate between pasture targets with and without applied superphosphate. This finding further suggested that Landsat might have value in estimating the fertiliser requirements of improved pasture.

Vickery (1983) confirmed these findings, identifying that the use of Landsat imagery had the potential to provide a cost-effective method of monitoring the fertility status of pastures, as a function of pasture growth rate, with an aim of developing a fertiliser precision management strategy, to increase gains in agricultural productivity. Vickery (1983) also identified the requirement, for the then next generation of satellites to increase spatial and spectral resolution.

Hedges *et al.* (1987) further developed the use of remote sensing, to classify and map more complex vegetation types than the relatively homogenous surfaces of

forestry and crops. This was achieved by the development of a principal component strategy for the unsupervised classification process of Landsat data.

When comparisons of aircraft and satellite imagery were undertaken to measure the response of pasture to superphosphate (Reid *et al.* 1993), differences in classifications based on data acquired by both satellite and aircraft reflected the contrasting boundaries between areas treated and untreated with superphosphate. This confirmed Vickery's (1983) findings that Landsat type radiance data strongly reflect the fertiliser status but extended this further to pastures over differing types and environments.

The use of remote sensing in grazing systems has not been limited to nutrient status and classification of pasture types but has also been used in animal production. The production of wool and its relationship to maximum normalised difference vegetation index (NDVI) on pastoral and agricultural zones of Western Australia, was studied by Smith (1994), where it was found that wool production could indeed be related maximum NDVI.

3.2 Broadacre Agriculture

Satellite remote sensing has been used widely as a means of estimating crop production areas (Kuhnell and Danaher 1996) and physiological status in many facets of Australian agriculture. Spectral response detected within the area of any pixel, represents the integration of all factors such as crop phenology, soil water status, and nutrient status, which in turn determine plant vigour, biomass and ultimately yield potential (Button 2001). However, detailed algorithms linking remotely sensed data to actual biophysical parameters work mainly in the context of single or localised areas, and the applicability of these relationships remains largely unverified across entire regions (Lamb 2000).

3.2.1 Cotton (*Gossypium hirsutum* L.)

The development of remote sensing techniques is continually expanding in Australian agriculture. Allen and Lonergan (1999) successfully demonstrated the use of thermal imagery to detect Fusarium wilt, caused by (*Fusarium oxysporum*) of cotton (*Gossypium hirsutum* L.) near Boggabilla and Moree in New South Wales.

3.2.2 Sugar Cane (*Saccharum officinarum* L.)

Prior to the work of Noonan (1999), the application of remote sensing in the sugar cane industry in Australia had been limited to studies in which Lee-Lovick and Kirchner (1990, 1991) concluded, that the use of remote sensing with Landsat Thematic Mapper was, "*inappropriate technology for the Australian sugar industry.*" In the 1990 study by Lee-Lovick and Kirchner, the spectral response patterns for mature cane were clearly distinguishable from fallow blocks. However, one of the problems faced in this study was distinguishing low productivity sugar cane, which had been damaged by flood, from rich grassy fallow blocks. Areas which suffered major damage after the flood were very difficult to separate from fallow blocks and they were therefore included in the estimate.

Conversely, Noonan's (1999) preliminary study showed that Landsat TM data was potentially useful for the detection of fallow blocks, and for the classification of flood damaged sugar cane in the Lower Herbert and Stone River catchments of Queensland.

3.2.3 (*Triticum aestivum* L.)

In 1998, a service known as AgImage (Smith *et al.* 1998) was developed, based on correlations between NDVI measurements derived from Landsat TM and SPOT XS imagery and yields on a paddock by paddock basis. The development of AgImage evolved from earlier findings by Smith *et al.* (1995), which determined relationships between NDVI data derived from NOAA satellite imagery and wheat yield. Stovold *et al.* (1996) later determined relationships

between NDVI data derived from resolution systems (e.g. Landsat and SPOT) and wheat yield.

Field spectral radiometers were investigated by Bellairs *et al.* (1996) as another means of estimating the biomass of wheat at early growth stages. It was found however that the technique, in order to be optimised, should be applied to a weed free site, with a uniform dark soil background and on material that is relatively homogenous in structure. It was concluded that unless such precautions were taken, field spectral radiometers were limited.

Corner *et al.* (1998) indicated that the use of high-resolution NDVI measurements was best suited to a diagnostic tool, rather than to a yield predictor. This summation was inferred from the finding that, whilst reasonable relationships at a regional scale between NDVI and grain yield could be derived, at a sub-paddock scale, the relationship could no longer be sustained, due not only to spatial and temporal averaging, but also to crop production factors.

Aigner *et al.* (2001) also concluded, that NDVI, growing season rainfall, grainfilling stage and water stress degree days from National Oceanic and Atmospheric Administration - Advanced Very High Resolution Radiometer (NOAA – AVHRR) data, correlated with the grain yield of wheat. These findings were based on large data subsets (area under crop) where homogeneity in the crop environment was present. As this is rarely the case with crops, reliable predictions are not possible unless the remote sensing data can be derived from smaller subsets.

3.2.4 Rice (*Oryza sativa*)

Heermann *et al.* (1998) showed that remote sensing was an effective tool in gaining knowledge of within paddock variability in Australian irrigated rice and thereby allowed more effective management to improve productivity. Development of decision making models such as MaNage Rice™ from remotely

sensed data have allowed the prediction of crop growth, biomass and potential yield, based on fertiliser application and weather conditions. The model has averaged these parameters across entire fields, in order to reduce heterogeneity of crops. Spackman *et al.* (2000) further refined the MaNage Rice ™ model by generating calibrated surface reflectance data within the growing season. The correlation between NDVI and biomass at mid-tillering enabled the MaNage Rice™ model to be adjusted to actual conditions within the field, hence providing more detailed and precise field management.

CHAPTER 4

A REVIEW OF THE AGRONOMY AND PHYSIOLOGY OF POPPY (*PAPAVER SOMNIFERUM*) AND PYRETHRUM (*TANACETUM CINERARIIFOLIUM*)

In this chapter, Section 4.1 provides a brief historical background to the development of the poppy industry in Tasmania, a description of the poppy plant and the agronomy, physiology and utilisation of the crop.

Section 4.2 provides a brief historical background to the development of the pyrethrum industry in Tasmania, a description of pyrethrum and the agronomy, physiology and utilisation of the crop.

4.1 Introduction to the Poppy Industry in Tasmania

The poppy industry is a major financial contributor to Tasmania's economy. The area sown to poppies (*Papaver somniferum*) in Tasmania exceeds 20 000 hectares (Anon 2000). With an annual average crop yield of around 2.5 tonnes per hectare, Tasmania supplies about half of the world's production of concentrated poppy straw (CPS) from about ten per cent of the area grown (Anon 2000; Fist 2001).

As well as cultivation and initial processing, some of the extraction of medicinal compounds is undertaken in Tasmania, but some manufacturing is also undertaken in Victoria. Two pharmaceutical companies, GlaxoSmithKline Australia and Tasmanian Alkaloids Pty Ltd contract land from farmers and undertake processing.

4.1.1 Brief History of the Poppy Industry in Tasmania

The Tasmanian Department of Agriculture in 1960 - 1961 undertook an experimental program of poppy production (Laughlin *et al.* 1998) at Don, Scottsdale and Cressy (Anon 1994). The trials were conducted on behalf of the English pharmaceutical company, McFarlane Smith Ltd, Edinburgh, a subsidiary of Glaxo, currently known as GlaxoSmithKline Australia. A decision was made in 1964 - 1965 to concentrate all future poppy crop development in Tasmania and control of Tasmanian poppy crop production was transferred from Edinburgh to Glaxo Australia Pty. Ltd.

Advances in 1969 saw the identification of a reliable and productive cultivar suited to Tasmanian conditions, effective selective weed control and the development of a modified forage harvester. These provided the breakthroughs needed to allow expansion of the industry. The first season of commercial production began in 1970. In 1972, a joint decision by Commonwealth and State Governments restricted the growing of *Papaver somniferum* to Tasmania. This restriction lead to regulation through the Poppy Advisory and Control Board, and expansion with the construction of a factory at Latrobe in Tasmania for the receival, storage and processing of the crop.

Tasmanian Alkaloids Pty Ltd was established at Westbury Tasmania in 1975 and is a fully integrated manufacturer of medicinal opiate products.

4.1.2 Nomenclature and Description

The specific name *Papaver sominferum* is derived from the Latin *somnus,* meaning "sleep" and *ferro*, meaning "bring" or "carry." Hence, "bringing sleep" alludes to the narcotic properties of the dried latex, (Parsons and Cuthbertson, 1992).

King (1994) states the family is particularly distinct with its flowers of four petals and two green sepals surrounding numerous stamens (Figure 4.1).

Figure 4.1: *Papaver somniferum* flower showing the distinct four petals and numerous stamens

Köhler (1887), Hyde-Wyatt (1989) and Parsons and Cuthbertson (1992) describe *Papaver somniferum* as an erect annual herb approximately one metre in height (Figure 4.2). The seedling has a hypocotyl but no epicotyl and stems are robust, solid, pithy and fluted in cross section with scattered stiff hairs. Leaves are alternate, obovate-lanceolate, tapering to a stalk-like base, forming a dense rosette. Leaf margins are unevenly but sharply toothed.

Flowers (four large overlapping petals) are white, pale violet to mauve with darker blotches at the base and are borne singly on long, erect stiffly bristled stalks. Two sepals cup and shed as the flower opens. The capsule (fruit) is a dull bluish-green, sub-globular in shape and has seven to nine persistent ridges at the apex, forming a flat plate-like cap (Figure 4.2). It produces numerous minute, dark brown seeds that are naturally spread by dehiscence (Köhler 1887; Hyde-Wyatt 1989; Parsons and Cuthbertson 1992).

4.1.3 Agronomy of Papaver somniferum

Poppy growing is carried out in a cool, temperate climate (Laughlin *et al.* 1998), on well drained, fertile soils with a pH_w (1:5, soil:water) of at least 5.7 as poppies do not grow well on acid soils (Temple-Smith *et al.* 1982).

Figure 4.2: *Papaver somniferum*, an erect annual herb with a dull bluish-green capsule with a flat plate-like cap

The necessary climatic and soil factors, in conjunction with the requirement for terrain which is amenable to cultivation, harvesting, low frost incidence, and ease of logistics for transport of harvested crops, has lead to the poppy industry being located in the North West Coastal region, North East region and in the Midlands region of the State (Figure 4.3).

Poppies are grown in mixed farming enterprises, which include pasture, green peas (*Pisum sativum*), potatoes (*Solanum tuberosum*), onions (*Allium cepa*), brassicas (*Brassica spp.*) and pyrethrum (*Tanacetum cinerariifolium*). The area sown to poppies is currently equal to that sown to potatoes, peas, green beans, onions, brassicas and pyrethrum combined (Fist 2001). It is preferable to grow poppies early in the crop rotation (soils which have not been heavily cropped and after a pasture or legume crop).

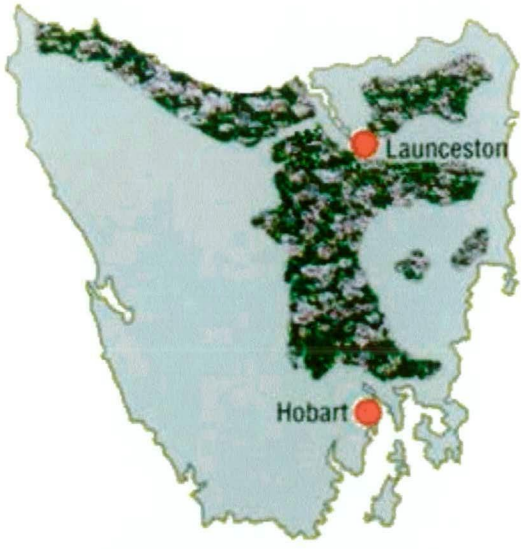

Figure 4.3: Distribution of poppy growing areas in Tasmania

Well drained, fertile soils are essential for the successful production of poppies, with approximately 70% of poppy crops grown on red basaltic krasnozem soils of Tasmania (Laughlin *et al.* 1998).

Early spring (August, September) is the ideal sowing time with flowering occurring in December and a dry mature harvest (12% moisture in capsules) occurring in February/March.

Poppies require a well prepared seedbed, not too firm and with the surface free from turf, straw, weeds and other vegetable matter. Adoption of raised beds in soil preparation has been critical in increasing Tasmania's poppy crop area to the current levels (Fist 2001), through expansion of production on poorly drained sands over clays in the Tasmanian midlands.

Seed is drilled at a rate of 0.75 – 1.0 kg of seed/ha with an objective of achieving a plant density of 50 – 70 plants per square metre. Lower densities may result in reduced yields whereas crop of higher densities, are susceptible to lodging and fungal diseases.

Weed control is important in achieving high poppy crop yields and successful herbicide strategies have been important in industry expansion. Herbicides are generally applied at the four to six leaf stage, when the crop is growing vigorously. Moisture stress at the time of application often results in unacceptable damage to the poppy and inadequate control of the weed species.

Insect pests of poppies are sporadic, but locally damaging if not treated. Infestations of red-legged earth mites, springtails (*Collembola* spp.) and slugs occur. The European skylark (*Alauda arvensis*) can cause damage to autumn sown crops in some areas (Walker *et al.* 1977). Native bud worm (*Heliothis punctigera*) is an occasional pest of the Tasmanian poppy crop, with damage usually occurring from the green capsule stage to the time of dry commercial harvesting. Insecticides to control *Heliothis punctigera* are occasionally required.

Downy mildew (*Peronospora arborescens*) was not recorded in the Tasmanian poppy crop until 1996 and since its' initial reporting the disease has become prevalent and a major limiting factor in production (Scott *et al.* 2001). Whilst current methods of control (fungicide application strategies) are effective, only one fungicide is available and resistance is expected to reduce the effectiveness of current control measures (Scott 2001). Poppy fire (*Pleospora papaveraceae*) causes yield reduction under conditions of high temperature and humidity, but seed and crop hygiene and adequate rotation limit losses. Sclerotinia wilt (*Sclerotinia sclerotiorum*) makes the plants more susceptible to lodging by wind and reduces yield (Laughlin *et al.* 1998). Poppy leaf smut (*Entyloma fuscum*) also sporadically requires fungicidal control (Laughlin *et al.* 1998).

It is important that during the summer months in Tasmania, water is applied and a range of overhead systems are used in response to monitored soil moisture levels.

Poppies are harvested when the crop is dry (12% moisture content) and the alkaloids in the latex have formed a dried deposit on the walls of the capsules.

Harvesting is carried out with specialised machinery, which removes the poppy head and a small portion of the stem. Sieving then separates capsules and seed.

4.1.4 Utilisation of *Papaver somniferum* Alkaloids

All members of the *Papaveraceae* family contain a milky sap or latex in which alkaloids may occur. The constituent alkaloids of the latex vary widely between species. *Papaver somniferum* contains many different alkaloids, with morphine usually being the predominant type.

The alkaloids are extracted from dried poppy capsules and stalk, using ethanol and water. This technique was developed by the Hungarian, Janos Kabay, in 1931, (Kabay 1990; Anon 2001). The morphine is then extracted using a precipitation process.

4.1.5 Characteristic Phases of Development of *Papaver somniferum*

The length of the vegetative period of poppies varies from 120 – 160 days, depending on the cultivar characteristics, climatic conditions and sowing time (Bernath and Nemeth 1998).

Despite the variation in the length of the vegetative period of poppies, six developmental stages in the course of poppy development have been observed (Bernath and Nemeth 1998). The first phase is termed the embryo or dormant stage, where the seed is in the pre-germinating stage. This first phase can be extended as poppy seeds can maintain viability for, four to six years.

The second phase is termed the germination stage, in which the testa (seed coat) ruptures and the first leaves appear. Under optimal conditions, (7°C to 10°C and optimal soil humidity) the germination phase occurs over a period of 15 to 20 days.

The leaf rosette stage, or third phase lasts from the appearance of the first leaves until the emergence of the flower shoot and the formation of generative organs. This is the longest period of development of the poppy and under typical seasonal conditions lasts for 50 to 60 days. Climatic conditions and agronomic practices such as nutrient supply, season temperatures, time of sowing and soil moisture levels significantly influence the duration of this phase.

Elongation of internodes and branching is referred to as the fourth phase. The fourth phase lasts from the beginning of shooting until blossoming of the main axis and is generally about 21 to 30 days duration in optimal weather conditions of 16°C to 18°C average temperature and moderate rainfall. The uptake of water and nutrients is most intensive during this phase.

The fifth developmental phase (blossoming and the formation of capsules and seeds) last on average 20 to 30 days. The flowers are open for 24 hours and petals begin to shed two days later. A further 10 to 14 days lapse after the shedding of flowers for the capsules and seeds to reach their final shape and size. Growth of the capsules then halts although the capsules are still green.

The sixth and final phase (ripening of the capsules and seeds) lasts for approximately 15 to 25 days depending on climatic conditions. During this phase the leaves senesce, the capsules obtain their characteristic dull bluish-green and the seeds will separate from the septa within the capsule. The poppy is then ready for harvest when the leaves and stems are dry and brittle and the seeds rattle in the capsule.

The graphical representation of the characteristic phases of development for the 1998/99 poppy crops on the North West Coast (Figure 4.4) is a characteristic sigmoid curve. The curve was obtained by simply plotting the poppy growth stage number (developed by Serve-Ag Pty. Ltd., Table 4.1) against days after planting and executing a regression analysis. The growth stage descriptor is merely a

numerical value to describe the characteristic phase of development and growth stage.

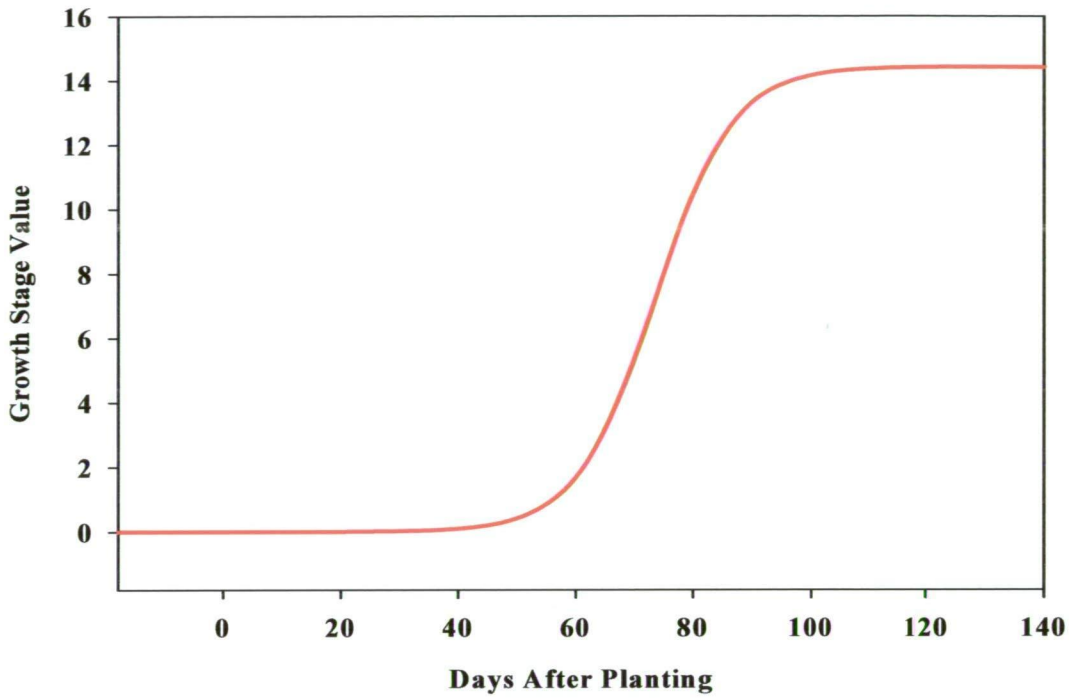

Figure 4.4: Characteristic phases of development for the 1998/99 poppy crop

Table 4.1: Characteristic phases of poppy development, used when the majority of plants in a paddock display the respective stage

Numerical Growth Stage Descriptor	Characteristic Phase of Development	Stage of Growth
0	2	cotyledon
0.2	2	2 leaf
0.4	3	4 leaf
0.6	3	6leaf
0.8	3	8 leaf
1	3	10 leaf (small rosette)
2	3	large rosette
3	3	running up
4	3	late running up
5	4	bud in apex
6	4	early hook
7	4	hook
8	4	upright bud
9	5	first flower
10	5	full flower
11	5	late flower
12	5	petal fall
13	6	green capsule
14	6	striped capsule
15	6	seed free

4.2 Introduction to the Pyrethrum Industry in Tasmania

Jones (1982) reported that as early as 1828, pyrethrum provided a natural insecticide. Pyrethrins have a low mammalian toxicity and rapid breakdown rate and, to date, no insects are known to have immunity to them (Salardini 2001).

Tasmania is an ideal environment for the production of pyrethrum because of the temperate climate, fertile well-drained soils and sufficient rainfall. The Tasmanian pyrethrum industry is a major supplier and multi-million dollar exporter of natural pyrethrum products to the world market.

Tasmanian natural pyrethrum products are exported to the U.S.A., Europe and Asia for use as the key ingredient of control formulations for household, food storage, medical and veterinary pests.

4.2.1 Brief History of the Pyrethrum Industry in Tasmania

Pyrethrum was first grown in Australia in the mid 1880's on the Lower Latrobe River in Victoria and later on during World War II, Prisoners of War in Australia grew pyrethrum, (Casida and Quistad 1995). It was not until the 1960's that the first experimental plots were established in Tasmania using techniques originating from Kenya, which was and currently still is the world's largest producer.

Attempts to grow pyrethrum on a commercial scale in Australia between 1932 and 1982 failed. Bhat and Menary (1984) attributed the failures to the introduction of inferior material, resulting in low flower and pyrethrin yields, disease and a lack of knowledge of the plant itself.

Since 1981, the company Commonwealth Industrial Gasses (CIG), the University of Tasmania, the State Government of Tasmania and GlaxoSmithKline Australia have grown pyrethrum commercially in Tasmania for pyrethrins (Casida and Quistad 1995).

In 1996, a management procurement of CIG Pyrethrum led to the formation of Botanical Resources Australia (BRA). BRA is a Tasmanian owned company, which contracts with local farmers to grow pyrethrum. Pyrethrum is harvested from early summer onwards and the company processes the harvested crop to a pale refined pyrethrum extract.

By 1992, Australia had become the world's second largest producer of pyrethrum, with the first fully mechanised production system. In comparison with the world's major producer, Kenya, the Australian levels of production are comparatively low. However, a fully mechanised and intensively managed production system has developed.

4.2.2 Nomenclature and Description

Pyrethrum (*Tanacetum cinerariifolium*) is a small herbaceous, perennial plant (Figure 4.5) of the Compositae family with many shoots originating from the crown and growing on average to 75cm, with pinnate leaves, which are white and silky-hairy on the underside.

Figure 4.5: Pyrethrum, a small herbaceous perennial plant

Casida and Quistad (1995), describe the flower head of pyrethrum as typical of the Compositae family, a compound inflorescence with small flowers (florets) aggregated together on a convex receptacle, the capitulum (Figure 4.6).

Figure 4.6: Pyrethrum flower head. (A) Whole flower showing white coloured ray florets and yellow coloured disc florets. (B) Flower head – vertical section. (After Casida and Quistad 1995)

Five petals join to form the yellow tubular corolla and five stamens, borne on short stalks, are located inside the tubular corolla. The stigma is two lobed and each lobe is tipped with a minute brush of short hairs.

4.2.3 Agronomy of *Tanacetum cinerariifolium*

Since 1988, the Australian pyrethrum industry has progressed to a commercial industry.

The temperate conditions of Tasmania are ideal for pyrethrum production. Mild winters provide a period of sufficiently low average temperatures to ensure vernalisation (essential for flowering) but rarely low enough to develop damaging frosts. The increasing day length during spring promotes the photoperiodic response in the plant (Brown 1990). Dependable rainfall during spring and early summer greatly reduces the requirement for supplementary irrigation (Casida and Quistad 1995). The coastal stretches of the Northwest coast (Figure 4.7) are particularly suited, not only climatically but also because of the already existing high level of farming and management skills developed for vegetable production.

Pyrethrum is typically grown in mixed farming enterprises, which include pasture, green peas (*Pisum sativum*), potatoes (*Solanum tuberosum*), onions (*Allium cepa*), brassicas (*Brassica spp.*) and poppies (*Papaver somniferum).*

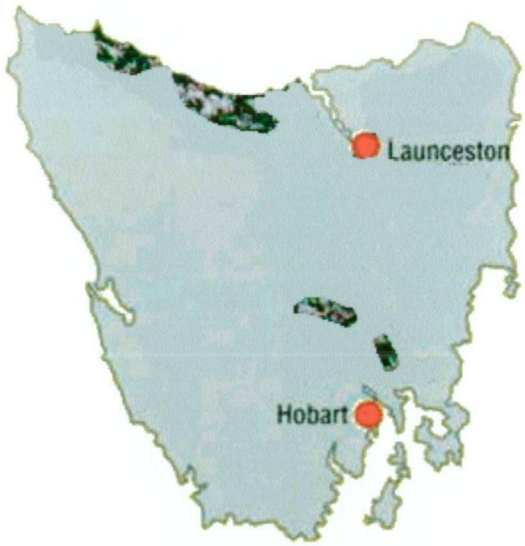

Figure 4.7: Distribution of pyrethrum growing areas in Tasmania

In Tasmania, the two common soils in which pyrethrum is cultivated are high phosphorus fixing ferrosols and non-phosphorus fixing vertisols (Salardini 2001). These soils are also selected for their free draining characteristic. It is critical that the area to be sown down to pyrethrum is free of weeds, is well drained, the pH is suitable (at least 5.7) and the nutrient status is suitable.

Autumn planting is preferred for good establishment. Prior to 1997, material was prepared from split crowns of mature plants and transplanted seedlings. Since 1997, seed has been precision drilled. Depending on each sites' soil analysis, compound fertilisers are banded at planting with subsequent top dressings of nitrogen during spring and further nutrients added during each autumn period over the life of the crop. Pre-planting and post-planting herbicides are applied to reduce weed competition during the winter. Sheep are occasionally used to graze weeds but control of weeds during the growing period is primarily based on the use of chemical herbicides.

Some of pyrethrums' usual economic pests, including thrips, aphids and mites, are not yet significant in Tasmania. However, economic damage due to nematodes is still to be fully determined. Slugs can damage pyrethrum until such times, as the

plant becomes established (Young and Armstrong 2001). Control of slugs is achieved by timely applications of chemical baits.

The fungal pathogens *Sclerotinia sclerotiorum* and *Sclerotinia minor*, causing crown rot, are common in the intensive vegetable production areas of the North West Coast. Selection for "resistant" varieties continues to be the preferred method of control. A bacterial leaf rot caused by *Pseudomonas sp.* has caused damage in commercial crops and has been controlled with copper-based sprays. Pethybridge and Hay (2001) identified *Phoma ligulicola* as the causal agent in the failure of recent first year pyrethrum crops to produce economic yields.

Casida and Quistad (1995) have shown that, significant yield increases can be obtained through careful water management within the soil profile by using neutron probes.

Harvesting is undertaken in January/February when the crop is field dry or the flowers are at the ideal maturity index (flowering maturity index (FMI) 5 to 6, Figure 4.8) to maximise pyrethrin content.

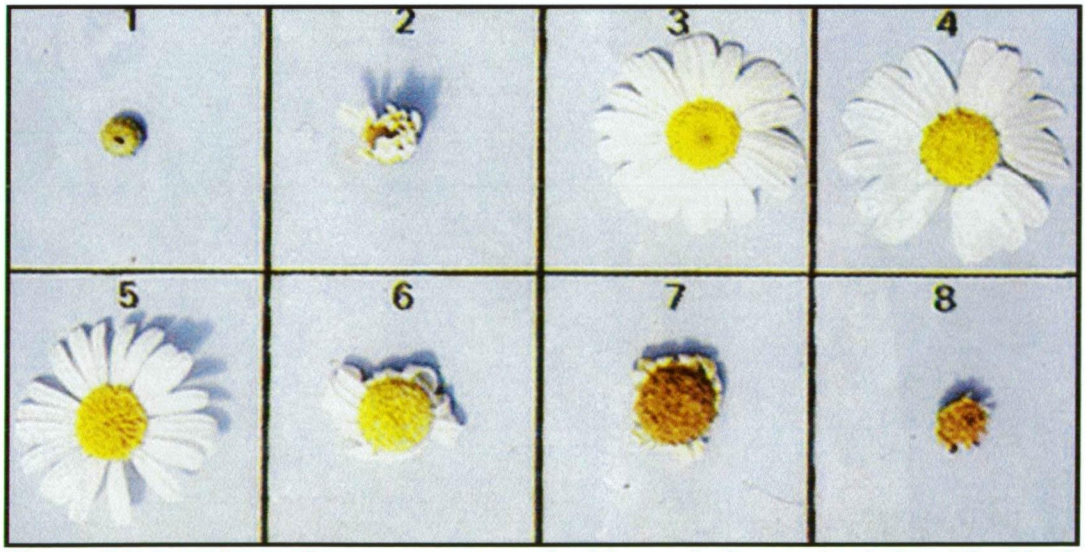

Figure 4.8: Pyrethrum flowers are categorised into a 1–8 maturity index. The ideal harvesting stage to maximise pyrethrin content is index 5 –6

Flowering occurs when the shoots originating from the crown have branched and terminated in tight flower buds, FMI 1. During FMI 2 and FMI 3, the petals of the flower open fully, and FMI 4, FMI 5 and FMI 6 denote stages at which the petals begin to senesce. FMI 7 and FMI 8 are the stages at which the achenes mature.

All aerial parts of the pyrethrum plant contain pyrethrin but the main concentration is in the seeds (achenes) produced by the central yellow disc florets of the flower. Crops are cut, windrowed and dried in the field before being threshed. The dried achenes are separated from the straw during the threshing process. Given the natural instability of pyrethrins once harvested, the crop must be processed rapidly (Casida and Quistad 1995). Processing involves crop cleaning, pelletising, storage and extraction of the pyrethrins into a crude oleoresin containing 25% active ingredient. Oleoresin is then refined via a supercritical carbon dioxide process. The yield of pyrethrin is a function of flower head (capitulum) yield, which is correlated, with high above ground dry matter production (Casida and Quistad 1995; Fulton *et al.* 2001).

4.2.5 Characteristic Phases of Development of *Tanacetum cinerariifolium*

Characteristic pyrethrum growth is graphically represented in Figure 4.9.

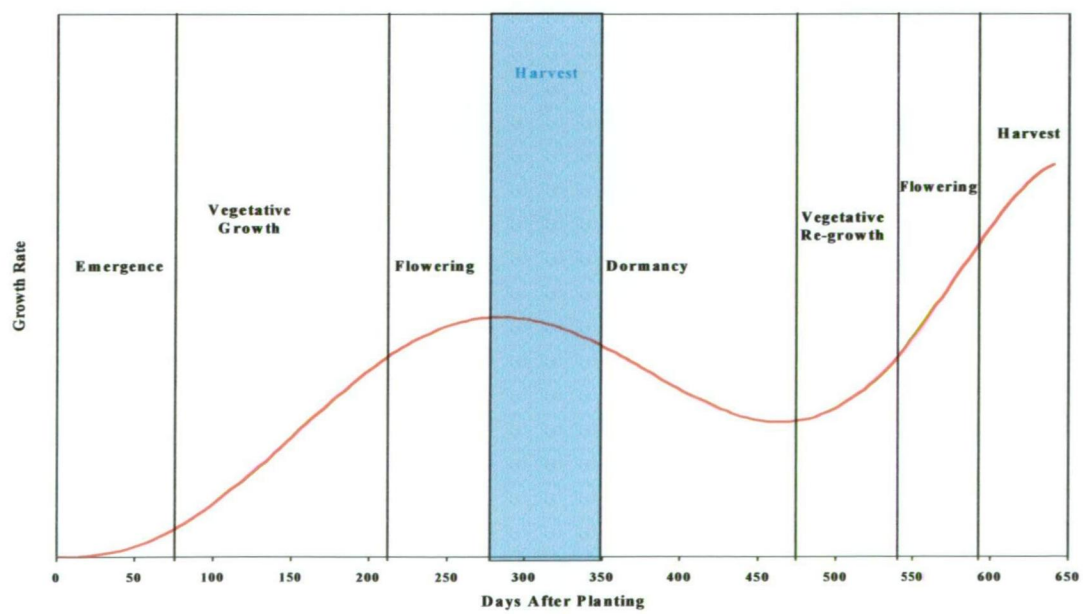

Figure 4.9: Characteristic growth of pyrethrum over a two year phase

Four stages of development are observed: emergence, vegetative growth, flowering and dormancy.

Harvesting promotes further branching of the plant and vegetative re-growth in the following spring generates more branches, more flower heads per plant and increased pyrethrin yield in the second year of the crop.

CHAPTER 5

REGIONAL SETTINGS

Tasmania Australia, is a source of many, high value, commercial crops, including poppies for the pharmaceutical industry and pyrethrum for the production of natural insecticides. Horticultural crops are grown in areas from about two up to 20 hectares.

5.1 Geographic Location

The North West Coast study area of Tasmania lays between 41° 07' 13''S and 41° 18' 45''S and from 146° 04' 07''E to 146° 33' 58' E, (Figure 5.1).

Figure 5.1: Location of the North West Coast study area

5.2 Climatic Environment

Under the Köppen classification scheme, where climatic zones are based on temperature and rainfall, as indicated by the native vegetation, (Stern *et al.* 2001), Tasmania falls into the temperate zone (Figure 5.2). The temperate zone is generally characterised by mild to warm summers and cold winters.

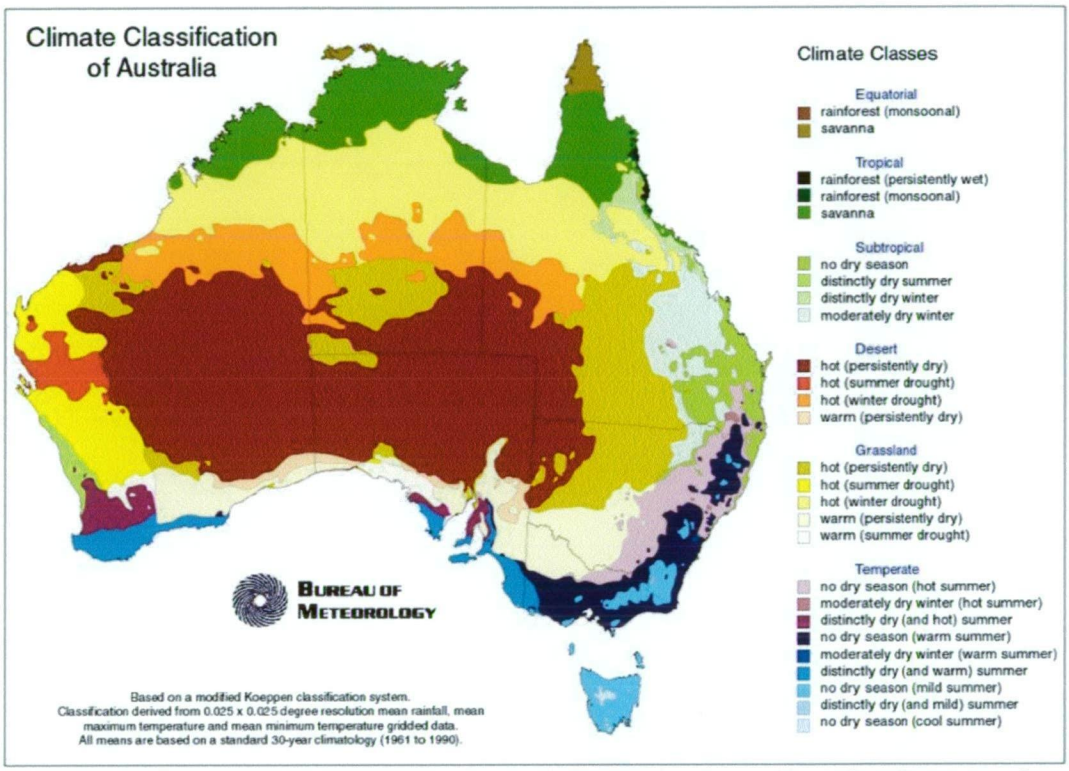

Figure 5.2: Tasmania in a classification of climate in Australia (after Stern *et al.* 2001)

Average annual rainfall in the study area ranges from 600 – 1200mm (Figure 5.3), of which approximately two thirds occurs in winter. The monthly average minimum temperature of 3 – 12 °C and monthly average maximum temperature of 12 – 21 °C (Figure 5.4), in conjunction with approximately four hours of direct sunlight in winter and seven in summer (Figure 5.5), typify the climate in this cool/temperate zone.

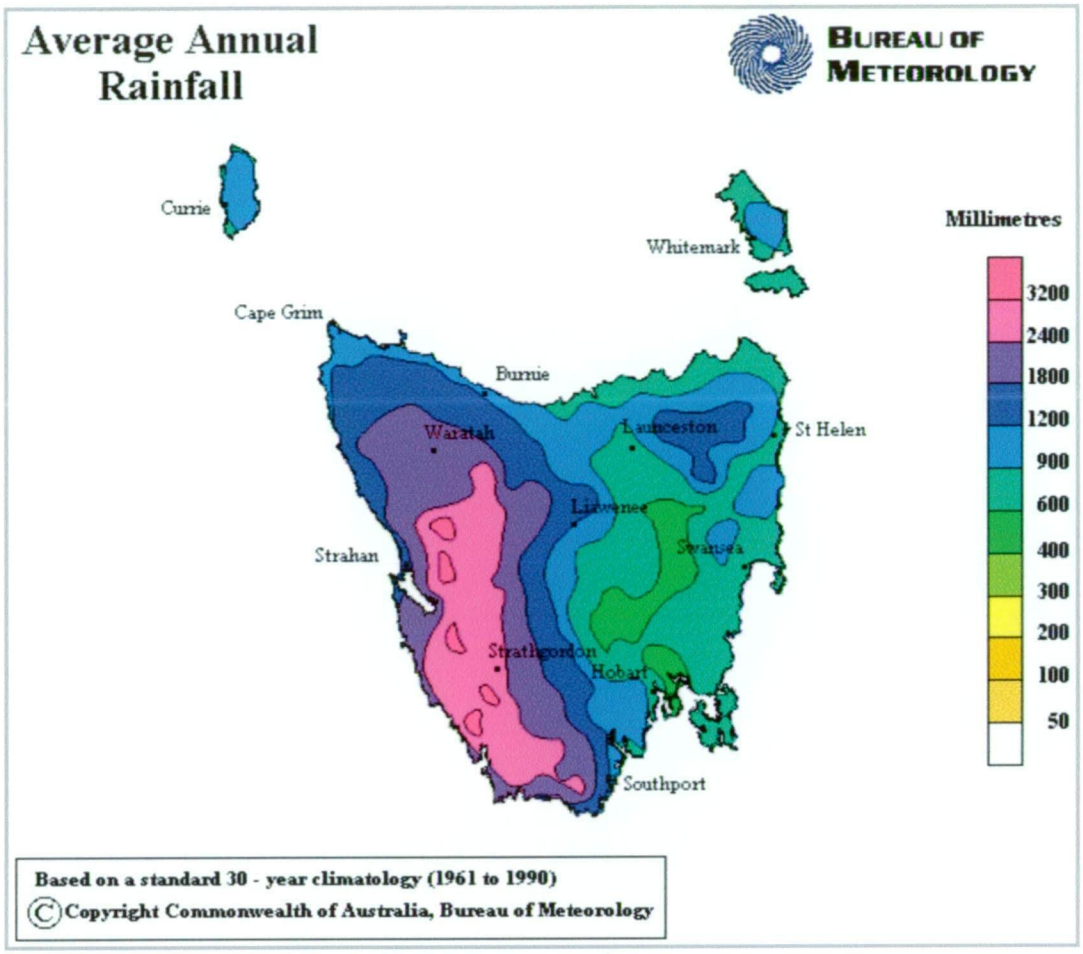

Figure 5.3: Average annual rainfall in Tasmania

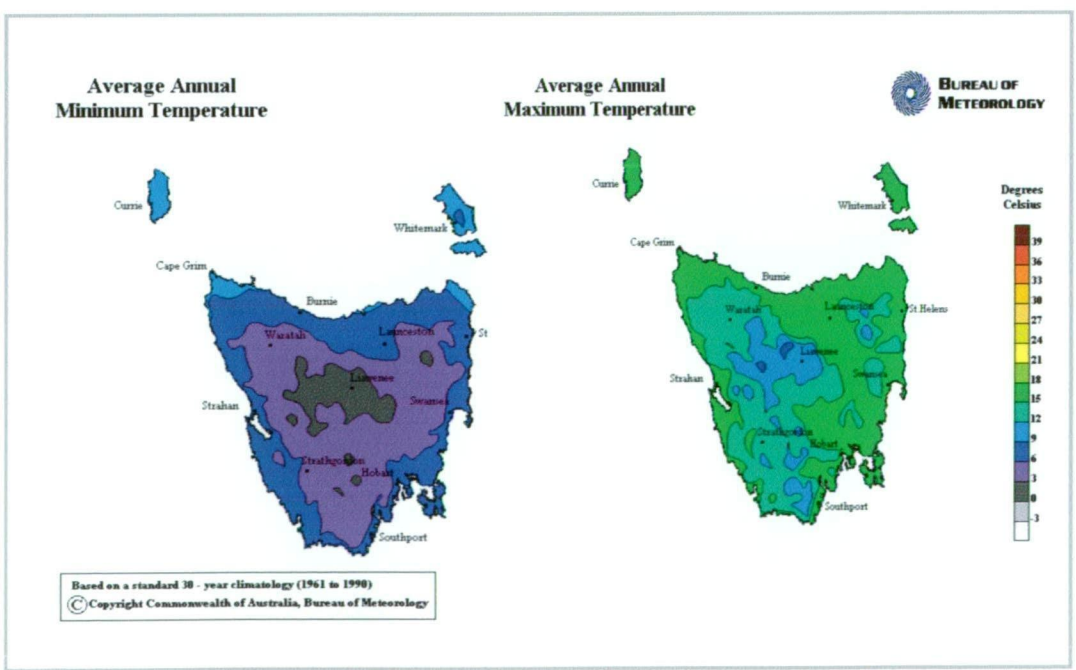

Figure 5.4: Average annual minimum and maximum temperatures in Tasmania

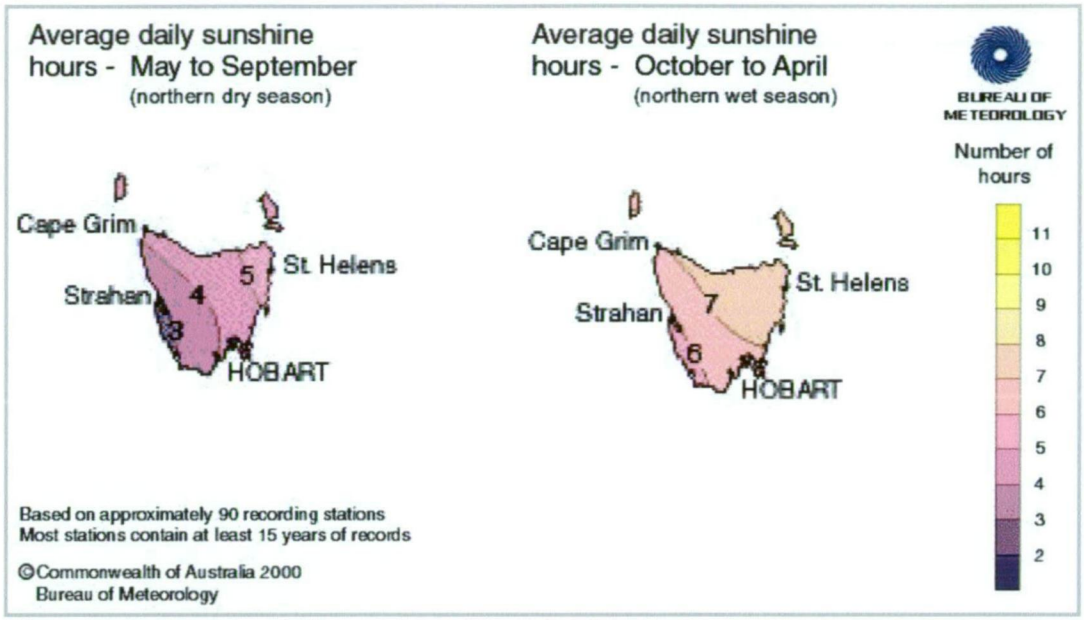

Figure 5.5: Average daily sunshine hours in Tasmania

5.3 Soil Environment

The soils of the study area are ferrosols, (Isbell 1996), with a significant proportion being from the krasnozem great soil group (Figure 5.6).

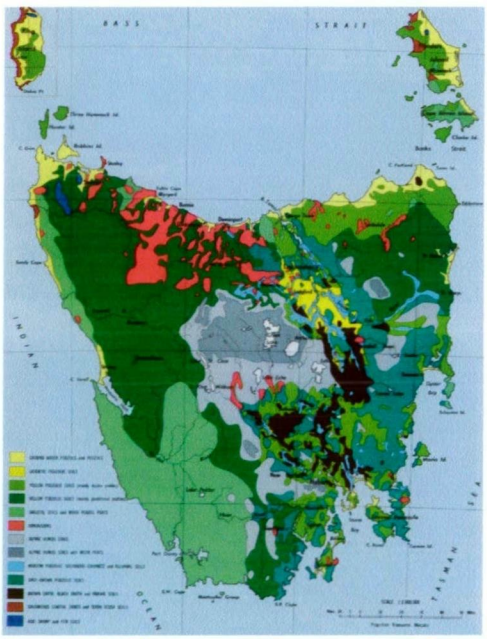

Figure 5.6: Great Soil Groups of Tasmania (after Davies 1965)

These soils are formed on basic or ultra-basic igneous rocks, their metamorphic equivalents, or alluvium parent material. Ferrosols are often intensively used because of their favourable properties, (basic subsoil pH, acidic topsoil pH, strong fine polyhedral structure, well drained). The soils are characterised by a B2 horizon that is high in free iron oxide.

CHAPTER 6

MATERIALS AND METHOD

6.1 Season 1997/98

6.1.1 Selection of Trial Area

The North West Coast study area of Tasmania lays between 41° 07' 13''S and 41° 18' 45''S (21.0 km, north to south) and from 146° 04' 07''E to 146° 33' 58''E (41.3 km, east to west), (Figure 4.1).

The cool, temperate climate, winter dominant rainfall and well structured soils enable a wide variety of horticultural crops to be grown in fields of 2- 20 hectares.

Average annual rainfall in the study area ranges from 600-1200mm, of which approximately two thirds occurs in winter. With mean daily maximum temperatures rarely exceeding 26°C, summers are mild. These meteorological conditions and irrigable krasnozem soils make the North West Coast of Tasmania, and the study area, particularly suited to the production of many crops including pharmaceutical poppies, pyrethrum, potatoes, peas, beans, carrots and onions for both processing and fresh market. Other vegetable crops include pumpkin, broccoli, cauliflower, and corn for the fresh domestic market and seed production. Cereals such as barley, oats, wheat and triticale are mainly grown for stock feed and sown pastures support dairying and other animal enterprises.

The study area was chosen not only because of the significance of the poppy and pyrethrum industries but also in order that as much ground truthing data as possible could be obtained within a single image. The Landsat 5 TM system acquired images in the Landsat worldwide reference system (WRS) from path 091 and row 089. The SPOT system acquired images in the SPOT grid reference system (GRS) with the K/J node 384/433 closest to the scene centre.

Further explanation of the Landsat worldwide reference system and the SPOT grid reference system are found in Appendix A, which also provides detailed technical information for the Landsat TM and SPOT sensors.

6.1.2 Image acquisition

Digital data from SPOT XS, XI and Landsat 5 TM systems were acquired in this research project, in order to increase the probabilities of acquiring good sequential information. The high incidence of cloud over Tasmania makes the acquisition of cloud-free images via the Landsat 5 TM system alone somewhat difficult (Reid *et al.* 1993). These limitations are also common elsewhere (Beaubien 1994; Stoney 1996; Wiegand *et al.* 1996). The SPOT system increases the ability to acquire cloud-free images by the use of off-nadir viewing. The use of both Landsat TM and SPOT increases the frequency of target overpass compared with the use of one system only.

Whilst a set temporal sequence of images was the ultimate target in acquisition strategy, there were inevitable difficulties obtaining cloudfree images and problems with partially clouded images.

The Landsat 5 TM satellite regularly passes over each region every 16 days. For this project, images were required at intervals of no more than 48 days during the critical growing periods.

In order to maximise the chances of the desired sequences, whenever three consecutive images acquired by Landsat TM were affected by cloud, it was arranged for the SPOT satellite to be programmed to acquire data for the area.

The Australian Centre for Remote Sensing (ACRES) acquires both SPOT and Landsat imagery routinely. However, ACRES does not routinely acquire all possible imagery. ACRES accommodates user requests for priority acquisition but regularly acquires SPOT and Landsat imagery as part of its public interest mapping (PIM) program.

Six satellite images were acquired between 02 July 1997 and 18 April 1998 (Table 6.1). There were four Landsat 5 TM images and two SPOT XS images. The data acquired were almost totally cloud-free.

Table 6.1: Images acquired for the North West Coast Study area in 1997/98

Image Type	Date	Status
LANDSAT 5 TM (6 bands)	02 July 1997	Successful
LANDSAT 5 TM (6 bands)	06 October 1997	Successful
LANDSAT 5 TM (6 bands)	23 November 1997	Successful
LANDSAT 5 TM (6 bands)	10 January 1998	Successful
SPOT 2 (3 bands)	23 February 1998	Successful – 2% cloud
SPOT 1 (3 bands)	18 April 1998	Successful

Some translucent cloud in the 23 February 1998 image was present however this did not affect the areas of interest under examination in this research. Full metadata details for each image are found in Appendix B.

Landsat TM band six was removed and not utilised in the analysis of the data for this project. Landsat TM band six has a spatial resolution of 120m (which is not entirely compatible with the 20m resolution of SPOT sensors and the 30m resolution of the five other Landsat bands (Shaha *et al.* 1990). A combination of low resolution and position in the thermal portion of the EMR spectrum makes Landsat TM band six unsuitable for many applications. These include yield or crop type discrimination (Lee-Lovick and Kirchner 1991; Noonan 1999), forestry applications (Cohen and Spies 1992; Fiorella and Ripple 1993; Bauer *et al.* 1994; Beaubien 1994; Collins and Woodcock 1996), and habitat mapping (Green *et al.* 1998). Band six was therefore removed and not considered in the analysis of the data.

6.1.3 Groundtruthing

Ground-based data were collected by the author, at fortnightly intervals, from 01 July 1997 through until 25 April 1998 for 83 poppy and 42 pyrethrum crops. The collected data recorded crop type, growth stage and percentage ground cover from randomly selected areas of interest (AOIs) (areas under crop), which constituted approximately 10% of the total area under cultivation. That is, the AOIs corresponded to 10% of the total area under cultivation.

The frequent interval of data collection was undertaken to ensure that data was available close to the time of the remotely sensed data acquisition, so that the data corresponded as much as possible (Star and Estes 1990).

6.1.4 Distribution of Areas of Interest

For the 1997/98 growing season, 83 poppy and 42 pyrethrum crops were surveyed Figures 6.1 and 6.2 illustrate the distribution of the poppy and pyrethrum AOIs in the growing seasons. Red polygons indicate the distribution of the AOIs.

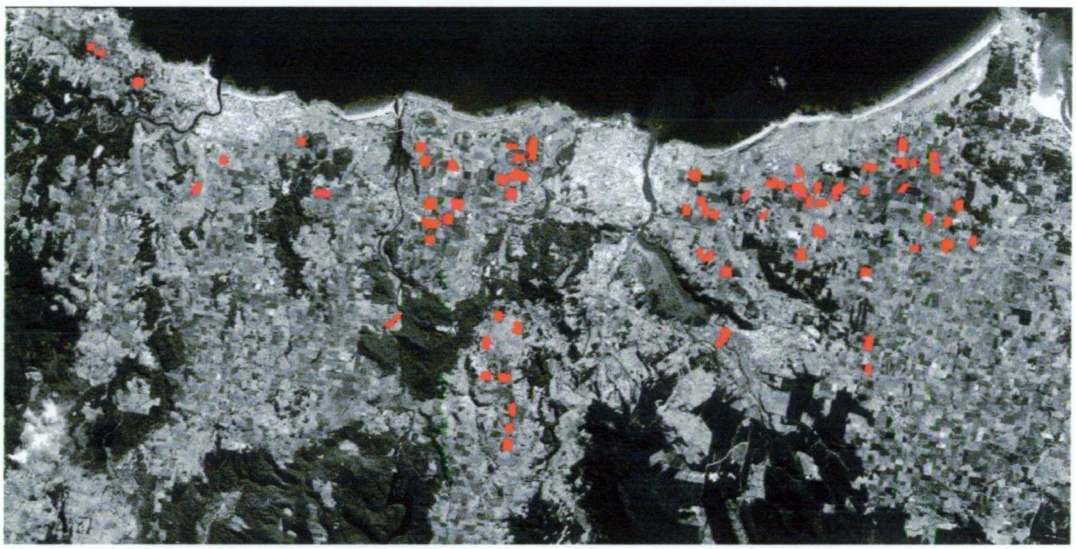

Figure 6.1: Distribution of the 1997/98 season poppy AOIs on the SPOT XS 18 April 1998 (gray scale) image

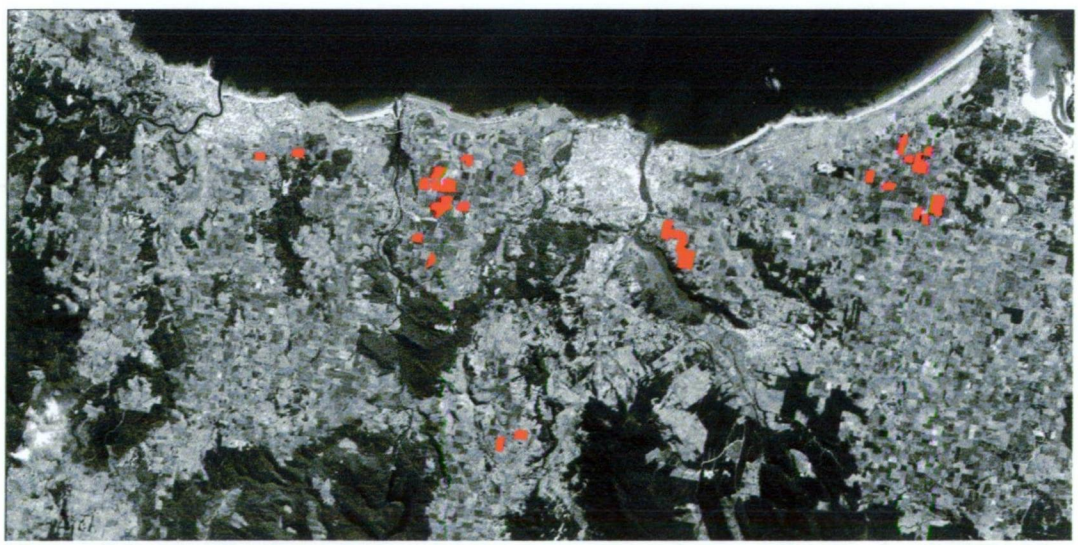

Figure 6.2: Distribution of the 1997/98 season pyrethrum AOIs on the SPOT XS 18 April 1998 (gray scale) image

The geographical distribution of the AOIs covered a significant proportion of the study area. This wide distribution enabled a representative sample to be analysed,

as different crops grown in distinct climatic and edaphic environments may have dissimilar growth signatures (Nieuwenhuis *et al*, 1996).

Crop boundaries were recorded utilising Tasmania 1:5000 orthophoto map series, referenced to the crop type and assessments. The crop type and assessments were utilised as training data for the analysis procedure and were stored in a database.

6.1.5 Database

Data was entered into the database using a data entry form developed in Microsoft Access® (Figure 6.3).

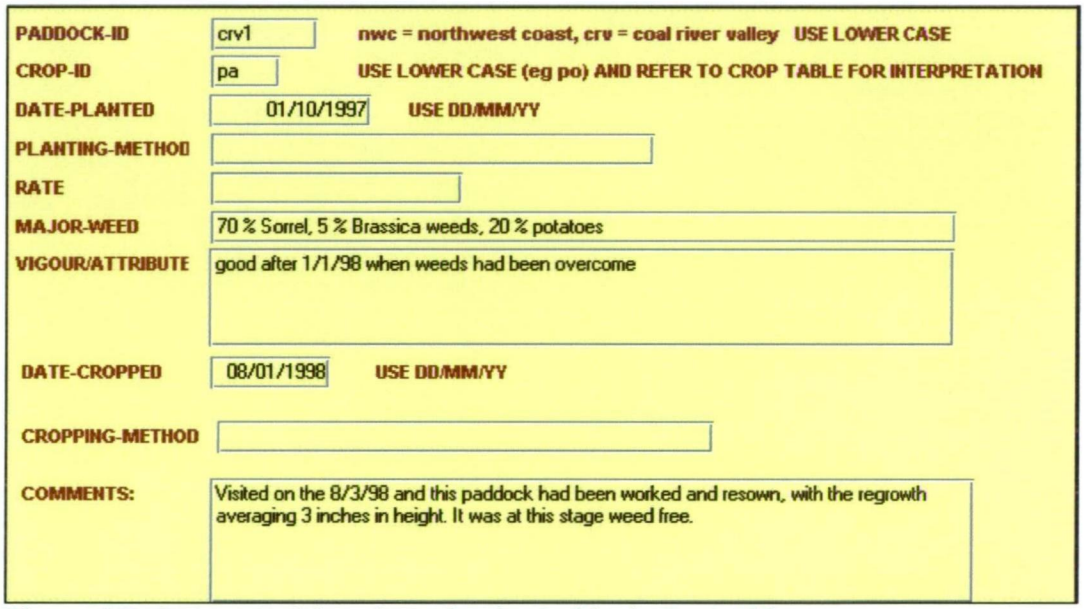

Figure 6.3: Data entry/view form for the Paddock-Crop table

This provided the user with meaningful field names and where necessary, help on how to fill in the fields. Individual paddock data were also viewed using this form, it being easier to use than the alternative data sheet view (Table 6.2).

The initial database design was developed from a list of known data about paddocks and crops. The standard technique of normalisation (Hoffer *et al.* 1999) was used to place this data in "third normal form". Third normal form is a three-step analysis of data, which results in the development of efficient database tables. The first step removed repetitive data and hence redundancy. The second step divided data into discrete data tables and the third step removed any data, which

was calculated and did not need to be stored. This methodology ensured there were no redundant data in the design and produced the most efficient relationships between tables. The main inefficiency removed, was that incurred with duplicate data, which would otherwise have had to be entered (and potentially modified) many times. The result of this normalisation process was the organization of the data, (attributes) into entities (tables).

Table 6.2: Datasheet view of data in the Paddock-Crop table

PADDOC	CROP ID	DATE-PI	PLANTING	RATE	MAJOR-WEED	VIGOUR/ATTRIBUTES	DATE-CI	CROPPIN	COMMENTS:
cn1	pa	/10/1997			70 % Sorrel, 5 % Brassic	good after 1/1/98 when we	/01/1998		Visited on the 8/3/98 and this paddo
cn10	fa	/11/1997			09/12/97 was 50 % groun				Was fallow throughout entire period
cn11	pp	/08/1997					/01/1998		12/1 stble remained and was still s
cn12	pp	/08/1997			Fat hen 30 %, Shepards F	Poor crop, only 1 to 1.5 fe	/01/1998		On the 8/3/98 was fallow and had b
cn13	ba	/08/1997					/01/1998		Visited on the 8/3/98 had been heac
cn14	lu	/06/1997							Cut twice, late November and early
cn15	pe	/08/1997					/11/1997		Visited on the 12/01/98 was fallow,
cn16	pa	/06/1997					/03/1998		Turf, Strathayr
cn17	pa	/06/1997							Turf, Strathayr
cn18	pe	/08/1997					/11/1997		Visited on the 12/1 was fallow, not v
cn19	po	/08/1997					/01/1998		24/10/97 was 20 % Row Cover, 09/
cn2	pe	/08/1997			Weed free	Good Vigour	/11/1997		Visited on the 12/1/98 was fallow, b
cn20	on	/08/1997					/01/1998		Tops were dying from late Decembe
cn21	pp	/08/1997					/01/1998		Headed on the 08/01/98, but stubbl
cn22	cs	/07/1997							Seed crop, were bolting and flowerir
cn23	pe	/08/1997				Excellent vigour	/01/1998		University Farm crop. Visited on the
cn24	pe	/07/1997					/11/1997		University Farm pea crop. Visited or
cn25	oa	/08/1997					/01/1998		Visited on the 8/03/98 this paddock
cn27	ca	/08/1997				Seed Crop	/01/1998		Visited on the 8/03/98 this paddock
cn28	ba	/08/1997					/01/1998		Stubble was still standing on the 09
cn29	pp	/08/1997					/01/1998		Stubble was still standing on the 12

After normalisation, an entity relationship diagram was produced. The entities, as mentioned, were analogous to tables in most database software, and the relationships to the links between the tables. These links were implemented by placing a single linking attribute in both tables. This is referred to as a "foreign key."

The result of applying normalisation to the project data was directly converted into an entity relationship diagram. This, along with the attributes organised into tables, was implemented directly in Microsoft Access®(Figure 6.4).

The relationships between the tables marked 1 - ∞ (or 1 to many) indicated the type of relationship. For example in Figure 6.4, one paddock can contain many crops, but only one crop at a time. Likewise the same crop can be grown in many paddocks. To show this relationship, the Paddock-Crop data table provided both a link and a temporal field to indicate what crop, in what paddock, at what time.

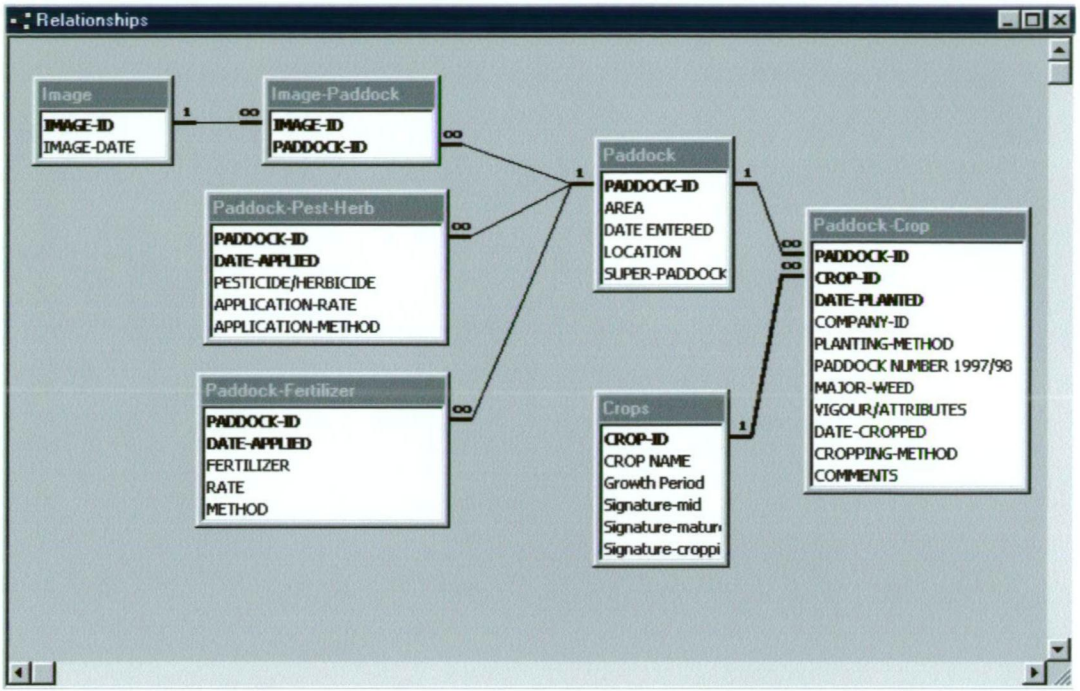

Figure 6.4: The original database relationship diagram showing all tables

6.2 Season 1998/99

6.2.1 Selection of Trial Area

The selected study area for the 1998/99 season was the same as in the 1997/98 season (between 41° 07' 13''S and 41° 18' 45''S, 21.0 km, north to south, and from 146° 04' 07''E to 146° 33' 58''E, 41.3 km, east to west.)

6.2.2 Image Acquisition

The timing of images acquired in the 1998/99 season, differed to those of the 1997/98 season due to the date of satellite overpass and the cloud cover present on the particular day of overpass.

In 1998/99 in the North West Coast area, seven satellite images were acquired between 21 July 1998 and 28 March 1999 (Table 6.3). There were four Landsat 5 TM images and three SPOT XI images. The image acquired on 03 March 1998 had about 10% cloud or shadow of cloud covering the study area. Cloud cover affected no areas of interest and, hence, there was no necessity to consider this effect in the analysis.

Table 6.3: Images acquired for the North West Coast Study area in 1998/99

Image Type	Date	Status
LANDSAT 5 TM (6 bands)	21 July 1998	Successful
LANDSAT 5 TM (6 bands)	27 September 1998	Successful
SPOT 4 (4 bands)	08 October 1998	Successful – 1% cloud
SPOT 4 (4 bands)	31 December 1998	Successful
LANDSAT 5 TM (6 bands)	29 January 1999	Successful – <1% cloud
LANDSAT 5 TM (6 bands)	03 March 1999	Successful – 10% cloud
SPOT 4 (4 bands)	29 March 1999	Successful

During the data collection phase of this project, there was one occasion on the North West Coast when images were not available within reasonable timeframes. No images were acquired in the 1998/99 season between 8 October 1998 and 31 December 1998, a period of 12 weeks at a critical phase of the cropping season. Full metadata details for each image are found in Appendix B.

6.2.3 Groundtruthing

During 1998/99, ground-based data were again collected by the author, at fortnightly intervals, from 21 July 1998 through until 30 March 1999 for 88 poppy and 60 pyrethrum crops. The collected data was assessed as for the 1997/98 growing season (section 6.1.3).

6.2.4 Distribution of the Areas of Interest

Figures 6.5 and 6.6 illustrate the distribution of the poppy and pyrethrum AOIs in these growing seasons. Red polygons indicate the distribution of the AOIs.

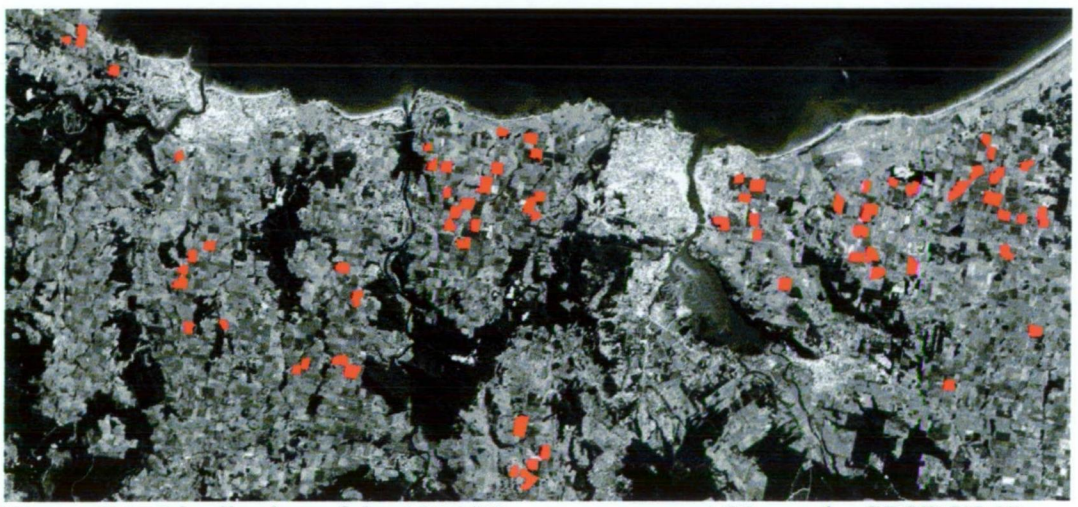

Figure 6.5: Distribution of the 1998/99 season poppy AOIs on the SPOT XI 29 March 1999 (gray scale) image

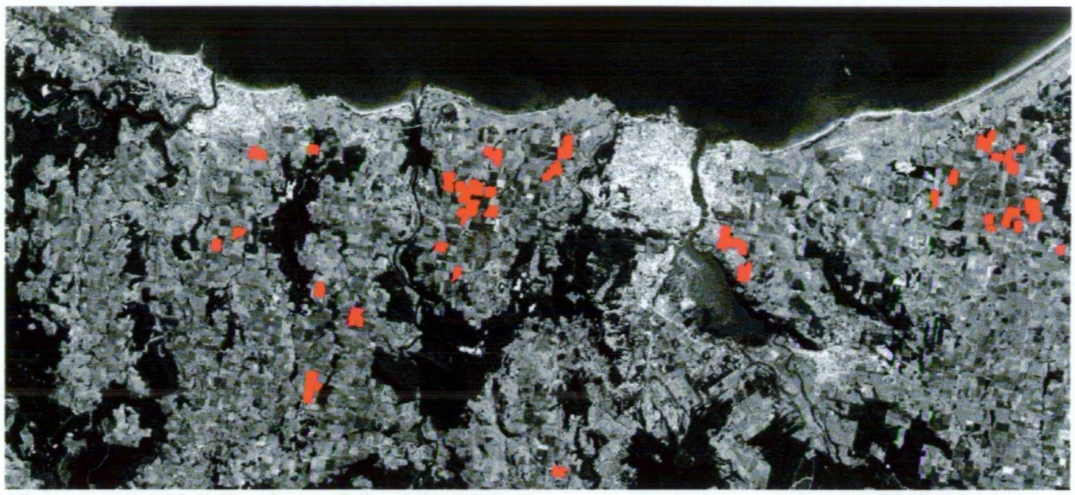

Figure 6.6: Distribution of the 1998/99 season pyrethrum AOIs on the SPOT XI 29 March 1999 (gray scale) image

6.3 Image Preprocesing

Errors and/or distortions in the imagery acquired were corrected to prepare the imagery for analysis. The images were rectified/registered to produce uniform 20 metre square "pixels" using the bilinear resampling method, (accounting for the 30m spatial resolution in the Landsat 5 TM sensor and the 20m resolution in the SPOT sensor) to accurately align the images.

It was considered necessary to perform image-to-image registration of the Landsat TM and SPOT imagery to enable comparison of separate images from the two sources, (Pouncey *et al.* 1999). Having decided to undertake image-to-image registration, it was then necessary to select the most appropriate resampling technique (nearest neighbour, bilinear interpolation or cubic convolution), taking into account the advantages and disadvantages of each.

It was taken into account that nearest neighbour resampling transfers original data values without averaging them and therefore maintains the extremes and subtleties of the data values (Pouncey *et al.* 1999). Modification of radiometric values is also avoided (Turner and Congalton 1998). However, when this method is used to resample a grid to a smaller size, there is usually a stair-stepped effect around diagonal lines and curves. Also, breaks or gaps in a network of linear data may result, when used on linear thematic data, (roads, paddock boundaries, Pouncey *et al.* 1999). Given that paddock boundaries contain a comprehensive combination

of diagonal lines, curves and linear data, the nearest neighbour resampling technique was not considered the most appropriate.

Cubic convolution produces layers with a mean and standard deviation matching the mean and standard deviation of the input pixels more closely than any other resampling method (Atkinson 1985) but data values may be altered (Pouncey *et al.* 1999). Atkinson (1985) reported that the effects of the cubic curve weighting can both sharpen the image and smooth out noise. However the actual effects depend on the data being used. Given that the cubic convolution method is most suited when the cell size is being dramatically changed (Landsat TM/aerial photo merges, Pouncey *et al.* 1999) it was not considered the most appropriate.

Bilinear interpolation has two advantages over the nearest neighbour resampling technique. Output images are smoother without the "stair-stepped" effect that is possible with nearest neighbour and they are more spatially accurate (Pouncey *et al.* 1999). This method is often used when changing the cell size of the data, such as the merge of SPOT/Landsat TM imagery (Pouncey *et al.* 1999). It was acknowledged that bilinear interpolation does result, in some extremes of the data file value being lost as some pixels are averaged and the edges are smoothed, and that subsequently the classification results may be affected (i.e. not necessarily representative of Landsat TM imagery). These effects were considered when the decision was made to undertake resampling using bilinear interpolation, as opposed to nearest neighbour and cubic convolution, when merging SPOT and Landsat TM imagery.

When considering the changes made to spatial parameters of the resampled imagery, not only is the bilinear interpolation technique more spatially accurate than the nearest neighbour technique, but also visual inspection of each layer in the signal-to-noise output image, (attained using hyperspectral image processing function) resulted in the inclusion of all Landsat TM layers in further processing. Furthermore, Hobma (1995) demonstrated that image-to-image registration could be used not only to improve rectification accuracies, to depict greater cartographic detail and to enhance spatial resolution but also to improve results of a supervised classification.

6.3.1 Rectification

The image processing software ERDAS Imagine (Version 8.4)® was used for image processing and analysis.

The most appropriate coordinate system for the data is detailed in Table 6.4. This system was selected as the projection, spheroid, horizontal datum and zone correspond to those of the Tasmania 1:5000 orthophoto map series, utilised in the recording of ground-truthed data.

Table 6.4: Coordinate system selected for image rectification

Projection Information	Projection Details
Projection Type	Universal Transverse Mercator (UTM)
Spheroid Name	Australian National
Horizontal Datum Name	Australian Geodetic Datum 1966
UTM Zone	55

Over 100 GCPs distributed throughout the study area were identified on the Tasmania 1:5000 orthophoto map series. Points selected as GCPs were dispersed throughout the 23 February 1998 SPOT image and included significant features easily recognisable on both imagery and the map series such as road intersections, airport runway, mobile phone towers and buildings. The reference coordinates (the coordinates of the Tasmania 1:5000 orthophoto map) were entered at the keyboard to identify a pixel on the 23 February 1998 SPOT image (source coordinates) and stored in a separate file to later facilitate image-to-image registration using the same GCPs.

A simple first order linear transformation was executed on the 23 February 1998 SPOT image displayed in the viewer. This transformation was selected to rectify the already transformed (to a plane) SPOT data to the desired map projection (Table 6.4).

The 23 February 1998 SPOT image was resampled using the nearest neighbour technique to avoid modification of radiometric values.

6.3.2 Image-to-Image Registration

Subsequent to the 23 February 1998 SPOT image being rectified to the Universal Transverse Mercator (UTM) map projection, all other imagery from 1997, 1998 and 1999 was registered to the 23 February 1998 SPOT image so that all images conformed and were accurately aligned.

For the registration of the Landsat 5 TM data (02 July 1997, 06 October 1997, 23 November 1997, 10 January 1998, 21 July 1998, 27 September 1998, 29 January 1999 and 03 March 1999), the Landsat Geometric Correction Model from ERDAS Imagine (Version 8.4)® was selected.

The same reference GCPs recorded in the rectification of the 23 February 1998 SPOT image, (reference image) were digitised on all individual Landsat 5 TM imagery (source imagery). Selected checkpoints were point matched until the checkpoint error was less than 0.5 (i.e. root mean square (RMS) values associated with each registration were less than or equal to 0.5), to create a transformation matrix for the source imagery to be resampled.

Resampling was undertaken utilising the Geo Correction Tools in ERDAS Imagine (Version 8.4)®, with the transformation matrix created from the point matched checkpoints and the bilinear resampling method (as cell size was being altered for the TM/SPOT merge).

For the registration of the SPOT data, (23 February 1998, 18 April 1998, 08 October 1998, 31 December 1998 and 29 March 1999) the SPOT Geometric Correction Model from ERDAS Imagine (Version 8.4)® was selected. As with the registration of the Landsat imagery, the same reference GCPs recorded in the rectification of the 23 February 1998 SPOT image (reference image) were digitised on all individual SPOT imagery (source imagery) and a transformation matrix generated. The transformation matrix and nearest neighbour resampling method were used in the Geo Correction Tools in ERDAS Imagine (Version 8.4)®. Root mean square (RMS) values associated with each registration were less than or equal to 0.5.

Once all imagery was rectified and registered, it was necessary for areas of interest (AOI's) to be defined.

6.4 Crop/Paddock Boundary Definitions and Digitising

The boundaries of paddocks were digitised directly on the computer screen on top of the satellite images (Figure 6.7), similar to the method used by Manière and Courboulès (1989), assisted by maps of the area with hand drawn paddock locations for reference. AOIs were simply polygon boundaries.

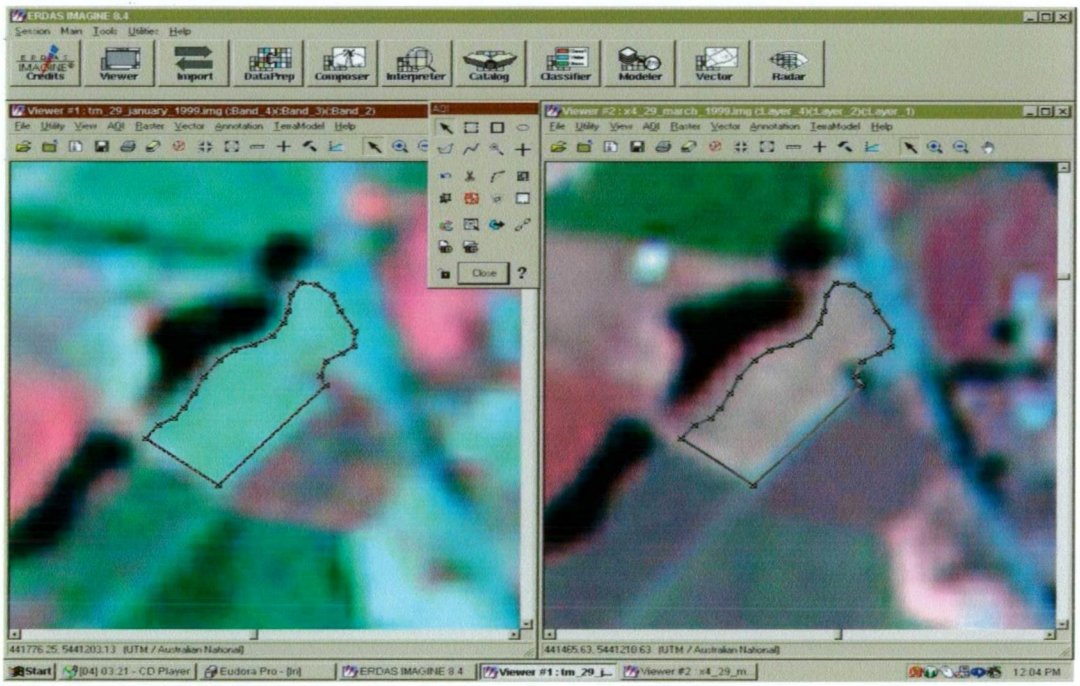

Figure 6.7: Digitising crop boundaries directly on the computer screen, superimposed on the TM 29 January 1999 image on the left and XI 29 March 1999 image on the right

This procedure was fast but it resulted in some paddock boundaries overlapping to a small extent. This was resolved by assigning the overlapping area to only one of the paddocks. The aim of the process was simply to delineate poppy and pyrethrum areas. The crop boundaries were saved, both as individual poppy or pyrethrum AOI's and in proportions of 10% of the total number of paddocks surveyed for each crop type in each season. For example, of the total population of poppy AOIs in the 1997/98 season, 10% were selected and saved as a training dataset, then a further 10% were added and this 20% were saved as a dataset and so on. The AOIs were selected and added using a random number generation table (Mead and Curnow 1987).

6.5 Preparation of Data for Classification

This project assessed three image analysis techniques as performed by Green *et al* (1998) and Noonan (1999), to determine the critical sample size and satellite image selection for the recognition of poppy and pyrethrum crops in North West Tasmania. Figure 6.8 provides a summary of the procedures used.

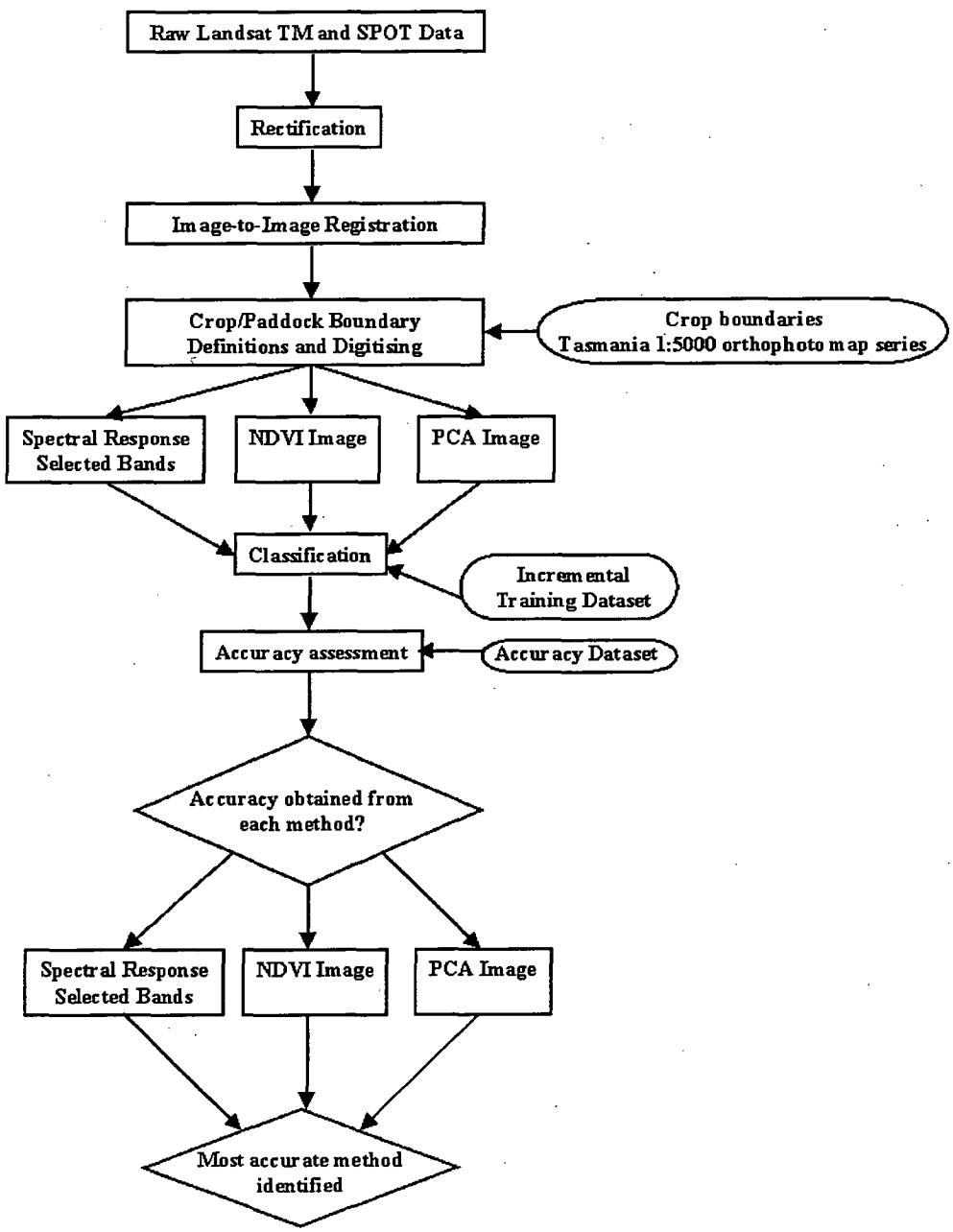

Figure 6.8: Flow diagram of the data analysis procedure.

6.5.1 Spectral Response Pattern Determination

Spectral response patterns were obtained for each AOI associated with poppies and pyrethrum in each of the individual images to determine whether pyrethrum and poppy crops exhibited spectrally distinct patterns using the automatic internal average relative reflectance (AIARR) function in ERDAS Imagine (Version 8.4)®.

AIARR executed three main steps. Firstly, the raw data were normalised using the same algorithm, which was used to normalise each pixel to the same total energy. This removed or minimized albedo variations and topographic effects. Secondly, the internal average relative reflectance function computed the logarithmic residuals of the spectra and raw digital number (DN) values were converted to extract absorption features. This was done by normalizing each pixel spectrum to flatten the convex background (i.e. normalize the baseline energy return to 1.0 for all wavelengths). The final step in this process was to rescale the data in three dimensions using the unsigned to 8-bit data option, which increased contrast between high and low values in the statistical layer, without altering the shape of the spectral curves. Zeros were ignored, in conjunction with a skip factor of one in the *X* and *Y* axis for the recalculation of the histograms for the AOIs only.

The outcome of the AIARR calculation on the data was a relative reflectance value for each pixel, for each layer per image. The mean and standard deviation of the relative reflectance values for the entire image were then obtained for each layer using the Layer Info Utility in ERDAS Imagine (Version 8.4)®. The summaries of the values for all pixels per layer were presented in Appendix C.

The relative reflectance values for the proportional AOIs associated with each crop type were then separately examined using the Layer Info Utility in ERDAS Imagine (Version 8.4)® to extract the mean and standard deviation for all pixels per crop type per layer. The mean and standard deviation of all AOIs for each crop type per layer for both the Landsat 5 TM and SPOT sensors were plotted to obtain the average spectral response curves.

The result of the AIARR calculation on the data was a set of relative reflectance values per pixel, per crop type, per layer, which were then used in classification with a decision rule, to assign the pixels to a class.

A histogram of the resulting AIARR values was exported for thematic layers, so that classification could be undertaken.

Normality of the resultant AIARR values for the AOIs were investigated using the following relationship (McBratney 1993):

If Mean = Median
then data is normally distributed.

This test of normaility is merely an extension of the statistical definition of mean and median (Mead and Curnow 1987). Mean is defined as the average of the values of the distribution and median is defined as that value for which exactly half the values in the population of the sample are greater and half smaller.

Skewness characterizes the degree of asymmetry of a distribution around its mean. Positive skewness (mean > median) indicates a distribution with an asymmetric tail extending toward more positive values. Negative skewness (mean < median) indicates a distribution with an asymmetric tail extending toward more negative values. Once the mean and median differed by more than the standard error of the mean:

$$SE\left(\overline{Y}\right) = \frac{S}{\sqrt{r}}$$

where:

S = sample standard deviation (σ)
r = number of observations

but less than the standard deviation the distibution was considered normal but skewed. For normal distribution, approximately 68% of the distribution is within a standard deviation of the mean (Mead and Curnow 1987). Hence, when the mean and median differed by more than the standard deviation the distribution was no longer considered normal.

6.5.2 Normalised Difference Vegetation Index Determination

The NDVI was calculated on the Landsat 5 TM imagery and SPOT imagery in ERDAS Imagine (Version 8.4)® utilising the spectral enhancement indices function, which calculated NDVI as:

$$NDVI_{TM} = \frac{TMBand4 - TMBand3}{TMBand4 + TMBand3} \quad \text{or} \quad NDVI_{SPOT} = \frac{SPOTBand3 - SPOTBand2}{SPOTBand3 + SPOTBand2}$$

This action produced a thematic statistical layer with values ranging from -1 (high biomass) to +1 (bare soil). The NDVI values were stretched between 0-255 (unsigned 8-bit) to increase contrast between high and low values in the statistical layer, without altering the shape of the spectral curves. The overall outcome of the NDVI calculation on the data was a value for each pixel, for each layer per image.

The mean and standard deviation of the NDVI values for all poppy and pyrethrum AOIs were then obtained for each layer using the Layer Info Utility in ERDAS Imagine (Version 8.4)®. Table 7.1 summarises the statistics of the NDVI calculation for the AOIs.

The result of the NDVI calculation on the data was a set of vegetation indices per pixel, per crop type per layer to be used in classification with a decision rule, to assign the pixels to a class.

A histogram of the resulting NDVI values was exported as for the thematic layer, so that classification could be undertaken. Normality of the data following the NDVI calculation for the AOIs was investigated as in Section 6.5.1.

Zeros were ignored, in conjunction with a skip factor of one in the X and Y axis for the recalculation of the histograms for the AOIs only.

6.5.3 Principal Components Analysis

A Principal Component Analysis (PCA) was carried out separately on each image in an approach similar to Turner and Congalton (1998). The spectral

enhancement, indices function in ERDAS Imagine (Version 8.4)® was utilised. The data was stretched to unsigned 8-bit to increase contrast between high and low values in the statistical layer, without altering the shape of the spectral curves. Eigen matrix and Eigenvalues were saved to separate files to enable determination of the required layers, which captured most of the information in the images. Components were calculated for six layers in the Landsat TM imagery, three layers in the SPOT XS imagery and four layers in the SPOT XI imagery. The resultant Eigenvalues and Eigenvectors presented in Tables 7.2 and 7.3. describe one value for each layer of the entire image.

From the PCA images, new images were created with the desired number of layers based on the examination of the Eigenvalues and Eigenvectors presented in Tables 7.2 and 7.3. Because a major goal of this merge was to retain the spectral information of all bands, the merging of layers was carried out in ERDAS Imagine (Version 8.4)® using the layerstack model. This algorithm assumed that PC 1 contained only overall scene luminance, and all interband variation was contained in the other PC bands. This remapping was done so that the mathematics of the reverse transform did not distort the thematic information. The number of input PC bands was dependent on the number of input bands in the multiband input image and was therefore, varied from image to image.
Given that, for all Landsat TM imagery, between 98.482% and 99.474% of variance was contained within the first three principal components, the layer stack was executed with the first three principal components. For all SPOT XI data between 99.189% and 99.845% of variance was contained within the first three principal components. Hence, the layer stack was executed with the first three principal components. Only the first and second principal components accounted for between 98.909% and 99.406% of the data variance in the SPOT XS data. Hence, the layer stack was executed with the first two principal components.

The mean and standard deviation of the new images generated through the layerstack model for both poppy and pyrethrum AOIs were then obtained for each layer using the Layer Info Utility in ERDAS Imagine (Version 8.4)®. Tables 7.4(a) and 7.4(b) summarise the statistics for the AOIs.

Normality of the merged PCA layers of all imagery, from the layerstack model histograms, was investigated using the normality McBratney (1993) relationship (Section 6.5.1).

Zeros were ignored, in conjunction with a skip factor of one in the *X* and *Y* axis for the recalculation of the histograms for the AOIs only.

6.6 Classification

Pouncey *et al.* (1999) state that using a combination of supervised and unsupervised classification may yield optimum results. Based on this information, it was decided to undertake both a supervised and unsupervised classification approach.

An unsupervised classification may be useful for generating a basic set of classes. Then, supervised classification can be used for further definition of the classes. Unsupervised classification is used in the initial stages of analysis when the classes within the data are to be determined by spectral distinctions inherent in the data alone, without superimposition of defined classes to be completed. An unsupervised classification was therefore performed to uncover statistical patterns inherent within the data, which had undergone AIARR, NDVI or PCA .

The approach taken to the classification of the imagery in this project was similar to that of Fiorella and Ripple (1993). ISODATA was used to develop 50 spectral classes at a convergence level of 99%. By specifying a convergence of 0.99 (99%) the iterative function ceased as soon as 99% or more of the pixels stayed in the same cluster between iterations. Iterations were set at 50 and colour scheme set at grayscale.

Clustering was initialised from statistics, which automatically computed the scaling range based on the number of classes requested and the assumption that the data were normally distributed. Means were initialised along the principal axis (computed to be along the first principal component vector and were evenly

distributed within the scaling range for the first principal component). Zeros were not classified and an *X* and *Y* skip factor of one was selected.

Given that the timing of image acquisition needed to coincide with presence of the target vegetation in order to assist the classification of imagery (Peştemalci *et al.* 1995) and that pyrethrum is a perennial crop, all images were classified for pyrethrum. However, as poppies are an annual crop, with a growing season of August until February, classification was executed on the 06 October 1997, 23 November 1997, 10 January 1998, 23 February 1998 and the 27 September 1998, 08 October 1998, 31 December 1998, 29 January 1999, 03 March 1999 images.

For each image the ISODATA was run 10 times with 10%, 20%, 30%, 40%, 50%, 60%, 70%, 80%, 90%, and 100% training data. The ISODATA was performed on the AOIs associated with each crop type (poppies and pyrethrum independently) for all data layers in each image.

Initially fifty classes were generated for each of the crop types per increment of training data so that paddock areas, which had similar signatures, were grouped into the same class. The 50 spectral classes for each 10% proportion were then merged, to produce one spectral class for each of the 10% proportions, on all images for pyrethrum and on the 06 October 1997, 23 November 1997, 10 January 1998, 23 February 1998 and the 27 September 1998, 08 October 1998, 31 December 1998, 29 January 1999, 03 March 1999 images for poppies. Those classes with a count of zero were removed.

The merged spectral response patterns generated from the AIARR, NDVI and PCA images with ISODATA provided the input for a supervised classification. As the spectral response patterns were the input for a supervised classification and were therefore essentially training data, only those signatures obtained from a specific image were used as the input for the supervised classification of that specific image.

As the AIARR, NDVI and PCA data were normally distributed and the spectral response patterns were parametric, a maximum likelihood parametric decision

rule was selected, which was based on the probability that a pixel belonged to a particular class. The maximum likelihood classification was performed once, for each crop type per procedure (AIARR, NDVI, or PCA) per image date, per proportion of training data (10%, 20%...) using all layers within the input data layers.

The basic equation assumed that the probabilities were equal for all classes and that the input bands had normal distributions. As *a priori* knowledge of the probabilities was unknown, the default probability weight of signatures (value of one) was accepted. Zeros were not classified.

Signature attribute statistics selected to be in the output, classified image were minimum, maximum, mean and standard deviation, ordered by layer. The statistics were based on the data file values for each layer for the signatures, rather than the entire classified image file.

Classification was performed for each class (poppy and pyrethrum independently) only on the AOIs associated with each class. It is acknowledged that if classification was performed on only the AOIs of one class then only that class will be distinguished. The objective of this project was however, not to distinguish class types but rather to determine whether the amount of training data had a significant effect on the contribution to classification, using the three methods, over two season's data for each of the crop types.

The supervised classification was executed on the 83 poppy crop AOIs and 42 pyrethrum crop AOIs for the 1997/98 growing season, and the 88 poppy crop AOIs and 60 pyrethrum crop AOIs for the 1998/99 growing season. This procedure was chosen as the classification of the areas external to the AOIs was of no significance, as ground truth data were not collected for these areas. Hence, validation/assessment of the results external to the AOIs was not possible.

6.7 Accuracy Assessment

Validation/assessment of the supervised classified image was measured as the number of crop pixels correctly classified as a proportion of the total population of crop pixels (where the total population equals all of the pixels in the crop's AOIs). This was achieved by determining, from the raster attribute editor, the number of pixels (histogram value), which were contributed to the final classification by the spectral classes for each of the 10% proportions of poppies and pyrethrum. For example, 10% of the poppy training data from the TM 23 November 1997 AIARR image contributed to the identification/classification of 1983 pixels out of a total of 11684 pixels associated with poppies in the image. Twenty percent of the poppy training data from the TM 23 November 1997 AIARR image contributed to the identification/classification of a further 3856 pixels. Subsequently the spectral response patterns obtained from 10% of the poppy training data classified 17% of the total 11684 pixels, and the spectral response patterns obtained from 20% of the poppy training data classified 50% of the total 11684 pixels.

To determine whether the amount of training data had a significant effect on the percentage contribution to classification for the three methods, over two season's data for each of the crop types, a one-way analysis of variance was undertaken. The least significant differences (LSD) at the 5% level of the AIARR, NDVI and PCA variates were determined in Genstat 5 (Release 4.1)®. Blocking effect was the image and percentage training data as the treatment.

It is important to note that the addition of more training data at any time would not necessarily lead to an "increase" in the number of pixels correctly classified, but would lead to the classification of a "different" sample of pixels. This was the hypothesis, which prompted this particular examination of the effect of quantity of training data on classification.

CHAPTER 7

RESULTS AND DISCUSSION

7.1 Spectral Response Pattern Determination

The mean and standard deviation from the automatic internal average relative reflectance calculation of each crop for both the Landsat 5 TM and SPOT sensors were plotted against the pixel value.

Figure 7.1, (Landsat TM spectral response pattern for poppies in the 1997/98 growing season) shows that there was a significant difference in the pixel values for the 06 October 1997, 23 November 1997 and 10 January 1998 images in bands one, two, three and five.

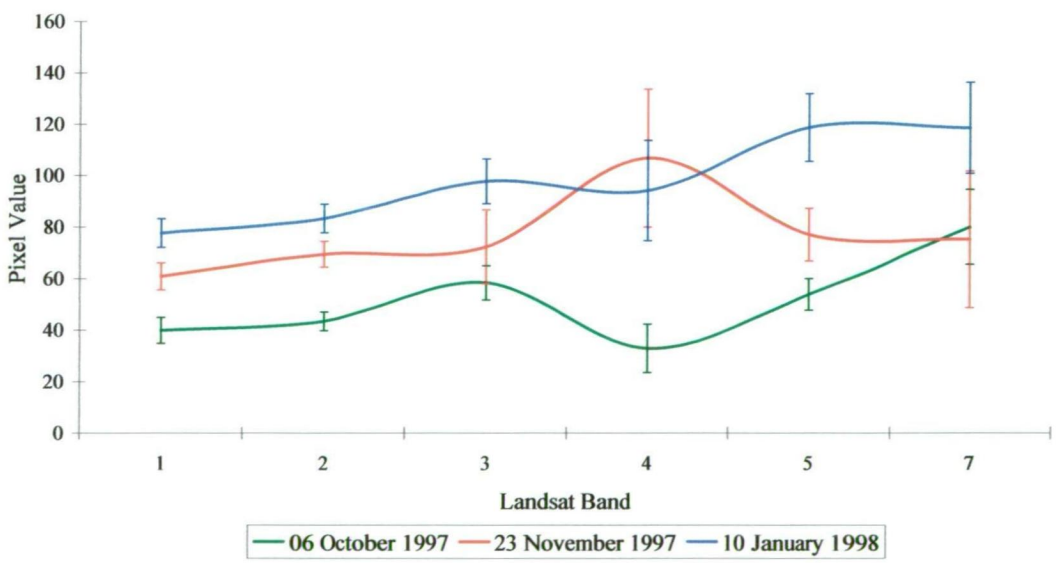

Figure 7.1: Landsat TM spectral response patterns for poppies in the 1997/98 growing season with bars indicating standard error associated with each band

This is consistent with Landsat TM bands one, two, three and five being generally applicable to the differentiation of vegetation from soils, assessment of vegetation

vigour, chlorophyll absorption and vegetation and soil moisture measurements respectively.

The pixel values for the 06 October 1997 image were considerably lower than those for the 23 November 1997 and 10 January 1998 images. This result can be explained in agronomic terms. As poppy crops were sown in August/September, by October the small rosette stage was near completion and the rapid increase in growth yet to commence (Figure 4.4).

Figure 7.2 shows the SPOT XS spectral response pattern for poppies in February 1997/98 and demonstrates a peak pixel value in band two (chlorophyll absorption by green vegetation). This characteristic can also be explained agronomically as the poppy crops had reached the sixth and final stage of development (ripening of the capsules and seeds) at this time. The capsules had obtained a characteristic dull bluish-green colour, distinct even to the naked eye.

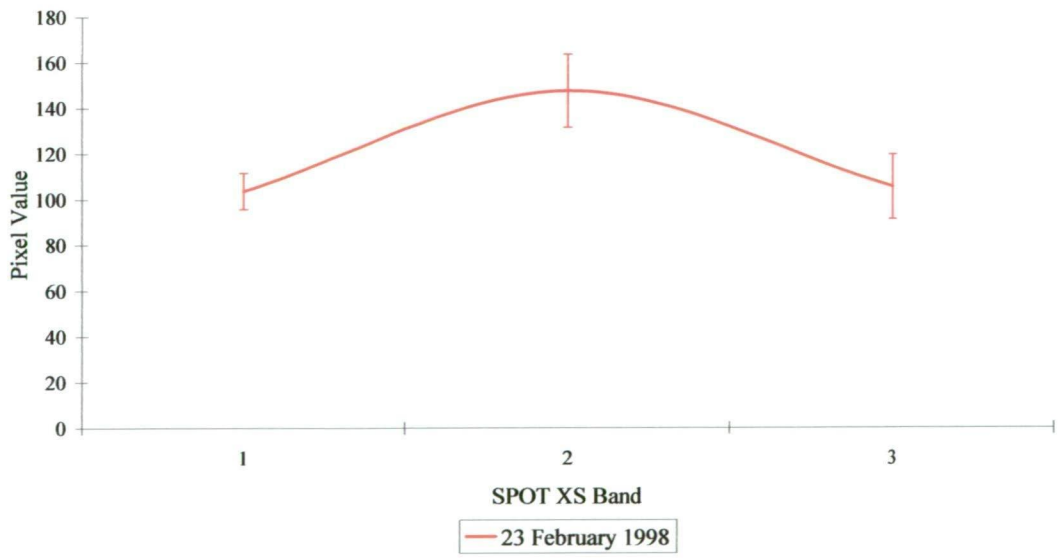

Figure 7.2: SPOT XS spectral response pattern for poppies in the 1997/98 growing season with bars indicating standard error associated with each band

Examination of the spectral response pattern for pyrethrum in the 1997/98 growing season, provided by the Landsat TM sensor (Figure 7.3), showed similarity with the poppy spectral response patterns. Figure 7.8 also illustrated

that the dormancy phase of growth (02 July 1997 image) resulted in low pixel values compared with the 23 November 1998 and 10 January 1998 imagery. From November to January, the pyrethrum crop reached a peak stage of growth, flowered and was harvested (Figure 4.9). Hence, the spectral response pattern for bands one, two, three and five was significantly different from that of the July and October images.

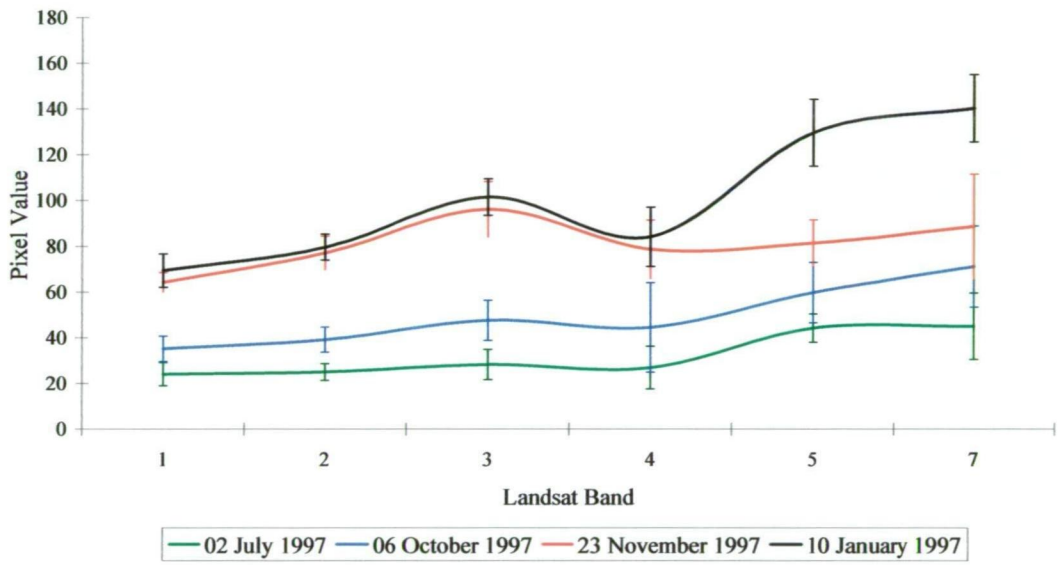

Figure 7.3: Landsat TM spectral response pattern for pyrethrum in the 1997/98 growing season with bars indicating standard error associated with each band

Significant increase was noted in pixel value for the January image in bands five and seven. This corresponded to bands generally applied to vegetation and soil moisture measurements and hydrothermal mapping. It was during this time (January) that the crop was cut, windrowed and dried in the field, exposing areas of soil.

The SPOT XS spectral response pattern for pyrethrum in the 1997/98 growing season (Figure 7.4) showed no significant difference in pixel values between the February and April images. As stated previously, it was during January and February that the crop was cut and harvested, exposing large areas of soil. Subsequently the crop progressed into a dormancy phase (Figure 4.9) where little

to no growth occurred. This is consistent with the result indicating little difference in spectral response between February and April.

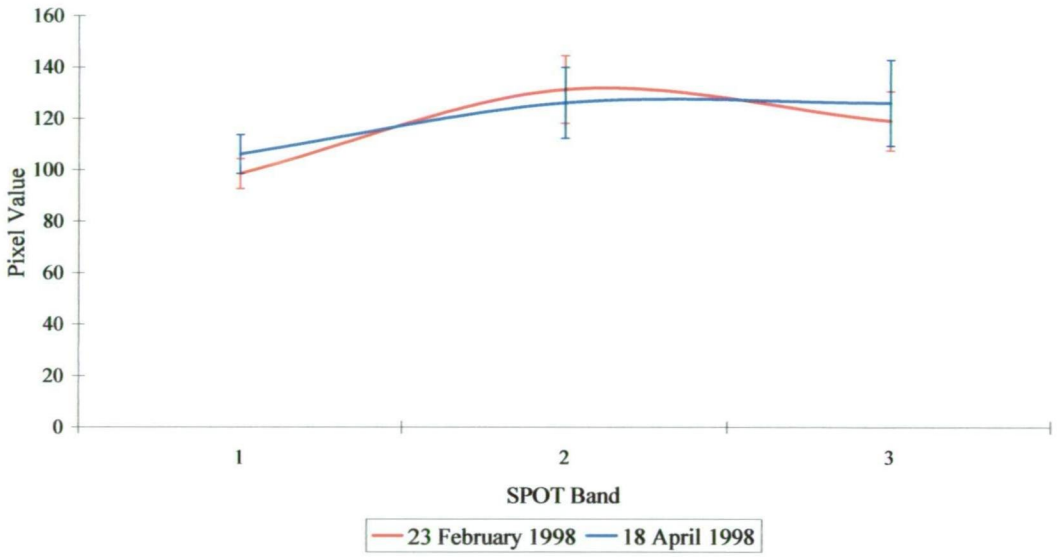

Figure 7.4: SPOT XS spectral response pattern for pyrethrum in the 1997/98 growing season with bars indicating standard error associated with each band

The results for the Landsat TM spectral response pattern for poppies in the 1998/99 growing season (Figure 7.5) differed from those of the previous growing season. Not only, were the overall pixel values lower, but the difference between the three methods were also not significantly different.

The 1998/99 poppy growing season was considered to be below average by the industry's personnel, as high rainfall was recorded during the January of 1999 which resulted in many crops lodging or exhibiting signs of disease in the capsules. Many crops were unable to dry off, reducing the expected variation in response between the January image and the September and March images. The minimal variation between the September and March images was explained by the limited presence of crop at both times, with the crop planted but still emerging in September. By March, the crop had been harvested and the ground fallow.

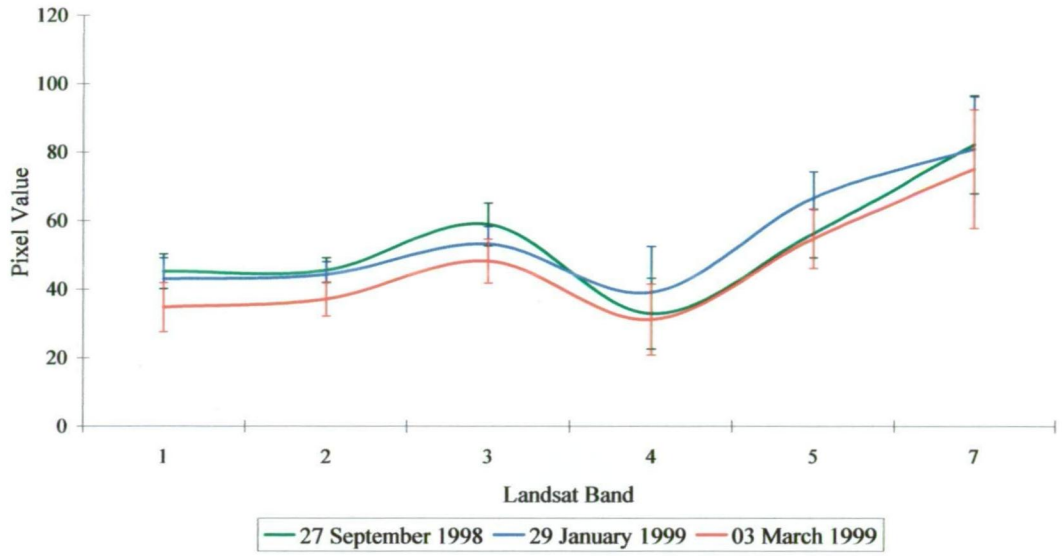

Figure 7.5: Landsat TM spectral response pattern for poppies in the 1998/99 growing season with bars indicating standard error associated with each band

The spectral response pattern for poppies in the 1998/99 growing season provided by the SPOT XI sensor (Figure 7.6) reflected the reduced variation between bands in the December image compared with the October image. The crops undergoing elongation of internodes and branching (fourth phase), where the uptake of water and nutrients was most intensive, may explain the reduced variation.

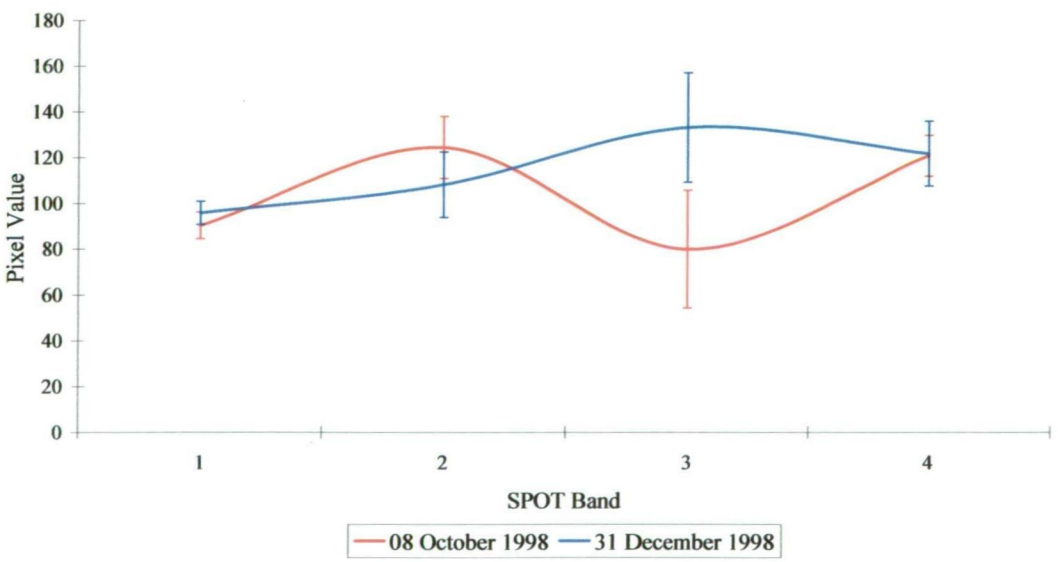

Figure 7.6: SPOT XI spectral response pattern for poppies in the 1998/99 growing season with bars indicating standard error associated with each band

The overall spectral response pattern trend, for pyrethrum in the 1998/99 growing season (Figure 7.7) was similar to that of the 1997/98 season. However, a reduction in pixel value for the January image in bands five and seven was recorded, as for the 1998/99 poppy crop attributed to the high rainfall in January 1999. The minimal variation between the July and March image pixel values was attributed to the crop dormancy phase.

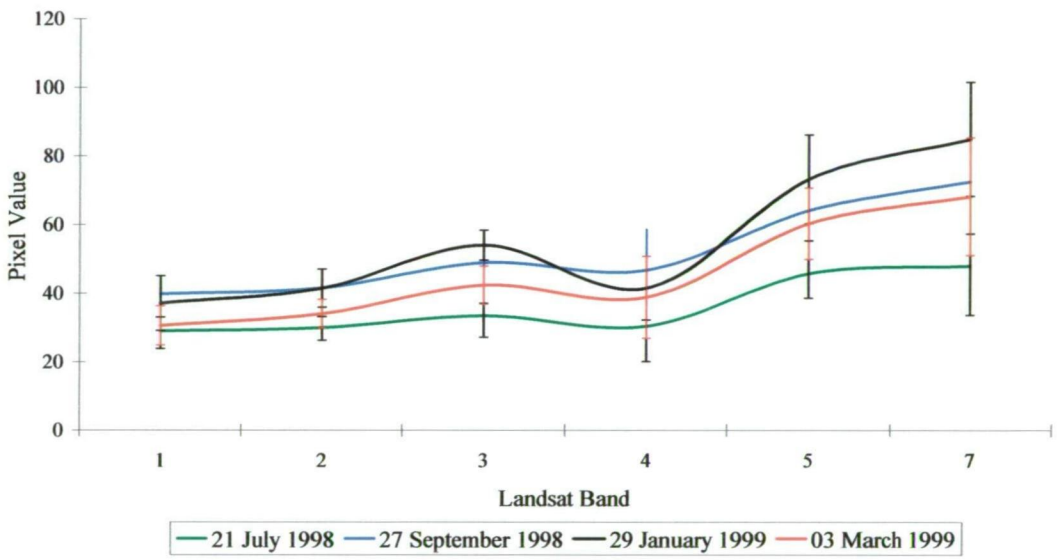

Figure 7.7: Landsat TM spectral response pattern for pyrethrum in the 1998/99 growing season with bars indicating standard error associated with each band

The most significant feature of the results obtained from the SPOT XI spectral response pattern for pyrethrum in the 1998/99 growing season (Figure 7.8) was the peak pixel value in the December image, band two. This high and distinct pixel value corresponded to the crop being in full flower.

The observations of the average spectral response pattern of poppies illustrated that Landsat TM bands one, two, three and five in November and January, provided significantly peakdifferent pixel values for the poppy crops. As stated previously, this is consistent with Landsat TM bands one, two, three and five being generally applicable to the differentiation of vegetation from soils, assessment of vegetation vigour, chlorophyll absorption and vegetation and soil moisture measurements respectively.

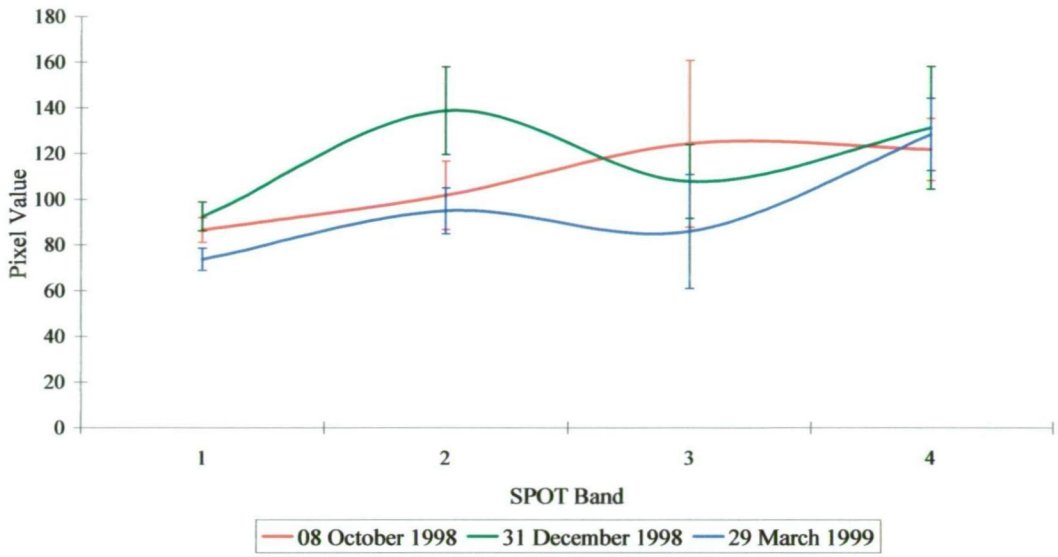

Figure 7.8: SPOT XI spectral response pattern for pyrethrum in the 1998/99 growing season with bars indicating standard error associated with each band

During November, the poppy crops were undergoing a rapid growth phase (elongation of internodes and branching). This fourth developmental phase (Chapter 4, section 4.1.5) was a period of rapid growth (Figure 4.4) in which the uptake of water and nutrients was most intensive. In January, the poppy crops were nearing completion of the fifth developmental phase. Flowers had shed and the capsules and seeds were reaching their final shape and size. Growth of the capsules had halted although the capsules were still green.

SPOT XS band two in February also provided peak pixel values. The peak pixel values in SPOT XS band two (chlorophyll absorption by green vegetation) corresponded to the poppy crops undergoing the sixth and final phase of development. During this phase the leaves senesced, the capsules obtained their characteristic dull bluish-green and the seeds separated from the septa within the capsule.

The spectral response pattern of pyrethrum indicated that the significant increase in pixel values of Landsat TM bands five and seven in January was unique to pyrethrum. This reflected the Landsat TM bands being responsive to vegetation,

soil moisture measurements and hydrothermal mapping. It was during this time (January) that the crop was cut, windrowed and dried in the field, exposing areas of soil. The peak pixel values in SPOT XI band two, during December corresponded to the crop being in full flower and reflected that SPOT XI band two is responsive to chlorophyll absorption by green vegetation and plant differentiation.

The result of the automatic internal average relative reflectance calculation on the data was a set of signatures corresponding to a class to be used in classification with a decision rule, to assign the pixels to a class. The generated signatures were parametric. A summary of the statistics for the AIARR values are presented in Appendix C. Normality of the resultant AIARR calculations was investigated using the McBratney (1993) relationship. When the mean and median of the AIARR values for the AOIs differed by more than the standard error of the mean but less than the standard deviation the distibution was considered normal but skewed. When the mean and median differed by more than the standard deviation the distribution was no longer considered normal.

All of the 1997/98 and 1998/99 AIARR values, from the Landsat TM, SPOT XS and SPOT XI sensors displayed a normal distribution of the data with varying degress of both positive and negative skewness.

For the 1997/98 growing season data, a negative skew was exhibited by the TM 02 July 1997 band seven, TM 06 October 1997 bands two and three, TM 23 November 1997 band three, TM 10 January 1998 bands one, five and seven, XS 23 February band two and XS 18 April bands one and two data.

The 1998/99 growing season data revealed a negative skew in Landsat TM bands three five and seven for 29 January 1999 and 03 March 1999. Landsat TM bands three and seven for 21 July 1998 and bands one, two, three and seven for 27 September 1998 displayed a negative skew. SPOT XI 08 October 1998 bands two

and four, XI 31 December 1998 band one, XI 29 March 1999 band one also displayed a negative skew.

7.2 Normalised Difference Vegetation Index (NDVI)

A histogram of the resulting NDVI values was exported for the thematic layer, so that classification could be undertaken. The resultant thematic layer for the entire image and histogram charts for the AOIs are shown fully in Appendix D. The result of the NDVI calculation on the data was a set of signatures corresponding to a class to be used in classification with a decision rule, to assign the pixels to a class. The generated signatures were parametric. Table 7.1 summarises the statistics of the NDVI calculation for the AOIs.The higher the values between 0–255, the greater the net primary productivity and leaf area index and thus the more photosythetically active the vegetation.

All of the 1997/98 and 1998/99 NDVI imagery, from the Landsat TM, SPOT XS and SPOT XI sensors, displayed a normal distribution of the data with varying degress of both positive and negative skewness. With the exception of the Landsat TM image of 21 July 1998, all imagery for both the 1997/98 and 1998/99 growing seasons exhibited a positive skewness. The Landsat TM image of 21 July 1998 however exhibited a negative skewness.

7.3 Principal Components Analysis

After a PCA was completed, the maximum content was found in the first principal component, decreasing with each subsequent principal component (Tables 7.2 and 7.3). Computation and examination of the Eigenvalues and Eigenvectors enabled determination of the percentage variance contained within a principal component (Dwivedi 1996). Tables 7.2 and 7.3 summarise the Eigenvalues and percentage variance for each image. For all Landsat TM imagery between 98.482% and 99.474% of variance was contained within the first three principal components.

Table 7.1: Summary of NDVI calculation statistics

Image	Minimum Value	Maximum Value	Mean	Median	Standard Deviation	Standard Error of Mean
TM 02 July 1997	32.000	249.000	164.232	164.000	32.375	0.225
TM 06 October 1997	91.000	248.000	167.438	163.000	27.870	0.193
TM 23 November 1997	118.000	245.000	193.504	192.000	25.944	0.180
TM 10 January 1998	121.000	241.000	161.637	158.000	14.756	0.102
XS 23 February 1998	105.000	222.000	143.786	143.000	17.543	0.122
XS 18 April 1998	89.000	238.000	136.581	134.000	27.269	0.189
TM 21 July 1998	26.000	250.000	160.205	161.000	32.558	0.205
TM 27 September 1998	59.000	234.000	153.531	149.000	29.089	0.183
XI 08 October 1998	38.000	232.000	115.128	105.000	38.635	0.243
XI 31 December 1998	107.000	244.000	174.790	172.000	25.566	0.161
TM 29 January 1999	54.000	243.000	159.801	157.000	20.639	0.130
TM 03 March 1999	23.000	246.000	161.284	159.000	27.276	0.171
XI 29 March 1999	70.000	240.000	125.936	121.000	32.970	0.207

Similarly, for all SPOT XI, data between 99.189% and 99.845% of variance was contained within the first three principal components. For SPOT XS data the first and second components accounted for between 98.909% and 99.406% of the data variance. This made it possible to exclude about one third of the layers in the PCA image, as they contained mostly noise and little information.

Resultant histogram charts for each layer of all imagery (calculated for AOIs) are shown in Appendix E. Tables 7.4 (a and b) summarise the statistics of the PCA for the AOIs.

All of the 1997/98 and 1998/99 layerstack model merged imagery, from the Landsat TM, SPOT XS and SPOT XI sensors, displayed a normal distribution of the data with varying degress of both positive and negative skewness. Those data for the 1997/98 growing season which displayed a positive skewness (mean > median) were TM 02 July 1997 PC1, TM 06 October 1997 PC1, TM 23 November 1997 PC2, TM 10 January 1998 PC1 and PC2, XS 23 February 1998 PC2 and XS 18 April 1998 PC1 and PC2.

For the 1998/98 growing season, a positive skewness was displayed for PC1 and PC 2 in all Landsat TM data (21 July 1998, 27 September 1998, 29 January 1999, and 03 March 1999). Principal component one in all XI data (08 October 1998, 31 December 1998, 29 March 1999) exhibited a positive skewness and PC2 in the XI 31 December 1998 image also resulted in a positive skewness of the data.

Table 7.2: Eigenvalues and percentage variance for1997/1998 imagery

Principal Component	Eigenvalue	Variance (%)
Landsat5 TM 02 July 1997		
PC1	228.810	85.187%
PC2	29.810	11.098%
PC3	5.902	2.197%
PC4	2.098	0.781%
PC5	1.417	0.527%
PC6	0.562	0.209%
Sum of eigenvalues =	268.599	
Landsat5 TM 06 October 1997		
PC1	1893.582	82.038%
PC2	352.136	15.256%
PC3	45.311	1.963%
PC4	10.463	0.453%
PC5	5.682	0.246%
PC6	1.001	0.043%
Sum of eigenvalues =	2308.175	
Landsat5 TM 23 November 1997		
PC1	2813.704	80.762%
PC2	542.250	15.564%
PC3	97.239	2.803%
PC4	18.210	0.523%
PC5	10.661	0.306%
PC6	1.493	0.043%
Sum of eigenvalues =	3483.958	

Principal Component	Eigenvalue	Variance (%)
Landsat5 TM 10 January 1998		
PC1	3857.052	87.824%
PC2	418.532	9.530%
PC3	85.386	1.944%
PC4	15.412	0.351%
PC5	13.842	0.315%
PC6	1.554	0.035%
Sum of eigenvalues =	4391.779	
SPOT2 H1XS 23 February 1998		
PC1	807.379	87.353%
PC2	111.407	12.053%
PC3	5.488	0.594%
Sum of eigenvalues =	924.275	
SPOT1 H1XS 18 April 1998		
PC1	150.860	80.936%
PC2	33.486	17.965%
PC3	2.048	1.009%
Sum of eigenvalues =	186.394	

Table 7.3: Eigenvalues and percentage variance for 1998/99 imagery

Principal Component	Eigenvalue	Variance (%)
Landsat5 TM 21 July 1998		
PC1	328.519	86.821%
PC2	37.476	9.904%
PC3	7.817	2.039%
PC4	2.379	0.629%
PC5	1.633	0.431%
PC6	0.663	0.175%
Sum of eigenvalues = 378.386		
Landsat5 TM 27 September 1998		
PC1	1072.504	82.953%
PC2	171.828	13.290%
PC3	35.921	2.778%
PC4	7.420	0.574%
PC5	4.007	0.310%
PC6	1.219	0.094%
Sum of eigenvalues = 1292.900		
SPOT4 HRV1XI 08 October 1998		
PC1	7654.418	81.156%
PC2	1321.951	14.016%
PC3	378.819	4.016%
PC4	76.500	0.811%
Sum of eigenvalues = 9431.688		
SPOT4 HRV1XI 31 December 1998		
PC1	10713.561	84.103%
PC2	1640.879	12.881%
PC3	300.736	2.361%
PC4	83.478	0.655%
Sum of eigenvalues = 12738.653		
Landsat5 TM 29 January 1999		
PC1	2726.831	81.736%
PC2	508.832	15.252%
PC3	78.430	2.351%
PC4	12.367	0.371%
PC5	8.186	0.245%
PC6	1.490	0.045%
Sum of eigenvalues = 3336.136		
Landsat5 TM 03 March 1999		
PC1	2441.168	81.941%
PC2	427.529	14.350%
PC3	94.836	3.183%
PC4	8.871	0.298%
PC5	5.427	0.182%
PC6	1.361	0.046%
Sum of eigenvalues = 2979.192		
SPOT4 HRV1XI 29 March 1999		
PC1	1569.661	84.521%
PC2	213.760	11.510%
PC3	58.291	3.139%
PC4	15.413	0.830%
Sum of eigenvalues = 1857.124		

Table 7.4 (a):Summary of PCA statistics for 1997/98 AOIs

Image	Band	Minimum Value	Maximum Value	Mean	Median	Standard Deviation	Standard Error of Mean
TM 02 July 1997	1	5.000	123.000	47.536	47.000	17.496	0.121
	2	156.000	242.000	196.882	197.000	10.346	0.072
	3	144.000	186.000	167.849	168.000	4.962	0.034
TM 06 October 1997	1	16.000	121.000	51.641	51.000	15.305	0.106
	2	120.000	237.000	180.929	181.000	12.612	0.087
	3	163.000	200.000	185.676	186.000	3.664	0.025
TM 23 November 1997	1	29.000	156.000	79.972	80.000	13.652	0.095
	2	111.000	254.000	192.065	188.000	21.750	0.151
	3	108.000	218.000	186.270	189.000	16.790	0.116
TM 10 January 1998	1	28.000	144.000	75.544	70.000	17.850	0.123
	2	79.000	211.000	107.012	104.000	13.099	0.091
	3	184.000	249.000	224.285	224.000	8.823	0.061
XS 23 February 1998	1	20.000	84.000	45.642	46.000	9.228	0.064
	2	166.000	229.000	200.166	200.000	5.794	0.040
XS 18 April 1998	1	26.000	115.000	52.712	51.000	12.358	0.086
	2	169.000	241.000	201.714	201.000	6.781	0.047

Table 7.4 (b):Summary of PCA statistics for 1998/99 AOIs

Image	Band	Minimum Value	Maximum Value	Mean	Median	Standard Deviation	Standard Error of Mean
TM 21 July 1998	1	6.000	116.000	40.220	39.000	15.767	0.099
	2	165.000	242.000	200.822	200.000	9.015	0.057
	3	128.000	175.000	159.693	160.000	4.682	0.029
TM 27 September 1998	1	16.000	129.000	55.432	52.000	17.321	0.109
	2	137.000	233.000	191.003	190.000	10.906	0.069
	3	189.000	228.000	214.839	215.000	3.687	0.023
XI 08 October 1998	1	35.000	226.000	110.700	107.000	23.518	0.148
	2	23.000	221.000	104.774	108.000	22.957	0.144
	3	75.000	226.000	169.930	175.000	23.054	0.145
XI 31 December 1998	1	45.000	242.000	149.651	144.000	33.225	0.209
	2	15.000	224.000	117.035	116.000	38.688	0.243
	3	33.000	228.000	117.542	122.000	33.990	0.214
TM 29 January 1999	1	8.000	189.000	66.500	64.000	21.175	0.133
	2	68.000	223.000	136.897	135.000	15.221	0.096
	3	94.000	245.000	225.960	227.000	7.841	0.049
TM 03 March 1999	1	7.000	145.000	55.210	55.000	18.326	0.115
	2	89.000	228.000	159.797	158.000	15.025	0.094
	3	94.000	183.000	142.312	143.000	11.590	0.073
XI 29 March 1999	1	17.000	108.000	57.267	57.000	14.240	0.089
	2	12.000	112.000	65.571	68.000	10.473	0.066
	3	89.000	170.000	132.069	134.000	9.927	0.062

The result of the PCA and layerstack model merge on the data was a set of signatures corresponding to a class to be used in classification with a decision rule, to assign the pixels to a class. The generated signatures were parametric.

7.4 Spectral Response Pattern Generation

Tables 7.5 to 7.8 are a summary of the output from the ERDAS Imagine (Version 8.4)® ISODATA signature files for each proportion of training data, for all layers per image (three or more for the AIARR, one for the NDVI, and two or three for the PCA) per crop type. The output of the signature files shows the red, green and blue values, where these were used to create the colour for the signature and class.

All signatures generated from the ISODATA clustering were parametric. Tables 7.5 (a) and (b) provide details of the merged spectral response patterns generated from the AIARR, NDVI and PCA images with ISODATA for the 1997/98 growing season poppy crop.

The spectral response patterns generated from the PCA of the SPOT XS 23 February 1998 image, mimicked a pattern equivalent to NDVI in that, the red, green and blue values were the same (red = green = blue). This feature was a result of only two bands having been included in the PCA image. The layerstack model algorithm assumed that PC1 contained only overall scene luminance, and all interband variation was contained in the other PC bands. Therefore, in the SPOT XS 23 February 1998 image, only one band was present to describe all interband variation. The NDVI calculation reduced the contrasting reflectance of the green biomass in the visible and near-infrared parts of the spectrum to a ratio contained within one band. Subsequently, a NDVI image and a PCA layerstack image (with only two bands) both resulted in the spectral response pattern variation between red, green and blue being nil.

The signatures generated for the 1998/99 poppy crop from the ISODATA clustering were parametric. Tables 7.6 (a) and (b) provide details of the merged spectral response patterns generated from the AIARR, NDVI and PCA images.

Tables 7.7 (a) and (b) provide details of the merged spectral response patterns generated from the AIARR, NDVI and PCA images with ISODATA for the 1997/98 growing season pyrethrum crop.

The merged pyrethrum spectral response patterns generated from the PCA of the SPOT XS data, (XS 23 February 1998 and XS 18 April 1998), mimicked a pattern equivalent to NDVI in that, the red, green and blue values were the same. This was also the case with the PCA of the XS 23 February 1998 image for poppies, confirming that all, interband variation was contained in the remaining PC bands. In the instance of the XS imagery, one band only remained.

Tables 7.8 (a), (b) and (c) provide details of the merged spectral response patterns generated from the AIARR, NDVI and PCA images with ISODATA for the 1998/99 growing season pyrethrum crop.

Table 7.5 (a): Merged spectral response patterns generated from the AIARR, NDVI and PCA images with ISODATA for the 1997/98 growing season poppy crop

Image	Percent Training	AIARR Red	AIARR Green	AIARR Blue	NDVI Red	NDVI Green	NDVI Blue	PCA Red	PCA Green	PCA Blue
TM 06 October 1997	10	0.326	0.688	0.694	0.335	0.335	0.335	0.465	0.494	0.367
	20	0.382	0.644	0.649	0.366	0.366	0.366	0.482	0.498	0.341
	30	0.397	0.628	0.629	0.380	0.380	0.380	0.472	0.502	0.348
	40	0.400	0.624	0.638	0.386	0.386	0.386	0.462	0.509	0.353
	50	0.395	0.631	0.636	0.379	0.379	0.379	0.461	0.504	0.351
	60	0.401	0.625	0.635	0.385	0.385	0.385	0.455	0.507	0.355
	70	0.401	0.632	0.626	0.384	0.384	0.384	0.452	0.488	0.372
	80	0.405	0.620	0.607	0.390	0.390	0.390	0.466	0.472	0.392
	90	0.409	0.620	0.606	0.394	0.394	0.394	0.46	0.472	0.395
	100	0.402	0.623	0.604	0.386	0.386	0.386	0.48	0.465	0.394
TM 23 November 1997	10	0.650	0.332	0.406	0.615	0.615	0.615	0.553	0.663	0.490
	20	0.703	0.292	0.350	0.699	0.699	0.699	0.544	0.705	0.493
	30	0.659	0.325	0.360	0.661	0.661	0.661	0.548	0.675	0.483
	40	0.656	0.332	0.377	0.658	0.658	0.658	0.550	0.662	0.473
	50	0.622	0.361	0.388	0.626	0.626	0.626	0.561	0.630	0.461
	60	0.618	0.360	0.392	0.626	0.626	0.626	0.566	0.627	0.454
	70	0.614	0.366	0.391	0.622	0.622	0.622	0.566	0.620	0.460
	80	0.610	0.372	0.395	0.618	0.618	0.618	0.559	0.616	0.477
	90	0.616	0.366	0.389	0.623	0.623	0.623	0.558	0.621	0.481
	100	0.605	0.370	0.395	0.617	0.617	0.617	0.569	0.611	0.472

Table 7.5 (b): Merged spectral response patterns generated from the AIARR, NDVI and PCA images with ISODATA for the 1997/98 growing season poppy crop

NDVI	Percent	AIARR			NDVI			PCA		
Image	Training	Red	Green	Blue	Red	Green	Blue	Red	Green	Blue
TM 10 January 1998	10	0.488	0.510	0.613	0.486	0.486	0.486	0.546	0.542	0.359
	20	0.484	0.448	0.544	0.506	0.506	0.506	0.586	0.521	0.339
	30	0.511	0.445	0.552	0.532	0.532	0.532	0.556	0.535	0.342
	40	0.518	0.455	0.548	0.533	0.533	0.533	0.536	0.547	0.356
	50	0.543	0.470	0.573	0.546	0.546	0.546	0.489	0.567	0.362
	60	0.546	0.468	0.576	0.550	0.550	0.550	0.484	0.570	0.361
	70	0.532	0.478	0.560	0.535	0.535	0.535	0.496	0.555	0.375
	80	0.547	0.460	0.553	0.553	0.553	0.553	0.496	0.568	0.378
	90	0.545	0.466	0.551	0.550	0.550	0.550	0.498	0.566	0.381
	100	0.555	0.458	0.565	0.562	0.562	0.562	0.492	0.574	0.376
XS 23 February 1998	10	0.309	0.650	0.727	0.324	0.324	0.324	0.352	0.352	0.352
	20	0.343	0.622	0.690	0.355	0.355	0.355	0.320	0.320	0.320
	30	0.355	0.619	0.664	0.364	0.364	0.364	0.331	0.331	0.331
	40	0.361	0.620	0.646	0.367	0.367	0.367	0.353	0.353	0.353
	50	0.373	0.613	0.629	0.376	0.376	0.376	0.361	0.361	0.361
	60	0.388	0.599	0.614	0.391	0.391	0.391	0.385	0.385	0.385
	70	0.384	0.612	0.601	0.383	0.383	0.383	0.391	0.391	0.391
	80	0.400	0.601	0.579	0.397	0.397	0.397	0.414	0.414	0.414
	90	0.399	0.602	0.581	0.396	0.396	0.396	0.451	0.451	0.451
	100	0.410	0.594	0.566	0.406	0.406	0.406	0.433	0.433	0.433

Table 7.6 (a): Merged spectral response patterns generated from the AIARR, NDVI and PCA images with ISODATA for the 1998/99 growing season poppy crop

Image	Percent Training	AIARR			NDVI			PCA		
		Red	Green	Blue	Red	Green	Blue	Red	Green	Blue
TM 27 September 1998	10	0.333	0.627	0.595	0.328	0.328	0.328	0.590	0.457	0.333
	20	0.364	0.641	0.601	0.348	0.348	0.348	0.548	0.476	0.353
	30	0.368	0.665	0.630	0.345	0.345	0.345	0.520	0.495	0.340
	40	0.395	0.620	0.576	0.378	0.378	0.378	0.516	0.465	0.396
	50	0.391	0.617	0.578	0.376	0.376	0.376	0.520	0.459	0.396
	60	0.390	0.617	0.594	0.375	0.375	0.375	0.510	0.474	0.384
	70	0.385	0.617	0.594	0.371	0.371	0.371	0.513	0.466	0.383
	80	0.383	0.621	0.602	0.369	0.369	0.369	0.519	0.473	0.375
	90	0.384	0.633	0.609	0.367	0.367	0.367	0.522	0.477	0.373
	100	0.384	0.637	0.604	0.366	0.366	0.366	0.529	0.474	0.375
XI 08 October 1998	10	0.452	0.607	0.684	0.380	0.380	0.380	0.553	0.590	0.396
	20	0.473	0.625	0.610	0.375	0.375	0.375	0.565	0.606	0.427
	30	0.455	0.653	0.608	0.359	0.359	0.359	0.577	0.604	0.396
	40	0.489	0.614	0.556	0.390	0.390	0.390	0.568	0.601	0.459
	50	0.500	0.607	0.552	0.393	0.393	0.393	0.569	0.601	0.467
	60	0.478	0.619	0.590	0.382	0.382	0.382	0.570	0.596	0.432
	70	0.486	0.626	0.587	0.373	0.373	0.373	0.578	0.607	0.437
	80	0.485	0.629	0.592	0.369	0.369	0.369	0.582	0.602	0.425
	90	0.481	0.633	0.585	0.369	0.369	0.369	0.580	0.607	0.428
	100	0.490	0.637	0.572	0.366	0.366	0.366	0.588	0.610	0.432

Table 7.6 (b): Merged spectral response patterns generated from the AIARR, NDVI and PCA images with ISODATA for the 1998/99 growing season poppy crop

NDVI	Percent	AIARR			NDVI			PCA		
Image	Training	Red	Green	Blue	Red	Green	Blue	Red	Green	Blue
XI 31 December 1998	10	0.451	0.359	0.591	0.634	0.634	0.634	0.532	0.362	0.380
	20	0.467	0.352	0.554	0.639	0.639	0.639	0.538	0.353	0.391
	30	0.416	0.325	0.527	0.683	0.683	0.683	0.493	0.304	0.418
	40	0.444	0.332	0.523	0.668	0.668	0.668	0.516	0.318	0.408
	50	0.451	0.346	0.532	0.652	0.652	0.652	0.522	0.334	0.403
	60	0.444	0.349	0.551	0.649	0.649	0.649	0.519	0.338	0.395
	70	0.445	0.352	0.560	0.645	0.645	0.645	0.519	0.343	0.394
	80	0.443	0.350	0.567	0.646	0.646	0.646	0.520	0.343	0.389
	90	0.448	0.352	0.561	0.644	0.644	0.644	0.524	0.343	0.387
	100	0.451	0.352	0.564	0.643	0.643	0.643	0.528	0.345	0.384
TM 29 January 1999	10	0.383	0.516	0.624	0.372	0.372	0.372	0.542	0.537	0.307
	20	0.418	0.521	0.620	0.396	0.396	0.396	0.515	0.549	0.332
	30	0.441	0.516	0.636	0.427	0.427	0.427	0.510	0.573	0.315
	40	0.466	0.488	0.585	0.455	0.455	0.455	0.508	0.560	0.370
	50	0.471	0.496	0.577	0.460	0.460	0.460	0.496	0.556	0.380
	60	0.466	0.495	0.567	0.458	0.458	0.458	0.498	0.545	0.387
	70	0.477	0.481	0.567	0.468	0.468	0.468	0.494	0.557	0.385
	80	0.481	0.466	0.568	0.478	0.478	0.478	0.501	0.564	0.377
	90	0.483	0.476	0.567	0.479	0.479	0.479	0.501	0.564	0.379
	100	0.477	0.481	0.565	0.473	0.473	0.473	0.506	0.559	0.379
TM 03 March 1999	10	0.320	0.693	0.635	0.278	0.278	0.278	0.499	0.437	0.312
	20	0.374	0.647	0.566	0.350	0.350	0.350	0.520	0.423	0.401
	30	0.403	0.610	0.570	0.388	0.388	0.388	0.510	0.457	0.392
	40	0.426	0.588	0.554	0.407	0.407	0.407	0.502	0.467	0.423
	50	0.425	0.585	0.550	0.409	0.409	0.409	0.506	0.461	0.430
	60	0.420	0.590	0.554	0.404	0.404	0.404	0.502	0.460	0.421
	70	0.430	0.577	0.551	0.418	0.418	0.418	0.501	0.466	0.428
	80	0.431	0.581	0.556	0.416	0.416	0.416	0.492	0.469	0.425
	90	0.432	0.587	0.571	0.416	0.416	0.416	0.483	0.478	0.414
	100	0.428	0.595	0.569	0.410	0.410	0.410	0.485	0.476	0.410

Table 7.7 (a): Merged spectral response patterns generated from the AIARR, NDVI and PCA images with ISODATA for the 1997/98 growing season pyrethrum crop

NDVI Image	Percent Training	AIARR Red	AIARR Green	AIARR Blue	NDVI Red	NDVI Green	NDVI Blue	PCA Red	PCA Green	PCA Blue
TM 02 July 1997	10	0.512	0.486	0.511	0.501	0.501	0.501	0.507	0.543	0.493
	20	0.554	0.440	0.477	0.558	0.558	0.558	0.493	0.550	0.537
	30	0.522	0.436	0.446	0.542	0.542	0.542	0.553	0.493	0.536
	40	0.524	0.442	0.465	0.543	0.543	0.543	0.540	0.504	0.526
	50	0.544	0.416	0.437	0.567	0.567	0.567	0.543	0.504	0.550
	60	0.511	0.424	0.428	0.541	0.541	0.541	0.569	0.453	0.550
	70	0.501	0.426	0.423	0.535	0.535	0.535	0.581	0.437	0.550
	80	0.495	0.432	0.427	0.530	0.530	0.530	0.586	0.430	0.547
	90	0.497	0.431	0.414	0.535	0.535	0.535	0.585	0.414	0.567
	100	0.496	0.428	0.390	0.537	0.537	0.537	0.606	0.389	0.588
TM 06 October 1997	10	0.543	0.490	0.571	0.527	0.527	0.527	0.421	0.629	0.428
	20	0.601	0.444	0.511	0.583	0.583	0.583	0.404	0.627	0.487
	30	0.606	0.397	0.449	0.610	0.610	0.610	0.480	0.595	0.534
	40	0.568	0.419	0.446	0.577	0.577	0.577	0.513	0.557	0.525
	50	0.637	0.370	0.431	0.629	0.629	0.629	0.452	0.626	0.549
	60	0.632	0.348	0.400	0.641	0.641	0.641	0.500	0.591	0.579
	70	0.501	0.426	0.423	0.659	0.659	0.659	0.498	0.598	0.596
	80	0.637	0.337	0.388	0.652	0.652	0.652	0.510	0.588	0.593
	90	0.648	0.321	0.365	0.667	0.667	0.667	0.509	0.571	0.636
	100	0.653	0.308	0.338	0.677	0.677	0.677	0.531	0.555	0.665
TM 23 November 1997	10	0.215	0.793	0.677	0.151	0.151	0.151	0.520	0.256	0.316
	20	0.281	0.746	0.668	0.242	0.242	0.242	0.485	0.310	0.358
	30	0.311	0.690	0.618	0.419	0.419	0.419	0.513	0.331	0.393
	40	0.307	0.666	0.577	0.302	0.302	0.302	0.554	0.329	0.382
	50	0.325	0.695	0.643	0.307	0.307	0.307	0.452	0.341	0.435
	60	0.330	0.705	0.666	0.309	0.309	0.309	0.421	0.338	0.469
	70	0.334	0.707	0.674	0.312	0.312	0.312	0.405	0.338	0.486
	80	0.330	0.705	0.666	0.310	0.310	0.310	0.422	0.336	0.477
	90	0.336	0.699	0.659	0.318	0.318	0.318	0.415	0.335	0.509
	100	0.337	0.703	0.663	0.318	0.318	0.318	0.393	0.327	0.542

Table 7.7 (b): Merged spectral response patterns generated from the AIARR, NDVI and PCA images with ISODATA for the 1997/98 growing season pyrethrum crop

NDVI Image	Percent Training	AIARR Red	AIARR Green	AIARR Blue	NDVI Red	NDVI Green	NDVI Blue	PCA Red	PCA Green	PCA Blue
TM 10 January 1998	10	0.387	0.746	0.650	0.316	0.316	0.316	0.380	0.374	0.513
	20	0.404	0.669	0.570	0.359	0.359	0.359	0.442	0.388	0.517
	30	0.441	0.560	0.478	0.419	0.419	0.419	0.489	0.421	0.572
	40	0.434	0.566	0.479	0.414	0.414	0.414	0.500	0.418	0.557
	50	0.425	0.598	0.493	0.396	0.396	0.396	0.481	0.409	0.572
	60	0.413	0.602	0.464	0.385	0.385	0.385	0.482	0.388	0.623
	70	0.411	0.594	0.448	0.386	0.386	0.386	0.498	0.598	0.596
	80	0.404	0.586	0.443	0.384	0.384	0.384	0.510	0.379	0.629
	90	0.408	0.582	0.421	0.390	0.390	0.390	0.504	0.380	0.669
	100	0.415	0.566	0.400	0.404	0.404	0.404	0.512	0.384	0.692
XS 23 February 1998	10	0.635	0.364	0.392	0.634	0.634	0.634	0.623	0.623	0.623
	20	0.628	0.367	0.405	0.633	0.633	0.633	0.568	0.568	0.568
	30	0.644	0.346	0.402	0.650	0.650	0.650	0.544	0.544	0.544
	40	0.671	0.316	0.385	0.678	0.678	0.678	0.539	0.539	0.539
	50	0.641	0.347	0.407	0.649	0.649	0.649	0.552	0.552	0.552
	60	0.618	0.368	0.428	0.627	0.627	0.627	0.550	0.550	0.550
	70	0.626	0.362	0.421	0.634	0.634	0.634	0.559	0.559	0.559
	80	0.632	0.356	0.414	0.641	0.641	0.641	0.558	0.558	0.558
	90	0.631	0.360	0.410	0.638	0.638	0.638	0.582	0.582	0.582
	100	0.640	0.355	0.397	0.646	0.646	0.646	0.603	0.603	0.603
XS 18 April 1998	10	0.685	0.297	0.359	0.700	0.700	0.700	0.637	0.637	0.637
	20	0.618	0.361	0.421	0.636	0.636	0.636	0.564	0.564	0.564
	30	0.599	0.390	0.425	0.612	0.612	0.612	0.542	0.542	0.542
	40	0.601	0.387	0.425	0.615	0.615	0.615	0.536	0.536	0.536
	50	0.634	0.359	0.390	0.646	0.646	0.646	0.588	0.588	0.588
	60	0.607	0.381	0.418	0.620	0.620	0.620	0.575	0.575	0.575
	70	0.615	0.375	0.411	0.628	0.628	0.628	0.586	0.586	0.586
	80	0.616	0.378	0.404	0.628	0.628	0.628	0.588	0.588	0.588
	90	0.616	0.387	0.394	0.624	0.624	0.624	0.611	0.611	0.611
	100	0.615	0.397	0.384	0.619	0.619	0.619	0.620	0.620	0.620

Table 7.8 (a): Merged spectral response patterns generated from the AIARR, NDVI and PCA images with ISODATA for the 1998/99 growing season pyrethrum crop

NDVI Image	Percent Training	AIARR Red	AIARR Green	AIARR Blue	NDVI Red	NDVI Green	NDVI Blue	PCA Red	PCA Green	PCA Blue
TM 21 July 1998	10	0.543	0.378	0.364	0.594	0.594	0.594	0.593	0.407	0.614
	20	0.550	0.353	0.376	0.608	0.608	0.608	0.598	0.450	0.582
	30	0.479	0.430	0.445	0.520	0.520	0.520	0.594	0.436	0.509
	40	0.479	0.426	0.424	0.524	0.524	0.524	0.605	0.406	0.533
	50	0.483	0.424	0.410	0.530	0.530	0.530	0.607	0.394	0.549
	60	0.493	0.421	0.387	0.539	0.539	0.539	0.608	0.376	0.578
	70	0.497	0.421	0.400	0.541	0.541	0.541	0.602	0.397	0.567
	80	0.490	0.440	0.424	0.526	0.526	0.526	0.585	0.411	0.548
	90	0.501	0.434	0.422	0.537	0.537	0.537	0.584	0.427	0.547
	100	0.500	0.432	0.413	0.603	0.603	0.603	0.596	0.414	0.556
TM 27 September 1998	10	0.729	0.253	0.355	0.750	0.750	0.750	0.396	0.625	0.673
	20	0.774	0.229	0.355	0.780	0.780	0.780	0.377	0.663	0.691
	30	0.663	0.327	0.404	0.673	0.673	0.673	0.432	0.596	0.612
	40	0.644	0.323	0.386	0.666	0.666	0.666	0.457	0.561	0.626
	50	0.644	0.312	0.366	0.674	0.674	0.674	0.471	0.542	0.646
	60	0.656	0.290	0.329	0.691	0.691	0.691	0.466	0.513	0.696
	70	0.663	0.295	0.339	0.690	0.690	0.690	0.454	0.530	0.688
	80	0.662	0.307	0.366	0.684	0.684	0.684	0.435	0.549	0.664
	90	0.654	0.324	0.375	0.674	0.674	0.674	0.445	0.548	0.653
	100	0.650	0.323	0.366	0.673	0.673	0.673	0.463	0.535	0.660

Table 7.8 (b): Merged spectral response patterns generated from the AIARR, NDVI and PCA images with ISODATA for the 1998/99 growing season pyrethrum crop

NDVI	Percent	AIARR			NDVI			PCA		
Image	Training	Red	Green	Blue	Red	Green	Blue	Red	Green	Blue
XI 08 October 1998	10	0.444	0.255	0.442	0.752	0.752	0.752	0.308	0.273	0.534
	20	0.428	0.221	0.415	0.790	0.790	0.790	0.269	0.236	0.550
	30	0.450	0.327	0.461	0.507	0.507	0.507	0.361	0.320	0.498
	40	0.478	0.330	0.455	0.686	0.686	0.686	0.383	0.333	0.514
	50	0.499	0.315	0.436	0.680	0.680	0.680	0.388	0.328	0.534
	60	0.535	0.291	0.390	0.699	0.699	0.699	0.390	0.319	0.583
	70	0.524	0.298	0.392	0.696	0.696	0.696	0.385	0.323	0.579
	80	0.490	0.308	0.419	0.691	0.691	0.691	0.369	0.326	0.561
	90	0.492	0.326	0.420	0.675	0.675	0.675	0.371	0.357	0.578
	100	0.512	0.323	0.407	0.673	0.673	0.673	0.386	0.358	0.587
XI 31 December 1998	10	0.432	0.789	0.360	0.302	0.302	0.302	0.271	0.750	0.817
	20	0.471	0.708	0.437	0.342	0.342	0.342	0.350	0.700	0.720
	30	0.478	0.695	0.492	0.336	0.336	0.336	0.399	0.666	0.614
	40	0.557	0.669	0.466	0.330	0.330	0.330	0.473	0.679	0.608
	50	0.591	0.663	0.453	0.322	0.322	0.322	0.500	0.692	0.616
	60	0.661	0.652	0.413	0.307	0.307	0.307	0.562	0.713	0.626
	70	0.634	0.658	0.424	0.311	0.311	0.311	0.537	0.708	0.627
	80	0.621	0.651	0.445	0.318	0.318	0.318	0.538	0.689	0.597
	90	0.589	0.670	0.435	0.319	0.319	0.319	0.499	0.692	0.621
	100	0.563	0.691	0.417	0.316	0.316	0.316	0.464	0.699	0.650

Table 7.8 (c): Merged spectral response patterns generated from the AIARR, NDVI and PCA images with ISODATA for the 1998/99 growing season pyrethrum crop

NDVI	Percent	AIARR			NDVI			PCA		
Image	Training	Red	Green	Blue	Red	Green	Blue	Red	Green	Blue
TM 29 January 1999	10	0.491	0.532	0.295	0.508	0.508	0.508	0.519	0.295	0.809
	20	0.455	0.550	0.378	0.467	0.467	0.467	0.536	0.315	0.732
	30	0.508	0.546	0.510	0.507	0.507	0.507	0.472	0.431	0.613
	40	0.521	0.533	0.460	0.524	0.524	0.524	0.484	0.419	0.651
	50	0.508	0.523	0.432	0.518	0.518	0.518	0.494	0.396	0.670
	60	0.502	0.518	0.414	0.515	0.515	0.515	0.504	0.385	0.680
	70	0.511	0.522	0.417	0.521	0.521	0.521	0.493	0.397	0.675
	80	0.524	0.537	0.434	0.527	0.527	0.527	0.469	0.420	0.655
	90	0.534	0.530	0.433	0.538	0.538	0.538	0.472	0.435	0.646
	100	0.529	0.526	0.416	0.535	0.535	0.535	0.491	0.424	0.656
TM 03 March 1999	10	0.522	0.406	0.451	0.574	0.574	0.574	0.576	0.498	0.562
	20	0.529	0.410	0.435	0.580	0.580	0.580	0.570	0.470	0.625
	30	0.671	0.330	0.418	0.675	0.675	0.675	0.433	0.615	0.617
	40	0.635	0.350	0.428	0.651	0.651	0.651	0.463	0.584	0.605
	50	0.606	0.372	0.419	0.627	0.627	0.627	0.482	0.524	0.648
	60	0.599	0.358	0.395	0.630	0.630	0.630	0.523	0.520	0.653
	70	0.596	0.363	0.404	0.627	0.627	0.627	0.521	0.522	0.644
	80	0.600	0.370	0.420	0.626	0.626	0.626	0.501	0.536	0.620
	90	0.610	0.366	0.418	0.632	0.632	0.632	0.495	0.551	0.612
	100	0.593	0.377	0.410	0.617	0.617	0.617	0.519	0.531	0.616
XI 29 March 1999	10	0.736	0.359	0.324	0.559	0.559	0.559	0.652	0.530	0.696
	20	0.735	0.366	0.292	0.565	0.565	0.565	0.641	0.533	0.721
	30	0.620	0.322	0.332	0.644	0.644	0.644	0.525	0.424	0.654
	40	0.611	0.328	0.351	0.636	0.636	0.636	0.523	0.419	0.631
	50	0.624	0.338	0.351	0.622	0.622	0.622	0.538	0.429	0.632
	60	0.639	0.327	0.324	0.635	0.635	0.635	0.535	0.426	0.666
	70	0.631	0.331	0.328	0.635	0.635	0.635	0.531	0.427	0.662
	80	0.603	0.339	0.363	0.630	0.630	0.630	0.519	0.418	0.628
	90	0.613	0.338	0.353	0.627	0.627	0.627	0.529	0.417	0.630
	100	0.632	0.351	0.341	0.610	0.610	0.610	0.553	0.436	0.639

7.5 An Assessment of the Contribution of the Amount of Training Data to Classification

The results and their discussion are presented in a tabular form in this section. The reader is referred, to the graphical presentation in the appropriate Appendix, Appendix F and Appendix G for poppies and pyrethrum respectively.

The amount of training data used had a significant effect on the percentage contribution to classification for the three methods, over two seasons' data for each of the crop types. Table 7.9 summarises the levels of significance of the treatment effect, provided by a one-way analysis of variance.

Table 7.9: F-probability values relating to the effect of the contribution to classification by proportional levels of training data using three methods for poppies and pyrethrum over two seasons

Crop/Season	AIARR F-Prob	NDVI F-Prob	PCA F-Prob
Poppies 1997/1998	<0.001	<0.001	<0.001
Poppies 1998/1999	<0.001	<0.001	<0.001
Pyrethrum 1997/1998	<0.001	<0.001	<0.001
Pyrethrum 1998/1999	<0.001	<0.001	<0.001

The F-probabilities associated with the proportional levels of training data for both poppy and pyrethrum crops over two seasons, was highly significant (F-prob <0.001), for each of the three methods (AIARR, NDVI and PCA). This finding confirmed that the amount of training data had a significant effect on the contribution to classification.

Whilst the proportional level of training data, significantly effected the contribution to classification, when the contribution to classification of the three methods were analysed, in only a few instances, were the results significant.

Results for both poppy seasons (1997/98 and 1998/99) are presented in Table 7.10. Appendix F shows the graphical presentation of the results. Table 7.10

shows the method, which returned the highest contribution to classification for the minimum effective level of training data. The quality (homogeneity) of the input data sets was reflected in the standard deviation (SD) statistics obtained from ERDAS Imagine (Version 8.4)®.

Using 90% of the total amount of data available for training, the Landsat TM 06 October 1997 image showed that the NDVI method returned a contribution to classification of 100% for poppies (Table 7.10). This result was however, not significantly different (P = 0.45), from the 87% contribution to classification by the AIARR method, or the 88% contribution to classification by the PCA method for the equivalent amount of training data (Figure F.1, Appendix F).

In the Landsat TM 23 November 1997 image, using 80% of the total amount of poppy data available for training, a contribution to classification of 88% was achieved with the PCA method (Table 7.10). However, this result was not significantly different (P = 0.97) from those achieved by the NDVI and AIARR methods (Figure F.2, Appendix F.). Both the NDVI and AIARR methods returned a 77% contribution to classification of poppies from 80% of the total amount of data available for training.

Using 80% of the total amount of data available for poppies as training data, the Landsat TM 10 January 1998 image showed that the PCA method returned a contribution to classification of 93% (Table 7.10). This result was however, not significantly different (P = 0.93) from the 76% contribution to classification by the NDVI method, or the 86% contribution to classification for the AIARR method for the equivalent amount of training data (Figure F.3, Appendix F).

Table 7.10: Summary of the method which returned the highest contribution to classification for the minimum effective level of training data for poppies

Image	Method	Contribution to Classification (%)	Amount of Training Data (%)	Standard Deviation of Input Data
TM 06 October 1997	NDVI	100	90	Layer 1 ± 22.520
TM 23 November 1997	PCA	88	80	Layer 1 ± 13.210 Layer 2 ± 202.123 Layer 3 ± 9.993
TM 10 January 1998	PCA	93	80	Layer 1 ± 9.339 Layer 2 ± 13.517 Layer 3 ± 9.870
XS 23 February 1998	NDVI	75	40	Layer 1 ± 15.629
TM 27 September 1998	NDVI	96	50	Layer 1 ± 24.478
XI 08 October 1998	NDVI	99	50	Layer 1 ± 30.804
XI 31 December 1998	NDVI	94	50	Layer 1 ± 24.131
TM 29 January 1999	PCA	94	80	Layer 1 ± 14.848 Layer 2 ± 140.311 Layer 3 ± 6.336
TM 03 March 1999	PCA	90	40	Layer 1 ± 16.573 Layer 2 ± 13.887 Layer 3 ± 9.621

In the SPOT XS 23 February 1998 image (Table 7.10), 40% of the total amount of data available used for training returned a contribution to classification of 75% with the NDVI method. This was not significantly different (P = 0.94) from the PCA and AIARR methods, which both contributed to 53% of the classification of poppies for the equivalent amount of training data (Figure F.4, Appendix F).

Figure F.4 further illustrates that the spectral response patterns developed through PCA on SPOT XS imagery (which mimicked those of the NDVI calculations, Table 7.5 (b)) resulted in similar classification results. For both the PCA and NDVI methods, using 70% of the total amount of data available for training, a contribution to the classification of 75% of the total poppy pixels was made. These findings are in contradiction to Turner and Congalton (1998) who reported that attempts to use the principal component database for SPOT XS data to map rice fields was unsuccessful. Turner and Congalton (1998) attributed this to the confusion between fallow areas and low lying areas, uncultivated areas with darker soils, which were found to have nearly identical PC scores to ploughed fields in lighter zones.

The results for the second poppy season reflected similar trends to those obtained in the first season. However, overall, the contributions to classification were improved on those obtained in the 1997/98 season. Eighty-three poppy crops were surveyed in 1997/98 and 88 crops in 1998/99. This increase, whilst appearing comparatively small compared to the improvement in results, also encompassed wider distribution of the poppy AOIs (Figures 7.1 and 7.2) which enabled a more representative sample to be analysed.

With 50% of the total amount of data available used for training and the Landsat TM 27 September 1998 image, the NDVI method returned a contribution to classification of 96% for poppies (Table 7.10). This result was not significantly different (P = 0.08) from the 91% contribution by the PCA method (Figure F.5, Appendix F) for the equivalent amount of training data. The 66% contribution to classification of poppies by the AIARR method, obtained with the equivalent

amount of training data available, was significantly lower (LSD = 1.97, Figure F.5, Appendix F) than the result obtained by the NDVI method.

In the SPOT XI 08 October 1998 image, use of 50% of the total amount of poppy data available for training, achieved a contribution to classification of 99% with the NDVI method (Table 7.10). This result was not significantly different (P = 0.64) from those achieved by the PCA and AIARR methods (Figure F.6, Appendix F.). The PCA method returned an 86% contribution to classification of poppies, for the equivalent amount of training data, and the AIARR method returned an 85% contribution.

Using 50% of the total amount of data available for poppies as training data, the SPOT XI 31 December 1998 image showed that the NDVI method returned a contribution to classification of 94% (Table 7.10). This NDVI result was significantly different (P = 0.002), from the 57% contribution by the PCA method (LSD = 13.60, Figure F.7, Appendix F), but not from the 85% contribution to classification achieved with the AIARR method (LSD = 10.50). The results obtained from the PCA were also significantly lower than those obtained from the AIARR method (LSD = 7.00).

In the Landsat TM 29 January 1999 image (Table 7.10), using 80% of the total amount data available for training, a contribution to classification of 94% with the PCA method was returned (Figure F.8, Appendix F). This was significantly different (P = 0.008) from the result obtained with the AIARR method (contribution to 66% classification of poppies, LSD = 10.24). The AIARR result was also significantly lower than the 76% obtained with the NDVI method (LSD = 2.37). The contribution to classification obtained with the PCA method, was however, not significantly different from the NDVI method.

When 40% of the total amount of data available used for training and the Landsat TM 03 March 1999 image was investigated, a contribution to classification of

90% was achieved using the PCA method (Table 7.10). This was not significantly different (P = 0.58) from the AIARR and NDVI methods, which contributed to 80% and 73% respectively to the classification of poppies for the equivalent amount of training data (Figure F.9, Appendix F).

In November and January of the first season, a contribution to poppy classification of 88% and 93% respectively, was achieved with 80% of the total amount available used for training, in conjunction with the PCA method. In the second poppy season, during January, a contribution to classification of 94 % was attained, for 80% of the total amount of data available used for training and the PCA method.

During November, the poppy crop was undergoing elongation of internodes and branching (the fourth phase). The uptake of water and nutrients was most intensive during this phase. The late fifth developmental phase was reached in January. The flowers had opened and the petals were shed. The capsules and seeds were reaching their final shape and size. The success of the PCA method during November and January on Landsat TM imagery was attributed to PC1 containing the "luminescence", PC2 containing "greenness" and PC3 "wetness," previously described in agricultural areas, (Crist and Cicone 1984a; 1984b; Torigoe *et al* 1992). The Eigenvectors for PC1, PC2 and PC3 (Table 7.2) of the November 1997 and January 1998 images were also the highest of all 1997/98 imagery. The Eigenvalues for PC1, PC2 and PC3 in the Landsat TM 29 January 1999 image (Table 7.3) were the highest of all Landsat imagery in 1998/99.

Abdel-Razik *et al.* (1984) found that the use of the PCA worked well with some but not with other vegetation data. In addition, the use of PCA worked well for imagery corresponding to particular growth stages of the vegetation being studied. This research confirmed Abdel-Razik *et al.* (1984), in that the November and January images corresponded to the fourth and late fifth phase (respectively) of poppy development. The PCA of November and January Landsat imagery resulted in Eigenvectors for PC1, PC2 and PC3 being the highest of all Landsat

imagery. Furthermore, Green *et al* (1998) and Mather (1987) concluded that the most accurate classification of Landsat TM necessitated the calculation of principal components. The classification of poppies using Landsat TM in the North West Coast of Tasmania was consistent with those findings. As shown in Table 7.10, 80% of the total amount of data available use for training contributed to an average classification of 90% of poppy crops. Therefore, to achieve a classification accuracy of 90% for poppies, the acquisition of Landsat data in either November or January, would require a PCA with 80% of the total poppy area used as training (calibration) data.

A high level of contribution to classification (94% - 99%) was achieved using only 50% of the total amount of data available for training and the NDVI method on SPOT XI data in October and December (Table 7.10).

During October the poppy crop had progressed from the leaf rosette stage to stem elongation, with rapid vegetative growth. During December, flowering and the formation of capsules and seeds occurred (early fifth developmental phase). These agronomic stages explained the high level of recognition achieved by the NDVI method with a low percentage of training data, consistent with the NDVI being sensitive to vegetative activity (Townshend and Justice 1998). The PCA of October and December XI imagery resulted in Eigenvectors for PC1, PC2 and PC3 being the highest of all 1998/99 imagery. This finding is in agreement with Dwivedi (1996) indicating that PCA is a powerful tool in change detection, as rapid growth occurs in the poppy crop in October and December. While PCA was not the most suitable method for SPOT XI data, it was, however, able to provide an insight into the levels of change within the ground cover.

Results for both pyrethrum seasons (1997/98 and 1998/99) are presented in Tables 7.11(a) and 7.11(b). Appendix G shows the graphical presentation of the results. Tables 7.11(a) and 7.11(b) show the method, which returned the highest contribution to classification for the minimum effective level of training data. The

quality (homogeneity) of the input data sets was reflected in the standard deviation (SD) statistics obtained from ERDAS Imagine (Version 8.4)®.

Using 90% of the total amount of data available for training, the Landsat TM 02 July 1997 image showed that the PCA method returned a contribution to classification of only 61% for pyrethrum (Table 7.11 (a)). This result was not significantly different (P = 0.51), from the 51% contribution by the AIARR method (Figure G.1, Appendix G) for the equivalent amount of training data.

In the Landsat TM 06 October 1997 image, with 90% of the total amount of pyrethrum data available used for training, a contribution to classification of only 68% was achieved with the PCA method (Table 7.11 (a)). This result was not significantly different (P = 0.43) from the 40% contribution to classification with the AIARR and the 23% contribution to classification with the NDVI methods (Figure G.2, Appendix G).

Using 90% of the total amount of pyrethrum data available for training, the Landsat TM 23 November 1997 image showed that the NDVI method returned a contribution to classification of 100% (Table 7.11 (a)). This result was not significantly different (P = 0.59) from the 73% contribution to classification with the PCA method and 61% contribution to classification with the AIARR method (Figure G.3, Appendix G) for the equivalent amount of training data.

Table 7.11 (a): Summary of the method which returned the highest contribution to classification for the minimum effective level of training data for the 1997/1998 pyrethrum season

Image	Method	Contribution to Classification (%)	Amount of Training Data (%)	Standard Deviation of Input Data
TM 02 July 1997	PCA	61	90	Layer 1 ± 15.0 Layer 2 ± 10.285 Layer 3 ± 4.551
TM 06 October 1997	PCA	68	90	Layer 1 ± 13.530 Layer 2 ± 13.114 Layer 3 ± 4.182
TM 23 November 1997	NDVI	100	90	Layer 1 ± 15.60
TM 10 January 1998	NDVI	81	40	Layer 1 ± 14.662
XS 23 February 1998	PCA	79	90	Layer 1 ± 7.252 Layer 2 ± 5.556
XS 18 April 1998	PCA	61	90	Layer 1 ± 9.342 Layer 2 ± 5.159

Table 7.11 (b): Summary of the method which returned the highest contribution to classification for the minimum effective level of training data for the 1998/1999 pyrethrum season

Image	Method	Contribution to Classification (%)	Amount of Training Data (%)	Standard Deviation of Input Data
TM 21 July 1998	PCA	95	80	Layer 1 ± 14.307 Layer 2 ± 8.642 Layer 3 ± 3.70
TM 27 September 1998	NDVI	100	60	Layer 1± 21.158
XI 08 October 1998	PCA	96	90	Layer 1 ± 22.362 Layer 2 ± 22.359 Layer 3 ± 26.334
XI 31 December 1998	NDVI	93	40	Layer 1 ± 14.151
TM 29 January 1999	NDVI	79	30	Layer 1 ± 16.977
TM 03 March 1999	PCA	97	50	Layer 1 ± 19.625 Layer 2 ± 19.058 Layer 3 ± 14.884
XI 29 March 1999	NDVI	89	40	Layer 1± 28.296

In the Landsat TM 10 January 1998 image (Table 7.11 (a)), the use of 40% of the total amount of data available for training, returned a contribution to classification of 81% with the NDVI method. This result was significantly different (P = 0.006) from the PCA and AIARR methods. The PCA contributed only 50% (LSD = 1.38) and the AIARR 35% (LSD = 13.18) respectively, for the equivalent amount of training data (Figure G.4, Appendix G).

Using 90% of the total amount of data available for training, the SPOT XS 23 February 1998 image showed that the PCA method returned a contribution to classification of 79% for pyrethrum (Table 7.11 (a), Figure G.5, Appendix G). This result was significantly different (P = 0.02), from the 46% contribution by the NDVI method (LSD = 9.98) for the equivalent amount of training data. However, the result for the PCA method was not significantly different from the 54% contribution to classification obtained with the AIARR method (LSD = 1.21).

In the SPOT XS 18 April 1998 image, using 90% of the total amount of pyrethrum data available for training, a contribution to classification of only 61% was achieved with the PCA method (Table 7.11 (a)). This result was not significantly different (P = 0.59) from the 45% contribution by the NDVI method and the 58% contribution by the AIARR method (Figure G.6, Appendix G.).

With 80% of the total amount of data for pyrethrum available used for training, the Landsat TM 21 July 1998 image showed that the PCA method returned a contribution to classification of 95% (Table 7.11 (b)). This result was however, not significantly different (P = 0.99), from the 90% contribution by the NDVI and AIARR methods (Figure G.7, Appendix G) for the equivalent amount of training data.

In the Landsat TM 27 September 1998 image (Table 7.11 (b)), using 60% of the total amount of data available for training, a contribution to classification of 100%

with the NDVI method was returned. This was not significantly different (P = 0.25) from the PCA method, which contributed to 90% of the classification or the AIARR method, which contributed to 78% classification of pyrethrum, for the equivalent amount of training data (Figure G.8, Appendix G).

When 90% of the total amount of data available was used for training and the SPOT XI 08 October 1998 image were investigated, a contribution to classification of 96% was achieved using the PCA method (Table 7.11 (b)). This was not significantly different (P = 0.98) from the AIARR and NDVI methods, which contributed to 92% and 94% respectively, to the classification of pyrethrum for the equivalent amount of training data (Figure G.9, Appendix G).

Using 40% of the total amount of data available for training, the SPOT XI 31 December 1998 image showed that the NDVI method returned a contribution to classification of 93% (Table 7.11 (b)). This result was not significantly different (P = 0.35) from the PCA method, which contributed to 75% of the classification of pyrethrum or the AIARR method, which contributed to 70% of the classification of pyrethrum, (Figure G.10, Appendix G).

In the Landsat TM 29 January 1999 image (Table 7.11 (b)), the use of 30% of the total amount of data available for training returned a contribution to classification of 79% with the NDVI method. This was not significantly different from the AIARR method, which contributed to 74% of the classification of pyrethrum, for the equivalent amount of training data (Figure G.11, Appendix G). The NDVI result however, was significantly different (P = 0.001) from the PCA method (LSD = 12.15), which contributed to only 46% of the classification of pyrethrum.

With 50% of the total amount of data available used for training, the Landsat TM 03 March 1999 image showed that the PCA method returned a contribution to classification of 97% for pyrethrum (Table 7.11 (b)). This result was not significantly different (P = 0.37), from the 78% contribution by the AIARR

method. The contribution to classification of 90% with the equivalent amount of training data and the use of the NDVI method was also not significantly different from the PCA result (Figure G.12, Appendix G).

In the SPOT XI 29 March 1999 image, using 40% of the total amount of pyrethrum data available for training, a contribution to classification of 89% was achieved with the NDVI method (Table 7.11 (b)). However, this result was not significantly different (P = 0.70) from the PCA method, which contributed to 73% of the classification of pyrethrum or the AIARR method, which contributed to 77% of the classification of pyrethrum (Figure G.13, Appendix G).

For pyrethrum in two images, during the 1997/98 growing season, the selection of method was significant. The NDVI analyses of the Landsat TM 10 January 1998 image produced a significantly higher contribution to classification and a significantly lower contribution to classification in the SPOT XS 23 February 1998 image. Whereas in the 1998/99 season, in only one instance the method was significantly lower, (NDVI method for the Landsat TM 29 January 1999 image). This finding was considered in terms of quality and quantity of training data. It was noted that only 42 pyrethrum crops were surveyed in 1997/98, whereas 60 crops were surveyed with a wider distribution in the 1998/99 season (Figures 7.2 and 7.4). It was concluded therefore, that the selection of method was critical, when the total amount of training data was low and its distribution was limited. This is consistent with Shine and Wakefield (1999).

For imagery acquired in late December or early January, 40% of the total amount of pyrethrum data used for training, contributed on average, to the classification of 87% of the crop. This occurred when the data were analysed using the NDVI method (Figures G.4 and G.10). Examination of this finding and of the growth stage of the crop during this period, provide an explanation. During November through until early January, the pyrethrum crop underwent a rapid growth phase, and flowered in December, suggesting that the use of NDVI was particularly appropriate for monitoring during this vegetative development. This is consistent

with Davenport and Nicholson (1993), Marchetti and Ricotta (1994), Marchetti, *et al.* (1995) and Murthy, *et al.* (1996).

Further examination of the results presented in Table 7.11 showed that the selection of the PCA method was appropriate from late February until October. This coincided with the post harvest period when the crop was either dormant or when the crop had been removed from the area, resulting in little or no crop coverage. A contribution to an average classification of 80%, from the use of 90% of the total amount of data available for training (Figures G.2, G.6, G.7 and G.9, Appendix G) was obtained using the PCA technique. Whilst using 90% of the data available for training to achieve 80% classification does not seem successful, achievement of 100% classification was only possible using 100% of the data available for training. Given the high costs associated with collection of training data and the use of remote sensing as a method by which to recognise crops over a large area, if a certain level of error is acceptable, acquiring training data for 100% of the crop area is inefficient.

The relative success of the PCA was attributed to inherent characteristics of the analysis and the agronomic nature of the pyrethrum crop. The PCA technique was used to highlight anomalies in the data (Simpson 1990) and was adept at delineating fallow areas (Ceballos and Bottino 1997) or areas of low variance in multi-spectral space such as fire scars or monocrops (Noonan 1999). It was particularily suited to the analysis of pyrethrum crops for late February until October, as the crop area during this time had little crop coverage.

The inconsistencies to the above-mentioned conclusion, were the SPOT XI 29 March 1999 and Landsat TM 27 September 1998 images. In these two instances, the greatest contribution to classification from the least amount of training data was achieved using the NDVI method. Use of 40% of the total amount of pyrethrum data available for training achieved a contribution to classification of 89% in the SPOT XI 29 March 1999 image (Table 7.11, Figure G.13). In the Landsat TM 27 September 1998 image, using 60% of the total amount of data

available for training returned a 100% contribution to the classification of pyrethrum (Table 7.11, Figure G.8). The results obtained with the NDVI method in the SPOT XI 29 March 1999 and Landsat TM 27 September 1998 images were however, not significantly different, from those obtained with the PCA method.

As previously stated, in the Landsat TM 27 September 1998 image use of the NDVI method was not significantly different (P = 0.25) from the PCA method. When 60% of the total amount of data available was used for training, 90% contribution to the classification of pyrethrum was returned (LSD = 10.14, Figure G.8, Appendix G) using the PCA method. Similarly, in the SPOT XI 29 March 1999 image use of the NDVI method was not significantly different (P = 0.70) from the PCA method. When 40% of the total amount of data available was used for training, 73% contribution to classification of pyrethrum was returned (LSD = 17.59, Figure G.13, Appendix G) using the PCA method.

Whilst not significantly different, the increased contribution to classification of pyrethrum in the SPOT XI 29 March 1999 and Landsat TM 27 September 1998 images by the NDVI method, may be accounted for in terms of crop health. The XI 29 March 1999 and TM 27 September 1998 images fell within the second observation period (1998/99 season). Pethybridge and Hay (2001) identified *Phoma ligulicola* as the causal agent in the failure of many pyrethrum crops to produce economic yields. It has been documented, plants infected with disease show various signs of stress including temperature differences (Allen and Lonergan 1999), changes in reflectance due to water stress, photosynthetic reduction and leaf area index reduction (Nutter 2000). The PCA technique was no longer the most appropriate method for the classification of diseased crops, as differences in spectral response patterns of pyrethrum crops (and plants within crops) no longer exhibited a low variance within multi-spectral space.

This research found that, to achieve a classification accuracy of 87% for pyrethrum, the acquisition of Landsat or SPOT data in late December or early January, would require a NDVI analysis with 40% of the total pyrethrum area used as training (calibration) data (Figures G.4 and G.10). When the pyrethrum

crop was post harvest and dormant, it was necessary to use the PCA method and 90% of the total amount of data available for training, to achieve a classification accuracy of 80%. During the dormancy stage (late February to October), when crop health was suspected to be poor, use of 50% of the total amount of training data available returned a 90% contribution to the classification of pyrethrum (Figures G.8 and G.13).

CHAPTER 8

CONCLUSION

When the average spectral response pattern of poppies was examined, Landsat TM bands one, two, three and five in November and December and SPOT XS band two in February, provided peak pixel values for the poppy crop. This is consistent with Landsat TM bands one, two, three and five being generally responsive to the differentiation of vegetation from soils, assessment of vegetation vigour, chlorophyll absorption and vegetation and soil moisture measurements respectively. The values reflect during November, the poppy crops undergoing a rapid growth phase (elongation of internodes and branching). This was the fourth developmental phase.

SPOT XS band two in February also provided peak pixel values. The peak pixel values in SPOT XS band two corresponded to the poppy crops undergoing the sixth and final phase of development. During this phase the leaves senesced and the capsules obtained their characteristic dull bluish-green colour.

The average spectral response pattern of pyrethrum indicated that the significant increase in pixel value for the Landsat TM January image, in bands five and seven was characteristic, as was the peak in SPOT XI band two during December.

The significant increase in pixel values of Landsat TM bands five and seven in January corresponded to the Landsat TM bands being generally responsive to soil moisture measurements and hydrothermal mapping. It was during this time (January) that the crop was cut, windrowed and dried in the field, exposing areas of soil. The peak pixel values in SPOT XI band two, during December corresponded to the crop being in full flower.

Automatic internal average relative reflectance, principal components analysis and normalised difference vegetation index operations resulted in normal distribution of data, consequently the use of an unsupervised classification with parametric signatures was a valid operation in this research.

The F-probabilities associated with the proportional levels of training data for both poppy and pyrethrum crops over two seasons, was highly significant, for each of the three methods (AIARR, NDVI and PCA). Therefore, it was deduced that the amount of training data had a significant effect on the contribution to classification.

Whilst the proportional level of data used for training, significantly affected the contribution to classification, when the contribution to classification of the three methods (AIARR, NDVI and PCA) were analysed, in only a few instances, were the results significant.

For poppies, a significantly lower contribution to classification in the Landsat TM 27 September 1998 and TM 29 January 1999 images was attained with the use of the AIARR method, compared to the NDVI and PCA methods respectively. During September when the crop is in the leaf rosette or third phase, not only is chlorophyll highly active but also the dense rosette causes much of the light in the near-infrared part of the spectrum to be reflected.

The findings in this research confirm those of Green *et al* (1998) and Mather's (1987) conclusion that the most accurate classification of Landsat TM necessitates the calculation of principal components and band ratios. In January of 1999, high rainfall resulted in many crops lodging or exhibiting signs of disease, the PCA method was highly suitable as the fundamental spectral dimensionality of the six reflective bands essentially occupied the first three Eigenvectors. The first PC is associated with "brightness", PC2 is associated with "greenness" and PC3 with "wetness." For all Landsat TM imagery, between 98.482% and 99.474% of

variance was contained within the first three principal components. Therefore, the PCA method was able to explain the total variation in the data associated with the lodged crops.

For pyrethrum in January, a significantly higher contribution to classification of Landsat TM was attained with the use of the NDVI method compared to the AIARR and PCA methods. It was during this time that the crop was cut, windrowed and dried in the field, exposing areas of soil. As stated previously, indices are related to the contrasting reflectance of the green biomass in the visible and near-infrared parts of the spectrum. A significantly lower contribution to classification in the SPOT XS 23 February 1998 and Landsat TM 29 January 1999 images (the crop had been cut and harvested, exposing large areas of soil, and was progressing into a dormancy phase (Figure 3.9) where little to no growth occurred) was attained with the use of the NDVI method compared to the AIARR and PCA methods. It is during this time that there is little to no plant physiological activity. These results indicate that whilst the NDVI method is appropriate for pyrethrum crops, which have been harvested, it is not suitable for dormant pyrethrum crops.

The results for the second poppy season reflected similar trends to those obtained in the first growing season. However, overall, the contributions to classification were improved. The increase was attributed to the wider distribution of the poppy crops, which enabled a more representative sample to be analysed.

The results of using SPOT XS imagery for the classification of poppies were in contradiction to Turner and Congalton (1998), who reported that attempts to use the principal component database for SPOT XS data to map rice fields were unsuccessful, with two land types having a high potential for being misclassified as ploughed fields. Moreover, a large number of smaller areas were not discernable on SPOT XS imagery.

In this research, the poppy fields surveyed were between 2- 20 hectares, which ensured detection in a SPOT XS image. As classification was performed crop independently misclassification was and error only resulted where crop pixels were unclassified. The addition of more training data at any time did not necessarily lead to an "increase" in the number of pixels correctly classified, but to the classification of a "different" sample of pixels.

In this research, when 70% of the total amount of data available for training was used, both the PCA and NDVI methods returned a contribution to classification of 75% of the total poppy pixels. These results were similar to those from SPOT XS imagery in February, when the poppy crops had reached the sixth and final stage of development.

To achieve a classification accuracy of 90% for poppies, when the crop was in the fourth phase and the uptake of water and nutrients was most intensive or during the late fifth developmental phase (November or January), Landsat TM data required a PCA with 80% of the total poppy area used as training (calibration) data. To achieve a classification accuracy of 96% for poppies, when the crop underwent rapid vegetative growth or the early fifth developmental phase, (October or December), SPOT XI data required a NDVI analysis, with 50% of the total poppy area used as training data.

The classification of poppies on the North West Coast of Tasmania was consistent with Abdel-Razik *et al.* (1984) in that, the use of principal components analysis worked well for imagery corresponding to particular growth stages of the vegetation being studied. The analysis in this research was in agreement with Green *et al* (1998) and Mather (1987). The most accurate classification of poppies using Landsat TM in the North West Coast of Tasmania necessitated the calculation of principal components. The results were also consistent with the NDVI being sensitive to vegetative activity (Townshend and Justice 1998) and the PCA being a powerful tool in change detection (Dwivedi 1996). While PCA was

not, the most suitable method for SPOT XI data, it was however, able to provide an insight into the level of change within the ground cover.

For pyrethrum in two images during the 1997/98 growing season, the selection of preparation method was significant. In the Landsat TM 10 January 1998 image, the NDVI analysis resulted in a significantly higher contribution to classification. In the SPOT XS 23 February 1998 image, a significantly lower contribution to classification was attained with the NDVI method. Whereas in the 1998/99 season, in only one instance the preparation method was significantly lower, (NDVI method for the Landsat TM 29 January 1999 image). This finding was considered in terms of quality and quantity of training data. It was concluded that the selection of method was critical when the total amount of training data was low and its distribution was limited. This is consistent with Shine and Wakefield (1999).

To achieve a classification accuracy of 87% for pyrethrum, when the crop underwent a rapid growth phase, and flowering (late December or early January), Landsat TM data required a NDVI analysis with 40% of the total pyrethrum area used as training data. To achieve a classification accuracy of 80%, when the pyrethrum crop was post harvest and dormant, (late February to October) imagery required a PCA with 90% of the pyrethrum area used as training (calibration) data.

The use of NDVI was particularly appropriate for monitoring pyrethrum during late December through until early January. This coincided with the pyrethrum crop undergoing a rapid growth phase and flowering, suggesting that the use of NDVI was particularly appropriate for monitoring during rapid vegetative development. This was consistent with Davenport and Nicholson (1993), Marchetti and Ricotta (1994), Marchetti, *et al.* (1995) and Murthy, *et al.* (1996).

The PCA technique was used to highlight anomalies in the data (Simpson 1990) and was proficient at delineating fallow areas (Ceballos and Bottino 1997) or areas of low variance multi-spectral space such as fire scars or monocrops (Noonan 1999). It was therefore, relatively successful for the analysis of pyrethrum crops for late February until October, as the crop area during this time had little crop coverage.

The findings of this research were consistent with Peştemalci *et al* (1995), in that timely acquisition of imagery was required to achieve a satisfactory level of contribution to classification from training data of poppies and pyrethrum. The findings also reiterated Shine and Wakefield (1999) confirming that the choice of the training set (quality and quantity) had an influence on the success of the classification approach. Examination of the AIARR, NDIV and PCA methods, indicated that image analysis technique affected the success of a classification, to a lesser extent than timely acquisition of imagery and choice of training set. This was consistent with Green *et al* (1998) and Noonan (1999).

There are several benefits of using satellite imagery over other sources of geographic data available, such as aerial photography, field surveys and conventional maps. For example, nearly all satellite imagery is acquired digitally and there is no need for expensive data conversion before analysis. For large areas, satellite images are usually less expensive than aerial photography or field surveys.

Printed maps may be soon out-dated. In contrast, a satellite image is acquired rapidly and is the most up to date map available. The information it contains is accurate, objective and unbiased. In intensive cropping situations, such as field horticulture, the number of crop types, which are grown regularly in any paddock is large (for example, over twenty, including cereals and pasture, in the Tasmanian industry). Plant back problems with residues of herbicides applied to a previous crop can thus create difficulties, particularly with crop species sensitive to many herbicides, such as poppies. As markets demand documented proof of

crop production history, including assurance that products are free from residues, some of which may originate from applications to previous crops, industry requires adequate tracking of the exact location of crop plantings over the medium term. For these reasons, spatial recognition of crops is worthy of continuous improvement.

The probability that poppies and pyrethrum individually may be recognised with a high level of accuracy may be of most direct interest to stakeholders involved with those particular crops. The procedure may expedite crop recording by stakeholders and assist in making decisions about crop location from the point of view of pest and disease spread and crop hygiene. From this point of view, the information from the procedure is compatible with other digitally acquired industry information.

Programs to help producers with paddock recording based on aerial photographs/plans are available but these can be expensive and time-consuming to set up. The ever-pressing need to continue to reduce the costs of such crop monitoring as a best practice issue is not only an industry concern, but also a concern at the individual grower level.

Beyond recognition of the crops themselves, lay the potential recognition of patterns characteristic of growth, yield and pest and disease incidences or other agronomic limitations to crop growth. Such tools would add significantly to current developments referred to as 'precision agriculture'. With continually improving technology, crop recognition, growth, health monitoring and prediction of such agronomic influences are now considered achievable goals. This is already the case in larger areas of monoculture, such as rice.

This research has demonstrated that by selecting a specific remotely sensed data preparation method (AIARR, NDVI, or PCA) in relation to time of data acquisition, crop type and growth cycle, the high costs associated with collecting

ground truthing data can be reduced, and in turn enable the use of remote sensing data for crop recognition to become more cost effective.

REFERENCES

Abdel-Razik, M., Abdel-Aziz, M. and Ayyad, M. (1984). "Multivariate analysis of vegetational variation in different habitats at Omayed, Egypt." *Vegetatio*, 57(2-3), 167-175.

Agresti. (1990). *Categorical Data Analysis*, John Wiley and Sons.

Aigner, E., Coppa, I., and Wieneke, F. (2001). "Crop Yield Estimation Using NOAA - AVHRR Data and Meteorological Data in the Eastern Wimmera (South Eastern Australia)." *XIXth Congress of the International Society for Photogrammetry and Remote Sensing*, Amsterdam, The Netherlands, 19 - 26.

Ajai, D. S., Kamat, G.S., Chaturvedi, A.K., Singh. and Sinha, S.K. (1983). "Spectral assessment of leaf area index, chlorophyll content, and biomass of chickpea." *Photogrammetric Engineering and Remote Sensing*, 49, 1721-1727.

Allen, S. J., and Lonergan, P.A. (1999) "Thermal imagery for the detection of Fusarium wilt of cotton." *Asia- Pacific Plant Pathology for the New Millennium*, Rydges, Canberra, Australian Capital Territory, Australia, 47.

Anon. (1994). "A Brief history: Poppy Industry Pioneers." *DAAPR/GLX 8-85.*

Anon. (2000). "Draft Regulatory Impact Statement, Proposed Poppy Industry Act." *http://www.justice.tas.gov.au/pacb/ris.htm.*

Anon. (2001). "A Short History, Poppy Control and Advisory Board." *Department of Justice and Industrial Relations, Tasmania. http://www.justice.tas.gov.au/pacb/history.htm.*

Atkinson, P. (1985) "Preliminary results of the effect of resampling on thematic mapper imagery." Falls Church, Virginia.

Australia Map http://www.expedia.com/pub/agent.dll

Barrett, R. M., Crowther, P., Laurence, R.C.N and Lincolne, R. (2000) "Agricultural Crop Identification Using SPOT and LANDSAT Images in Tasmania." *International Society for Photogrammetry and Remote Sensing XIXth Congress.* Amsterdam, The Netherlands, 133-139.

Bauer, M. E., Burk, T.E. Ek, A.R., Coppin, P.R., Lime, S.D., Walsh, T.A., Walters, D.K., Befort, W. and Heinzen, D.F. (1994). "Satellite inventory of Minnesota forest resources." *Photogrammetric Engineering & Remote Sensing*, 60(3), 287-298.

Beaubien, J. (1994). "Landsat TM satellite images of forests: From enhancement to classification." *Canadian Journal of Remote Sensing*, 20(1), 17-27.

Bellairs, S. M., Turner, N.C., Hick, P.T. and Smith R.C.G. (1996). "Plant and soil influences on estimating biomass of wheat in plant breeding plots using field spectral radiometers." *Australian Journal of Agricultural Research*, 47(7), 1017 - 1134.

Bernath, J. and Nemeth, E. (1998). "Physiological- Ecological aspects." Poppy The Genus Papaver, J. Bernath, ed., Harwood Academic Press, Amsterdam, The Netherlands, 65-91.

Bhat, B. K. and. Menar, R.C. (1984). "Pyrethrum production in Australia: It's past and present potential." *Journal of the Australian Institute of Agricultural Science*, 50(3), 189 - 192.

Birth, G. S., and McVey, G. (1968). "Measuring the colour of growing turf with a reflectance spectrophotometer." *Agronomy Journal*, 60, 640-643.

Blasco, F., Lavenu, F. and Baraza, J. (1986) "Remote sensing data applied to mangroves of Kenya Coast." *International Symposium on Remote Sensing of the Environment*, 1465 - 1480.

Brown, P. H. (1990). "Morphological and physiological aspects of flower initiation and development in *Tanacetum cinerariaefolium* L.," PhD, University of Tasmania.

Bureau of Meteorology (2001) http://www.bom.gov.au

Button, B. J. (2001). "Satellite Imagery as a Data Source for Prescription and Precision farming in Australia." *Geospatial Information and Agriculture*, Austalian Technology Park, Eveleigh, Sydney.

Byun, H. G., Persaud, K.C., Khaffaf, S.M., Hobbs, P.J., Misselbrook, T.H., (1997). "Application of unsupervised clustering methods to the assessment of malodour in agriculture using an array of conducting polymer odour sensors." *Computers and Electronics in Agriculture*, 17(2), 233-247.

Campbell, J. B. (1996). *Introduction to Remote Sensing*, Taylor & Francis, London.

Casida, J. E. and Quistad, G. B. (1995). *Pyrethrum flowers, production, chemistry toxicology and uses*, Oxford University Press, New York.

Ceballos, J.C. and Bottino, M.J. (1997). "The discrimination of scenes by principal components analysis of multi-spectral imagery." *International Journal of Remote Sensing*, 18(11), 2437 - 2449.

Chavez, P. S., Guptill, S.C. and Bowell, J. (1984) "Image processing techniques for Thematic Mapper Data." *50th Annual ASP-ACSM Symposium*, Washington, D.C., 728 - 743.

Chavez, P.S. and Kwarteng, A.Y. (1989). "Extracting spectral contrast in Landsat Thematic Mapper image data using selective principal component analysis." *Photgrammetric Engineering and Remote Sensing*, 55(3), 339-348.

Clarke, R.N. and Roush, T.L. (1984). "Reflectance Spectroscopy: Quantitative Analysis Techniques for Remote Sensing Applications." *Journal of Geophysical Research*, 89(B7), 6329 - 6340.

Cohen, J. (1960). "A coefficient of agreement for nominal scales." *Educational and Psychological Measurement*, 20(1), 37 - 46.

Cohen, W.B. and Spies, T.A. (1992). "Estimating structural attributes of Douglas-fir/western hemlock forest stands from Landsat and SPOT imagery." *Remote Sensing of the Environment*, 41(1), 1-17.

Collins, J.B. and Woodcock, C.E. (1996). "An assessment of several linear change detection techniques for mapping forest mortality using multi temporal Landsat TM data." *Remote Sensing of Environment*, 56(1), 66-77.

Colwell, R. N. (1983). "Manual of Remote Sensing.", American Society of Photogrammetry, Falls Church, Virginia.

Congalton, R. G., Oderwald, R.G. and Mead, R. A. (1983). "Assessing Landsat classification accuracy using discrete multivariate statistical techniques." *Photogrammetric Engineering and Remote Sensing*, 49(12), 1671 - 1678.

Congalton, R. G. (1991). "A review of assessing the accuracy of classifications of remotely sensed data." *Remote Sensing of Environment*, 37(1), 35-46.

Corner, R. J., Cook, S.E., Wheaton, G.A., and Caccetta, P.A. (1998). "The effect of scale on the utility of remotely sensed grain yield estimates." Sydney.

Crist, E.P. and Cicone, R.C.. (1984a). "Application of the tasseled cap concept to simulated Thematic Mapper data." *Photogrammetric Engineering and Remote Sensing*, 50(3), 343 - 352.

Crist, E.P. and Cicone, R.C. (1984b). "A physically-based transformation of Thematic Mapper data - The TM tasseled cap." *IEEE Transactions on Geoscience and Remote Sensing*, GE 22(3), 256 - 263.

Cruz-Castillo, J. G., Ganeshanandam, S., MacKay, B.R., Lawes, G.S., Lawoko, C.R.O. and Woolley, D.J. (1994). "Applications of canonical discriminant analysis in horticultural research." *HortScience*, 29(10), 1115-1995.

Davenport, M. L. and Nicholson, S. E. (1993). "On the relation between rainfall and the Normalised Difference Vegetation Index for diverse vegetation types in East Africa." *International Journal of Remote Sensing*, 14(12), 2369 - 2389.

Davies, J. L. (1965). "Atlas of Tasmania." Lands and Surveys Department, Hobart, Tasmania, 128.

Deering, D. W., Rouse, J.W., Haas, R.H. and Schell, J.A. (1975). "Measuring forage production of grazing units from Landsat MSS data." *Tenth International Symposium on Remote Sensing of Environment*, 1169-1179.

Dwivedi, R. S., Sankar, T.R., Venkataratnam, L. and Rao, D.P. (1993). "Detection and delineation of various desert terrain features using Landsat-TM derived image transforms." *Journal of Arid Environments*, 25(1), 151-162.

Dwivedi, R. S. (1996). "Monitoring of salt-affected soils of the ino-Gaangetic alluvial plains using principal component analysis." *International Journal of Remote Sensing*, 17(10), 1907-1914.

Eastman, R. J. (1993). "IDIRISI 4.1 Update Manual." Clark University, Graduate School of Geography.

Elachi, C. (1987). *Introduction to the Physics and Techniques of Remote Sensing*, John Wiley and Sons, New York.

Fassnacht, K. S., Gower, S.T., MacKenzie, M.D., Nordheim, E.V. and Lillesand, T.M. (1997). "Estimating the leaf area index of North Central Wisconsin forests using the Landsat Thematic Mapper." *Remote Sensing of Environment*, 61(2), 229-245.

Faust, N. L. (1989). "Image Enhancement." Encyclopedia of Computer Science and Technology, A. a. W. Kent, J.G., ed., Marcel Dekker, Inc., New York.

Fiorella, M. and Ripple, W. J. (1993). "Determining successional stage of temperate coniferous forests with Landsat satellite data." *Photogrammetric Engineering & Remote Sensing*, 59(2), 239-246.

Fist, A. J. (2001). "The Tasmanian Poppy Industry: A Case Study of the Application of Science and Technology." *Proceedings of the 10th Australian Agronomy Conference,* Hobart http://www.regional.org.au/au/asa/2001/plenery/1/fist.htm

Flaschka, H. A. (1969). *Quantitative Analytical Chemistry:* Barnes and Noble Inc, New York.

Franklin, S. E., Connery, D.R. and Williams, J.A. (1994). "Classification of alpine vegetation using Landsat Thematic Mapper SPOT HRV and DEM data." *Canadian Journal of Remote Sensing*, 20(1), 49-58.

Fulton, D., Clark, R. and Fulton, A. (2001). "Effects of plant population on pyrethrins yield of pyrethrum, (Tanacetum cinerariifolium) in Tasmania." *Proceedings of the 10th Australian Agronomy Conference*, Hobart. http://www.regional.org.au/au/asa/2001/2/d/fulton.htm

Gong, P., Marceau, D.J. and Howarth, P.J. (1992). " A comparison of spatial feature extraction algorithms for landuse classification using SPOT HRV data." *Remote Sensing of the Environment*, 40(2), 137 - 151.

Gonzalez, R.C. and Wintz, P. (1977). *Digital Image Processing*, Addison-Wesley Publishing Company, Reading, Massachusetts.

Green, E. P., Clark, C.D., Mumby, P.J., Edwards, A.J., and Ellis, A.C. (1998). "Remote sensing techniques for mangrove mapping." *International Journal of Remote Sensing*, 19(5), 935-956.

Hedges, D. A., and Vickery, P.J. (1987) "Use of a principal components strategy as the basis for an unsupervised classification routine to examine Landsat data from grassland vegetation." *4th Australasian Remote Sensing Conference "Operational remote sensing and the aerospace industry"*, Adelaide Convention Centre, North Terrace, Adelaide, South Australia, 178-188.

Heermann, D. F., Buchleiter, G.W., and Fleming, K.L. (1998) "Multidisciplinary team research of irrigated precision farming" *First International Conference on Geospatial Information in Agriculture and Forestry*, 140 - 147.

Hoffer, J. A., George, J.F and Valacich, J.S. (1999). *Modern Systems Analysis and Design*, Addison Wesley.

Hord, R. M. (1982). *Digital Image Processing of Remotely Sensed Data*, Academic Press, New York.

Hobma, T. J. (1995). Merging SPOT for landscape-ecological studies, applied to a coastal dune environment. *Journal of Coastal Research* 11 (4):1003-1019.

Hyde-Wyatt, B. H. (1989). *Tasmanian Weed Handbook: A guide to the identification of the main broad-leaf weeds of crops and pastures in Tasmania.*, Department of Agriculture, Tasmania.

Isbell, R. F. (1996). *The Australian Soil Classification*, CSIRO Publishing, Collingwood, Victoria.

Jensen, J. R. (1996). *Introductory Digital Image Processing: A Remote Sensing Perspective*, Prentice-Hall, Englewood Cliffs, New Jersey.

Jones, L. C. (1982) "Chemicals - Friend or Foe." *1982 Let us spray - Weeds. Bugs and Deadly Potions 25 years of the Riverina Outlook Conference,* Wagga Wagga 1973-1998.

Jupp, D. L. B., and Mayo, K.K. (1982). "The use of residual images in Landsat image analysis." *Photogrammetric Engineering and Remote Sensing*, 48(4), 595-604.

Jupp. D.L.B., H., S.J., Mayo, K.K., Kendal, S.W., Bolton, J.R., Harrison, B.A. (1985). *The BRIAN Handbook: An introduction to Landsat and the BRIAN (Barrier Reef Image Analysis) System for Users*, Institute of Biological Resources; Commonwealth Scientific and Industrial Research Organisation, Canberra. A.C.T.

Kabay, J. J. (1990). *Janos Kabay - The Life of an Inventor*, John Kabay, Harbord.

King, S. M. (1994). "Patter About Poppies." GlaxoWellcome.

Kittler, J. and Young, P.C. (1973). "A new approach to feature selection based on the Karhunen-Loeve expansion." *Pattern Recognition*, 5(4), 335 - 352.

Kloer, B. R. (1994) "Hybrid parametric/non-parametric image classification." Reno, Nevada.

Köhler, F. E. (1887). *Köhler's Medizinal-Pflanzen in naturgetreuen Abbildungen mit kurz erläuterndem Texte*, Gera-Untermhaus.

Koppi, A. J. (1994). "The Soil Resource." Department of Agricultural Chemistry and Soil Science, University of Sydney, Sydney, 167.

Kuhnell, C. and Danaher, T. (1996). "Mapping broadacre cropping areas in Queensland Using Landsat TM and NOAA AVHRR Imagery." *8th Australasian Remote Sensing and Photogrammetry Conference* , Canberra.

Lamb, D. W. (2000). "The use of qualitative airborne multispectral imaging for managing agricultural crops - a case study in south-eastern Australia." *Australian Journal of Experimental Agriculture*, 40(5), 725 - 738.

Lark, R. M. (1995). "A reappraisal of unsupervised classification, I: correspondence between spectral and conceptual classes." *International Journal of Remote Sensing*, 16(8), 1425 - 1443.

Laughlin, J. C., Chung, B., and Beattie, B. M. (1998). Poppy cultivation in Australia. In *Poppy The Genus Papaver*, edited by Bernath, J. Amsterdam, The Netherlands: Harwood Academic Press.3:249 - 277

Laurence, R. C. N., Barrett, R.M., Crowther, P. and Linclone R. (2001). "Remote Sensing as an Aid to Horticultural Crop Recording and Husbandry." *Final Report to Horticulture Australia Ltd. HRDC VG97011,* University of Tasmania, Tasmanian Institute for Agricultural Research.

Lee-Lovick, L.G. and Kirchner L (1990). "The application of remotely sensed (Landsat TM) data to monitor growth and predict yields in sugarcane." *Proceedings of Australian Society of Sugar Cane Technologists*, 65 - 71.

Lee-Lovick, L.G. and Kirchner L (1991). . "Limitations of Landsat TM data in monitoring growth and predicting yields in sugarcane." *Proceedings of Australian. Society of Sugar Cane Technologists*, 124-130.

Lillesand, T.M. and Kiefer, R.W. (1994). *Remote Sensing and Image Analysis*, Wiley and Sons, London.

Manière, R. and Courboulès, J. (1989). "Comparative performance results between Landsat Thematic Mapper and SPOT 1 High Resolution Visible imagery for Mediterranean forest inventory." *Advances in Space Research*, 9(1), 125-134.

Marchetti, M., Ricotta, C. and Volpe, F. (1995). "A qualitative approach to the mapping of post-fire regrowth in Mediterranean vegetation with Landsat TM data." *International Journal of Remote Sensing*, 16(13), 2487 - 2494.

Marchetti, M and Ricotta, C. (1994). " The use of remote sensing data to compile a register of fires in Mediterranean areas." *Monti e Bosch*, 45(1), 5 - 10.

Mather, P. M. (1987). *Computer Processing of Remotely sensed Images: An Introduction*, John Wiley, Chichester.

Mather, P. M. (1991). *Computer Applications in Geography*, John Wiley and Sons, Chichester.

Mazzoleni, S., French, D.D. and Miles, J. (1991). "A comparative study of classification and ordination methods on successional data." *COENOSES*, 6(2), 91 - 101.

McBratney, A. B. (1993). "Rudiments of Soil Sampling and Data Analysis." Soil Technology: Applied Soil Science, P. A. Hazelton, and Koppi, A.J., ed., Australian Society of Soil Science Inc., Sydney, 103 - 133.

Mead, R. and Curnow, R.N. (1987). *Statistical Methods in Agriculture and Experimental Biology*, Department of Applied Statistics, University of Reading, Chapman and Hall, London.

Murthy, C. S., Thiruvengadachari, S., Raju P.V. and Jonna, S. (1996). " Improved ground sampling and crop yield estimation using satellite data." *International Journal of Remote Sensing*, 17(5), 945 - 956.

Nieuwenhuis, G. J. A., Muncher, C.A., de Wit, A.J.W. (1996). "Monitoring of land use and crop growth conditions in Europe." *127*, DLO Winand Staring Centre (SC-DLO), Wageningen, Netherlands.

Noonan, M. (1999). "Classification of Fallow and Yields using Landsat TM data in the Sugarcane Lands of the Herbert River Catchment." *http://hric.tag.csiro.au/information/publications/index.html*, Herbert Resource Information Centre.

Nutter, F. W. J. (2000). "Quantifying and modelling biotic plant stress." Personal Communication.

Orlóci, L. (1966). "Geometric models in ecology I. The theory and application of some ordination methods." *The Journal of Ecology*, 54, 193 - 215.

Parsons, W. T., and Cuthbertson, E. G. (1992). *Noxious Weeds of Australia*, Inkarta Press, Melbourne.

Perakis, K. M., I. and Silleos, N. (1998) "Qualitative and spatial comparative study of satellite images classified by supervised and fuzzy logic based classification algorithms: A case study in Kilkis prefecture, Central Macedonia, Greece." *Control Applications and Ergonomics in Agriculture (CAEA '98)*, Athens, Greece, 195-200.

Pestemalci, V., Dinc, U.,Yegingi, I., Kandirmaz, M., Cullu, M.A., Ozturk, N. and Aksoy, E. (1995). Acreage estimation of wheat and barley fields in the province of Adana, Turkey. *International Journal of Remote Sensing* 16 (6):1075-1085.

Pethybridge, S.J. and Hay, F.S. (2001). "Influence of *Phoma ligulicola* on yield, and site factors on disease development, in Tasmanian pyrethrum crops." *Australasian Plant Pathology*, 30(1), 17-20.

Pouncey, R., Swanson, K. and Hart, K. (1999). "ERDAS Field Guide." R. Pouncey, Swanson, K. and Hart, K., ed., ERDAS Inc, Atlanta, Georgia, 672.

Pratt, W. K. (1991). *Digital Image Processing*, John Wiley and Sons, Inc, New York.

Reid, R. N. D., Vickery, P.J., Hedges, D.A., and Williams P.M. (1993). "Measuring the response of pasture to superphosphate using aircraft and satellite remote sensing." *Australian Journal of Experimental Agriculture*, 33(5), 597-600.

Richards, J. A. (1993). *Remote Sensing Digital Image Analysis: An Introduction*, Springer-Verlag, Berlin.

Rouse, J. W., Haas, R.H., Schell, J.A. and Deering, D.W. (1974). Monitoring vegetation systems in the Great Plains with ERTS. *Third Earth Resources Technology Satellite-1 Symposium.* NASA SP-351:309-317.

Saha, S. K., Kudrat, M. and Bhan, S.K. (1990). "Digital processing of Landsat TM data for wasteland mapping in parts of Aligarh District (Uttat Pradesh), India." *International Journal of Remote Sensing*, 11(3), 485-492.

Salardini, A. A. (2001). "The effect of hybrids, soil types and applied phosphorous on the growth and tissue composition of pyrethrum (Tanacetum cinerariifolium L.)." *Proceedings of the 10th Australian Agronomy Conference,* Hobart. http://www.regional.org.au/au/asa/2001/2/c/salardini.htm

Scott, J. B. (2001a). "Control of Downy Mildew in Tasmanian Crops." Personal Communication.

Scott, J. B., Hay, F.S., Wilson, C.R., Cotterill, P.J. and Fist, A.J. (2001) "Epidemiology of downy mildew of oilseed poppy in Tasmania." *Proceedings of the 13th Biennial Conference of the Australian Plant Pathology Society*, 303.

Shine, J. A. and Wakefield, G.I. (1999). "A comparison of supervised imagery classification using analyst-chosen and geostatistically-chosen training sets." GeoComputation 99, Alexandria, VA, USA. http://www.geovista.psu.edu/geocomp/geocomp99/Gc99/044/gc_044.htm

Simpson, C. J. (1990). "Deep weathering, vegetation and fireburn. Significant obstacles for geoscience remote sensing in Australia." *International Journal of Remote Sensing*, 11(11), 2019 - 2034.

Skidmore, A. J. (1989). "An expert system classifies eucalypt forest types using Thematic Mapper data and a digital terrain model." *Photogrammetric Engineering and Remote Sensing*, 55(10), 1449-1464.

Smith, R. C. G. (1994). "Australian Vegetation Watch, Near Real Time Satellite Information for Vegetation Management." *RIRDC reference No. DOL-1A.*

Smith, R. C. G., Adams, J., Stephens, D.J., and Hick, P.T. (1995). "Forecasting wheat yield in a mediterranean-type environment from the NOAA satellite." *Australian Journal of Agricultural Research*, 46(1), 113 - 125.

Smith, R. G. C., Stovold, R.G.H., Wheaton, G.A., Caccetta, P.A. and Evans, F. (1998) "AGIMAGE- mapping of within-field variability of crop yield from high resolution satellite data." 9th Australasian Remote Sensing and Photogrammetry Conference, Sydney.

Spackman, S., McKenzie, G., Lamb, D., and Louis, J. (2000)."Retrieving biophysical data from airborne multispectral imagery of rice crops." *XIXth Congress of the International Society for Photogrammetry and Remote Sensing*, Amsterdam, The Netherlands, 1447-1451.

Star, J. and Estes J. (1990). *Geographic Information Systems: An Introduction*, Prentice-Hall, Englewood Cliffs, New Jersey.

Stern, H., de Hoedt, G. and Ernst, J. (2001). "Objective Classification of Australian Climates http://www.bom.gov.au/climate/environ/other/koppen_explain.shtml.

Stoney, W. E. (1996) "Land observation satellites in the next ten years." Agriculture in the 21st Century; Proceedings of the Workshop on Remote Sensing at University of California, Davis, California. http://cstars.ucdavis.edu/proj/ag-21/ag21cen.html.

Story, M., and Congalton, R.G. (1986). Accuracy assessment: A user's perspective. *Photogrammetric Engineering & Remote Sensing* 52 (3):397 - 399.

Stovold, R. C. H., Smith, R.C.G., Allen, A and Evans, F. (1996) "A high resolution satellite information product for farm and catchment management in Western Australia." *8th Australasian Remote Sensing Conference,* Canberra.

Swain, P.H. and Davis, S.M. (1978). "Remote Sensing: The Quantitative Approach." , McGraw-Hill International Book Co., c1978 Company, London.

Swan, J. M. A. (1970). "An examination of some ordination problems by use of simulated vegetational data." *Ecology*, 51, 89 - 102.

Temple-Smith, M. G., Wright, D.N., Laughlin, J.C. and Hoare, B.J. (1982) "Effect of liming acid krasnozems on the yield of poppy (Papaver somniferum L.)." *Agronomy Australia*, Rivererina College of Advanced Education, Wagga Wagga, 261.

Torigoe, Y., Amano, T., Ogawa, K. and Fukuharam, M. (1992). "Discrimination of cabbage fields for detecting clubroot disease damage using Landsat Thematic Mapper Data." *Japanese Journal of Crop Science*, 6(3), 527-535.

Tou, J.T. and Gonzalez, R.C. (1974). *Pattern Recognition principles*, Addison-Wesley, Reading, MA.

Townshend, J. R. G. and Justice, C.O. (1995). "Spatial Variability of images and the monitoring of changes in the Normalised Difference Vegetation Index." *International Journal of Remote Sensing*, 16(12), 2187-2195.

Tucker, C. J. (1979). "Red and photographic infrared linear combinations for monitoring vegetation." *Remote Sensing of Environment*, 10(1), 127-150.

Tucker, C. J., Elgin, J.H., and McMurtrey, J.E. (1980). "Relationship of crop radiance to alfalfa agronomic values." *International Journal of Remote Sensing*, 1(1), 69-75.

Turner, M. D., Congalton, R.G. (1998). "Classification of multi-temporal SPOT-XS satellite data for mapping rice fields on a West African floodplain." *International Journal of Remote Sensing*, 19(1), 21-41.

Vickery, P. J., Hedges, D.A., Duggin, M.J. (1980). "Assessment of the fertilizer requirement of improved pasture from remote sensing information." *Remote Sensing of Environment*, 9(2), 131-148.

Vickery, P. J. (1983) "Use of satellite data to monitor fertility status of improved pastures." *The First National Conference on Computers in Agriculture*, University of Western Australia, 337.

Walker, M. R., Thorp, J.R. and Peacock, F.S. (1977). "*Report on poppy seedling damage in autumn sown crops in the Midlands 1976/77 season.*" Tasmanian Department of Agriculture.

Wallender, W. W. (1996). *Remote sensing data, agricultural and ecological models, and the balance between profitability and the environment. Lecture Outline/Papers from the Workshop on Remote Sensing for Agriculture in the 21st Century.* (Internet). University of California, October 23 - 25, 1996 (last viewed 2000). Available from http://cstars.ucdavis.edu/proj/ag-21/lect0912.pdf.

Wiegand, C., Anderson, G., Lingle, S., and Escobar, D. (1996). "Soil salinity effects on crop growth and yield - illustration of an analysis and mapping methodology for sugarcane." *Journal of Plant Physiology Special issue: vegetation stress II. First international symposium on vegetation stress, Munich, Germany, 19-21 June 1995.*, 145(3-4), 418 - 424.

Williams, R. S. (1983). "Geological Application." Manual of Remote Sensing, American Society of Photogrammetry, 1667 - 2100.

Young, C.L. and Armstrong, G.D. (2001) "Slugs, snails and iron based baits: An increasing problem and a low toxic specific action solution." *Proceedings of the 10th Australian Agronomy Conference*, Hobart. http://www.regional.org.au/au/asa/2001/6/c/young.htm.

APPENDIX A

TECHNICAL SENSOR DETAILS

A.1 Landsat 5 TM Satellite Platform and Sensor Characteristics

The Landsat series of satellites (operated by the Earth Resources Observation Systems (EROS) Data Center (EDC) of the United States Geological Survey (USGS)) was the first commercially viable system of land-use satellites, initially run by NASA as an experiment. The first Landsat satellite was launched in July 1972.

Landsat 5 (Figure A.1), launched on 01 March 1994, operates from a repetitive, circular, sun-synchronous, near-polar orbit and on each day-side pass, scans a ground swath 185 km wide beneath the satellite, and operates at a nominal altitude of 705km.

Figure A.1: Landsat 5 satellite

Landsat 5 has a repeat cycle of 16 days and has an equatorial crossing at approximately 10 am local time. Landsat 5 satellite acquires data from a multi-spectral Scanner (MSS) and a thematic mapper (TM) sensor. Australian Centre for Remote Sensing (ACRES) data reception for TM was effective from 1987 until 1999 and MSS data from 1979 until 1997.

The Landsat TM sensor bands utilised in this project provide information on the Earth's surface in the visible, near, middle and thermal infrared regions of the electromagnetic spectrum (Figure A.2). The TM scanner, which first appeared on Landsat 4 in 1982, was designed to provide improved spectral and spatial resolution over the MSS instrument. The basic mode of operation is similar, however the use of more sensitive detectors, better optics and a lower orbit has enabled the collection of radiation in seven spectral bands and improved ground resolution.

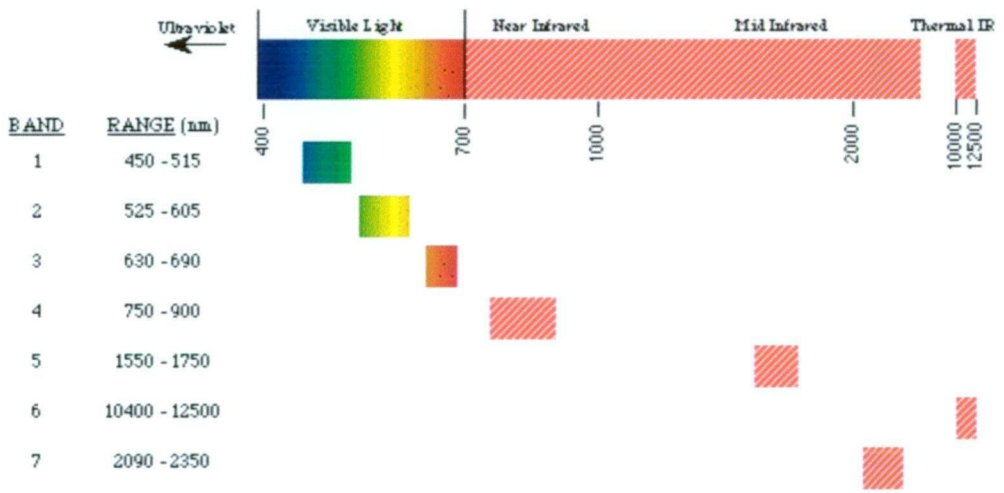

Figure A.2: Landsat 5 Thematic Mapper Bands

Data is collected using banks of 16 detectors in each band and 16 lines of data are collected during both the forward and backward sweeps of the oscillating mirror system. In the TM scanner's seven spectral modes, bands from one to six are chosen primarily for vegetation monitoring and Band 7 for geological applications. Table A.1 outlines the band designations, spectral ranges and principal applications.

Each full TM scene covers an area of approximately 185km EW by 170km NS. The pixel (picture element) resolution of the TM scanner is 30 metres for Bands one to five and seven, and 120 metres for Band 6. TM scenes are designated in a path/row system referred to as the Landsat Worldwide Reference System (WRS). Data is collected in a continuous stream along a near vertical path as the satellite moves from north to south. The data is arbitrarily divided into nominal scenes, which are about 24 second increments of spacecraft time apart, corresponding to a spacing of approximately 160km. The rows have been positioned in such a way that Row 60 coincides with the equator. Landsat path designations increase from east to west while SPOT are the reverse.

Table A.1:Band designations, spectral ranges and applications of Landsat 5 TM

Band Number	Spectral Range (nm)	Electromagnetic region	Generalised Application Details
1	450 – 515	Blue	Coastal water mapping, differentiation of vegetation from soils
2	525 – 605	Green	Assessment of vegetation vigour
3	630 – 690	Visible Red	Chlorophyll absorption for vegetation differentiation
4	750 – 900	Near Infrared	Biomass surveys and delineation of water bodies
5	1555 – 1750	Middle Infrared	Vegetation and soil moisture measurements: differentiation between snow and cloud
6	10400 - 12500	Thermal Infrared	Thermal mapping, soil moisture studies and plant heat stress measurement
7	2090 – 2350	Middle Infrared	Hydrothermal mapping

A.2 SPOT Satellite Platform and Sensor Characteristics

The SPOT series of satellites is a joint venture between French, Swedish, and German organisations, operated by the Toulouse (France) based company, SPOT

Image. The first SPOT satellite was launched in February 1986 by the French Government Agency, Centre National d'Etudes Spatials (CNES). SPOT 2 and SPOT 4 were launched in 1990 and 1998 respectively. They operate from a repetitive, circular, sun-synchronous, 99 degree inclination, near polar orbit and on each day-side pass, scan a ground swath 60km wide (at vertical viewing) and 85km (at 27 degrees off-nadir viewing), and operate at a nominal altitude of 832km.

SPOT 2 and SPOT 4 (Figure A.3) are each fitted with two identical High Resolution Visible (HRV) scanners, each able to function independently with two modes of operation. These are multispectral modes (XS and Xi) with a pixel size of twenty metres, and a panchromatic (PAN) or monochromatic mode with a pixel size of ten metres.

Figure A.3: SPOT 2 and 4 Satellites

Data from the SPOT series have been recorded over Australia by ACRES since May 1990, although not every pass is routinely acquired. The SPOT series have a repeat cycle of 26 days and an equatorial crossing of approximately10.40 hrs local time. The SPOT 2 and SPOT 4 sensor bands utilised in this project provide information on the Earth's surface in the visible, near and short wave infrared regions of the electromagnetic spectrum (Figure A.4).

Each HRV scanner contains two rows of detectors moving along a path in a "push broom" technique, resulting in high geometric accuracy within a swath. One row comprises 3000 detectors to measure reflected radiation in multispectral (XS, Xi) mode with the other 6000 detectors measuring reflected radiation in panchromatic (Pan) mode. Table A.2 outlines the band designations, spectral ranges and principal applications.

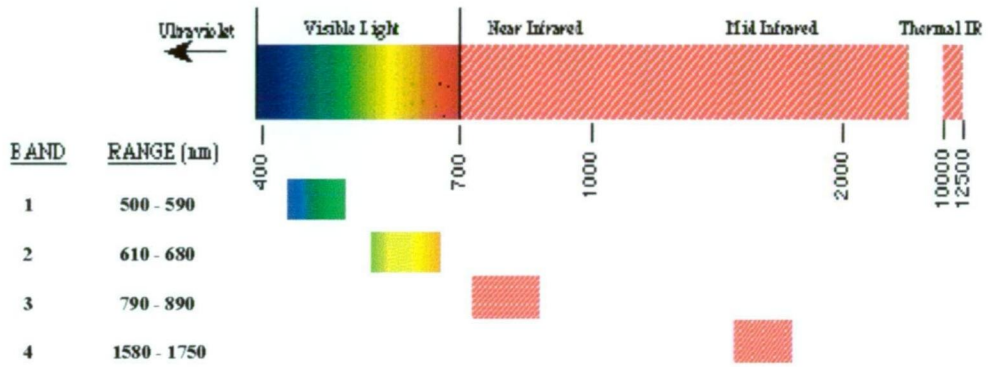

Figure A.4: SPOT XS and XI HRV Bands. Band 4 is available on SPOT 4 only.

Table A.2: Band designations, spectral ranges and applications of SPOT XS and XI sensors. Xi4 band is available on SPOT 4 only.

Band Number	Spectral Range (nm)	Electromagnetic region	Generalised Application Details
XS1 XI1	500 – 590	Visible Green	Green reflectance by healthy vegetation, some water details in shallow areas
XS2 XI2	610 – 680	Visible Red	Chlorophyll absorption by green vegetation for plant differentiation
XS3 XI3	790 – 890	Near Infrared	Vegetation reflectance, biomass studies, water body delineation
XI4*	1580 - 1750	Short Wave Infrared	Classification for agriculture and geoscience

Each scanner also has a moveable mirror in front of the optics, allowing the off-nadir viewing of areas up to 27 degrees east or west of the vertical, and hence more frequent re-visits of an area. This ability to oblique view allows the

production of stereoscopic pairs (multiple acquisitions of the same area) to be taken within the same cycle and also allows SPOT to image any area within a 950km swath.

The SPOT Grid Reference System (GRS) uses a K/J designation to locate a SPOT scene along and across its path. Column numbers (designated by K) increase easterly, while rows (designated by J) increase southerly. Scenes acquired offset from the track, are associated with the K/J node closest to the scene centre.

APPENDIX B.

METADATA DETAILS FOR ACQUIRED IMAGERY

B.1 Landsat5 TM 02 July 1997

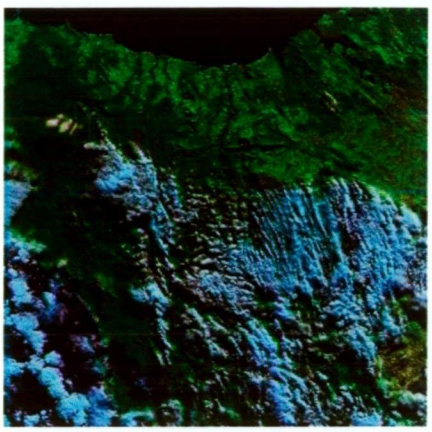

Date/Time Centre (UT):	1997-07-02 23:28:30
Satellite:	Landsat 5
Sensor:	TM
Path / Row:	91 / 89
Centre Latitude:	41°45'41" S
Centre Longitude:	146°04'19" E
Cloud Cover UL UR:	todo
Cloud Cover LL LR:	todo
Orbit Number:	70938
Bands Available:	1234567
Bands Gain:	+++++++
Bands Displayed:	1,4,7
Sun Elevation:	14.1°
Sun Azimuth:	40.2°
Average Cloud (0-100):	0
UL Latitude:	40°46'31" S
UL Longitude:	145°14'32" E
UR Latitude:	41°05'56" S
UR Longitude:	147°26'44" E
LL Latitude:	42°24'30" S
LL Longitude:	144°40'12" E
LR Latitude:	42°44'26" S
LR Longitude:	146°55'49" E
Missing Data %:	0
Ground Station:	Alice Springs
Scene ID:	10500910891997070223283O
AOS Time:	1997-07-02 23:19:43
LOS Time:	1997-07-02 23:28:54
Bit Error Rate:	.0E+00

B.2 Landsat5 TM 06 October 1997

Date/Time Centre (UT):	1997-10-06 23:31:29
Satellite:	Landsat 5
Sensor:	TM
Path / Row:	91 / 89
Centre Latitude:	41°45'41" S
Centre Longitude:	146°05'02" E
Cloud Cover UL UR:	20 10
Cloud Cover LL LR:	0 0
Orbit Number:	72336
Bands Available:	1234567
Bands Gain:	+++++++
Bands Displayed:	1,4,7
Sun Elevation:	40.4°
Sun Azimuth:	53.6°
Average Cloud (0-100):	7
UL Latitude:	40°46'32" S
UL Longitude:	145°15'15" E
UR Latitude:	41°05'55" S
UR Longitude:	147°27'27" E
LL Latitude:	42°24'31" S
LL Longitude:	144°40'57" E
LR Latitude:	42°44'25" S
LR Longitude:	146°56'33" E
Missing Data %:	0
Ground Station:	Alice Springs
Scene ID:	10500910891997100623312 9
AOS Time:	1997-10-06 23:22:49
LOS Time:	1997-10-06 23:32:08
Bit Error Rate:	.0E+00

B.3 Landsat5 TM 23 November 1997

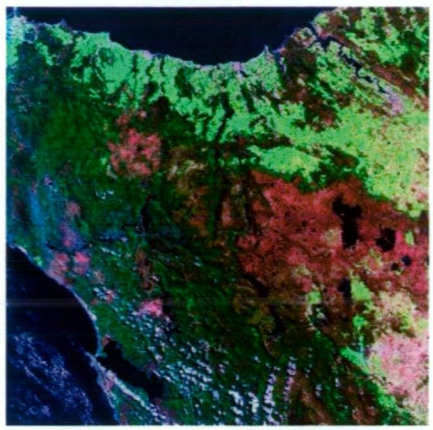

Date/Time Centre (UT):	1997-11-23 23:32:42
Satellite:	Landsat 5
Sensor:	TM
Path / Row:	91 / 89
Centre Latitude:	41°45'53" S
Centre Longitude:	146°05'54" E
Cloud Cover UL UR:	10 0
Cloud Cover LL LR:	50 20
Orbit Number:	73035
Bands Available:	1234567
Bands Gain:	+++++++
Bands Displayed:	1,4,7
Sun Elevation:	52.0°
Sun Azimuth:	67.6°
Average Cloud (0-100):	20
UL Latitude:	40°46'44" S
UL Longitude:	145°15'53" E
UR Latitude:	41°06'10" S
UR Longitude:	147°28'29" E
LL Latitude:	42°24'39" S
LL Longitude:	144°41'36" E
LR Latitude:	42°44'36" S
LR Longitude:	146°57'38" E
Missing Data %:	0
Ground Station:	Alice Springs
Scene ID:	10500910891997112323324 2
AOS Time:	1997-11-23 23:23:51
LOS Time:	1997-11-23 23:33:31
Bit Error Rate:	.0E+00

B.4 Landsat5 TM 10 January 1998

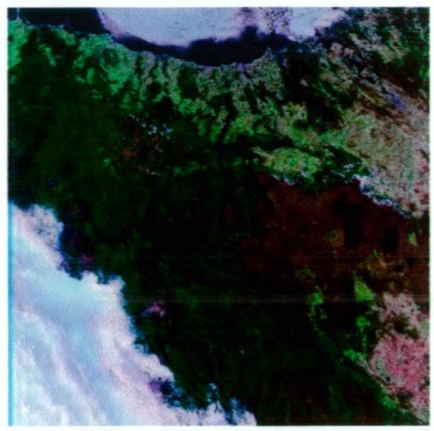

Date/Time Centre (UT):	1998-01-10 23:33:52
Satellite:	Landsat 5
Sensor:	TM
Path / Row:	91 / 89
Centre Latitude:	41°45'52" S
Centre Longitude:	146°05'16" E
Cloud Cover UL UR:	20 20
Cloud Cover LL LR:	70 10
Orbit Number:	73734
Bands Available:	1234567
Bands Gain:	+++++++
Bands Displayed:	1,4,7
Sun Elevation:	49.4°
Sun Azimuth:	74.0°
Average Cloud (0-100):	30
UL Latitude:	40°46'43" S
UL Longitude:	145°15'17" E
UR Latitude:	41°06'07" S
UR Longitude:	147°27'48" E
LL Latitude:	42°24'40" S
LL Longitude:	144°41'03" E
LR Latitude:	42°44'35" S
LR Longitude:	146°56'57" E
Missing Data %:	0
Ground Station:	Alice Springs
Scene ID:	10500910891998011023352
AOS Time:	1998-01-10 23:25:05
LOS Time:	1998-01-10 23:34:41
Bit Error Rate:	1.8E-07

B.5 SPOT2 H1XS 23 February 1998

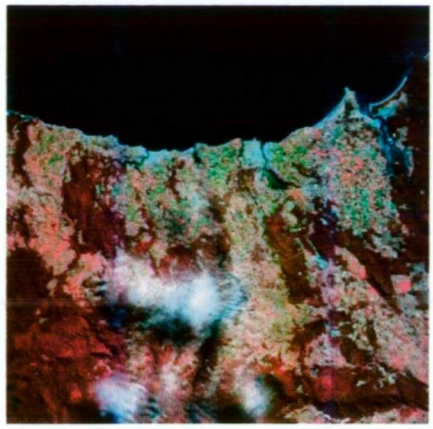

Date/Time Centre (UT):	1998-02-23 00:14:26
Satellite:	SPOT2
Sensor:	H1XS
GRS K/J:	384 / 433
Centre Latitude:	41°15'05" S
Centre Longitude:	146°15'33" E
Cloud Cover UL UR:	0 0
Cloud Cover LL LR:	20 10
Orbit Number:	93
Bands Available:	1,2,3
Bands Gain:	675
Bands Displayed:	123
Off Nadir Angle:	1.64° E (of Sat.)
Sun Elevation:	47.0°
Sun Azimuth:	52.9°
Programming Type:	Independent Instrument
Average Cloud (0-100):	7
UL Latitude:	40°56'09" S
UL Longitude:	145°59'39" E
UR Latitude:	41°02'36" S
UR Longitude:	146°42'07" E
LL Latitude:	41°27'28" S
LL Longitude:	145°48'52" E
LR Latitude:	41°33'59" S
LR Longitude:	146°31'40" E
DPCM Flag:	6 bit Pan data
Missing Data %:	0
Ground Station:	Alice Springs
Scene ID:	11223844331998022300 1426
AOS Time:	1998-02-23 00:09:16
LOS Time:	1998-02-23 00:15:13
Bit Error Rate:	.0E+00

B.6 SPOT1 H1XS 18 April 1998

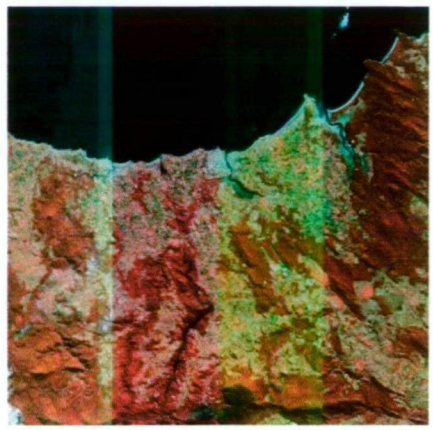

Date/Time Centre (UT):	1998-04-18 00:05:39
Satellite:	SPOT1
Sensor:	H1XS
GRS K/J:	384 / 433
Centre Latitude:	41°15'05" S
Centre Longitude:	146°19'19" E
Cloud Cover UL UR:	0 10
Cloud Cover LL LR:	10 0
Orbit Number:	320
Bands Available:	123
Bands Gain:	675
Bands Displayed:	1,2,3
Off Nadir Angle:	8.56° W (of Sat.)
Sun Elevation:	30.2°
Sun Azimuth:	37.2°
Programming Type:	Coupled Instrument
Average Cloud (0-100):	5
UL Latitude:	40°55'44" S
UL Longitude:	146°03'17" E
UR Latitude:	41°03'06" S
UR Longitude:	146°46'40" E
LL Latitude:	41°26'54" S
LL Longitude:	145°51'32" E
LR Latitude:	41°34'20" S
LR Longitude:	146°35'15" E
DPCM Flag:	6 bit Pan data
Missing Data %:	0
Ground Station:	Alice Springs
Scene ID:	1112384433199804180005 39
AOS Time:	1998-04-18 00:00:41
LOS Time:	1998-04-18 00:06:22
Bit Error Rate:	.0E+00

B.7 Landsat5 TM 21 July 1998

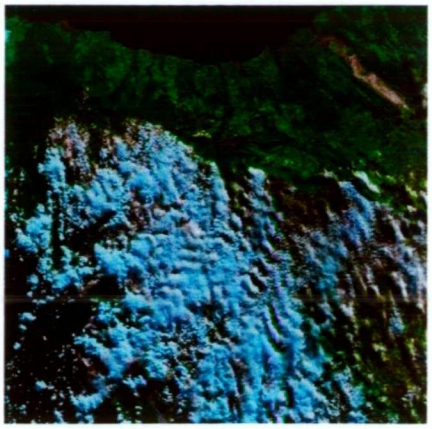

Date/Time Centre (UT):	1998-07-21 23:36:46
Satellite:	Landsat 5
Sensor:	TM
Path / Row:	91 / 89
Centre Latitude:	41°45'53" S
Centre Longitude:	146°05'14" E
Cloud Cover UL UR:	todo
Cloud Cover LL LR:	todo
Orbit Number:	76530
Bands Available:	1234567
Bands Gain:	+++++++
Bands Displayed:	1,4,7
Sun Elevation:	17.1°
Sun Azimuth:	40.4°
Average Cloud (0-100):	0
UL Latitude:	40°46'45" S
UL Longitude:	145°15'06" E
UR Latitude:	41°06'08" S
UR Longitude:	147°27'50" E
LL Latitude:	42°24'41" S
LL Longitude:	144°40'56" E
LR Latitude:	42°44'35" S
LR Longitude:	146°57'05" E
Missing Data %:	0
Ground Station:	Alice Springs
Scene ID:	10500910891998072123364 6
AOS Time:	1998-07-21 23:27:55
LOS Time:	1998-07-21 23:37:35
Bit Error Rate:	2.6E-07

B.8 Landsat5 TM 27 September 1998

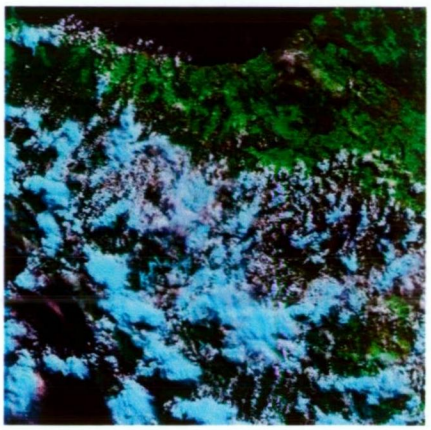

Date/Time Centre (UT):	1998-09-23 23:37:17
Satellite:	Landsat 5
Sensor:	TM
Path / Row:	91 / 89
Centre Latitude:	41°45'48" S
Centre Longitude:	146°06'00" E
Cloud Cover UL UR:	todo
Cloud Cover LL LR:	todo
Orbit Number:	77462
Bands Available:	1234567
Bands Gain:	+++++++
Bands Displayed:	1,4,7
Sun Elevation:	36.4°
Sun Azimuth:	49.4°
Average Cloud (0-100):	0
UL Latitude:	40°46'41" S
UL Longitude:	145°16'09" E
UR Latitude:	41°05'58" S
UR Longitude:	147°28'19" E
LL Latitude:	42°24'42" S
LL Longitude:	144°42'00" E
LR Latitude:	42°44'29" S
LR Longitude:	146°57'34" E
Missing Data %:	0
Ground Station:	Alice Springs
Scene ID:	10500910891998092323371 7
AOS Time:	1998-09-23 23:28:31
LOS Time:	1998-09-23 23:38:06
Bit Error Rate:	.0E+00

B.9 SPOT4 HRVIR1XI 08 October 1998

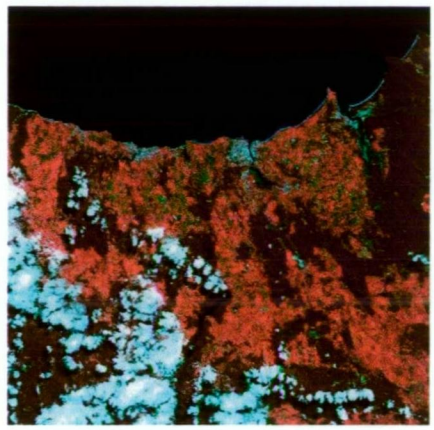

Date/Time Centre (UT):	1998-10-08 00:08:07
Satellite:	SPOT4
Sensor:	HRVIR1XI
GRS K/J:	384 / 433
Centre Latitude:	41°15'05" S
Centre Longitude:	146°03'03" E
Cloud Cover UL UR:	10 0
Cloud Cover LL LR:	10 30
Orbit Number:	320
Bands Available:	1234
Bands Gain:	3232
Bands Displayed:	1,2,3
Off Nadir Angle:	10.04° W (of Sat.)
Sun Elevation:	58.1°
Sun Azimuth:	57.8°
Programming Type:	Coupled Instrument
Average Cloud (0-100):	12
UL Latitude:	40°55'39" S
UL Longitude:	145°46'49" E
UR Latitude:	41°03'11" S
UR Longitude:	146°30'38" E
LL Latitude:	41°26'47" S
LL Longitude:	145°34'57" E
LR Latitude:	41°34'24" S
LR Longitude:	146°19'06" E
DPCM Flag:	8 bit Pan data
Missing Data %:	0
Ground Station:	Alice Springs
Scene ID:	1124384433200981008000807
AOS Time:	1998-10-08 00:02:33
LOS Time:	1998-10-08 00:08:49
Bit Error Rate :	.0E+00

B.10 SPOT4 HRVIR1XI 31 December 1998

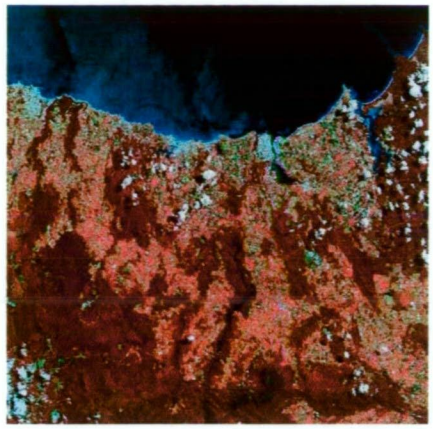

Date/Time Centre (UT):	1998-12-31 00:23:14
Satellite:	SPOT4
Sensor:	HRVIR1XI
GRS K/J:	384 / 433
Centre Latitude:	41°15'05" S
Centre Longitude:	145°58'58" E
Cloud Cover UL UR:	10 20
Cloud Cover LL LR:	40 30
Orbit Number :	235
Bands Available:	1234
Bands Gain:	3232
Bands Displayed:	1,2,3
Off Nadir Angle:	10.64° E (of Sat.)
Sun Elevation:	60.7°
Sun Azimuth:	53.8°
Programming Type:	Coupled Instrument
Average Cloud (0-100):	25
UL Latitude:	40°56'17" S
UL Longitude:	145°41'53" E
UR Latitude:	41°02'23" S
UR Longitude:	146°26'15" E
LL Latitude:	41°27'43" S
LL Longitude:	145°31'53" E
LR Latitude:	41°33'52" S
LR Longitude:	146°16'37" E
DPCM Flag:	8 bit Pan data
Missing Data %:	0
Ground Station:	Alice Springs
Scene ID:	1145384433200981231600 2314
AOS Time:	1998-12-31 00:17:31
LOS Time :	1998-12-31 00:23:23
Bit Error Rate:	.0E+00

Comments : Band 4 possible residue dead detectors

B.11 Landsat5 TM 29 January 1999

Date/Time Centre (UT):	1999-01-29 23:37:27
Satellite:	Landsat 5
Sensor:	TM
Path / Row:	91 / 89
Centre Latitude:	41°45'41" S
Centre Longitude:	146°07'58" E
Cloud Cover UL UR:	50 50
Cloud Cover LL LR:	0 0
Orbit Number :	79093
Bands Available:	1234567
Bands Gain:	+++++++
Bands Displayed:	1,4,7
Sun Elevation:	49.6°
Sun Azimuth:	72.9°
Average Cloud (0-100):	25
UL Latitude:	40°49'09" S
UL Longitude:	145°15'23" E
UR Latitude:	41°08'55" S
UR Longitude:	147°31'09" E
LL Latitude:	42°21'30" S
LL Longitude:	144°43'12" E
LR Latitude:	42°41'46" S
LR Longitude:	147°02'15" E
Missing Data %:	0
Ground Station:	Alice Springs
Scene ID:	105009108919990129233727 1
AOS Time:	1999-01-29 23:28:57
LOS Time:	1999-01-29 23:38:16
Bit Error Rate:	

B.12 Landsat5 TM 03 March 1999

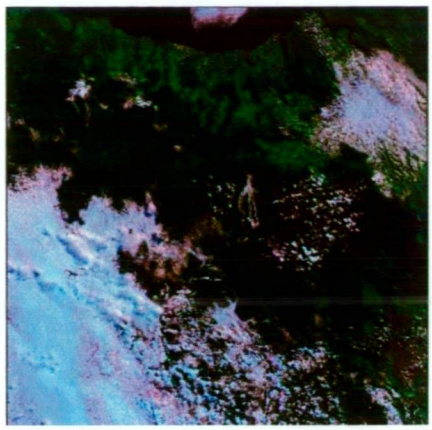

Date/Time Centre (UT):	1999-03-03 23:37:26
Satellite:	Landsat 5
Sensor:	TM
Path / Row:	91 / 89
Centre Latitude:	41°45'52" S
Centre Longitude:	146°05'16" E
Cloud Cover UL UR:	todo
Cloud Cover LL LR:	todo
Orbit Number:	80025
Bands Available:	1234567
Bands Gain:	+++++++
Bands Displayed:	1,4,7
Sun Elevation:	34.6°
Sun Azimuth:	53.7°
Average Cloud (0-100):	0
UL Latitude:	40°46'47" S
UL Longitude:	145°15'03" E
UR Latitude:	41°06'05" S
UR Longitude:	147°27'50" E
LL Latitude:	42°24'43" S
LL Longitude:	144°40'59" E
LR Latitude:	42°44'32" S
LR Longitude:	146°57'12" E
Missing Data %:	0
Ground Station:	Alice Springs
Scene ID:	10500910891999030323372 6
AOS Time:	1999-03-18 03:31:08
LOS Time:	1999-03-18 03:38:14
Bit Error Rate:	9.6E-07

B.13 SPOT4 HRVIR2XI 29 March 1999

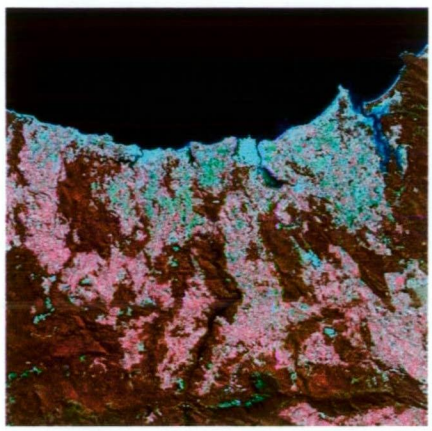

Date/Time Centre (UT):	1999-03-29 00:15:49
Satellite:	SPOT4
Sensor:	HRVIR2XI
GRS K/J:	384 / 433
Centre Latitude:	41°15'05" S
Centre Longitude:	146°18'20" E
Cloud Cover UL UR:	0 0
Cloud Cover LL LR:	10 0
Orbit Number:	93
Bands Available:	1234
Bands Gain:	3230
Bands Displayed:	1,2,3
Off Nadir Angle:	1.96° E (of Sat.)
Sun Elevation:	30.0°
Sun Azimuth:	33.6°
Programming Type:	
Average Cloud (0-100):	2
UL Latitude:	40°56'09" S
UL Longitude:	146°02'27" E
UR Latitude:	41°02'36" S
UR Longitude:	146°44'55" E
LL Latitude:	41°27'29" S
LL Longitude:	145°51'40" E
LR Latitude:	41°33'59" S
LR Longitude:	146°34'28" E
DPCM Flag:	8 bit Pan data
Missing Data %:	0
Ground Station:	Alice Springs
Scene ID:	1146384433200993290015491
AOS Time:	1998-03-29 00:09:30
LOS Time:	1998-03-29 00:16:39
Bit Error Rate:	

APPENDIX C

SUMMARY STATISTICS OF AIARR VALUES

Table C.1: Summary statistics of AIARR values for 1997/98 Growing season

Image	Band	Minimum Value	Maximum Value	Mean	Median	Standard Deviation	Standard Error of Mean
TM 02 July 1997	1	16.000	43.000	25.675	25.000	4.090	0.028
	2	17.000	41.000	26.447	26.000	13.311	0.092
	3	13.000	44.000	29.354	29.000	3.855	0.027
	4	2.000	71.000	27.056	25.000	10.562	0.073
	5	3.000	65.000	38.124	38.000	9.383	0.065
	7	5.000	94.000	41.781	42.000	11.536	0.080
TM 06 October 1997	1	27.000	61.000	38.029	37.000	5.226	0.036
	2	30.000	65.000	41.779	42.000	4.077	0.028
	3	26.000	78.000	54.113	56.000	8.523	0.059
	4	13.000	90.000	37.400	35.000	11.544	0.080
	5	25.000	76.000	56.150	56.000	7.302	0.051
	7	25.000	127.000	76.614	76.000	14.950	0.104
TM 23 November 1997	1	47.000	97.000	62.153	62.000	5.171	0.036
	2	55.000	98.000	72.449	71.000	7.057	0.049
	3	41.000	130.000	81.616	82.000	17.832	0.124
	4	36.000	167.000	95.837	90.000	26.317	0.183
	5	44.000	115.000	78.761	78.000	10.417	0.072
	7	30.000	187.000	80.515	77.000	26.016	0.180
TM 10 January 1998	1	55.000	117.000	74.425	75.000	7.456	0.052
	2	66.000	110.000	82.010	81.000	5.910	0.041
	3	50.000	135.000	99.228	99.000	8.671	0.060
	4	49.000	228.000	90.303	85.000	17.980	0.125
	5	70.000	155.000	123.076	124.000	14.791	0.103
	7	46.000	193.000	127.221	128.000	19.779	0.137
XS 23 February 1998	1	63.000	131.000	101.652	101.000	7.617	0.053
	2	62.000	178.000	141.142	143.000	16.955	0.118
	3	77.000	186.000	110.753	110.000	14.763	0.102
XS 18 April 1998	1	63.000	142.000	111.383	112.000	11.290	0.078
	2	48.000	176.000	134.584	137.000	20.676	1.096
	3	66.000	228.000	114.070	111.000	26.078	0.181

Table C.2: Summary statistics of AIARR values for 1998/99 Growing season

Image	Band	Minimum Value	Maximum Value	Mean	Median	Standard Deviation	Standard Error of Mean
TM 21 July 1998	1	17.000	48.000	30.178	30.000	4.537	0.028
	2	21.000	50.000	31.191	31.000	3.595	0.023
	3	17.000	52.000	34.748	35.000	4.881	0.031
	4	2.000	79.000	30.390	28.000	11.776	0.074
	5	6.000	70.000	41.047	40.000	9.208	0.058
	7	10.000	79.000	45.922	47.000	10.789	0.068
TM 27 September 1998	1	23.000	69.000	42.858	43.000	5.498	0.035
	2	31.000	66.000	43.802	44.000	4.185	0.026
	3	30.000	77.000	54.555	56.000	7.966	0.050
	4	11.000	91.000	38.914	36.000	13.080	0.082
	5	24.000	91.000	59.732	59.000	9.537	0.060
	7	25.000	134.000	78.095	79.000	15.323	0.096
XI 08 October 1998	1	67.000	125.000	88.733	88.000	5.948	0.037
	2	62.000	176.000	114.547	118.000	18.159	0.114
	3	30.000	230.000	99.328	88.000	37.906	0.238
	4	71.000	158.000	121.346	122.000	11.228	0.071
XI 31 December 1998	1	73.000	137.000	94.391	95.000	5.876	0.037
	2	66.000	183.000	121.553	119.000	22.525	0.141
	3	66.000	196.000	122.050	119.000	24.508	0.154
	4	77.000	215.000	126.044	123.000	21.240	0.133
TM 29 January 1999	1	28.000	89.000	40.421	40.000	7.597	0.048
	2	33.000	77.000	43.086	43.000	4.813	0.030
	3	30.000	77.000	53.569	54.000	4.808	0.030
	4	7.000	107.000	40.124	38.000	11.835	0.074
	5	10.000	93.000	69.578	70.000	10.785	0.068
	7	5.000	121.000	82.767	86.000	16.011	0.101
TM 03 March 1999	1	20.000	71.000	32.897	31.000	6.895	0.043
	2	26.000	65.000	35.762	35.000	4.906	0.031
	3	17.000	69.000	45.681	46.000	6.705	0.042
	4	2.000	87.000	34.510	32.000	11.758	0.074
	5	12.000	82.000	57.194	58.000	9.891	0.062
	7	10.000	120.000	72.140	75.000	17.625	0.111
XI 29 March 1999	1	59.000	109.000	77.474	78.000	5.897	0.037
	2	56.000	141.000	103.773	103.000	14.834	0.093
	3	41.000	197.000	77.558	70.000	25.585	0.161
	4	64.000	170.000	120.824	120.000	14.506	0.091

APPENDIX D.

NDVI RESULTANT THEMATIC LAYERS AND HISTOGRAMS

D.1 Landsat5 TM 02 July 1997

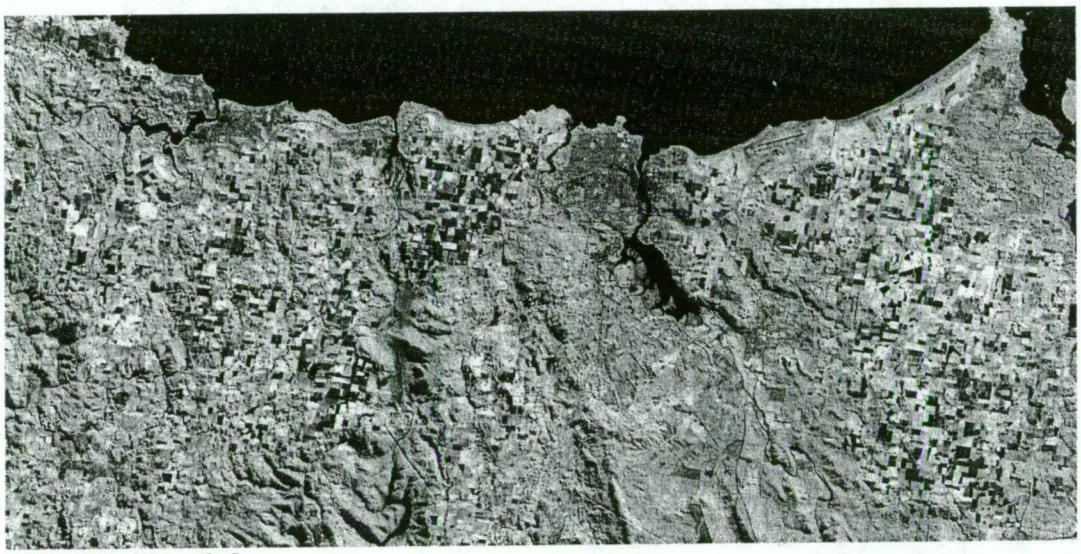

Resultant thematic layer

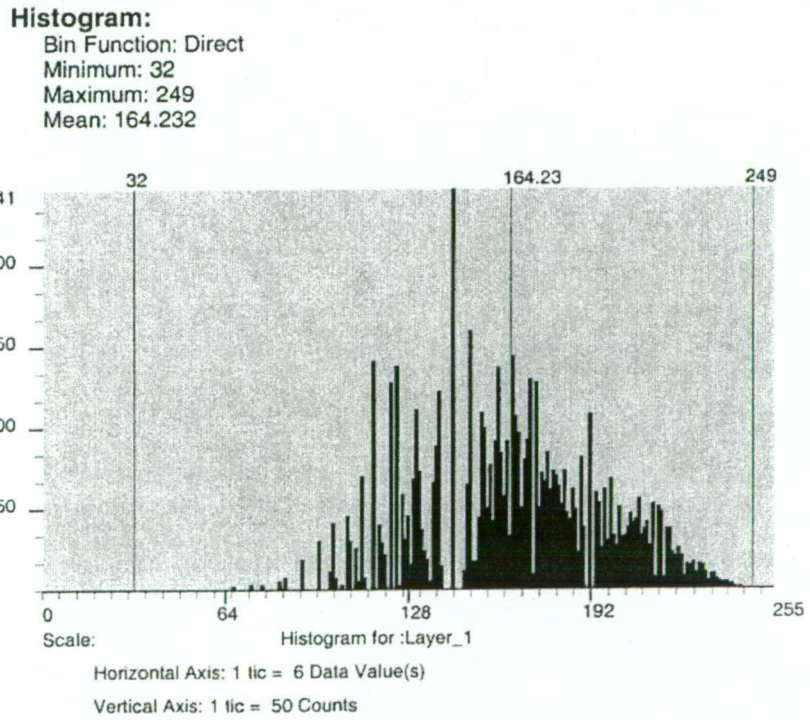

D.2 Landsat5 TM 06 October 1997

Resultant thematic layer

Histogram:

Bin Function: Direct
Minimum: 91
Maximum: 248
Mean: 167.438

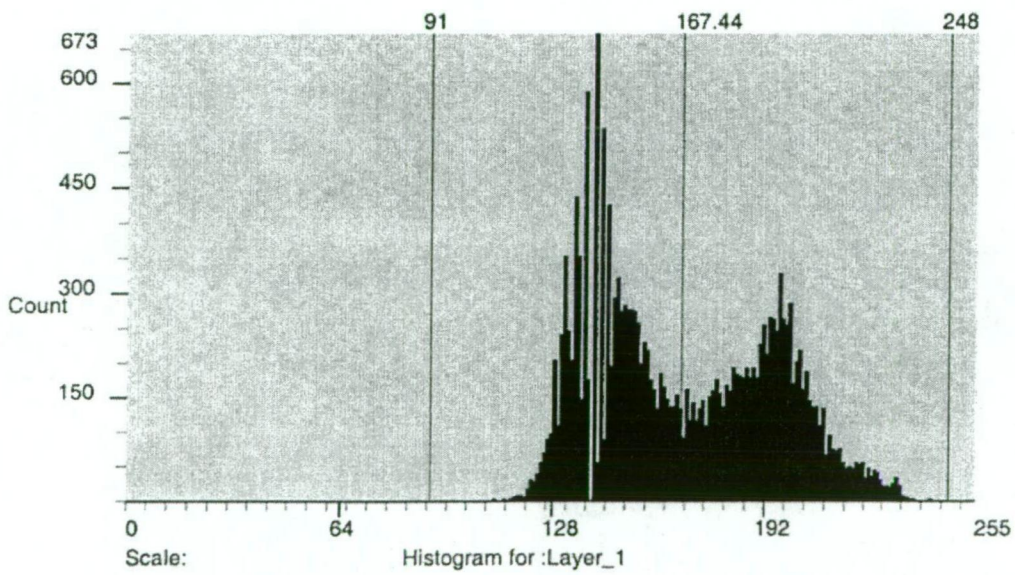

Horizontal Axis: 1 tic = 6 Data Value(s)

Vertical Axis: 1 tic = 50 Counts

D.3 Landsat5 TM 23 November 1997

Resultant thematic layer

Histogram:

Bin Function: Direct
Minimum: 118
Maximum: 245
Mean: 193.504

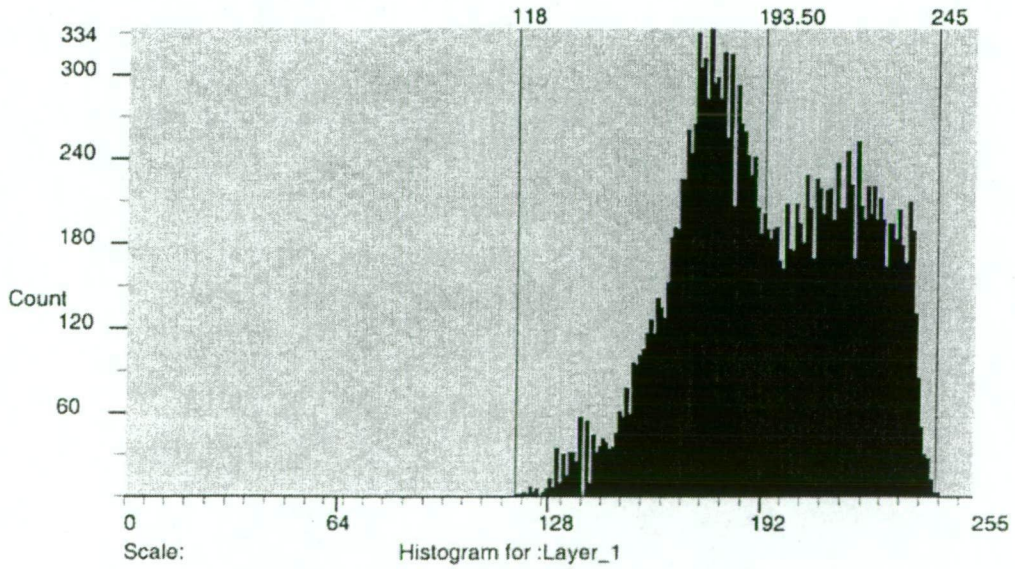

Horizontal Axis: 1 tic = 6 Data Value(s)

Vertical Axis: 1 tic = 30 Counts

D.4 Landsat5 TM 10 January 1998

Resultant thematic layer

Histogram:

Bin Function: Direct
Minimum: 121
Maximum: 241
Mean: 161.637

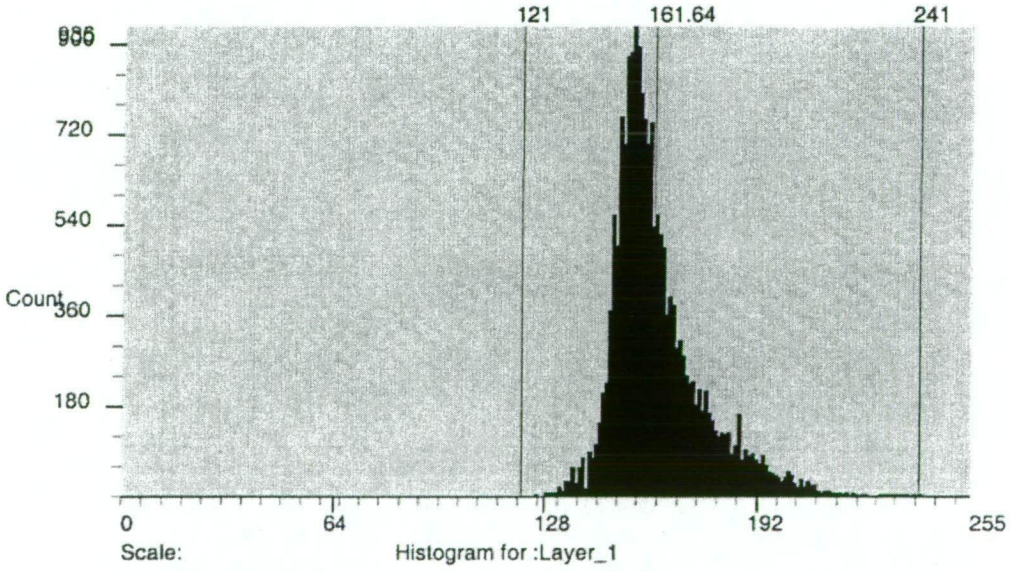

D.5 SPOT2 H1XS 23 February 1998

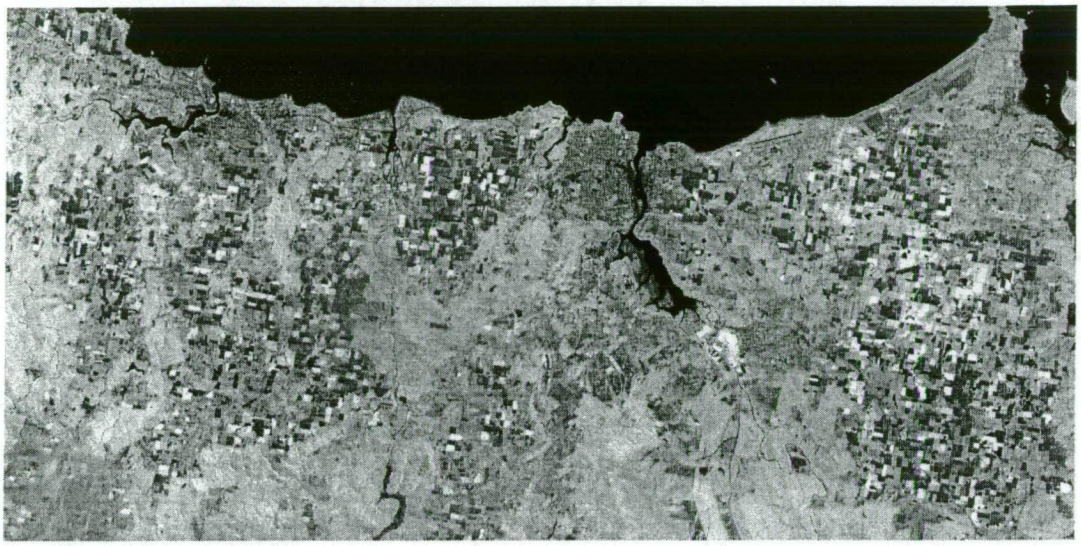

Resultant thematic layer

Histogram:

Bin Function: Direct
Minimum: 105
Maximum: 222
Mean: 143.786

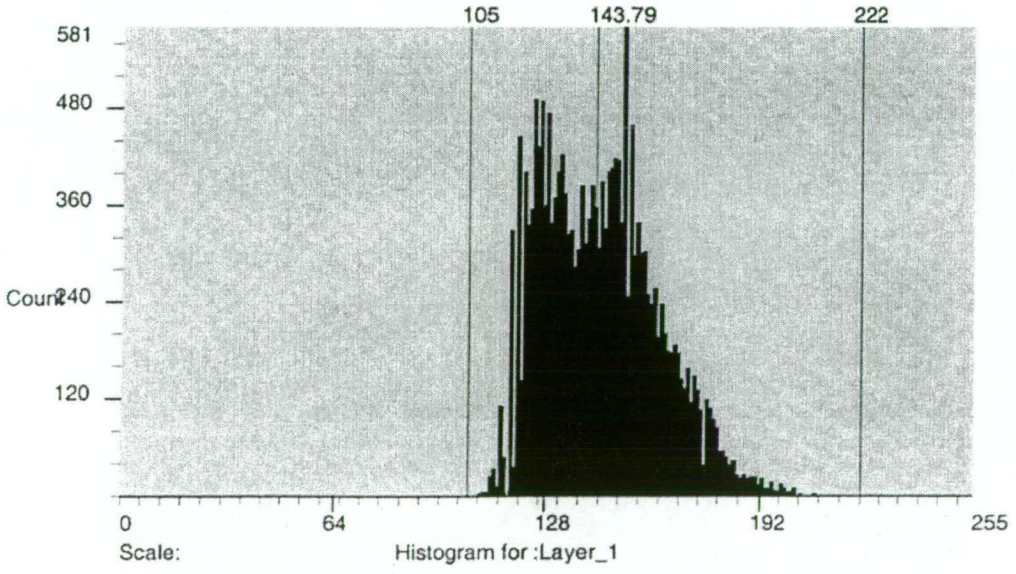

D.6 SPOT1 H1XS 18 April 1998

Resultant thematic layer

Histogram:

Bin Function: Direct
Minimum: 89
Maximum: 238
Mean: 136.581

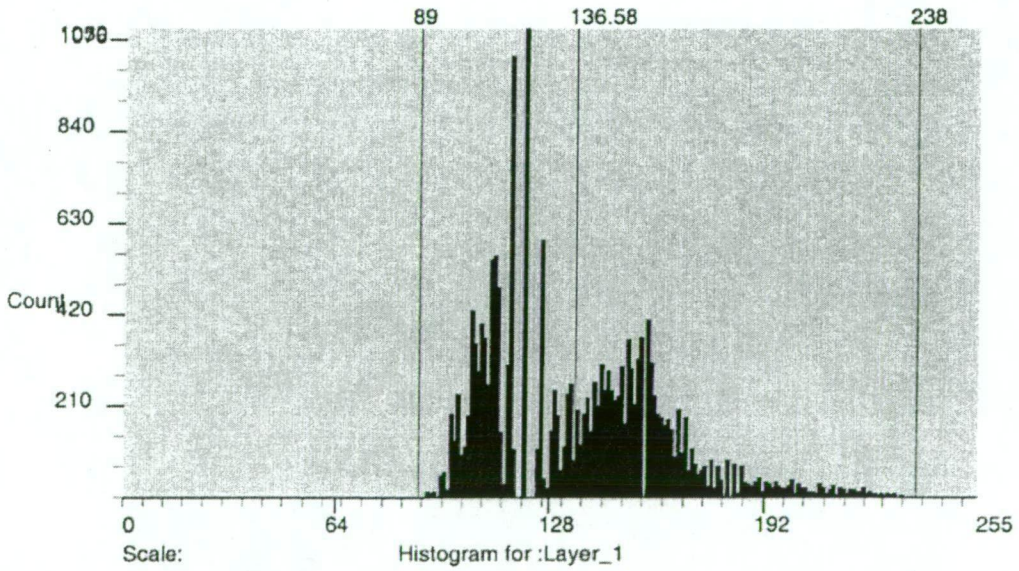

D.7 Landsat5 TM 21 July 1998

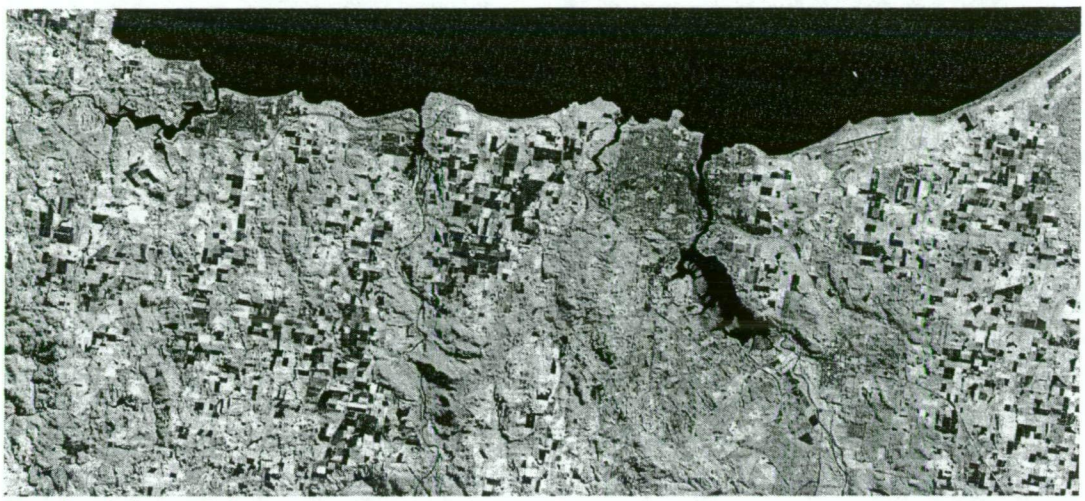

Resultant thematic layer

Histogram:

Bin Function: Direct
Minimum: 26
Maximum: 250
Mean: 160.205

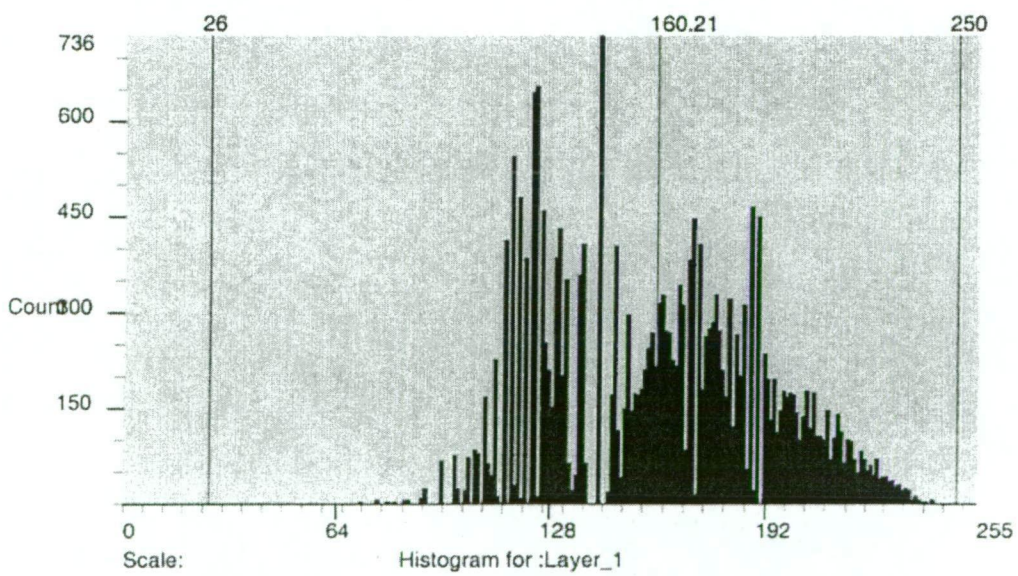

D.8 Landsat5 TM 27 September 1998

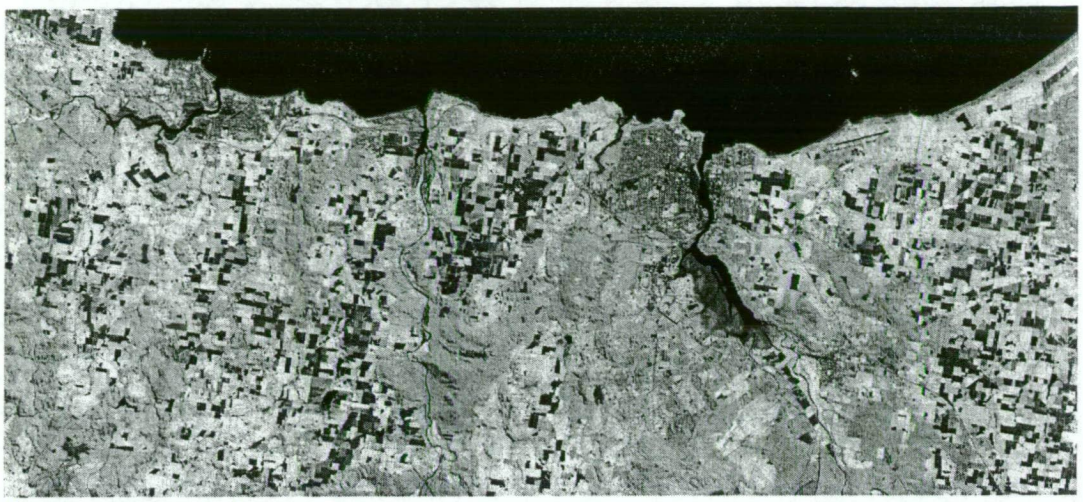

Resultant thematic layer

Histogram:

Bin Function: Direct
Minimum: 59
Maximum: 234
Mean: 153.531

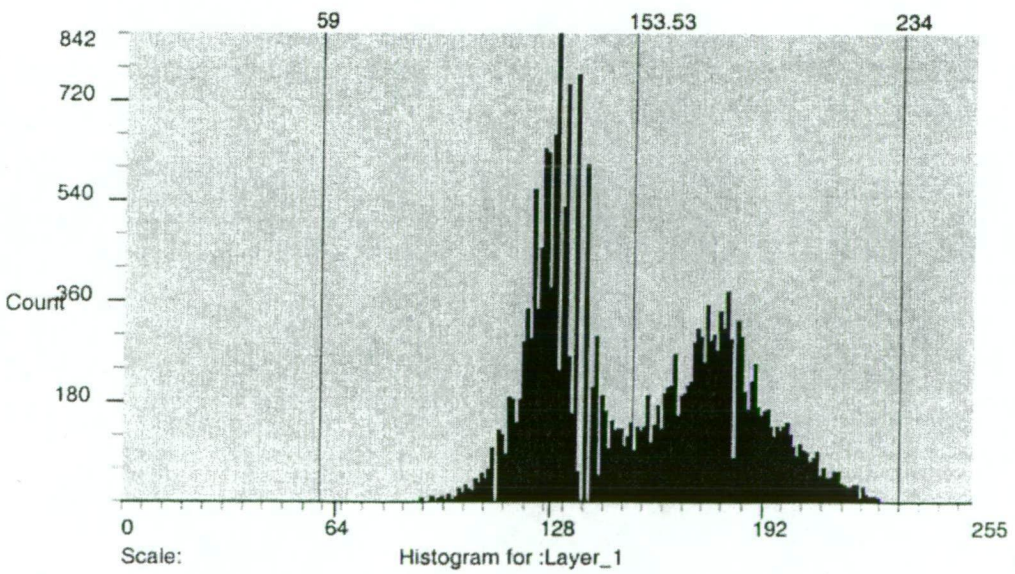

D.9 SPOT4 HRVIR1XI 08 October 1998

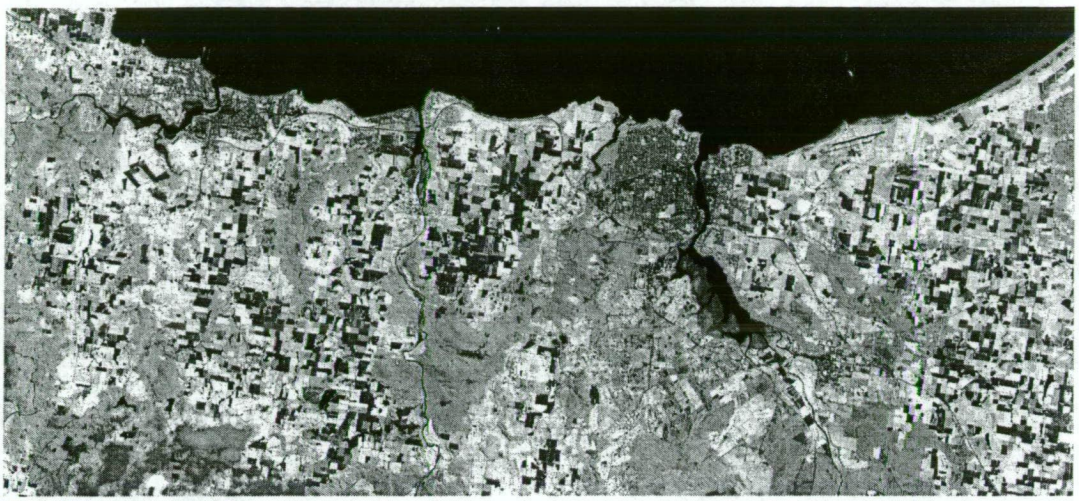

Resultant thematic layer

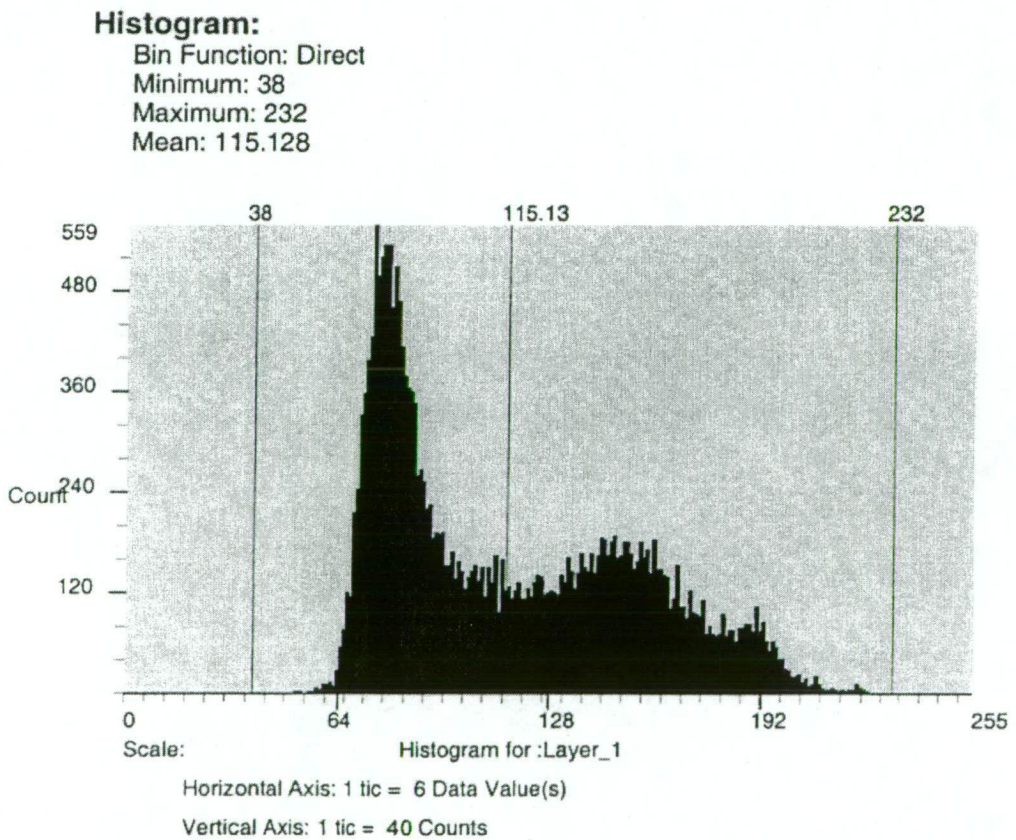

D.10 SPOT4 HRVIR1XI 31 December 1998

Resultant thematic layer

Histogram:
Bin Function: Direct
Minimum: 107
Maximum: 244
Mean: 174.79

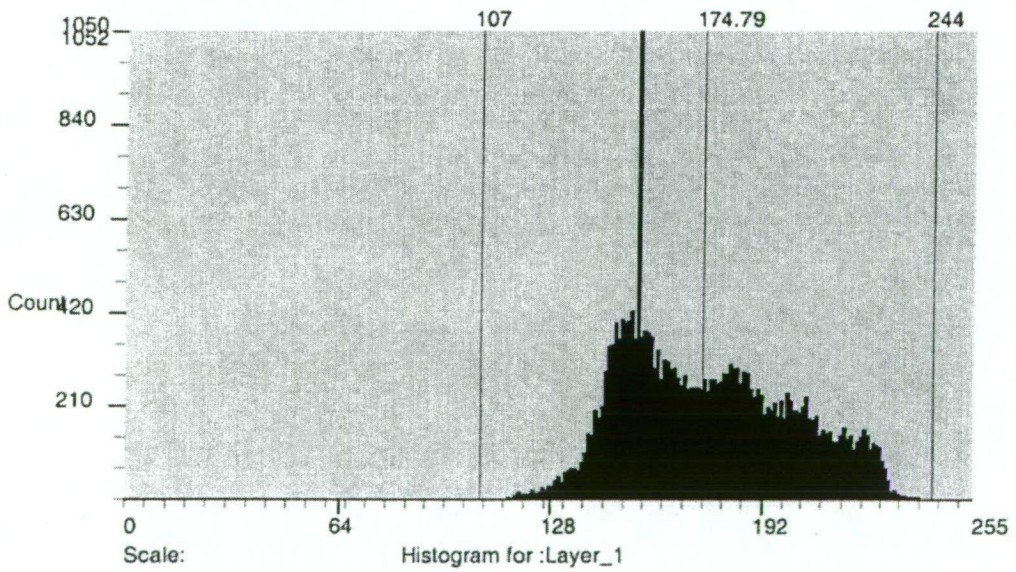

D.11 Landsat5 TM 29 January 1999

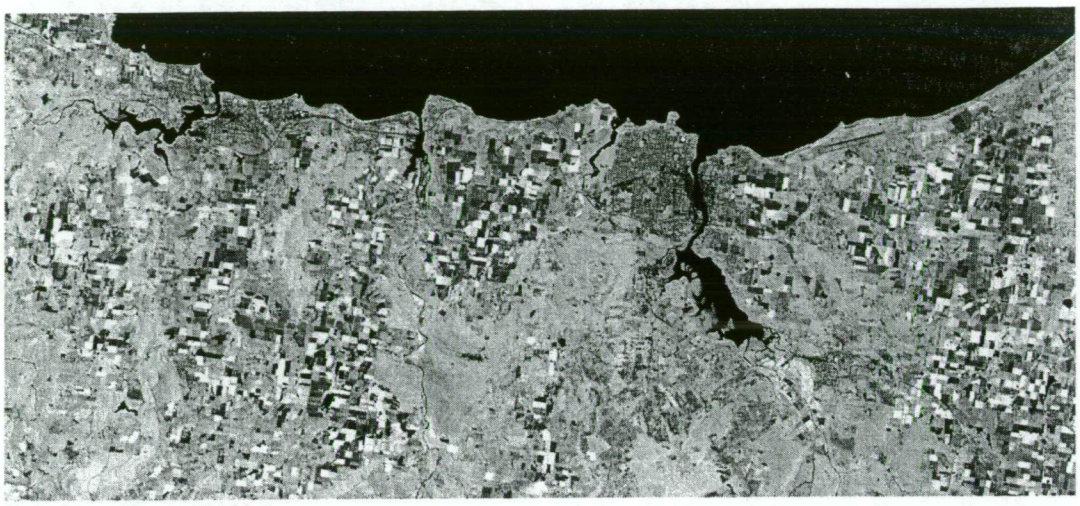

Resultant thematic layer

Histogram:

Bin Function: Direct
Minimum: 54
Maximum: 243
Mean: 159.801

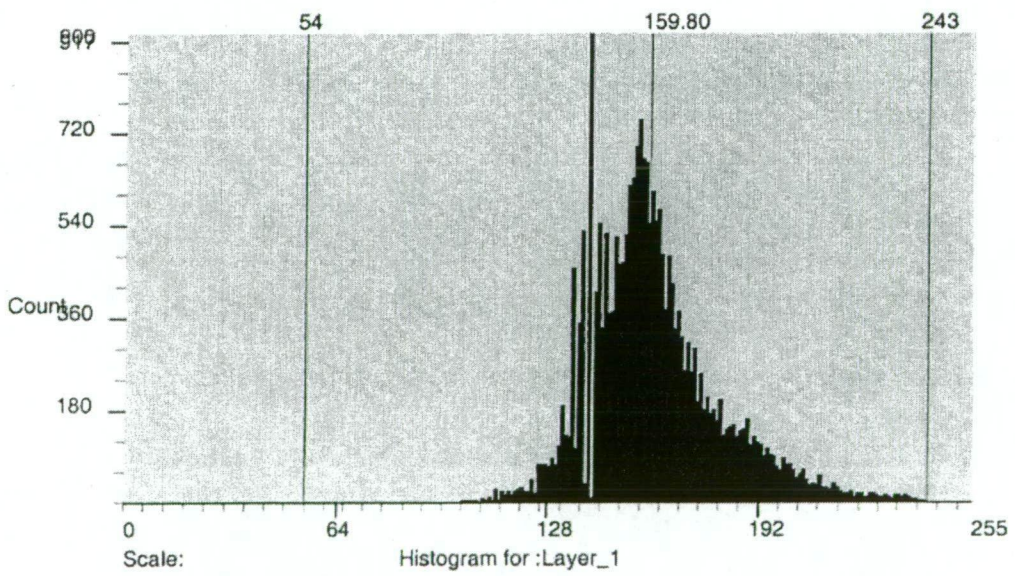

D.12 Landsat5 TM 03 March 1999

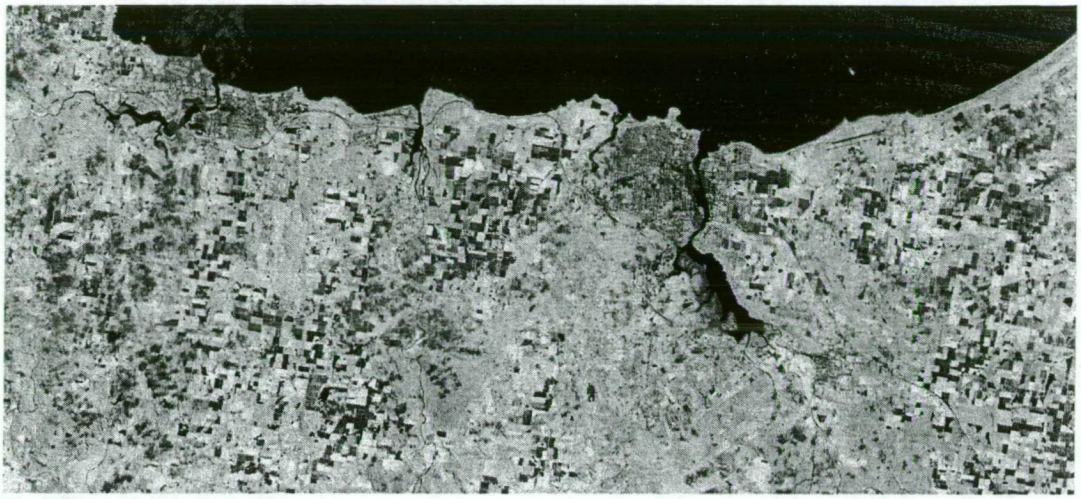

Resultant thematic layer

Histogram:

Bin Function: Direct
Minimum: 23
Maximum: 246
Mean: 161.284

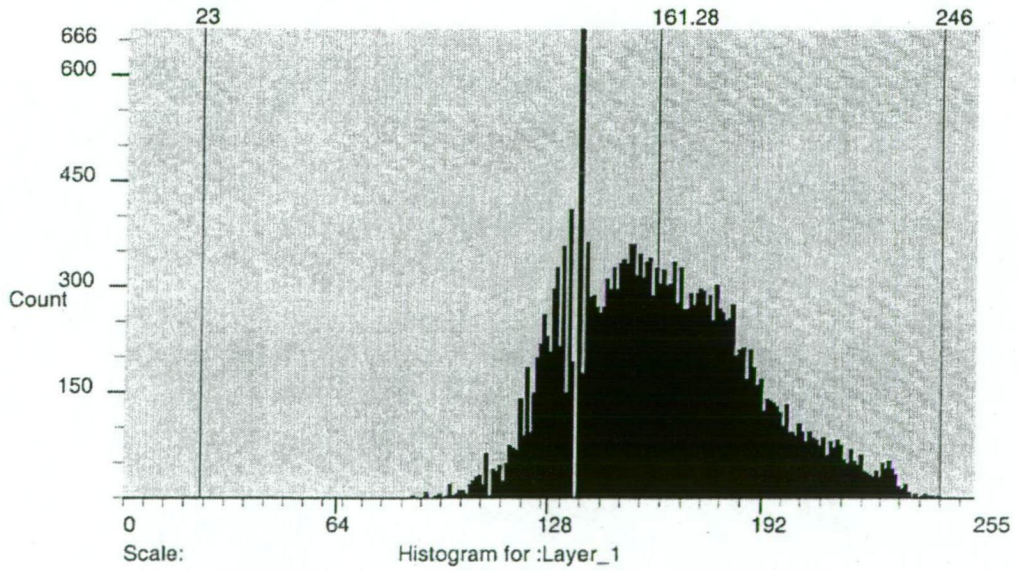

Horizontal Axis: 1 tic = 6 Data Value(s)

Vertical Axis: 1 tic = 50 Counts

D.13 SPOT4 HRVIR2XI 29 March 1999

Resultant thematic layer

Histogram:

Bin Function: Direct
Minimum: 70
Maximum: 240
Mean: 125.936

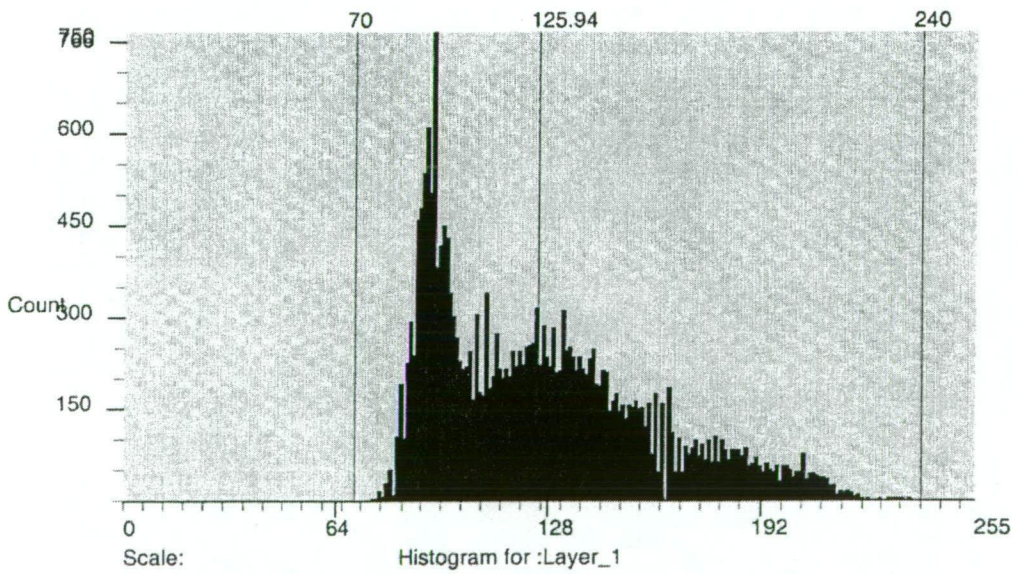

Horizontal Axis: 1 tic = 6 Data Value(s)

Vertical Axis: 1 tic = 50 Counts

APPENDIX E.

PCA LAYER STACK HISTOGRAMS

E.1 Landsat5 TM 02 July 1997

Histogram:
Bin Function: Direct
Minimum: 5
Maximum: 123
Mean: 47.536

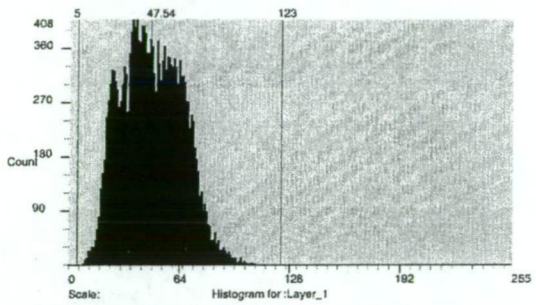

Histogram:
Bin Function: Direct
Minimum: 156
Maximum: 242
Mean: 196.882

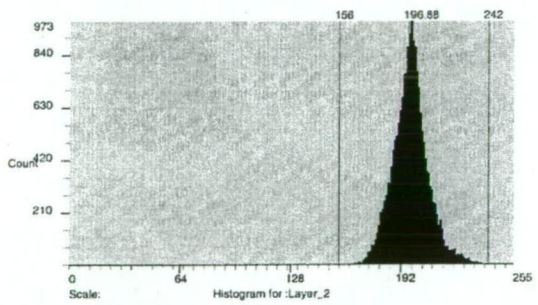

Histogram:
Bin Function: Direct
Minimum: 144
Maximum: 186
Mean: 167.849

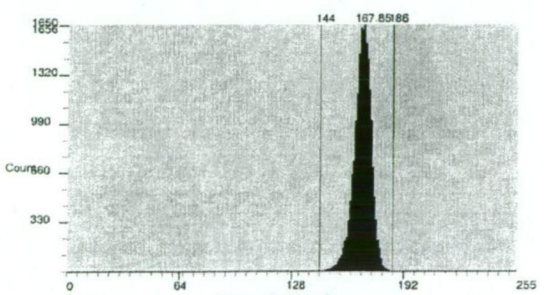

E.2 Landsat5 TM 06 October 1997

Histogram:
Bin Function: Direct
Minimum: 16
Maximum: 121
Mean: 51.6407

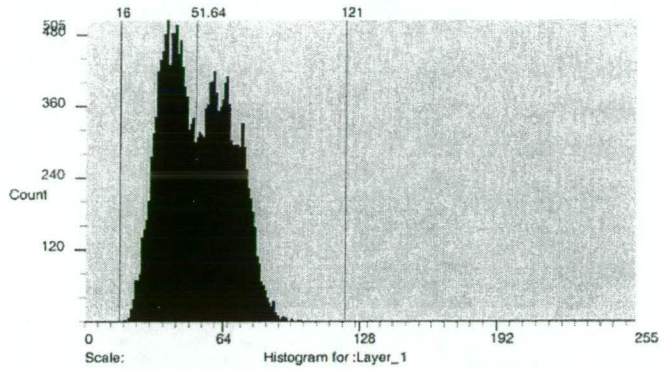

Horizontal Axis: 1 tic = 6 Data Value(s)
Vertical Axis: 1 tic = 40 Counts

Histogram:
Bin Function: Direct
Minimum: 120
Maximum: 237
Mean: 180.929

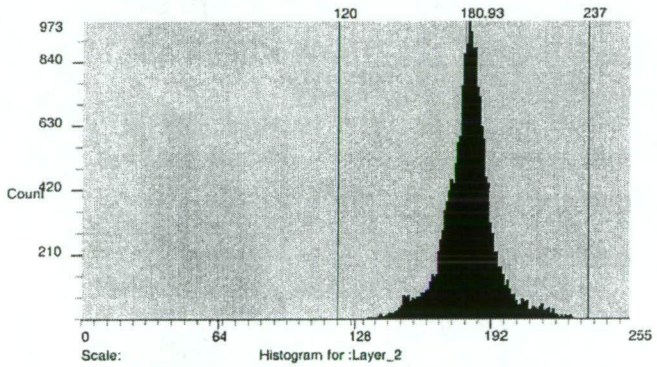

Horizontal Axis: 1 tic = 6 Data Value(s)
Vertical Axis: 1 tic = 70 Counts

Histogram:
Bin Function: Direct
Minimum: 163
Maximum: 200
Mean: 185.676

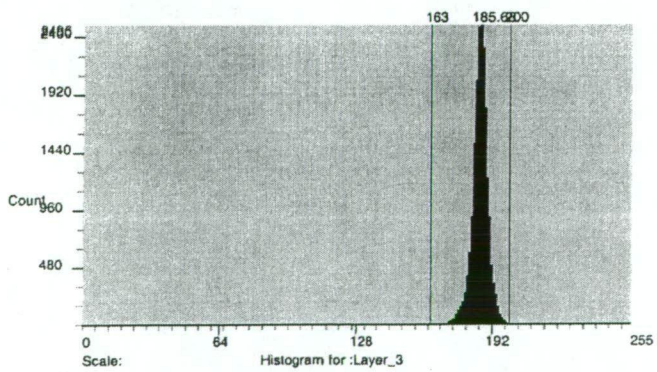

Horizontal Axis: 1 tic = 6 Data Value(s)
Vertical Axis: 1 tic = 160 Counts

E.3 Landsat5 TM 23 November 1997

Histogram:
Bin Function: Direct
Minimum: 29
Maximum: 156
Mean: 79.3719

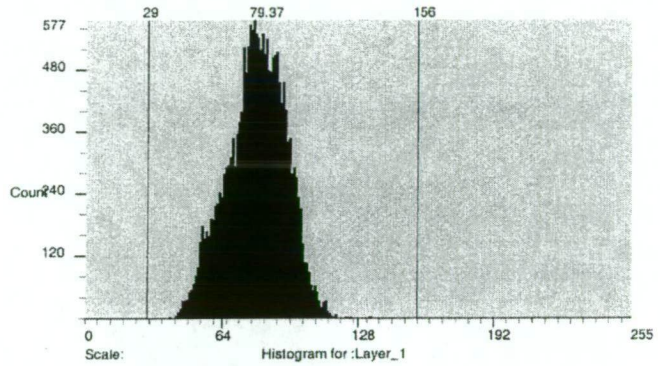

Histogram:
Bin Function: Direct
Minimum: 111
Maximum: 254
Mean: 192.065

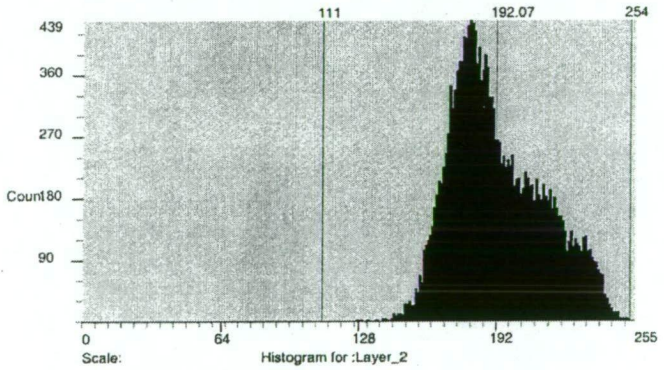

Histogram:
Bin Function: Direct
Minimum: 108
Maximum: 218
Mean: 186.27

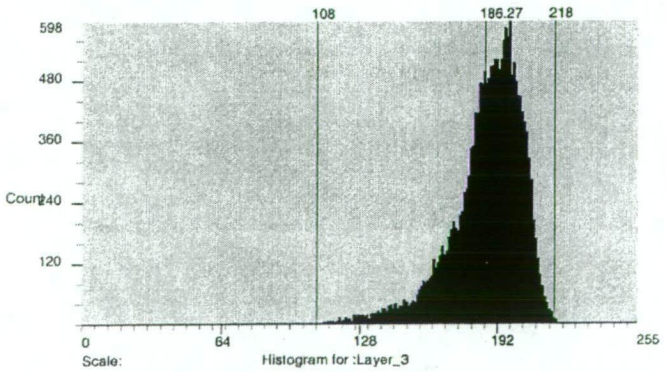

E.4 Landsat5 TM 10 January 1998

Histogram:
Bin Function: Direct
Minimum: 28
Maximum: 144
Mean: 75.5444

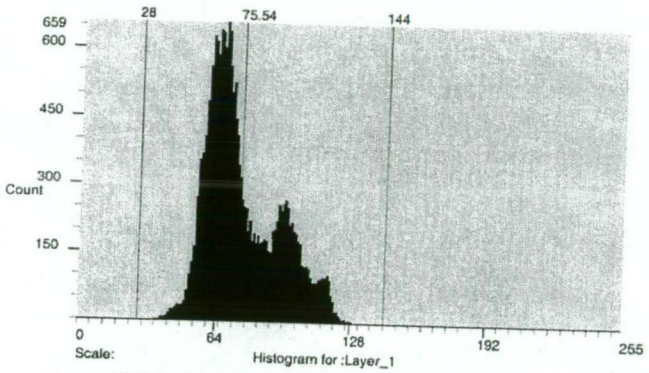

Horizontal Axis: 1 tic = 6 Data Value(s)
Vertical Axis: 1 tic = 50 Counts

Histogram:
Bin Function: Direct
Minimum: 79
Maximum: 211
Mean: 107.012

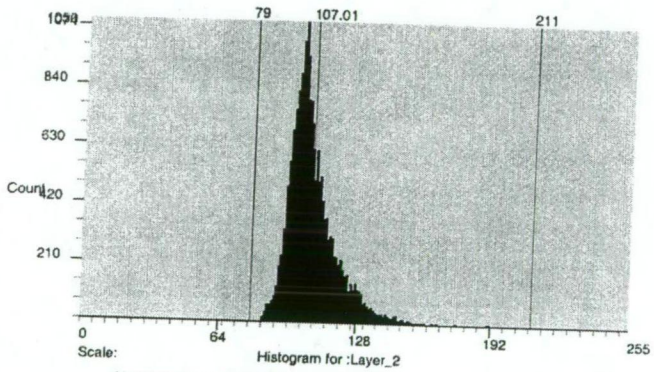

Horizontal Axis: 1 tic = 6 Data Value(s)
Vertical Axis: 1 tic = 70 Counts

Histogram:
Bin Function: Direct
Minimum: 184
Maximum: 249
Mean: 224.285

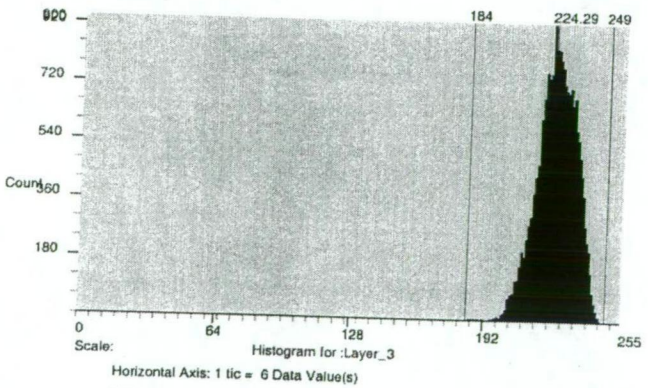

Horizontal Axis: 1 tic = 6 Data Value(s)
Vertical Axis: 1 tic = 60 Counts

E.5 SPOT2 H1XS 23 February 1998

Histogram:
Bin Function: Direct
Minimum: 20
Maximum: 84
Mean: 45.6421

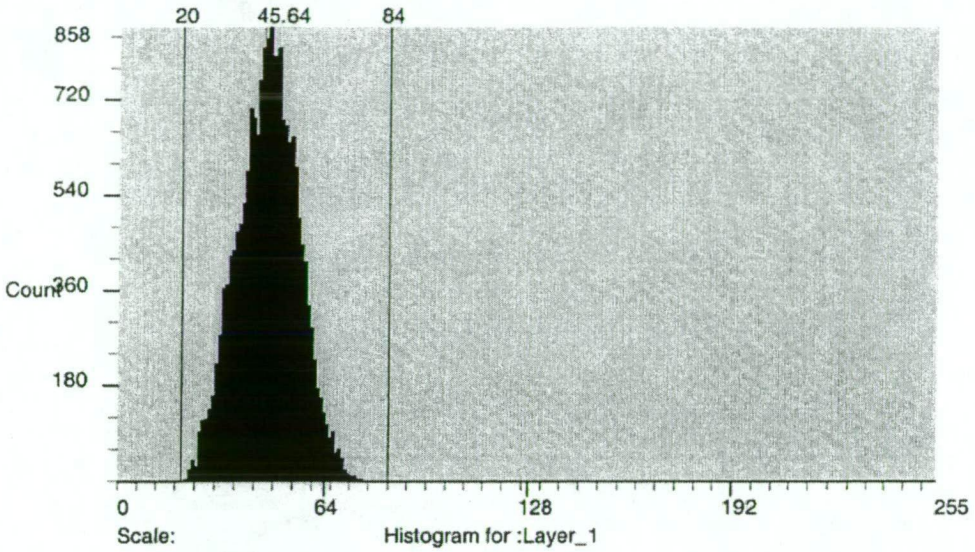

Horizontal Axis: 1 tic = 6 Data Value(s)
Vertical Axis: 1 tic = 60 Counts

Histogram:
Bin Function: Direct
Minimum: 166
Maximum: 229
Mean: 200.166

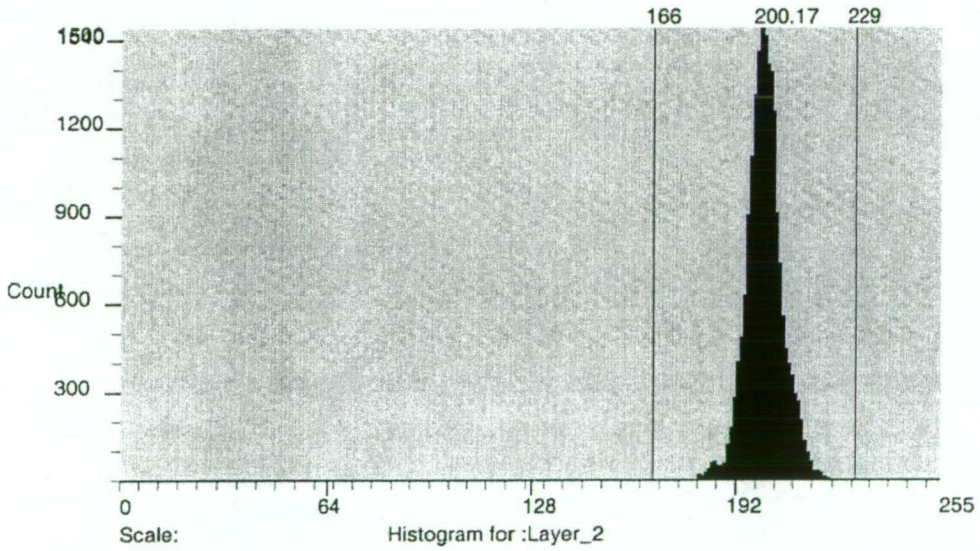

Horizontal Axis: 1 tic = 6 Data Value(s)
Vertical Axis: 1 tic = 100 Counts

E.6 SPOT1 H1XS 18 April 1998

Histogram:
Bin Function: Direct
Minimum: 26
Maximum: 115
Mean: 52.712

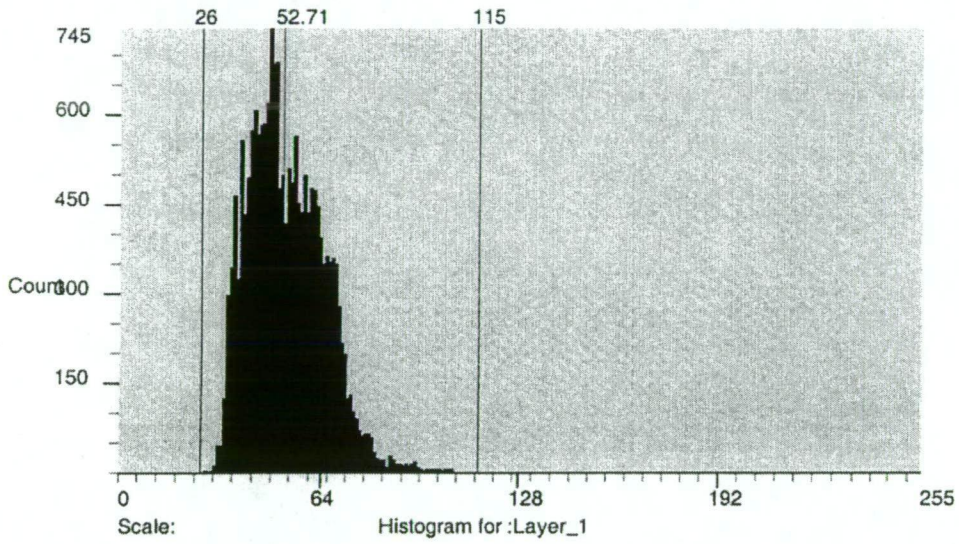

Horizontal Axis: 1 tic = 6 Data Value(s)
Vertical Axis: 1 tic = 50 Counts

Histogram:
Bin Function: Direct
Minimum: 169
Maximum: 241
Mean: 201.714

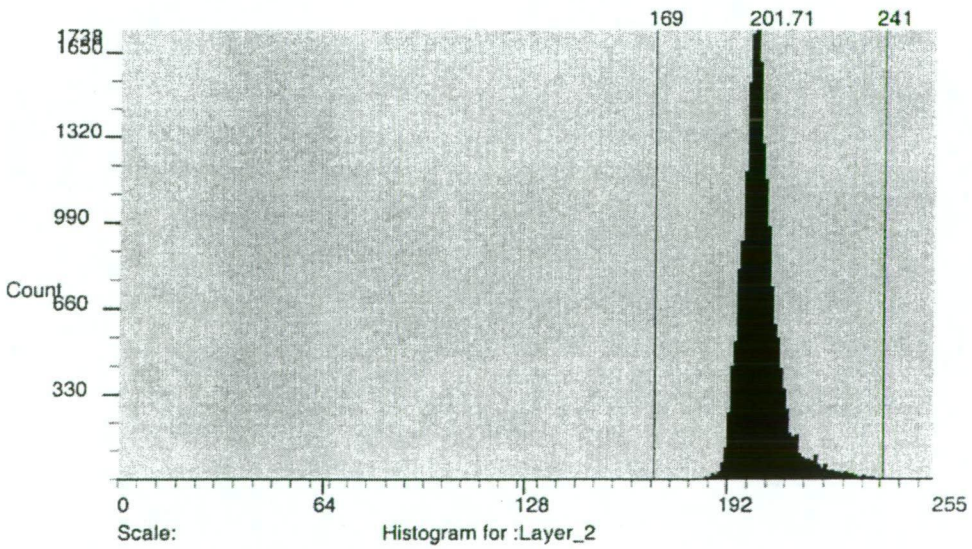

Horizontal Axis: 1 tic = 6 Data Value(s)
Vertical Axis: 1 tic = 110 Counts

E.7 Landsat5 TM 21 July 1998

Histogram:
Bin Function: Direct
Minimum: 6
Maximum: 116
Mean: 40.2196

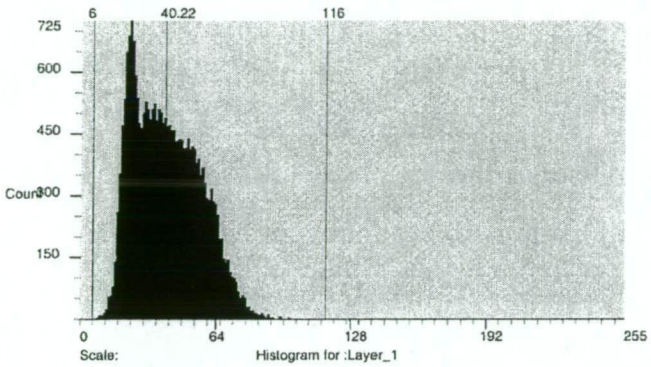

Scale: Histogram for :Layer_1
Horizontal Axis: 1 tic = 6 Data Value(s)
Vertical Axis: 1 tic = 50 Counts

Histogram:
Bin Function: Direct
Minimum: 165
Maximum: 242
Mean: 200.822

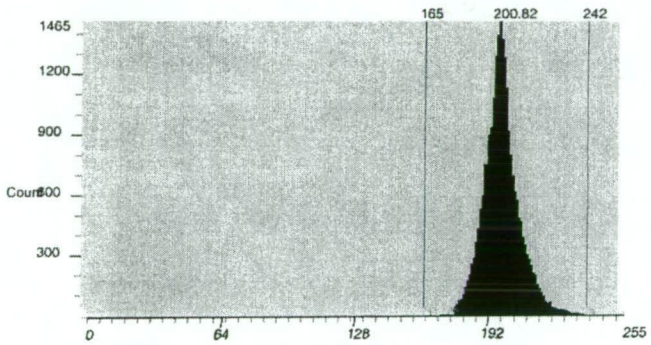

Scale: Histogram for :Layer_2
Horizontal Axis: 1 tic = 6 Data Value(s)
Vertical Axis: 1 tic = 100 Counts

Histogram:
Bin Function: Direct
Minimum: 128
Maximum: 175
Mean: 159.693

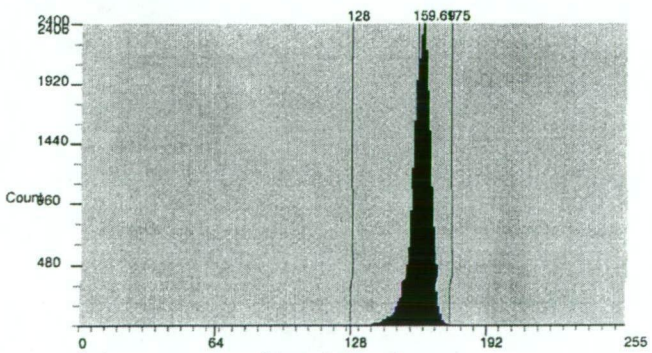

Scale: Histogram for :Layer_3
Horizontal Axis: 1 tic = 6 Data Value(s)
Vertical Axis: 1 tic = 160 Counts

E.8 Landsat5 TM 27 September 1998

Histogram:
Bin Function: Direct
Minimum: 16
Maximum: 129
Mean: 55.4317

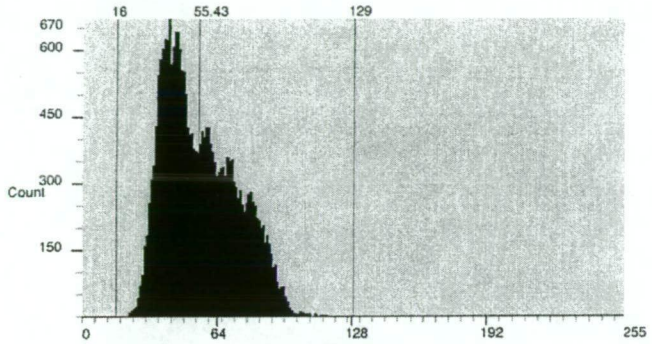

Horizontal Axis: 1 tic = 6 Data Value(s)
Vertical Axis: 1 tic = 50 Counts

Histogram:
Bin Function: Direct
Minimum: 137
Maximum: 233
Mean: 191.003

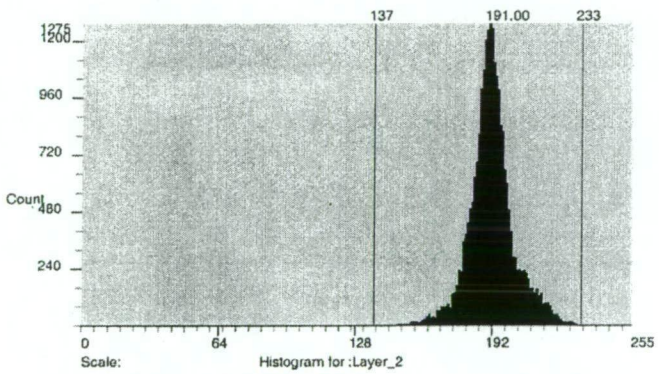

Horizontal Axis: 1 tic = 6 Data Value(s)
Vertical Axis: 1 tic = 80 Counts

Histogram:
Bin Function: Direct
Minimum: 189
Maximum: 228
Mean: 214.839

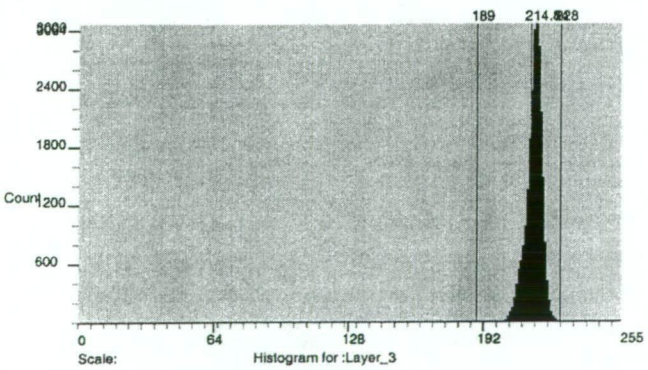

Horizontal Axis: 1 tic = 6 Data Value(s)
Vertical Axis: 1 tic = 200 Counts

E.9 SPOT4 HRVIR1XI 08 October 1998

Histogram:
Bin Function: Direct
Minimum: 35
Maximum: 226
Mean: 110.7

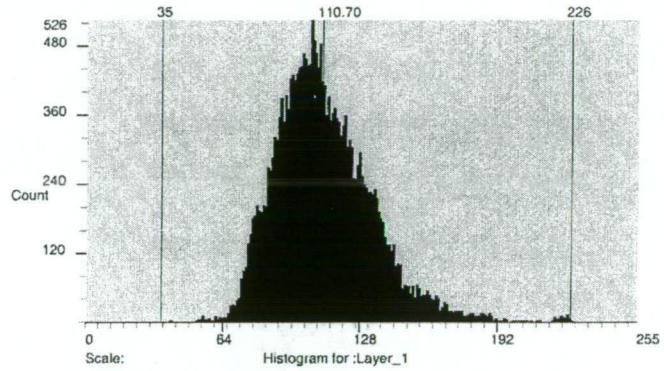

Horizontal Axis: 1 tic = 6 Data Value(s)
Vertical Axis: 1 tic = 40 Counts

Histogram:
Bin Function: Direct
Minimum: 23
Maximum: 221
Mean: 104.774

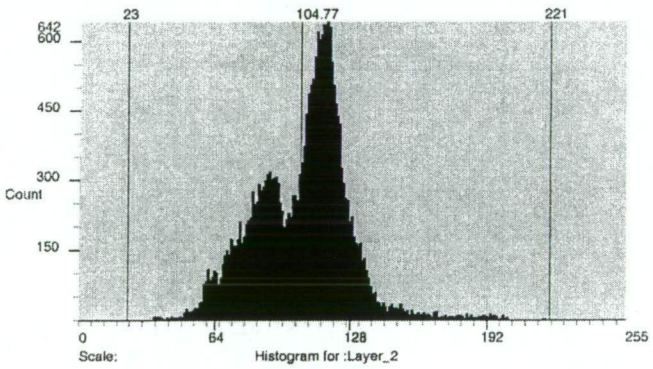

Horizontal Axis: 1 tic = 6 Data Value(s)
Vertical Axis: 1 tic = 50 Counts

Histogram:
Bin Function: Direct
Minimum: 75
Maximum: 226
Mean: 169.93

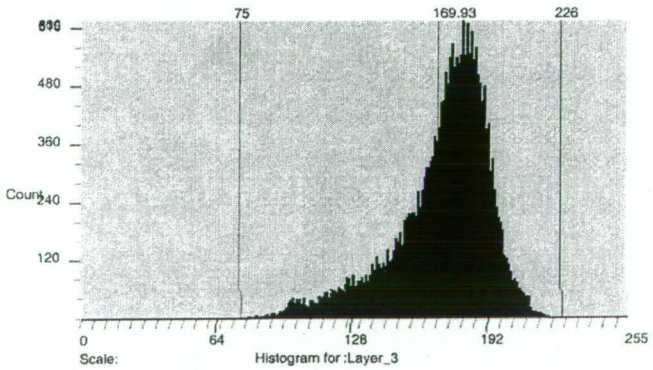

Horizontal Axis: 1 tic = 6 Data Value(s)
Vertical Axis: 1 tic = 40 Counts

E.10 SPOT4 HRVIR1XI 31 December 1998

Histogram:
Bin Function: Direct
Minimum: 45
Maximum: 242
Mean: 149.651

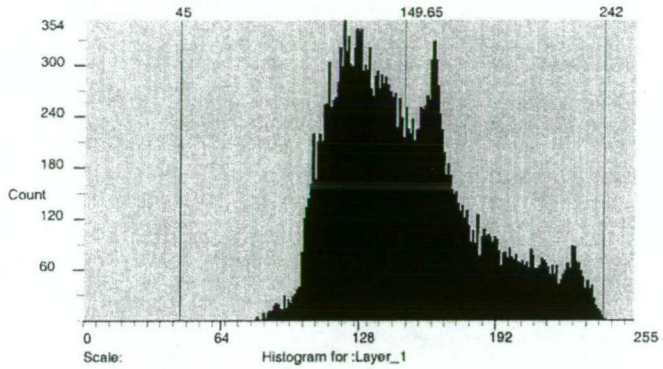

Histogram:
Bin Function: Direct
Minimum: 15
Maximum: 224
Mean: 117.035

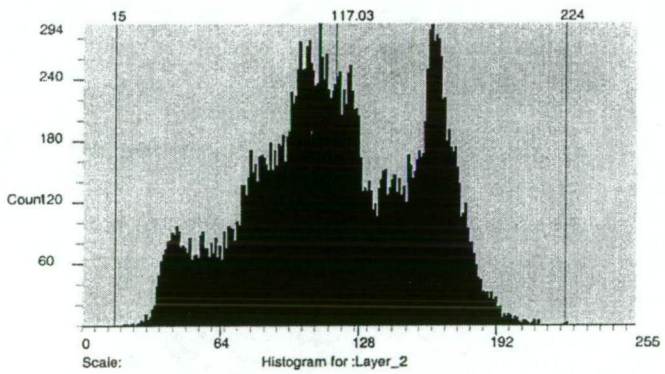

Histogram:
Bin Function: Direct
Minimum: 33
Maximum: 228
Mean: 117.542

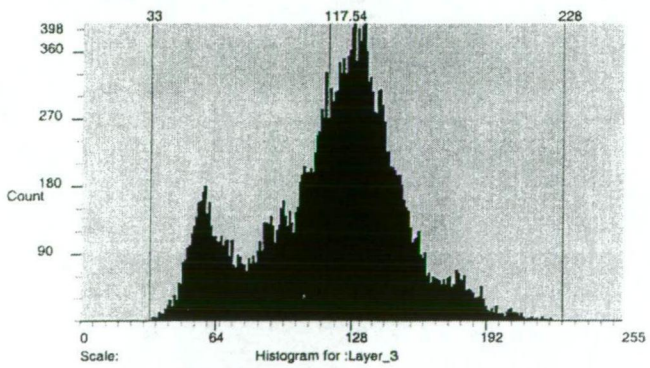

E.11 Landsat5 TM 29 January 1999

Histogram:
Bin Function: Direct
Minimum: 8
Maximum: 189
Mean: 66.5001

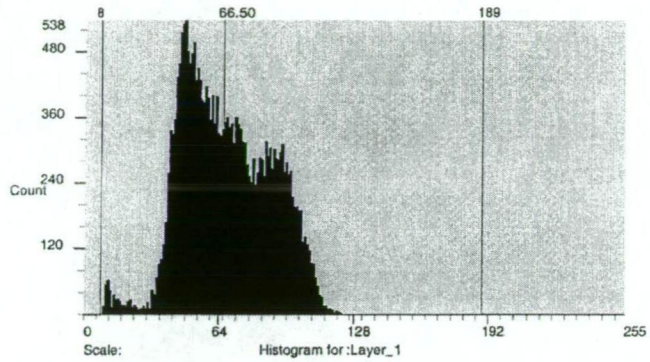

Horizontal Axis: 1 tic = 6 Data Value(s)
Vertical Axis: 1 tic = 40 Counts

Histogram:
Bin Function: Direct
Minimum: 68
Maximum: 223
Mean: 136.897

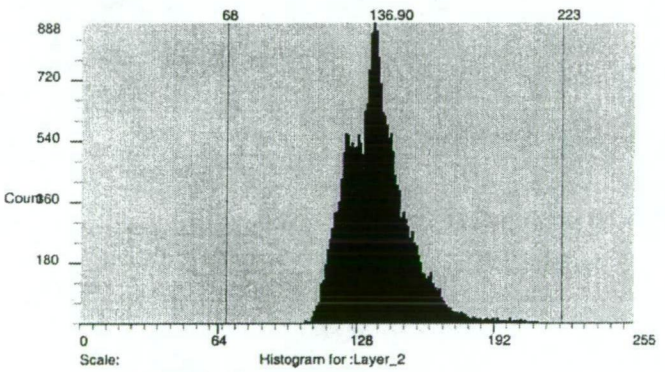

Horizontal Axis: 1 tic = 6 Data Value(s)
Vertical Axis: 1 tic = 60 Counts

Histogram:
Bin Function: Direct
Minimum: 94
Maximum: 245
Mean: 225.96

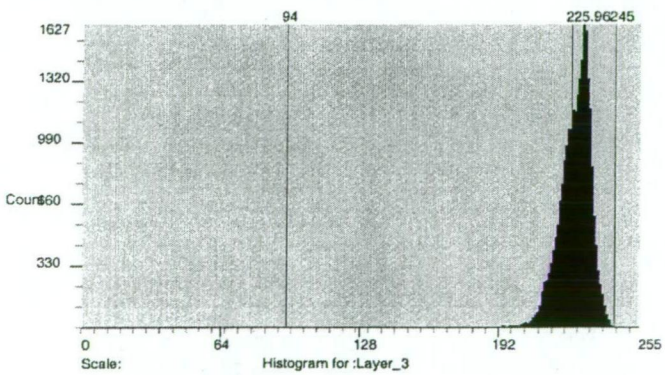

Horizontal Axis: 1 tic = 6 Data Value(s)
Vertical Axis: 1 tic = 110 Counts

E.12 Landsat5 TM 03 March 1999

Histogram:
Bin Function: Direct
Minimum: 7
Maximum: 145
Mean: 55.2102

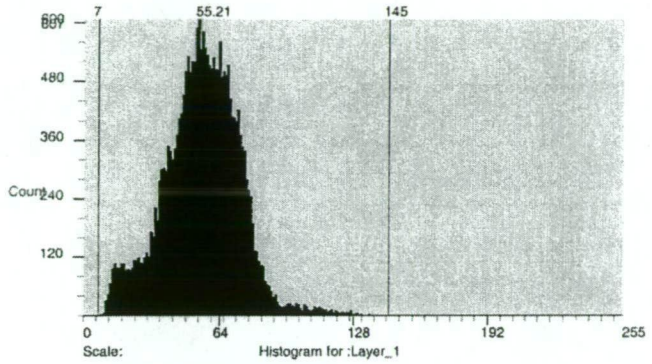

Histogram:
Bin Function: Direct
Minimum: 89
Maximum: 228
Mean: 159.797

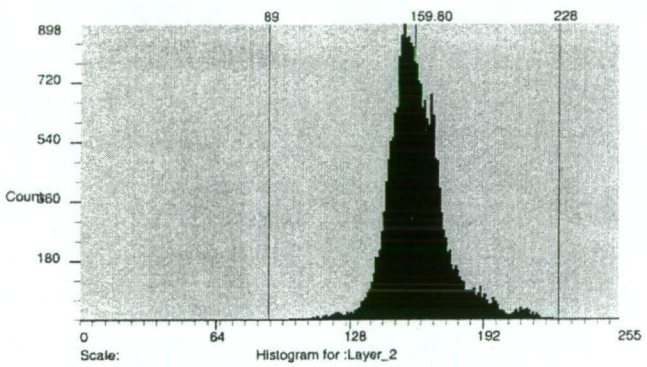

Histogram:
Bin Function: Direct
Minimum: 94
Maximum: 183
Mean: 142.312

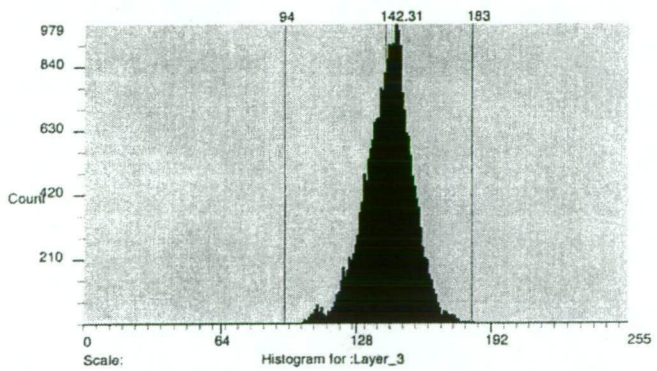

E.13 SPOT4 HRVIR2XI 29 March 1999

Histogram:
Bin Function: Direct
Minimum: 17
Maximum: 108
Mean: 57.6672

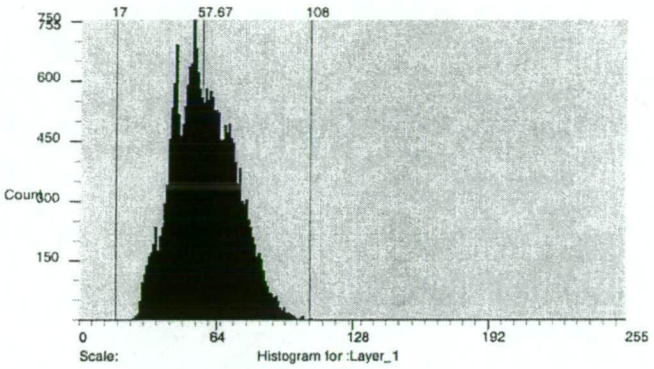

Histogram:
Bin Function: Direct
Minimum: 12
Maximum: 112
Mean: 65.5711

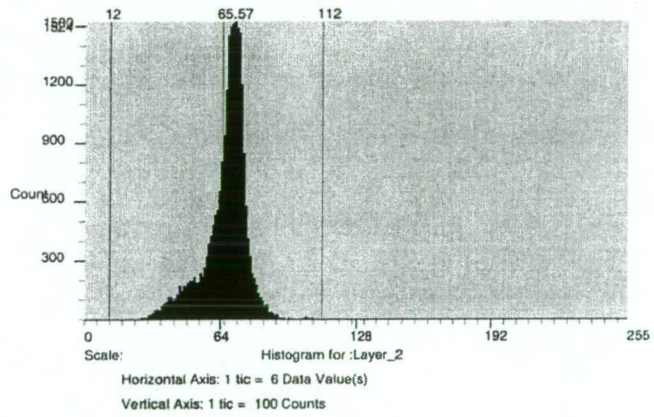

Histogram:
Bin Function: Direct
Minimum: 89
Maximum: 170
Mean: 132.069

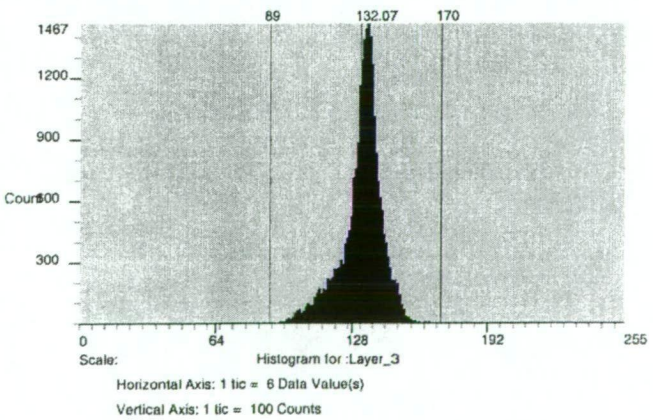

APPENDIX F.

CONTRIBUTION OF TRAINING DATA TO CLASSIFICATION

POPPIES

F.1 Landsat TM 06 October 1997

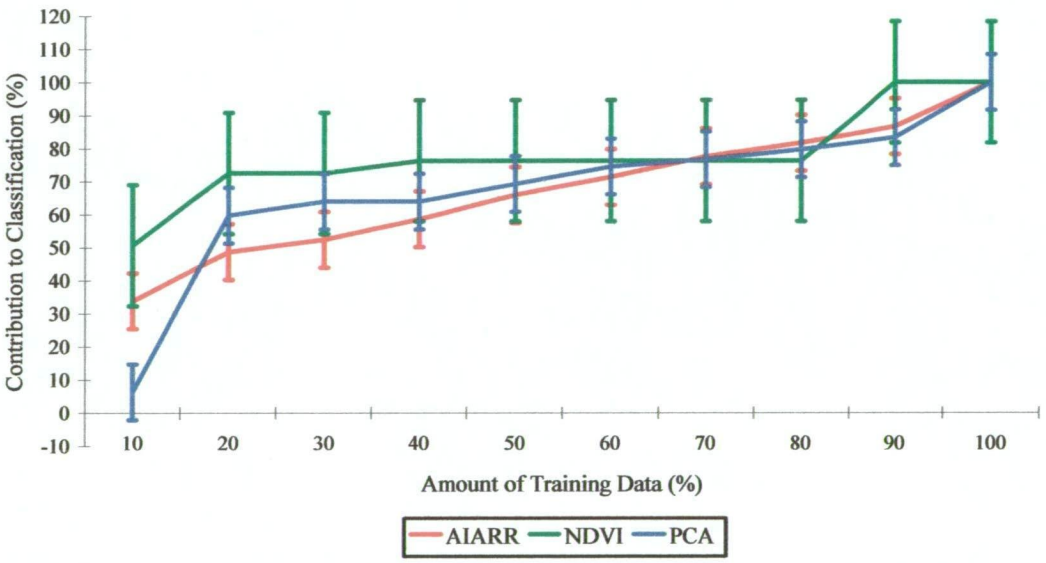

Figure F.1: Contribution of training data to classification of poppies in Landsat TM 06 October 1997 image, using three analysis methods, with bars indicating least significant difference associated with each processing method

Oneway Analysis of TM 06 October 1997 By Method

Analysis of Variance

Source	DF	Sum of Squares	Mean Square	F Ratio	Prob > F
Method	2	653.400	326.700	0.8185	0.4518
Error	27	10777.300	399.159		
C. Total	29	11430.700			

Means for Oneway Anova

Level	Number	Mean	Std Error	Lower 95%	Upper 95%
AIARR	10	67.8000	6.3179	54.837	80.763
NDVI	10	77.7000	6.3179	64.737	90.663
PCA	10	67.8000	6.3179	54.837	80.763

Std Error uses a pooled estimate of error variance

Means Comparisons

Dif=Mean[i]-Mean[j]	NDVI	AIARR	PCA
NDVI	0.00000	9.90000	9.90000
AIARR	-9.90000	0.00000	0.00000
PCA	-9.90000	0.00000	0.00000

Alpha= 0.05

Comparisons for each pair using Student's t

t
2.05183

Abs(Dif)-LSD	NDVI	AIARR	PCA
NDVI	-18.3328	-8.4328	-8.4328
AIARR	-8.4328	-18.3328	-18.3328
PCA	-8.4328	-18.3328	-18.3328

Positive values show pairs of means that are significantly different.

F.2 Landsat TM 23 November 1997

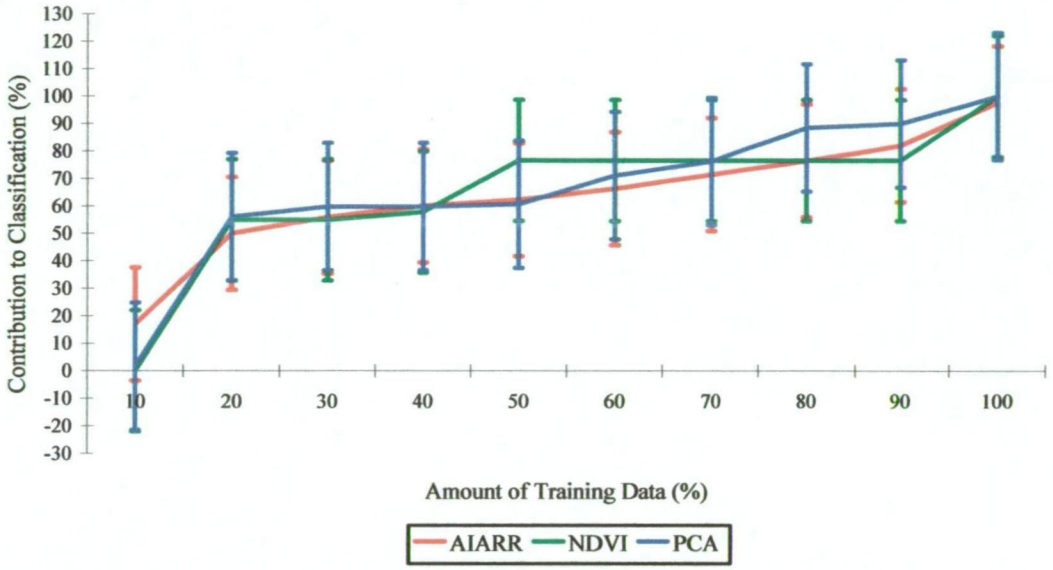

Figure F.2: Contribution of training data to classification of poppies in Landsat TM 23 November 1997 image, using three analysis methods, with bars indicating least significant difference associated with each processing method

Oneway Analysis of TM 23 November 1997 By Method

Analysis of Variance

Source	DF	Sum of Squares	Mean Square	F Ratio	Prob > F
Method	2	34.067	17.033	0.0267	0.9737
Error	27	17216.100	637.633		
C. Total	29	17250.167			

Means for Oneway Anova

Level	Number	Mean	Std Error	Lower 95%	Upper 95%
AIARR	10	63.8000	7.9852	47.416	80.184
NDVI	10	65.3000	7.9852	48.916	81.684
PCA	10	66.4000	7.9852	50.016	82.784

Std Error uses a pooled estimate of error variance

Means Comparisons

Dif=Mean[i]-Mean[j]	PCA	NDVI	AIARR
PCA	0.00000	1.10000	2.60000
NDVI	-1.10000	0.00000	1.50000
AIARR	-2.60000	-1.50000	0.00000

Alpha=0.05

Comparisons for each pair using Student's t

t
2.05183

Abs(Dif)-LSD	PCA	NDVI	AIARR
PCA	-23.1709	-22.0709	-20.5709
NDVI	-22.0709	-23.1709	-21.6709
AIARR	-20.5709	-21.6709	-23.1709

Positive values show pairs of means that are significantly different.

F.3 Landsat TM 10 January 1998

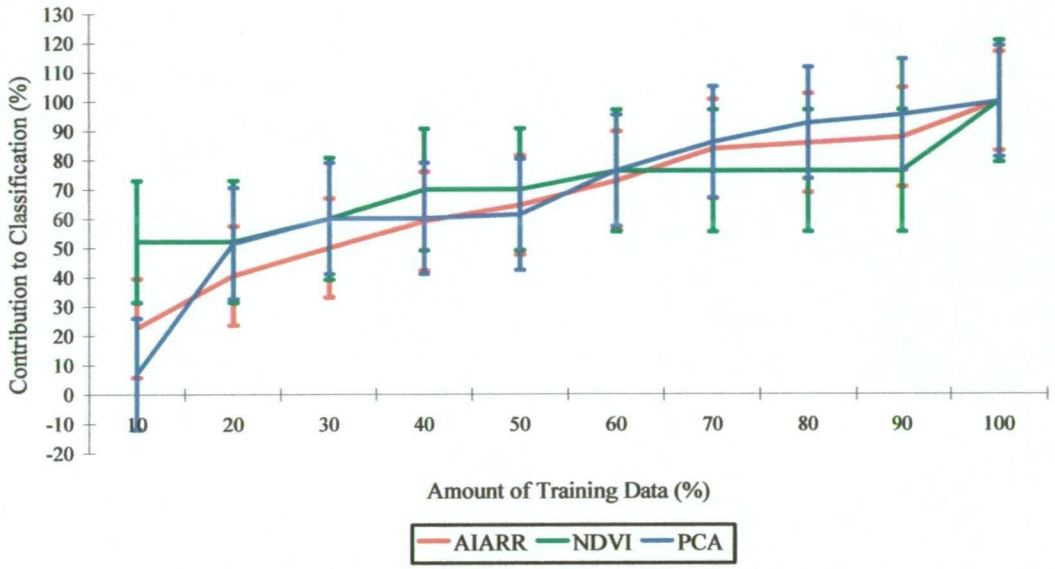

Figure F.3: Contribution of training data to classification of poppies in Landsat TM 10 January 1998 image, using three analysis methods, with bars indicating least significant difference associated with each processing method

Oneway Analysis of TM 10 January 1998 By Method

Analysis of Variance

Source	DF	Sum of Squares	Mean Square	F Ratio	Prob > F
Method	2	76.200	38.100	0.0741	0.9288
Error	27	13880.500	514.093		
C. Total	29	13956.700			

Means for Oneway Anova

Level	Number	Mean	Std Error	Lower 95%	Upper 95%
AIARR	10	66.9000	7.1700	52.188	81.612
NDVI	10	70.8000	7.1700	56.088	85.512
PCA	10	69.0000	7.1700	54.288	83.712

Std Error uses a pooled estimate of error variance

Means Comparisons

Dif=Mean[i]-Mean[j]	NDVI	PCA	AIARR
NDVI	0.00000	1.80000	3.90000
PCA	-1.80000	0.00000	2.10000
AIARR	-3.90000	-2.10000	0.00000

Alpha=0.05

Comparisons for each pair using Student's t

t
2.05183

Abs(Dif)-LSD	NDVI	PCA	AIARR
NDVI	-20.8055	-19.0055	-16.9055
PCA	-19.0055	-20.8055	-18.7055
AIARR	-16.9055	-18.7055	-20.8055

Positive values show pairs of means that are significantly different.

F.4 SPOT XS 23 February 1998

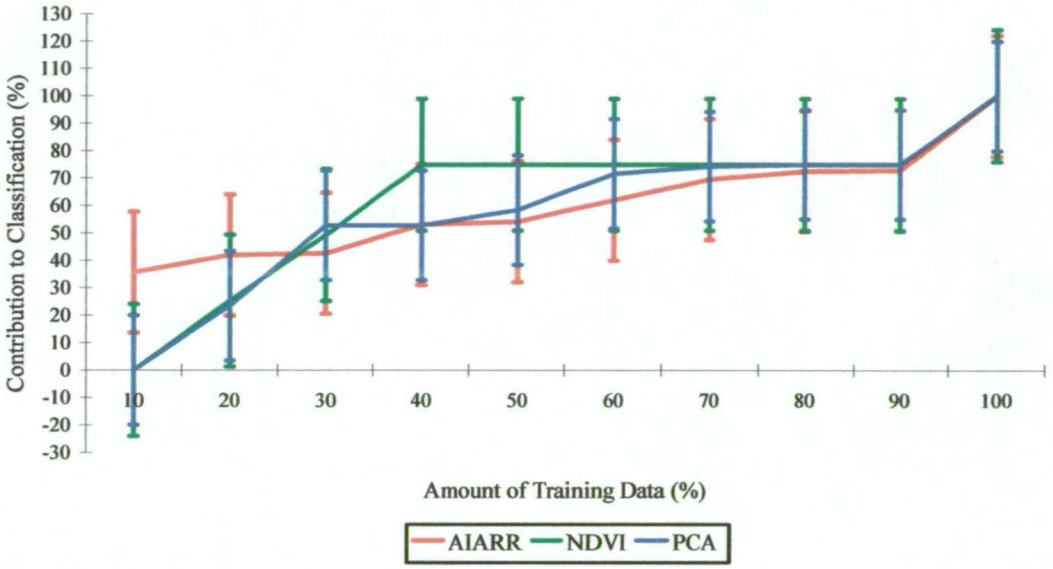

Figure F.4: Contribution of training data to classification of poppies in SPOT XS 23 February 1998 image, using three analysis methods, with bars indicating least significant difference associated with each processing method

Oneway Analysis of XS 23 February 1998 By Method

Analysis of Variance

Source	DF	Sum of Squares	Mean Square	F Ratio	Prob > F
Method	2	84.067	42.033	0.0612	0.9408
Error	27	18540.900	686.700		
C. Total	29	18624.967			

Means for Oneway Anova

Level	Number	Mean	Std Error	Lower 95%	Upper 95%
AIARR	10	60.4000	8.2867	43.397	77.403
NDVI	10	62.4000	8.2867	45.397	79.403
PCA	10	58.3000	8.2867	41.297	75.303

Std Error uses a pooled estimate of error variance

Means Comparisons

Dif=Mean[i]-Mean[j]	NDVI	AIARR	PCA
NDVI	0.00000	2.00000	4.10000
AIARR	-2.00000	0.00000	2.10000
PCA	-4.10000	-2.10000	0.00000

Alpha=0.05

Comparisons for each pair using Student's t

t
2.05183

Abs(Dif)-LSD	NDVI	AIARR	PCA
NDVI	-24.0458	-22.0458	-19.9458
AIARR	-22.0458	-24.0458	-21.9458
PCA	-19.9458	-21.9458	-24.0458

Positive values show pairs of means that are significantly different.

F.5 Landsat TM 27 September 1998

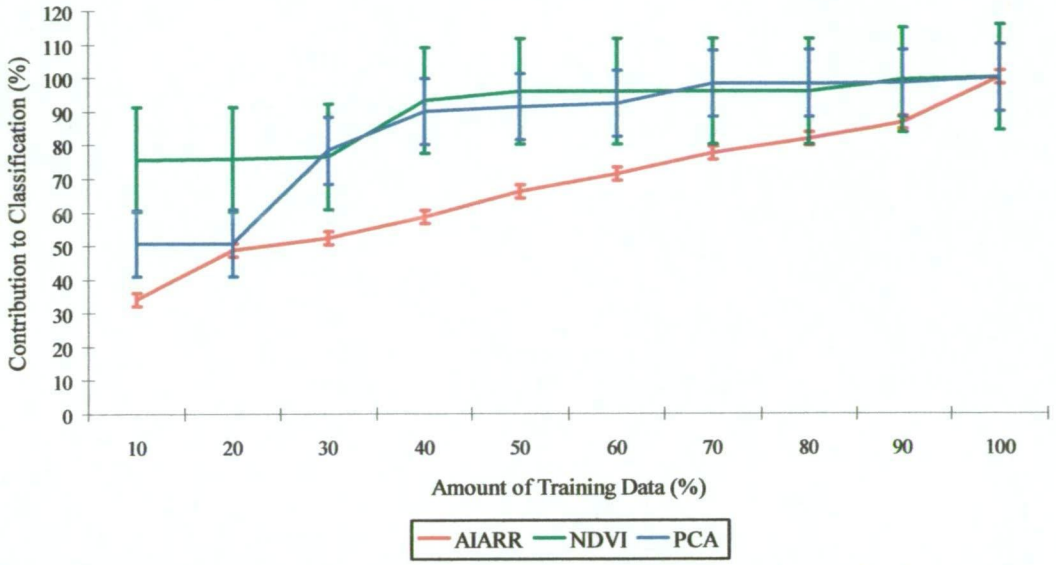

Figure F.5: Contribution of training data to classification of poppies in Landsat TM 27 September 1998 image, using three analysis methods, with bars indicating least significant difference associated with each processing method

Oneway Analysis of TM 27 September 1998 By Method

Analysis of Variance

Source	DF	Sum of Squares	Mean Square	F Ratio	Prob > F
Method	2	1612.8667	806.433	2.7808	0.0798
Error	27	7830.1000	290.004		
C. Total	29	9442.9667			

Means for Oneway Anova

Level	Number	Mean	Std Error	Lower 95%	Upper 95%
AIARR	10	72.8000	5.3852	61.750	83.85
NDVI	10	90.4000	5.3852	79.350	101.45
PCA	10	84.7000	5.3852	73.650	95.75

Std Error uses a pooled estimate of error variance

Means Comparisons

Dif=Mean[i]-Mean[j]	NDVI	PCA	AIARR
NDVI	0.0000	5.7000	17.6000
PCA	-5.7000	0.0000	11.9000
AIARR	-17.6000	-11.9000	0.0000

Alpha=0.05

Comparisons for each pair using Student's t

t
2.05183

Abs(Dif)-LSD	NDVI	PCA	AIARR
NDVI	-15.6264	-9.9264	1.9736
PCA	-9.9264	-15.6264	-3.7264
AIARR	1.9736	-3.7264	-15.6264

Positive values show pairs of means that are significantly different.

F.6 SPOT XI 08 October 1998

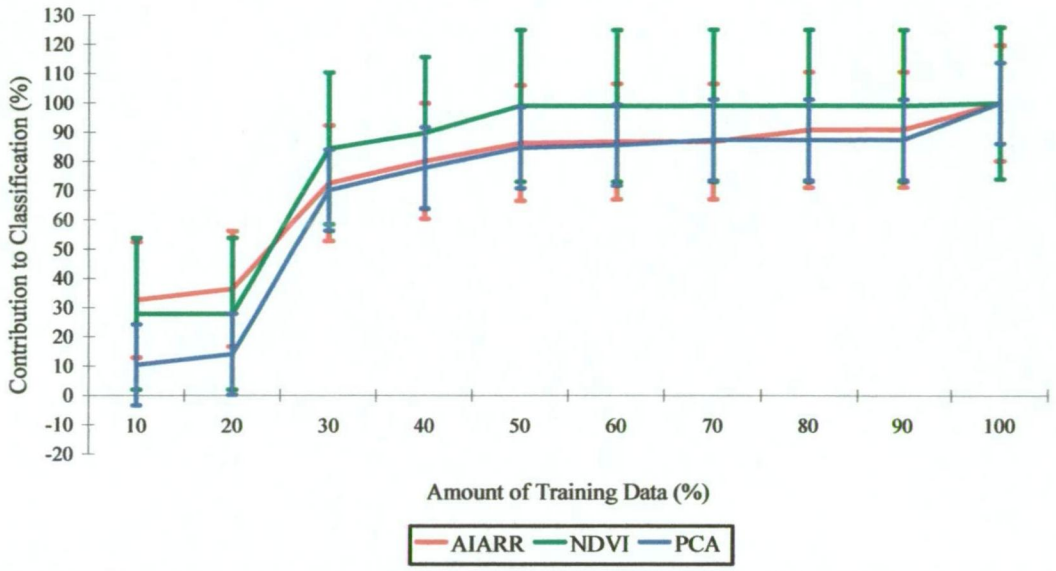

Figure F.6: Contribution of training data to classification of poppies in SPOT XI 08 October 1998 image, using three analysis methods, with bars indicating least significant difference associated with each processing method

Oneway Analysis of XI 08 October 1998 By Method

Analysis of Variance

Source	DF	Sum of Squares	Mean Square	F Ratio	Prob > F
Method	2	732.200	366.100	0.4585	0.6371
Error	27	21561.000	798.556		
C. Total	29	22293.200			

Means for Oneway Anova

Level	Number	Mean	Std Error	Lower 95%	Upper 95%
AIARR	10	76.3000	8.9362	57.964	94.64
NDVI	10	82.5000	8.9362	64.164	100.84
PCA	10	70.4000	8.9362	52.064	88.74

Std Error uses a pooled estimate of error variance

Means Comparisons

Dif=Mean[i]-Mean[j]	NDVI	AIARR	PCA
NDVI	0.0000	6.2000	12.1000
AIARR	-6.2000	0.0000	5.9000
PCA	-12.1000	-5.9000	0.0000

Alpha=0.05

Comparisons for each pair using Student's t

t
2.05183

Abs(Dif)-LSD	NDVI	AIARR	PCA
NDVI	-25.9304	-19.7304	-13.8304
AIARR	-19.7304	-25.9304	-20.0304
PCA	-13.8304	-20.0304	-25.9304

Positive values show pairs of means that are significantly different.

F.7 SPOT XI 31 December 1998

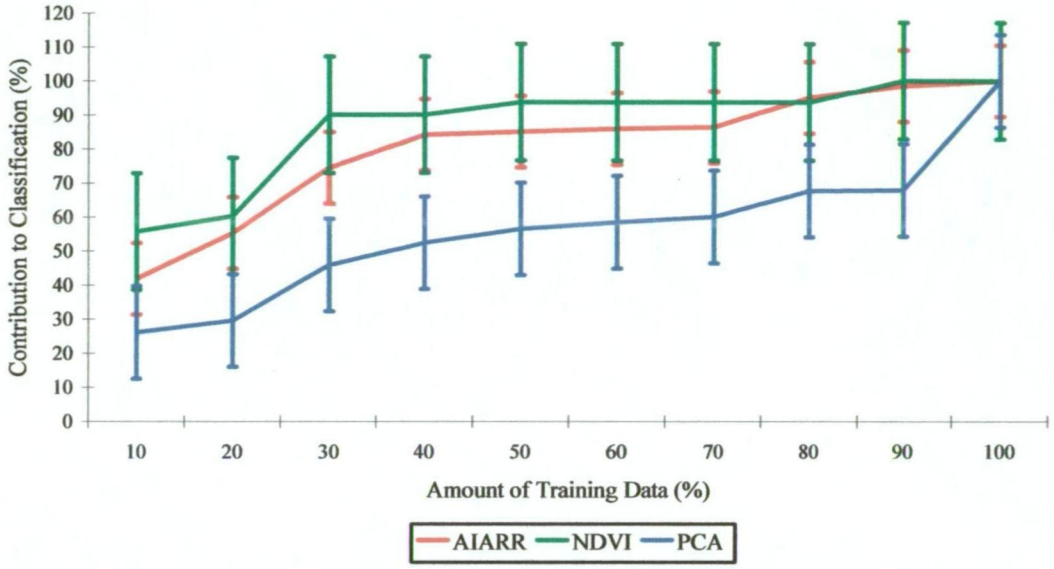

Figure F.7: Contribution of training data to classification of poppies in SPOT XI 31 December 1998 image, using three analysis methods, with bars indicating least significant difference associated with each processing method

Oneway Analysis of XI 31 December 1998 By Method

Analysis of Variance

Source	DF	Sum of Squares	Mean Square	F Ratio	Prob > F
Method	2	5222.867	2611.43	7.5197	0.0025
Error	27	9376.500	347.28		
C. Total	29	14599.367			

Means for Oneway Anova

Level	Number	Mean	Std Error	Lower 95%	Upper 95%
AIARR	10	80.6000	5.8930	68.509	92.691
NDVI	10	87.2000	5.8930	75.109	99.291
PCA	10	56.5000	5.8930	44.409	68.591

Std Error uses a pooled estimate of error variance

Means Comparisons

Dif=Mean[i]-Mean[j]	NDVI	AIARR	PCA
NDVI	0.0000	6.6000	30.7000
AIARR	-6.6000	0.0000	24.1000
PCA	-30.7000	-24.1000	0.0000

Alpha=0.05

Comparisons for each pair using Student's t

t
2.05183

Abs(Dif)-LSD	NDVI	AIARR	PCA
NDVI	-17.1000	-10.5000	13.6000
AIARR	-10.5000	-17.1000	7.0000
PCA	13.6000	7.0000	-17.1000

Positive values show pairs of means that are significantly different.

F.9 Landsat TM 29 January 1999

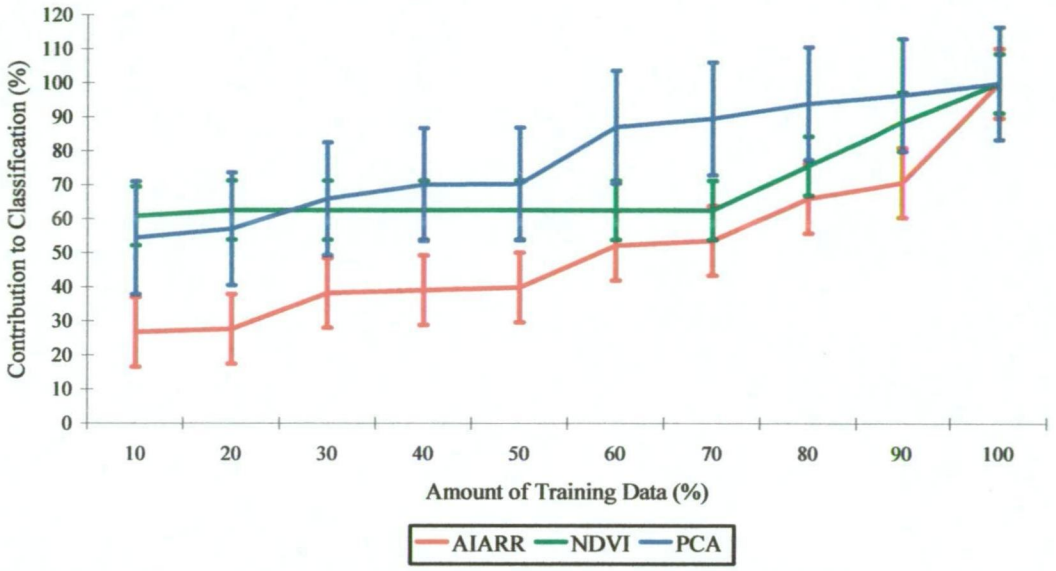

Figure F.8: Contribution of training data to classification of poppies in Landsat TM 29 January 1999 image, using three analysis methods, with bars indicating least significant difference associated with each processing method

Oneway Analysis of TM 29 January 1999 By Method

Analysis of Variance

Source	DF	Sum of Squares	Mean Square	F Ratio	Prob > F
Method	2	3792.867	1896.43	5.8206	0.0079
Error	27	8797.000	325.81		
C. Total	29	12589.867			

Means for Oneway Anova

Level	Number	Mean	Std Error	Lower 95%	Upper 95%
AIARR	10	51.5000	5.7080	39.788	63.212
NDVI	10	70.4000	5.7080	58.688	82.112
PCA	10	78.3000	5.7080	66.588	90.012

Std Error uses a pooled estimate of error variance

Means Comparisons

Dif=Mean[i]-Mean[j]	PCA	NDVI	AIARR
PCA	0.0000	7.9000	26.8000
NDVI	-7.9000	0.0000	18.9000
AIARR	-26.8000	-18.9000	0.0000

Alpha=0.05

Comparisons for each pair using Student's t

t
2.05183

Abs(Dif)-LSD	PCA	NDVI	AIARR
PCA	-16.5631	-8.6631	10.2369
NDVI	-8.6631	-16.5631	2.3369
AIARR	10.2369	2.3369	-16.5631

Positive values show pairs of means that are significantly different.

F.9 Landsat TM 03 March 1999

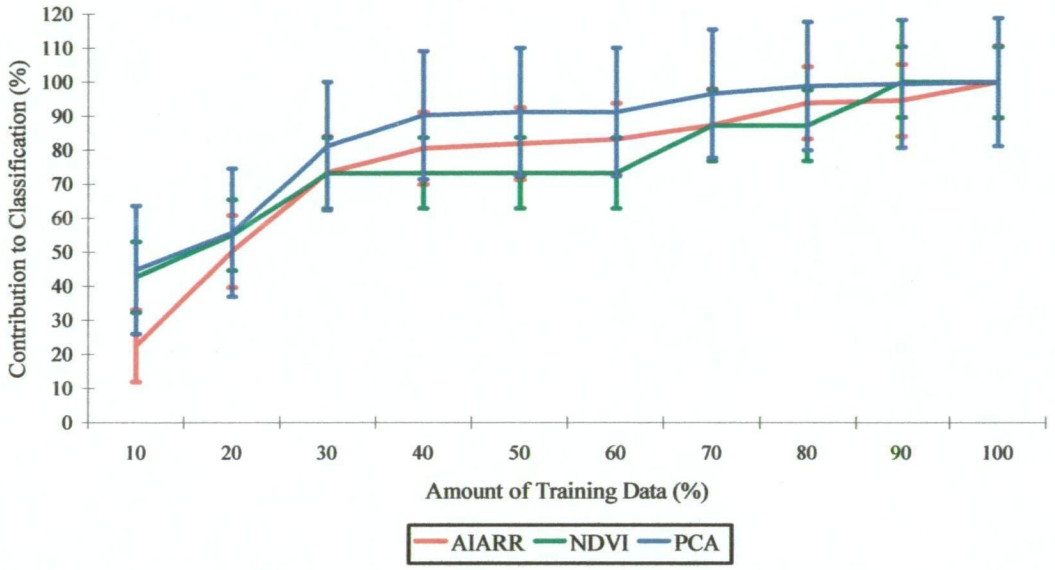

Figure F.9: Contribution of training data to classification of poppies in Landsat TM 03 March 1999 image, using three analysis methods, with bars indicating least significant difference associated with each processing method

Oneway Analysis of TM 03 March 1999 By Method

Analysis of Variance

Source	DF	Sum of Squares	Mean Square	F Ratio	Prob > F
Method	2	459.467	229.733	0.5474	0.5847
Error	27	11330.400	419.644		
C. Total	29	11789.867			

Means for Oneway Anova

Level	Number	Mean	Std Error	Lower 95%	Upper 95%
AIARR	10	76.6000	6.4780	63.308	89.892
NDVI	10	76.4000	6.4780	63.108	89.692
PCA	10	84.8000	6.4780	71.508	98.092

Std Error uses a pooled estimate of error variance

Means Comparisons

Dif=Mean[i]-Mean[j]	PCA	AIARR	NDVI
PCA	0.00000	8.20000	8.40000
AIARR	-8.20000	0.00000	0.20000
NDVI	-8.40000	-0.20000	0.00000

Alpha=0.05

Comparisons for each pair using Student's t

t
2.05183

Abs(Dif)-LSD	PCA	AIARR	NDVI
PCA	-18.7974	-10.5974	-10.3974
AIARR	-10.5974	-18.7974	-18.5974
NDVI	-10.3974	-18.5974	-18.7974

Positive values show pairs of means that are significantly different.

APPENDIX G.

CONTRIBUTION OF TRAINING DATA TO CLASSIFICATION

PYRETHRUM

G.1 Landsat TM 02 July 1997

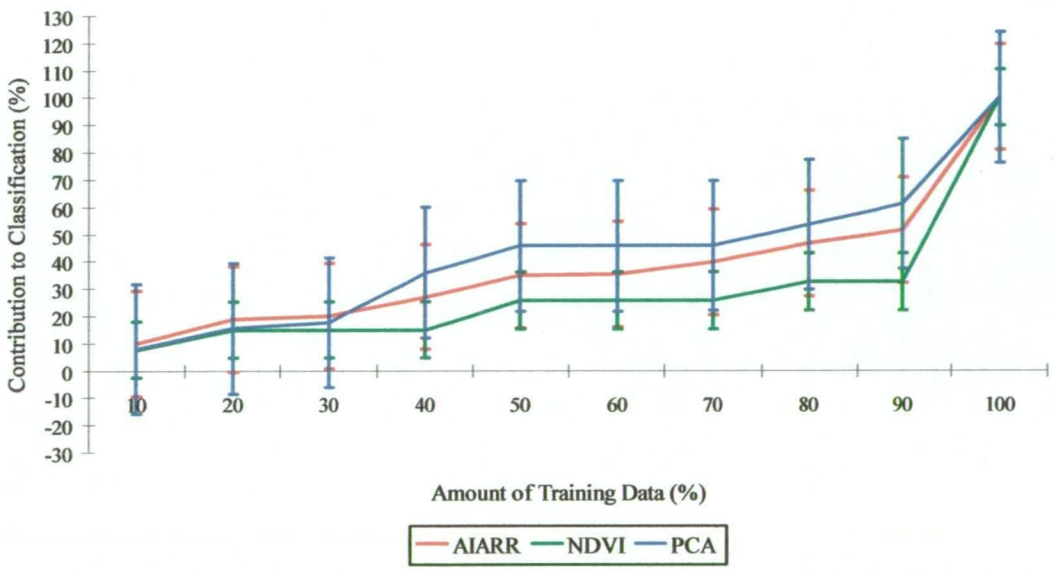

Figure G.1: Contribution of training data to classification of pyrethrum in Landsat TM 02 July 1997 image, using three analysis methods, with bars indicating least significant difference associated with each processing method

Oneway Analysis of TM 02 July 1997 By Method

Analysis of Variance

Source	DF	Sum of Squares	Mean Square	F Ratio	Prob > F
Method	2	930.067	465.033	0.6899	0.5103
Error	27	18199.800	674.067		
C. Total	29	19129.867			

Means for Oneway Anova

Level	Number	Mean	Std Error	Lower 95%	Upper 95%
AIARR	10	38.4000	8.2102	21.554	55.246
NDVI	10	29.5000	8.2102	12.654	46.346
PCA	10	42.9000	8.2102	26.054	59.746

Std Error uses a pooled estimate of error variance

Means Comparisons

Dif=Mean[i]-Mean[j]	PCA	AIARR	NDVI
PCA	0.0000	4.5000	13.4000
AIARR	-4.5000	0.0000	8.9000
NDVI	-13.4000	-8.9000	0.0000

Alpha=0.05

Comparisons for each pair using Student's t

t
2.05183

Abs(Dif)-LSD	PCA	AIARR	NDVI
PCA	-23.8236	-19.3236	-10.4236
AIARR	-19.3236	-23.8236	-14.9236
NDVI	-10.4236	-14.9236	-23.8236

Positive values show pairs of means that are significantly different.

G.2 Landsat TM 06 October 1997

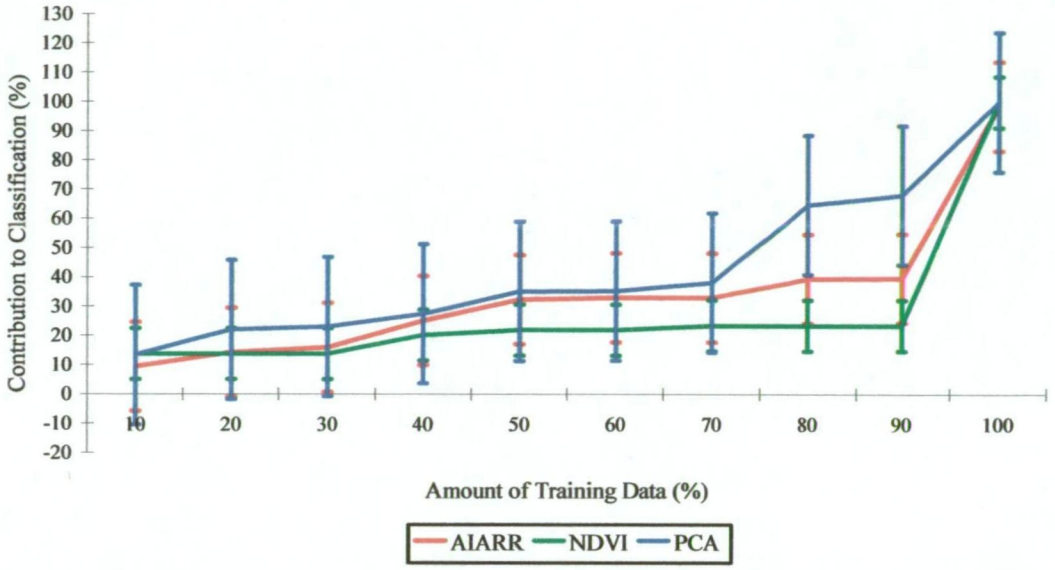

Figure G.2: Contribution of training data to classification of pyrethrum in Landsat TM 06 October 1997 image, using three analysis methods, with bars indicating least significant difference associated with each processing method

Oneway Analysis of TM 06 October 1997 By Method

Analysis of Variance

Source	DF	Sum of Squares	Mean Square	F Ratio	Prob > F
Method	2	1147.400	573.700	0.8507	0.4383
Error	27	18208.900	674.404		
C. Total	29	19356.300			

Means for Oneway Anova

Level	Number	Mean	Std Error	Lower 95%	Upper 95%
AIARR	10	34.0000	8.2122	17.150	50.850
NDVI	10	27.5000	8.2122	10.650	44.350
PCA	10	42.6000	8.2122	25.750	59.450

Std Error uses a pooled estimate of error variance

Means Comparisons

Dif=Mean[i]-Mean[j]	PCA	AIARR	NDVI
PCA	0.0000	8.6000	15.1000
AIARR	-8.6000	0.0000	6.5000
NDVI	-15.1000	-6.5000	0.0000

Alpha=0.05

Comparisons for each pair using Student's t

t
2.05183

Abs(Dif)-LSD	PCA	AIARR	NDVI
PCA	-23.8296	-15.2296	-8.7296
AIARR	-15.2296	-23.8296	-17.3296
NDVI	-8.7296	-17.3296	-23.8296

Positive values show pairs of means that are significantly different.

G.3 Landsat TM 23 November 1997

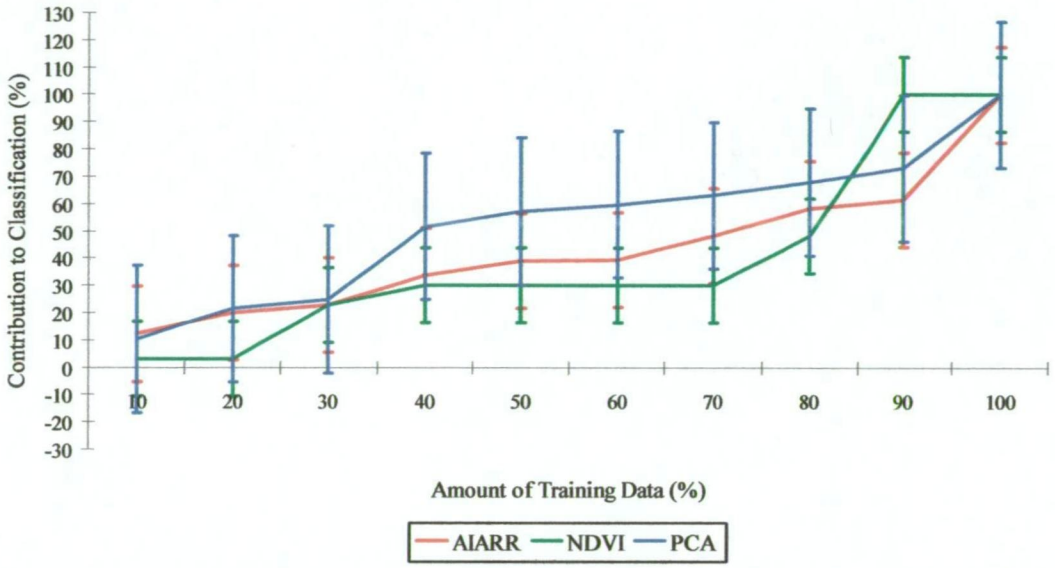

Figure G.3: Contribution of training data to classification of pyrethrum in Landsat TM 23 November 1997 image, using three analysis methods, with bars indicating least significant difference associated with each processing method

Oneway Analysis of TM 23 November 1997 By Method

Analysis of Variance

Source	DF	Sum of Squares	Mean Square	F Ratio	Prob > F
Method	2	927.267	463.633	0.5402	0.5888
Error	27	23171.400	858.200		
C. Total	29	24098.667			

Means for Oneway Anova

Level	Number	Mean	Std Error	Lower 95%	Upper 95%
AIARR	10	43.4000	9.2639	24.392	62.408
NDVI	10	39.7000	9.2639	20.692	58.708
PCA	10	52.9000	9.2639	33.892	71.908

Std Error uses a pooled estimate of error variance

Means Comparisons

Dif=Mean[i]-Mean[j]	PCA	AIARR	NDVI
PCA	0.0000	9.5000	13.2000
AIARR	-9.5000	0.0000	3.7000
NDVI	-13.2000	-3.7000	0.0000

Alpha=0.05

Comparisons for each pair using Student's t

t
2.05183

Abs(Dif)-LSD	PCA	AIARR	NDVI
PCA	-26.8813	-17.3813	-13.6813
AIARR	-17.3813	-26.8813	-23.1813
NDVI	-13.6813	-23.1813	-26.8813

Positive values show pairs of means that are significantly different.

G.4 Landsat TM 10 January 1998

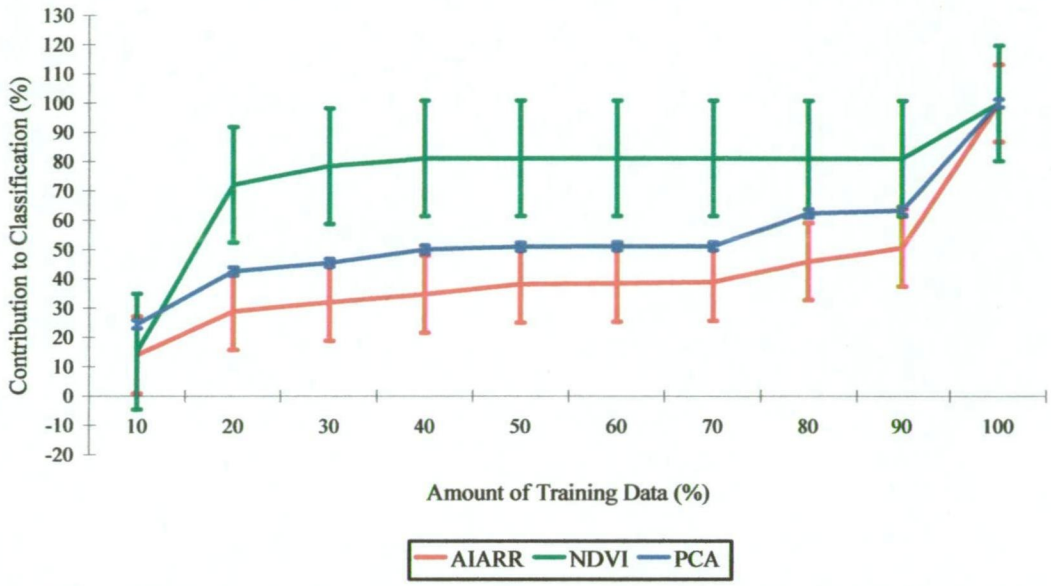

Figure G.4: Contribution of training data to classification of pyrethrum in Landsat TM 10 January 1998 image, using three analysis methods, with bars indicating least significant difference associated with each processing method

Oneway Analysis of TM 10 January 1998 By Method

Analysis of Variance

Source	DF	Sum of Squares	Mean Square	F Ratio	Prob > F
Method	2	5556.200	2778.10	6.0159	0.0069
Error	27	12468.500	461.80		
C. Total	29	18024.700			

Means for Oneway Anova

Level	Number	Mean	Std Error	Lower 95%	Upper 95%
AIARR	10	42.2000	6.7956	28.257	56.143
NDVI	10	75.1000	6.7956	61.157	89.043
PCA	10	54.0000	6.7956	40.057	67.943

Std Error uses a pooled estimate of error variance

Means Comparisons

Dif=Mean[i]-Mean[j]	NDVI	PCA	AIARR
NDVI	0.0000	21.1000	32.9000
PCA	-21.1000	0.0000	11.8000
AIARR	-32.9000	-11.8000	0.0000

Alpha=0.05

Comparisons for each pair using Student's t

t
2.05183

Abs(Dif)-LSD	NDVI	PCA	AIARR
NDVI	-19.7189	1.3811	13.1811
PCA	1.3811	-19.7189	-7.9189
AIARR	13.1811	-7.9189	-19.7189

Positive values show pairs of means that are significantly different.

G.5 SPOT XS 23 February 1998

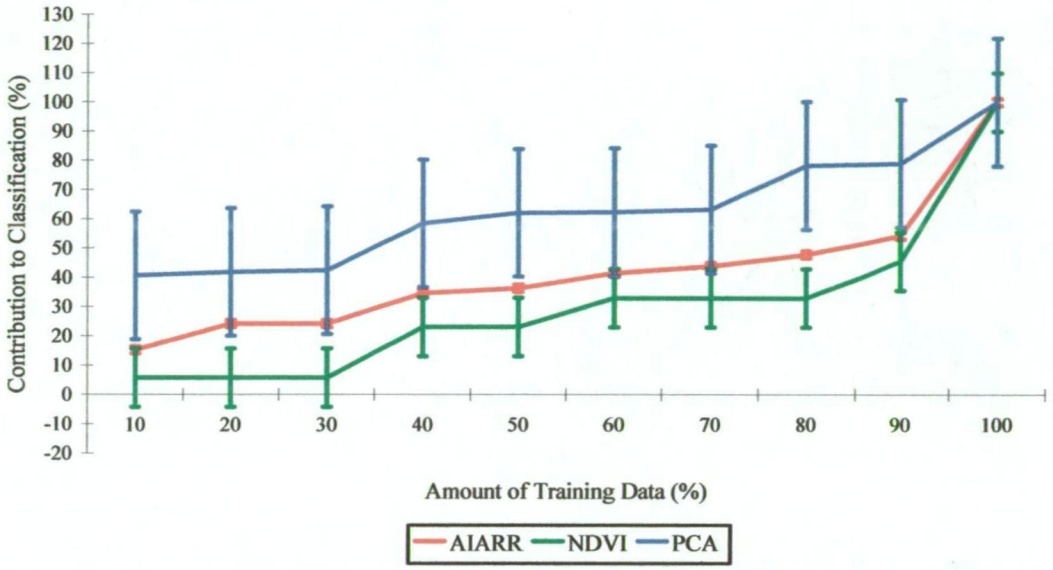

Figure G.5: Contribution of training data to classification of poppies in SPOT XS 23 February 1998 image, using three analysis methods, with bars indicating least significant difference associated with each processing method

Oneway Analysis of XS 23 February 1998 By Method

Analysis of Variance

Source	DF	Sum of Squares	Mean Square	F Ratio	Prob > F
Method	2	5203.467	2601.73	4.6052	0.0190
Error	27	15253.900	564.96		
C. Total	29	20457.367			

Means for Oneway Anova

Level	Number	Mean	Std Error	Lower 95%	Upper 95%
AIARR	10	42.1000	7.5164	26.678	57.522
NDVI	10	30.9000	7.5164	15.478	46.322
PCA	10	62.7000	7.5164	47.278	78.122

Std Error uses a pooled estimate of error variance

Means Comparisons

Dif=Mean[i]-Mean[j]	PCA	AIARR	NDVI
PCA	0.0000	20.6000	31.8000
AIARR	-20.6000	0.0000	11.2000
NDVI	-31.8000	-11.2000	0.0000

Alpha=0.05

Comparisons for each pair using Student's t

t
2.05183

Abs(Dif)-LSD	PCA	AIARR	NDVI
PCA	-21.8105	-1.2105	9.9895
AIARR	-1.2105	-21.8105	-10.6105
NDVI	9.9895	-10.6105	-21.8105

Positive values show pairs of means that are significantly different.

G.6 SPOT XS 18 April 1998

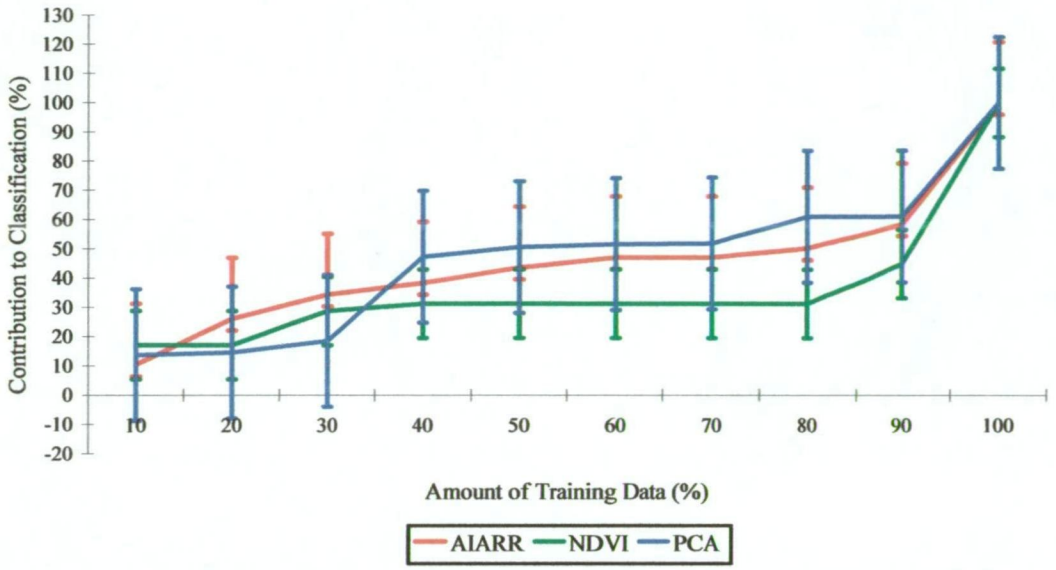

Figure G.6: Contribution of training data to classification of poppies in SPOT XS 18 April 1998 image, using three analysis methods, with bars indicating least significant difference associated with each processing method

Oneway Analysis of XS 18 April 1998 By Method

Analysis of Variance

Source	DF	Sum of Squares	Mean Square	F Ratio	Prob > F
Method	2	674.467	337.233	0.5595	0.5780
Error	27	16275.400	602.793		
C. Total	29	16949.867			

Means for Oneway Anova

Level	Number	Mean	Std Error	Lower 95%	Upper 95%
AIARR	10	45.4000	7.7640	29.470	61.330
NDVI	10	36.3000	7.7640	20.370	52.230
PCA	10	47.1000	7.7640	31.170	63.030

Std Error uses a pooled estimate of error variance

Means Comparisons

Dif=Mean[i]-Mean[j]	PCA	AIARR	NDVI
PCA	0.0000	1.7000	10.8000
AIARR	-1.7000	0.0000	9.1000
NDVI	-10.8000	-9.1000	0.0000

Alpha=0.05

Comparisons for each pair using Student's t

t
2.05183

Abs(Dif)-LSD	PCA	AIARR	NDVI
PCA	-22.5289	-20.8289	-11.7289
AIARR	-20.8289	-22.5289	-13.4289
NDVI	-11.7289	-13.4289	-22.5289

Positive values show pairs of means that are significantly different.

G.7 Landsat TM 21 July 1998

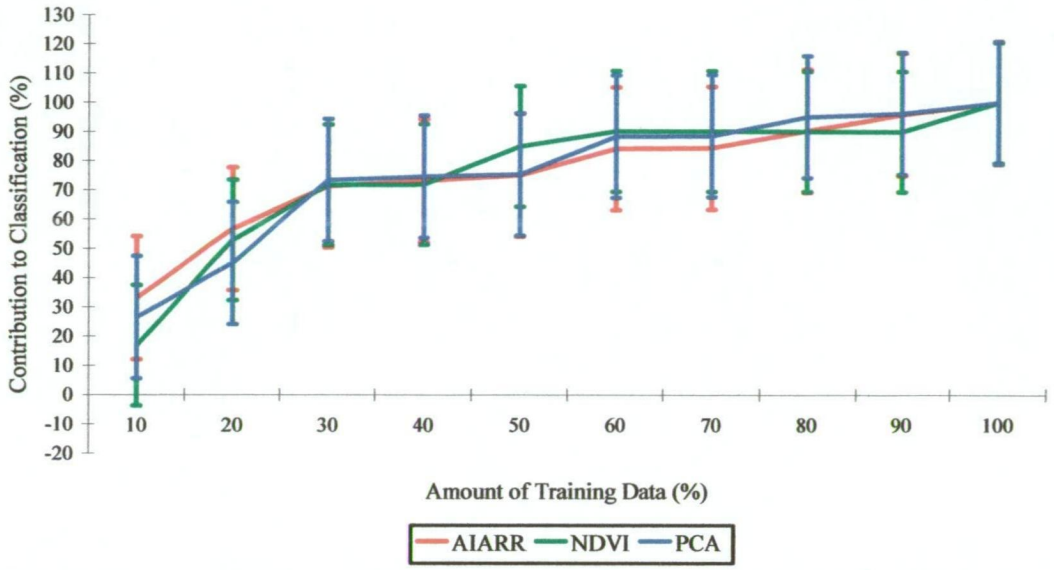

Figure G.7: Contribution of training data to classification of poppies in Landsat TM 21 July 1998 image, using three analysis methods, with bars indicating least significant difference associated with each processing method

Oneway Analysis of TM 21 July 1998 By Method

Analysis of Variance

Source	DF	Sum of Squares	Mean Square	F Ratio	Prob > F
Method	2	0.867	0.433	0.0008	0.9992
Error	27	14148.600	524.022		
C. Total	29	14149.467			

Means for Oneway Anova

Level	Number	Mean	Std Error	Lower 95%	Upper 95%
AIARR	10	76.3000	7.2389	61.447	91.153
NDVI	10	75.9000	7.2389	61.047	90.753
PCA	10	76.2000	7.2389	61.347	91.053

Std Error uses a pooled estimate of error variance

Means Comparisons

Dif=Mean[i]-Mean[j]	AIARR	PCA	NDVI
AIARR	0.000000	0.100000	0.400000
PCA	-0.1	0.000000	0.300000
NDVI	-0.4	-0.3	0.000000

Alpha=0.05

Comparisons for each pair using Student's t

t
2.05183

Abs(Dif)-LSD	AIARR	PCA	NDVI
AIARR	-21.0054	-20.9054	-20.6054
PCA	-20.9054	-21.0054	-20.7054
NDVI	-20.6054	-20.7054	-21.0054

Positive values show pairs of means that are significantly different.

G.8 Landsat TM 27 September 1998

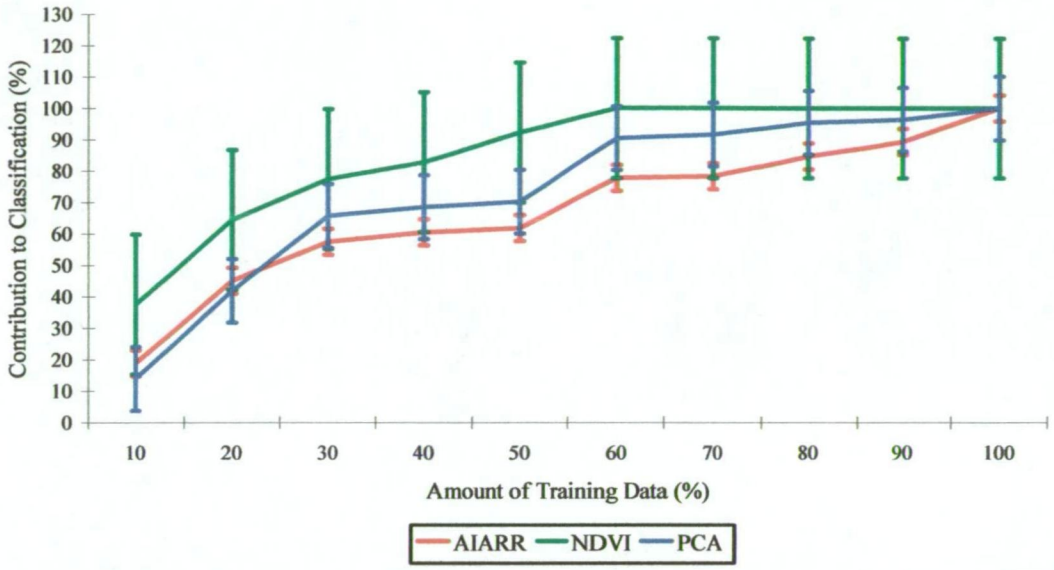

Figure G.8: Contribution of training data to classification of poppies in Landsat TM 27 September 1998 image, using three analysis methods, with bars indicating least significant difference associated with each processing method

Oneway Analysis of TM 27 September 1998 By Method

Analysis of Variance

Source	DF	Sum of Squares	Mean Square	F Ratio	Prob > F
Method	2	1700.067	850.033	1.4470	0.2530
Error	27	15861.300	587.456		
C. Total	29	17561.367			

Means for Oneway Anova

Level	Number	Mean	Std Error	Lower 95%	Upper 95%
AIARR	10	67.4000	7.6646	51.674	83.13
NDVI	10	85.5000	7.6646	69.774	101.23
PCA	10	73.4000	7.6646	57.674	89.13

Std Error uses a pooled estimate of error variance

Means Comparisons

Dif=Mean[i]-Mean[j]	NDVI	PCA	AIARR
NDVI	0.0000	12.1000	18.1000
PCA	-12.1000	0.0000	6.0000
AIARR	-18.1000	-6.0000	0.0000

Alpha=0.05

Comparisons for each pair using Student's t

t
2.05183

Abs(Dif)-LSD	NDVI	PCA	AIARR
NDVI	-22.2405	-10.1405	-4.1405
PCA	-10.1405	-22.2405	-16.2405
AIARR	-4.1405	-16.2405	-22.2405

Positive values show pairs of means that are significantly different.

G.9 SPOT XI 08 October 1998

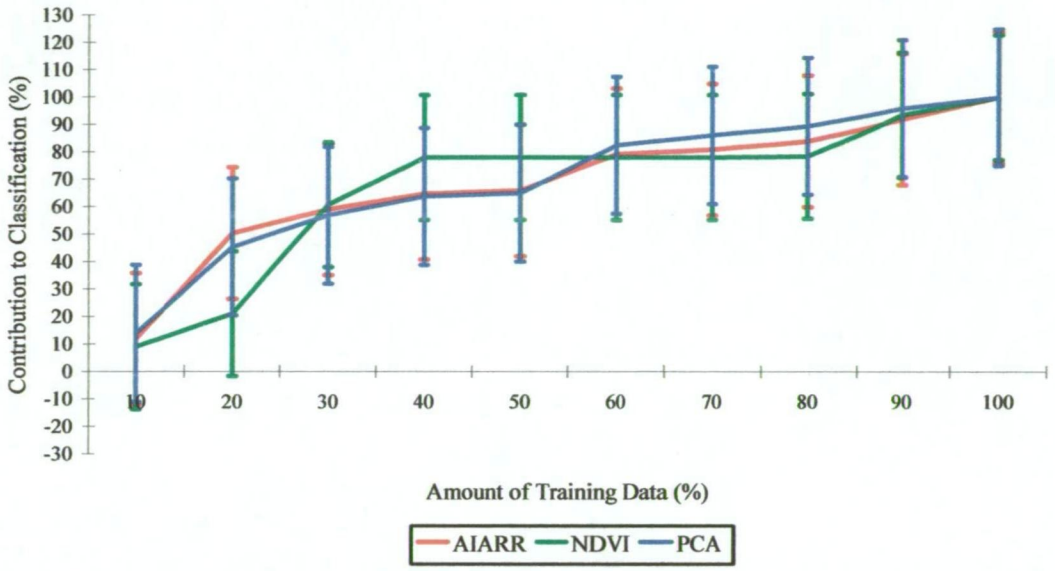

Figure G.9: Contribution of training data to classification of poppies in SPOT XI 08 October 1998 image, using three analysis methods, with bars indicating least significant difference associated with each processing method

Oneway Analysis of XI 08 October 1998 By Method

Analysis of Variance

Source	DF	Sum of Squares	Mean Square	F Ratio	Prob > F
Method	2	24.267	12.133	0.0164	0.9837
Error	27	19979.600	739.985		
C. Total	29	20003.867			

Means for Oneway Anova

Level	Number	Mean	Std Error	Lower 95%	Upper 95%
AIARR	10	68.8000	8.6022	51.150	86.450
NDVI	10	67.6000	8.6022	49.950	85.250
PCA	10	69.8000	8.6022	52.150	87.450

Std Error uses a pooled estimate of error variance

Means Comparisons

Dif=Mean[i]-Mean[j]	PCA	AIARR	NDVI
PCA	0.00000	1.00000	2.20000
AIARR	-1.00000	0.00000	1.20000
NDVI	-2.20000	-1.20000	0.00000

Alpha=0.05

Comparisons for each pair using Student's t

t
2.05183

Abs(Dif)-LSD	PCA	AIARR	NDVI
PCA	-24.9613	-23.9613	-22.7613
AIARR	-23.9613	-24.9613	-23.7613
NDVI	-22.7613	-23.7613	-24.9613

Positive values show pairs of means that are significantly different.

G.10 SPOT XI 31 December 1998

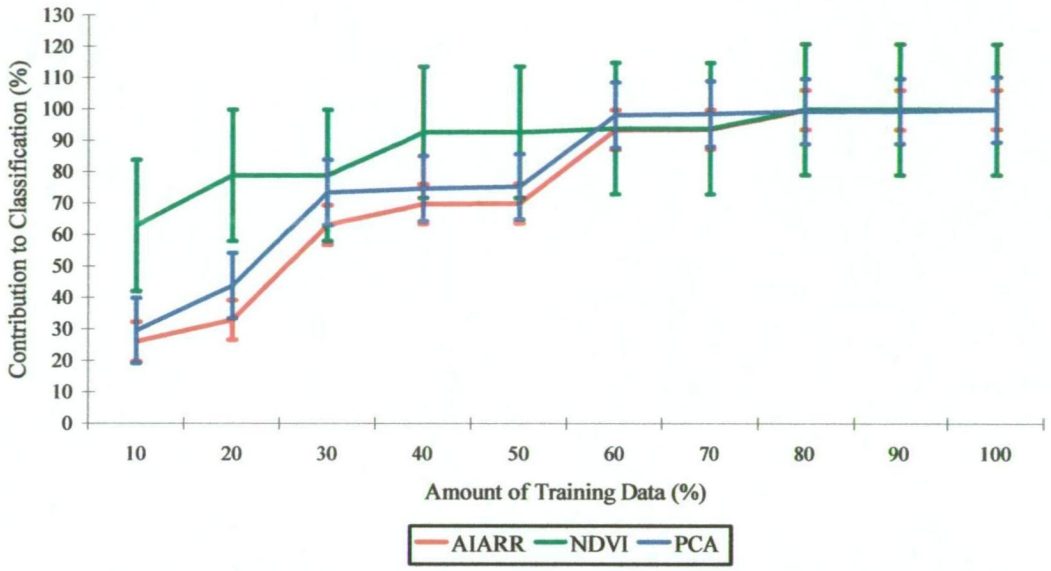

Figure G.10: Contribution of training data to classification of poppies in SPOT XI 31 December 1998 image, using three analysis methods, with bars indicating least significant difference associated with each processing method

Oneway Analysis of XI 31 December 1998 By Method

Analysis of Variance

Source	DF	Sum of Squares	Mean Square	F Ratio	Prob > F
Method	2	1134.067	567.033	1.0941	0.3492
Error	27	13993.400	518.274		
C. Total	29	15127.467			

Means for Oneway Anova

Level	Number	Mean	Std Error	Lower 95%	Upper 95%
AIARR	10	74.9000	7.1991	60.129	89.67
NDVI	10	89.5000	7.1991	74.729	104.27
PCA	10	79.0000	7.1991	64.229	93.77

Std Error uses a pooled estimate of error variance

Means Comparisons

Dif=Mean[i]-Mean[j]	NDVI	PCA	AIARR
NDVI	0.0000	10.5000	14.6000
PCA	-10.5000	0.0000	4.1000
AIARR	-14.6000	-4.1000	0.0000

Alpha=0.05

Comparisons for each pair using Student's t

t
2.05183

Abs(Dif)-LSD	NDVI	PCA	AIARR
NDVI	-20.8899	-10.3899	-6.2899
PCA	-10.3899	-20.8899	-16.7899
AIARR	-6.2899	-16.7899	-20.8899

Positive values show pairs of means that are significantly different.

G.11 Landsat TM 29 January 1999

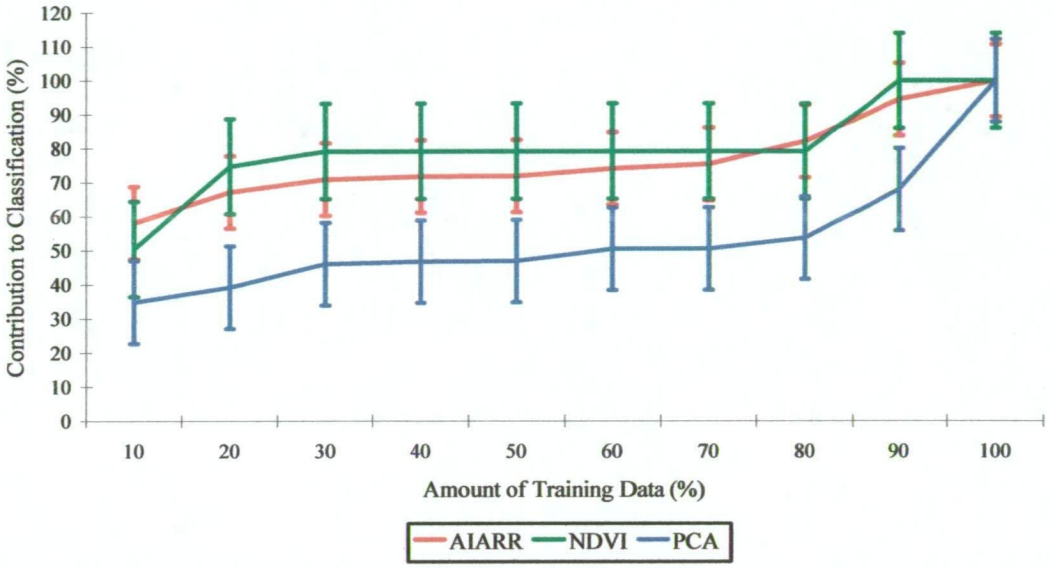

Figure G.11: Contribution of training data to classification of poppies in Landsat TM 29 January 1999 image, using three analysis methods, with bars indicating least significant difference associated with each processing method

Oneway Analysis of TM 29 January 1999 By Method

Analysis of Variance

Source	DF	Sum of Squares	Mean Square	F Ratio	Prob > F
Method	2	4039.800	2019.90	8.7331	0.0012
Error	27	6244.900	231.29		
C. Total	29	10284.700			

Means for Oneway Anova

Level	Number	Mean	Std Error	Lower 95%	Upper 95%
AIARR	10	76.6000	4.8093	66.732	86.468
NDVI	10	79.9000	4.8093	70.032	89.768
PCA	10	53.8000	4.8093	43.932	63.668

Std Error uses a pooled estimate of error variance

Means Comparisons

Dif=Mean[i]-Mean[j]	NDVI	AIARR	PCA
NDVI	0.0000	3.3000	26.1000
AIARR	-3.3000	0.0000	22.8000
PCA	-26.1000	-22.8000	0.0000

Alpha=0.05

Comparisons for each pair using Student's t

t
2.05183

Abs(Dif)-LSD	NDVI	AIARR	PCA
NDVI	-13.9552	-10.6552	12.1448
AIARR	-10.6552	-13.9552	8.8448
PCA	12.1448	8.8448	-13.9552

Positive values show pairs of means that are significantly different.

G.12 Landsat TM 03 March 1999

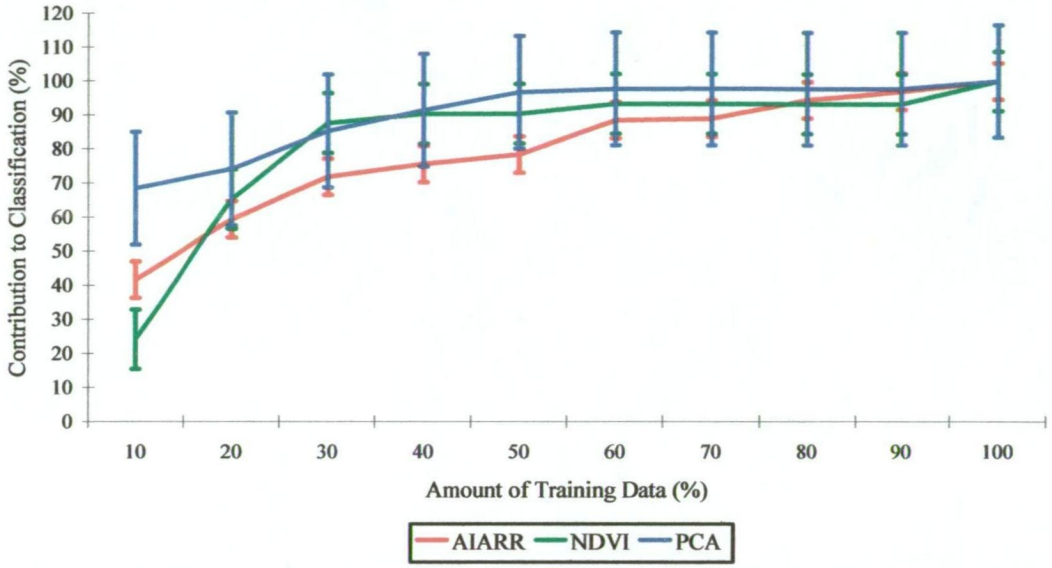

Figure G.12: Contribution of training data to classification of poppies in Landsat TM 03 March 1999 image, using three analysis methods, with bars indicating least significant difference associated with each processing method

Oneway Analysis of TM 03 March 1999 By Method

Analysis of Variance

Source	DF	Sum of Squares	Mean Square	F Ratio	Prob > F
Method	2	659.4667	329.733	1.0140	0.3762
Error	27	8779.5000	325.167		
C. Total	29	9438.9667			

Means for Oneway Anova

Level	Number	Mean	Std Error	Lower 95%	Upper 95%
AIARR	10	79.5000	5.7023	67.800	91.20
NDVI	10	82.9000	5.7023	71.200	94.60
PCA	10	90.7000	5.7023	79.000	102.40

Std Error uses a pooled estimate of error variance

Means Comparisons

Dif=Mean[i]-Mean[j]	PCA	NDVI	AIARR
PCA	0.0000	7.8000	11.2000
NDVI	-7.8000	0.0000	3.4000
AIARR	-11.2000	-3.4000	0.0000

Alpha=0.05

Comparisons for each pair using Student's t

t
2.05183

Abs(Dif)-LSD	PCA	NDVI	AIARR
PCA	-16.5466	-8.7466	-5.3466
NDVI	-8.7466	-16.5466	-13.1466
AIARR	-5.3466	-13.1466	-16.5466

Positive values show pairs of means that are significantly different.

G.13 SPOT XI 29 March1999

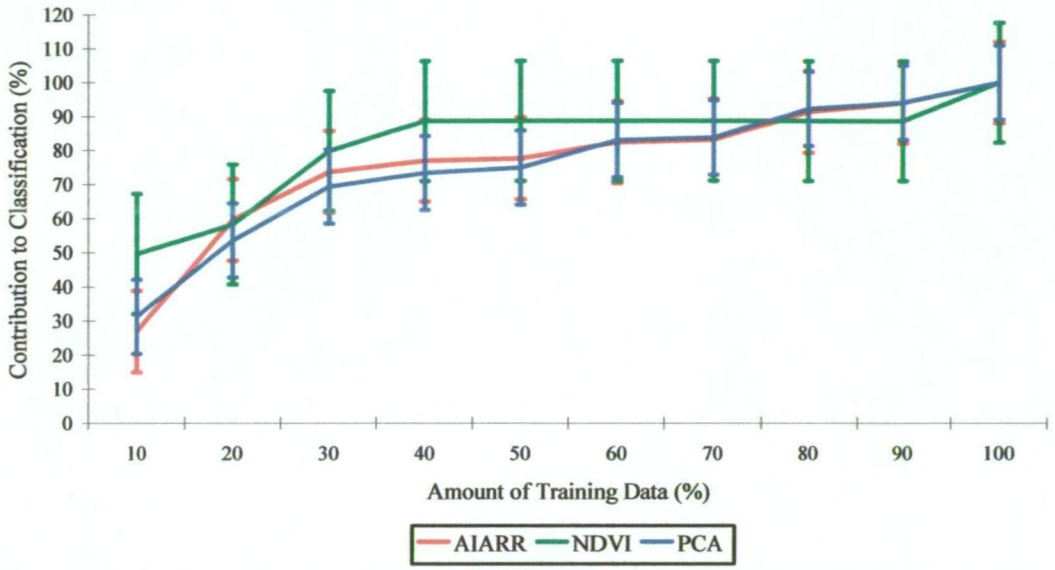

Figure G.13: Contribution of training data to classification of poppies in SPOT XI 29 March 1999 image, using three analysis methods, with bars indicating least significant difference associated with each processing method

Oneway Analysis of XI 29 March 1999 By Method

Analysis of Variance

Source	DF	Sum of Squares	Mean Square	F Ratio	Prob > F
Method	2	258.200	129.100	0.3511	0.7071
Error	27	9928.500	367.722		
C. Total	29	10186.700			

Means for Oneway Anova

Level	Number	Mean	Std Error	Lower 95%	Upper 95%
AIARR	10	76.6000	6.0640	64.158	89.042
NDVI	10	82.2000	6.0640	69.758	94.642
PCA	10	75.5000	6.0640	63.058	87.942

Std Error uses a pooled estimate of error variance

Means Comparisons

Dif=Mean[i]-Mean[j]	NDVI	AIARR	PCA
NDVI	0.00000	5.60000	6.70000
AIARR	-5.60000	0.00000	1.10000
PCA	-6.70000	-1.10000	0.00000

Alpha=0.05

Comparisons for each pair using Student's t

t
2.05183

Abs(Dif)-LSD	NDVI	AIARR	PCA
NDVI	-17.5961	-11.9961	-10.8961
AIARR	-11.9961	-17.5961	-16.4961
PCA	-10.8961	-16.4961	-17.5961

Positive values show pairs of means that are significantly different.